



University of
Nottingham

UK | CHINA | MALAYSIA

Synthesis and biological evaluation of novel PqsR antagonists
to combat *Pseudomonas aeruginosa* infections

Alaa Mashabi

Thesis submitted to the University of Nottingham for the degree of Doctor of
Philosophy

January 2021

Declaration

This thesis is submitted to the University of Nottingham for the degree of Doctor of Philosophy.

The work described in this thesis has been conducted by myself, unless stated otherwise. No part has been used for submission of another degree at the University of Nottingham or elsewhere.

The work presented in this thesis that was not conducted by myself is outlined below:

- The *in silico* virtual screening of MCCC library and biological evaluation of the high scored compounds which results of five hits was carried out by Dr. Fadi Soukarieh.
- Any compounds presented in Chapter 2 (SAR discussion) but were not discussed in synthesis and experimental were synthesised by Dr. Fadi Soukarieh.
- The initial SAR study presented in Chapter 3 (Table 3-1) was carried out by Dr. Fadi Soukarieh.
- Some biological work presented in Chapter 4 was carried out by Nigel Halliday and Eduard Vico Oton.
- The crystallography and isothermal calorimetry titration experiment were performed by William Richardson.

Alaa Mashabi

Contents

1	Introduction.....	1
1.1	Background.....	1
1.1.1	The history of antibiotic resistance	1
1.1.2	The opportunistic pathogen <i>Pseudomonas aeruginosa</i>	3
1.1.3	Clinical manifestations.....	4
1.1.4	Genomic structure and diversity	6
1.2	Current therapy for <i>Pseudomonas aeruginosa</i> infections	8
1.2.1	‘Traditional’ approaches	8
1.2.2	The ‘modifications of current classes’ approach	9
1.2.3	The ‘novel mechanism of action’ approach.....	11
1.3	<i>Pseudomonas aeruginosa</i> resistance and tolerance	14
1.3.1	Intrinsic resistance.....	14
1.3.2	Acquired resistance.....	17
1.3.3	Adaptive resistance	18
1.4	Establishment of <i>Pseudomonas aeruginosa</i> infection	21
1.5	Quorum sensing networks of <i>Pseudomonas aeruginosa</i>	24
1.5.1	<i>N</i> -acyl-L-homoserine lactone-dependent quorum sensing.....	25
1.5.2	Alkyl quinoline-dependant quorum sensing	27
1.5.3	Key effectors of the <i>pqs</i> QS system in virulence	29
1.6	Targeting quorum sensing as a novel strategy for treatment of <i>Pseudomonas aeruginosa</i> infections.....	32
1.6.1	Targeting the <i>las</i> system	33
1.6.2	Targeting the <i>rhl</i> system	34
1.6.3	Targeting the <i>pqs</i> system.....	34
1.7	PqsR receptor as a transcriptional regulator in <i>Pseudomonas aeruginosa</i> QS	37
1.7.1	Validation of PqsR receptor as a therapeutic target in <i>Pseudomonas aeruginosa</i> infections	37

1.7.2	Molecular insight of PqsR receptor.....	40
1.8	The design of an anti-virulence development project.....	42
1.8.1	Physicochemical properties of antibacterial compounds.....	45
1.8.2	Biological evaluation of novel quorum sensing inhibitors.....	49
1.9	Project overview and objectives.....	57
2	Design, Synthesis and Evaluation of Novel quinazolin-4(3 <i>H</i>)-one-based PqsR antagonists as Adjuvant Therapies to Treat <i>Pseudomonas aeruginosa</i> Infection.....	58
2.1	Background of the project.....	58
2.2	Hit characterization.....	60
2.3	Rationale of the design.....	63
2.4	Results and discussion.....	65
2.4.1	Synthesis of 2-(4-(3-(6-chloro-4-oxoquinazolin-3(4 <i>H</i>)-yl)-2-hydroxypropoxy) phenyl) acetonitrile, 1.6 and its analogues.....	65
2.4.2	Oxidizing the hydroxyl functional group in 2-(4-(3-(6-chloro-4-oxoquinazolin-3(4 <i>H</i>)-yl)-2-hydroxypropoxy) phenyl) acetonitrile, 1.6	70
2.4.3	Synthesis of 2-(4-(2-amino-3-(6-chloro-4-oxoquinazolin-3(4 <i>H</i>)-yl) propoxy) phenyl) acetonitrile 2.40 and its analogues.....	71
2.4.4	Nitrile hydrolysis in 1.6 to synthesis 2-(4-(3-(6-chloro-4-oxoquinazolin-3(4 <i>H</i>)-yl) -2-hydroxypropoxy) phenyl) acetamide 2.51	76
2.4.5	Modification of the nitrile group to different heterocycles.....	78
2.4.6	Different approaches for linker modifications.....	79
2.5	Molecular analysis.....	81
2.5.1	Isothermal calorimetry titration (ITC) of PqsR ^{CBD} with 1.13	81
2.5.2	Crystal structure of PqsR ^{CBD} complexed with PqsR antagonists 1.13 and 2.34	83
2.6	Structure–activity relationship analysis.....	85
2.6.1	Analysing the optimal position of electron-withdrawing substitution on the quinazolin-4(3 <i>H</i>)-one core.....	85
2.6.2	Amino propan-2-ol linker investigation.....	87
2.6.3	Analysing the substituents on the 2-(4-hydroxyphenyl) acetonitrile ring.....	90
2.6.4	The analysis of 1.6 enantiomer activity.....	93

2.7	Conclusion and future work.....	94
3	Hit to lead Optimisation of Novel 1 <i>H</i> -benzo[<i>d</i>]imidazole based PqsR Inhibitors as Adjuvant Therapy to Treat <i>Pseudomonas aeruginosa</i> Infections.....	96
3.1	Background and aim of the project.....	96
3.2	Rationale of the design.....	98
3.3	Results and discussion	100
3.3.1	Synthesis overview	100
3.3.2	The first synthetic route employing amino functional group in 3.10	102
3.3.3	The second synthetic route employing epoxide moiety in 2.29	105
3.3.4	The third synthetic route employing isothiocyanate moiety.....	109
3.3.5	The design of the final synthetic route of 2-aminobenzimidazole series.....	111
3.4	Molecular analysis	119
3.4.1	Crystal structure of PqsR ^{CBD} complexed with active compounds belonging to the 2-amino benzimidazole series	120
3.5	Structure activity relationship analysis	123
3.5.1	SAR study of 2-aminobenzimidazole series	123
3.5.2	Comparison between 3.20 and 1.3	125
3.5.3	Analysis of 3.20 enantiomers activity.....	127
3.6	Conclusion and future work.....	130
4	Biological Characterisation of PqsR Inhibitors based on Crystal Structure and <i>In Vitro</i> Studies, and their Effect on Quorum Sensing in <i>Pseudomonas aeruginosa</i>	131
4.1	Overview.....	131
4.2	Primary <i>in vitro</i> assays.....	133
4.2.1	The CTX:: <i>Pkm</i> -lux PAO1-L strain	133
4.2.2	Growth measurement	134
4.3	Secondary <i>in vitro</i> assays.....	135
4.3.1	Pyocyanin signal quantification	136
4.3.2	Alkyl quinolone signal quantification.....	138
4.4	Biofilm formation analysis.....	140
4.5	Cytotoxicity study.....	144

4.6	Conclusions and future work	146
5	General Discussion and Future Work	147
5.1	Antivirulence drugs in the clinic	147
5.2	The pharmacophore of PqsR antagonists.....	150
5.3	Physicochemical properties analysis.....	153
5.3.1	Lipophilicity analysis	157
5.3.2	Molecular weight analysis	159
5.3.3	Hydrogen bond donor and acceptor analysis	161
5.4	Conclusions and future work	162
6	Experimental	166
6.1	Chemistry	166
6.1.1	Reagents and instruments.....	166
6.1.2	Experimental of chapter 2	168
6.1.3	Experimental of chapter 3	188
6.2	Biological evaluation	244
6.2.1	Bioluminescence reporter gene fusion assay	244
6.2.2	Pyocyanin and alkyl quinoline quantification.....	246
6.2.3	<i>Ex vivo</i> pig lung model.....	247
6.2.4	Cytotoxicity study	249
7	Appendix.....	250
8	References.....	258

Poster presentation

- Mashabi, A. *et al.* Design, synthesis and evaluation of novel PqsR inhibitors as adjuvant therapy to treat *pseudomonas aeruginosa* infections. 27th Annual GP2A Medicinal Chemistry Conference– Nottingham UK, 21st – 23rd August 2019

Publication

- Soukarieh, F. *et al.* Hit identification of new potent PqsR antagonists as inhibitors of quorum sensing in planktonic and biofilm grown *Pseudomonas aeruginosa*. *Front Chem* **8**, 1–14 (2020).
- Grossman, S. *et al.* Novel quinazolinone inhibitors of the *Pseudomonas aeruginosa* quorum sensing transcriptional regulator PqsR. *Eur J Med Chem* **208**, (2020).
- Soukarieh, F. *et al.* Design and evaluation of new quinazolin-4(3*H*)-one derived PqsR antagonists as quorum sensing quenchers in *pseudomonas aeruginosa*. *ACS Infect Dis* (in press)

Abstract

Pseudomonas aeruginosa is an important opportunistic pathogen that belongs to superbug microorganisms and shows an increased number of multi-drug resistant (MDR) clinical isolates. *P. aeruginosa* has three hierarchically organised quorum sensing (QS) or cell to cell communication systems named *las*, *rhl* and *pqs*. The *las* and *rhl* are classic QS systems that use an *N*-(3-oxododecanoyl) -L-homoserine lactone as autoinducers. The *las* system is the major QS system of the cell and controls the other two and there is partial redundancy with the *rhl* system regarding the genes and functions controlled by the system. The *pqs* quorum sensing system of *P. aeruginosa* is a major regulatory network that controls the expression of genes involved in virulence, biofilms, oxidative stress and iron acquisition, especially in chronic conditions. The transcriptional regulator of the *pqs* system is PqsR which becomes functional upon direct binding to the main autoinducer of the receptor, PQS and its precursor HHQ. The inhibition of QS and in particular the *pqs* system is an approach to decrease the virulence of *P. aeruginosa in vivo*, improve the outcome of antibiotic treatments and decrease the *P. aeruginosa* associated morbidity. This work aims to develop PqsR antagonists that attenuating the pathogenicity and resistance of one of the most critical pathogens by designing and developing a range of novel QS inhibitors targeting the transcriptional regulator (PqsR) of the *pqs* system which is distinct to *P. aeruginosa*. Different chemical approaches are employed to synthesise a range of compounds, and the selected candidates are validated through different biological evaluations and molecular structure analysis. Chapter 2 focuses mainly on a SAR study for the selected hit, founded by *in silico* screening, with a quinazolin-4(3*H*)-one scaffold which is similar to the natural substrate of the receptor. In Chapter 3, the work aimed to expand the SAR further by replacing the quinazolin-4(3*H*)-one moiety with different heterocyclic ring systems; it was concluded that the optimal replacement is the 1-methyl-1*H*-benzo[*d*]imidazol-2-amine ring. Many attempts were established to identify the optimal conditions to synthesise

this series by employing different strategies, and the selected pathway was successful in synthesising a range of analogues with good yield. Cell based reporter gene assay with PAO1-L CTX::P_{pqsA}-lux strain of *P. aeruginosa* was employed to evaluate the activity of the compounds. Furthermore, the active compounds with sub-micromolar potency were analysed in pyocyanin quantification assay. **3.20** was analysed further in alkyl quinoline quantification assay against different genomic classes of *P. aeruginosa*. The crystal structures of PqsR^{CBD} complexed with key compounds presented in chapter 2 and 3 were attained. These biological evaluations are presented in this work in an attempt to prove the concept and validate PqsR as a relevant therapeutic target. Furthermore, a cytotoxicity study of the most active compounds in the series was conducted to investigate the therapeutic-toxicity index of these compounds before proceeding to the *in vivo* study. Overall, this project has led to the successful development of hit to lead optimization study starting with previously identified compound **2-(4-(3-(6-chloro-4-oxoquinazolin-3(4H)-yl)-2-hydroxypropoxy) phenyl) acetonitrile**, **1.6** (IC₅₀ = 3.2 μM in PAO1-L) leading to a new series of potent benzimidazole containing compounds. **2-(4-(3-((6-chloro-1-isopropyl-1H-benzo[d]imidazol-2-yl) amino)-2-hydroxypropoxy) phenyl) acetonitrile** **3.20** (PAO1-L IC₅₀ 0.13 ± 0.04 μM, PA14 IC₅₀ 0.09 ± 0.01 μM) is one of the most potent PqsR antagonists in this series with high potency inhibition of *pqs* system signalling. In addition, **3.20** showed wide spectrum efficacy against different genomic classes of *P. aeruginosa* with significant inhibition of *P. aeruginosa* pyocyanin and AQ production. The co-crystal structure of **3.20** and some analogues with PqsR^{LBD} were determined which revealed specific binding interactions of this new class of inhibitors. In addition, cytotoxicity studies revealed that **3.20** had a good safety margin against a human cell line which support **3.20** progression to a murine *in vivo* study. However, it is critical to establish further pharmacokinetics *in vitro* and *in vivo* assays as well as a biofilm formation model to evaluate the efficacy or safety of the novel candidate which are beyond the scope of this thesis.

Abbreviations

2-ABA	2-aminobenzoylacetate
2-ABA-CoA	2-aminobenzoylacetyl-CoA
AQ	2-alkyl-4-quinoline
ASM	artificial sputum medium
BOP	benzotriazol-1-yl-oxy-ris-(dimethylamino)-phosphonium hexafluorophosphate
bp	base pair
CBD	Co-inducer binding domain
CDI	Carbonyl diimidazole
c-di-GMP	3',5'-cyclic diguanylic acid
CF	Cystic fibrosis
CFU	Colony-forming unit
CFTR	Cystic fibrosis transmembrane conductance regulator
CIP	Ciprofloxacin
CMC	Comprehensive medicinal chemistry
COPD	Chronic obstructive pulmonary disease
DIAD	Di-isopropyl azodicarboxylate
DMEM	Dulbecco's Modified Essential Medium
DMP	Dess–Martin periodinane
DPPA	Di-phenyl phosphoryl azide
eDNA	Extracellular DNA
EDG	electron-donating group
ee	enantiomeric excess
EPS	Extracellular polymeric substances
EWG	electron-withdrawing group
EVPL	<i>ex vivo</i> pig lung
FBS	fetal bovine serum
GFP	green fluorescent protein
h	hours
HBA	hydrogen bond acceptor
HBD	hydrogen bond donor
HCN	hydrogen cyanide
HHQ	2-Heptyl-3,4-dihydroxyquinoline
HMBC	heteronuclear multiple-bond correlation
HQNO	4-hydroxy-2-heptylquinoline-N-oxide
HSL	<i>N</i> -acyl-L-homoserine lactone
HTH	Helix-turn-helix domain
HPLC	high-performance liquid chromatography
HTS	high-throughput screening
IC ₅₀	Inhibitory concentration 50%
ITC	Isothermal titration calorimetry

K_D	Dissociation constant
LB	Lysogeny broth media
LBD	Ligand binding domain
LLE	lipophilic ligand efficiency
LPS	Lipopolysaccharide
LTTR	LysR-type transcriptional regulator
MCCC	University of Nottingham managed chemical compound collection
MIC	minimum inhibitory concentration
MDR	multi-drug resistant
MW	molecular weight
NHQ	2-nonyl-4-hydroxyquinoline
OD	Optical density
OMV	Outer membrane vesicle
PABN	Phenylalanine arginyl β -naphthylamide
PQS	<i>Pseudomonas</i> quinolone signal, 4-hydroxy-2-heptylquinoline
PyBop	benzotriazol-1-yl-oxy-tris-pyrrolidino-phosphonium hexafluorophosphate
PyBrop	bromo tri-(pyrrolidino) phosphonium hexafluorophosphate
QQ	quorum quenching
QS	Quorum sensing
QSI	Quorum sensing inhibitors
QZN	Quinazolinone
SCV	Small Colony Variant
Tc	Tetracycline
TLC	Thin-layer chromatography
t_R	retention time
UV	Ultraviolet light
μM	Micromolar concentration
WHO	World Health Organization

Acknowledgment

First of all, I want to express all my thanks to ALLAH who without his guidance I would never be able to conduct and complete this long journey.

I would like also to express my deep sense of gratitude to my supervisors Michael Stocks, Barrie Kellam and Miguel Camara for their valuable guidance, motivation and encouragement at various stages of my project conduction. It is also my duty to record my thankfulness to Fadi Soukarieh who had carried a heavy load of responsibilities and concerns in bringing this project to a successful end with his patience, motivation, and immense knowledge.

I can't forget my parents, the source of my power who had been always beside me, supported me with their prayers, as well as with their countless love. I wish to expand my deepest gratitude and appreciation to my husband who has inspired me with his hope, love, and support and to my little kids Basel, Noor and Mohammad. Also, to my siblings, who have been an untiring shoulder, always keeping me on my feet, Najlaa, Ohood, Abdulaziz, Hossam and Moayd.

I dedicate this piece of work to my uncle's soul who die with complication of COVID-19 in October 2020 due to resistance strain of opportunistic pathogen, *Acinetobacter baumannii* complex haemolyticus which caused resistance pneumonia, in the hope that mankind will find the ideal strategy to fight these resistance strains in near future.

Alaa Mashabi

January 2021.

1 Introduction

1.1 Background

1.1.1 The history of antibiotic resistance

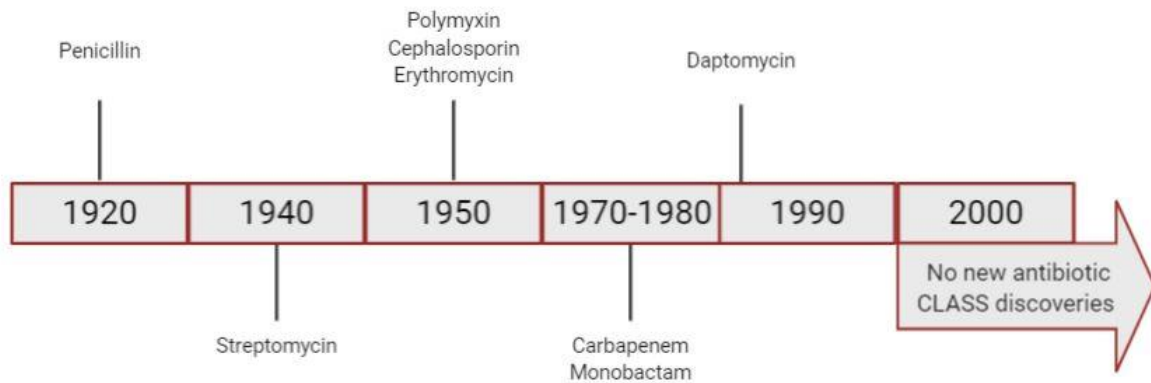


Figure 1-1: **The timeline of antibiotic development over the last century.** No new class of antibiotic has been identified since 1987.

Over the past decades, the number of multi-drug resistant (MDR) bacterial clinical isolates, specifically gram-negative pathogens, has rapidly increased. At the same time, since 1987, no new class of antibiotic has been developed for gram-negative bacteria (Figure 1-1), and all new recently approved antibiotics have been based on modifications of existing antibiotic classes. This latter fact is surprising not only because industrial and academic research was heavily supported during this period but also because of the revolution in novel technologies, such as genomic and high-throughput screening, which were introduced and applied to improve the productivity of drug discovery programmes. The combination of increasing emergence of MDR strains and the lack of discovery of new classes of antibiotics represents a serious threat to human health, as it could lead to the disarming of healthcare providers in the battle against bacterial pathogens at some point. MDR strains are the primary threat to hospitalised patients

and have been associated with mortality rates of 30–70 %.¹ As a result of this increasing morbidity, mortality rates could reach the levels seen prior to the antibiotic era. However, the emergence of MDR clinical isolates is not recent; it has been a persistent threat from the beginning of the antibiotic period. For example, penicillin was discovered by Alexander Fleming in 1928, and in 1940, several years before it was used to treat infections in patients, a bacterial penicillinase was identified by two members of the penicillin discovery team.² In addition, penicillin-resistant strains of *Staphylococcus aureus* were isolated in 1944, only two years after the introduction of this antibiotic into the market.³

The spread of resistance before the introduction of antibiotics into clinical practice was limited because of the absence of selective pressure from antibiotics. This pressure is a result of external influences, such as antibiotics, which lead to natural selection and differential survival of one group of organisms over another. In this case, antibiotics cause selective pressure by killing susceptible bacteria which allows antibiotic-resistant bacteria to survive and proliferate, thereby considerably accelerating the emergence of MDR strains. A similar trend has been observed for all antibiotics developed to date, with resistance observed before or shortly after first clinical use and a gradual increase in the proportion of resistant isolates over time. Typically, resistance usually affected a single antibiotic or antibiotic class. However, this has changed with the phenomenon of multi-drug resistance, which was first observed in enterobacteria during the late 1950s and has been spreading ever since.⁴ The situation has now become highly critical with the increase in the number of MDR microorganisms, popularly known as 'superbugs'. This term refers to any type of bacterium highly resistant, due to multiple mutations, to most antibacterial agents currently available causing severe therapeutic challenge. The gram-negative *Pseudomonas aeruginosa* is a superbug which usually causes different types of acute and chronic infections associated with high morbidity and mortality rates.⁴ In 2017, the World Health Organization (WHO) called for urgent development of new

antibiotics against a list of antibiotic-resistant strains which pose the greatest threat to human health. One of the top-priority pathogens in the list which needs immediate intervention is the carbapenem-resistant strain of *P. aeruginosa*;⁵ therefore, *P. aeruginosa* is the scope of this work.

1.1.2 The opportunistic pathogen *Pseudomonas aeruginosa*

P. aeruginosa is a ubiquitous aerobic monotrichous rod with a polar flagellum conferring motility to this organism. It also has protein structures on the surface known as pili which are responsible for adherence to the infected epithelium. As a gram-negative bacterium, its cell wall is made of a single layer of peptidoglycan surrounded by a membranous structure called the outer membrane (Figure 1-2). It produces several fluorescent siderophores, including pyoverdine and pyochelin, as well as a blue-green pigment called pyocyanin which gives *P. aeruginosa* a characteristic appearance in culture media.⁶

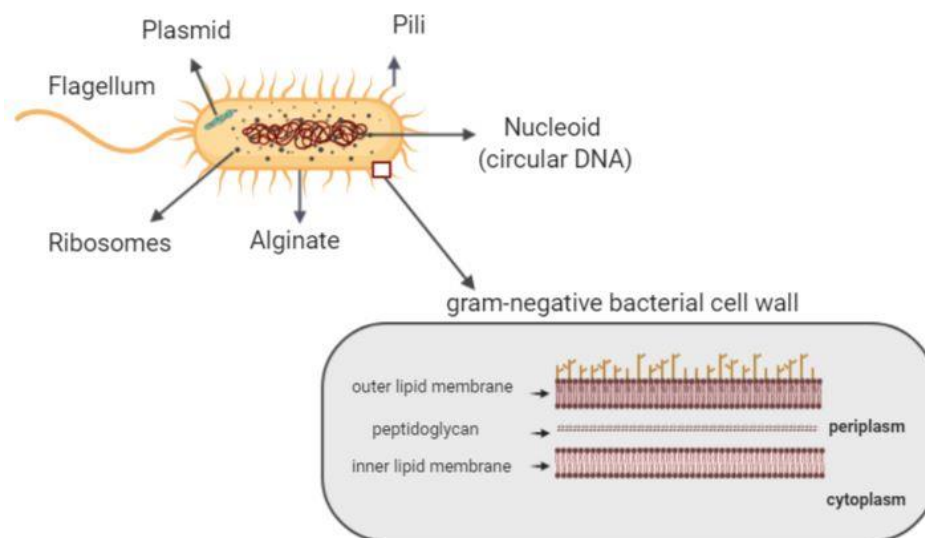


Figure 1-2: **The basic structure of *Pseudomonas aeruginosa*.** The enlarged section shows the common structure of the gram-negative cell wall, including that of *P. aeruginosa*.

The adaptability of *P. aeruginosa* allows it to grow in a wide range of environments and conditions with temperatures ranging from 5.5 to 45 °C and pH from 4 to 9.⁶ This adaptability

to different environments is due to the genetic flexibility provided by its large and complex genome, as will be discussed later (section 1.1.4). The pathogen can be found in different locations in the hospital environment and on medical equipment; as a result, it can be transmitted from patient to patient by healthcare providers.⁷ *P. aeruginosa* is an opportunistic pathogen which means that it rarely affects healthy individuals, and the infection can be initiated by different triggers that cause a break in first-line defences of eukaryotic host cells. These triggers engender breaks in normal cutaneous or mucosal barriers can result from trauma, surgery, serious burns, or catheter devices or disruption of normal protective mucosal flora by broad-spectrum antibiotics. Another possible factor is alteration of immunological defence mechanisms in cases such as chemotherapy-induced neutropenia, mucosal clearance defects in cystic fibrosis (CF), AIDS, and diabetes mellitus.⁸

1.1.3 Clinical manifestations

P. aeruginosa is an uncommon cause of pneumonia in healthy individuals or of community-acquired pneumonia. *Pseudomonas* pneumonia mostly occurs in an immune-compromised host with haemorrhagic and necrotising lung pathology.⁹ Hospital-acquired *pseudomonas* pneumonia is most likely to occur in patients with HIV or chronic obstructive pulmonary disease (COPD), or in patients who have undergone surgery or tracheostomy.¹⁰ *P. aeruginosa* is the most frequent and important pathogen responsible for chronic infection in patients with CF, with a reported rate of colonisation up to 80%.¹¹ The major determinant of morbidity and mortality due to this infection is recurrent endobronchial infection and exaggerated neutrophilic inflammation.¹²

CF is a genetic condition caused by autosomal recessive inheritance of mutations, or in other words, both parents carry one copy of the mutated gene, cystic fibrosis transmembrane conductance regulator (*CFTR*) gene.¹² This mutation causes dysfunction of the CFTR protein which is an ion channel in epithelial tissue and controls the flow of water and chloride ions into

and out of cells. This protein is present inside the cells that produce mucus, sweat, saliva, tears, and digestive enzymes, and its malfunction leads to the disruption of the balance of ions and fluid and production of mucus that is abnormally thick and sticky. The abnormal mucus obstructs the airways and limits pathogen clearance from the lung, which is the main cause of CF symptoms.¹³ Deficiency in the physical clearance defence mechanism of the respiratory system leads to early recruitment of inflammatory defence mechanisms involving polymorphonuclear leukocytes (PMN) and antibodies.¹⁴ Therefore, from early childhood, CF patients have recurrent and chronic respiratory tract infections characterised by PMN inflammation.¹⁵ Despite the inflammatory response and intensive antibiotic therapy, biofilm formation is initiated by *Staphylococcus aureus* (*S. aureus*) at an early stage, and as infection progresses, *P. aeruginosa* eventually becomes the predominant pathogenic resident and persists for decades as a chronic infection leading to treatment failure and sometimes the need for lung transplantation.¹⁶

Furthermore, *P. aeruginosa* is associated with bacteraemia, and it currently accounts for 15% of gram-negative bacteraemia cases.¹⁷ Interestingly, CF patients are rarely diagnosed with *P. aeruginosa* bacteraemia, which may be due to the high levels of circulating *P. aeruginosa* antibodies and the main infection of CF patients being localised pneumonia.¹⁸ The hospital mortality associated with *P. aeruginosa* bloodstream infections is reported to be greater than 20% in most cases and is higher among patients who have been under inappropriate initial antimicrobial regimens.¹⁷ Some local infections, such as eye or ear infections, remain at the infection site while others, such as wound or burn infections, result in bacteraemia. The difference in response may be due to host defences and initial treatment.¹⁹ Furthermore, *P. aeruginosa* causes urinary tract infections associated with the use of catheters as a major factor; no specific characteristic distinguishes the infection caused by this organism from other types

of urinary tract infections. This type of infection is usually treated with a variety of antipseudomonal drugs with good results.⁹

1.1.4 Genomic structure and diversity

The large genome size (5.5–7 million base pairs [Mbp]) and genetic complexity of *P. aeruginosa*, compared to the other 25 sequenced bacterial genomes, reflect the evolutionary adaptations which permit this pathogen to thrive in diverse ecological niches.²⁰ Analysis of its genome sequence has shown that this pathogen has a core genome found in all *P. aeruginosa* strains which is highly conserved among clonal complexes with sequence diversities between 0.5–0.7%. In addition, *P. aeruginosa* has an accessory genome which consists of extrachromosomal elements like prophages, transposons, insertion sequences (IS), genomic islands (GI) and plasmids which are inserted into the chromosome at various loci.²¹ The transferable genetic elements of the accessory genome can be present in subgroups of the *P. aeruginosa* population, but may also occur only in single strains in variable proportions up to 20% of the whole genome. The composition of the accessory genome accounts for most intra- and inter-clonal genomic diversity and rapid antibiotic resistance in *P. aeruginosa* which is apparently acquired by horizontal gene transfer from different sources as will be discussed in Section 1.3.2.²⁰ It is important to consider these variations in drug discovery projects and identify targets conserved in all strains of this bacterium by focusing on core genes and avoiding targeting the accessory genome. Indeed, the fast increase in available *P. aeruginosa* genome sequences, due to the revolution in sequencing technologies, is expected to provide the field with an unbiased overview of the genetic repertoire of *P. aeruginosa* populations which can guide target selection.

The first complete genome sequence analysis was performed for the PAO1 strain of *P. aeruginosa* which was isolated from the infected wound of an Australian patient.²² This strain is regarded as the major reference for genetic and functional studies in most laboratories. PAO1

consists of a 6.264-Mbp circular chromosome encoding 5,570 predicted protein-coding sequences. The second most studied *P. aeruginosa* strain is PA14, a clinical isolate which is considered more virulent than PAO1. According to open reading frame (ORF) analysis, PA14 contains 58 regions that are absent in PAO1, including the PA14 pathogenicity islands PAPI-1 and PAPI-2.²³ Both PAPI islands encode a cluster of discrete virulence genes which may confer additional pathogenic functions to this strain. Another clinical isolate (PA7) of Argentinian origin shows an unusual antimicrobial resistance pattern and is considered a taxonomic outlier of *P. aeruginosa*. In addition, LESB58 (Liverpool epidemic strain) is a strain isolated in 1988 from a CF patient from Liverpool. It is characterised by early overexpression of the cell-density-dependent quorum sensing (QS) regulon (for more details see Section 1.5), including virulence-related secreted factors such as elastase and pyocyanin. Furthermore, LESB58 is known to be a biofilm hyperproducer and has the potential to cause severe infections even in non-CF patients.²⁴

1.2 Current therapy for *Pseudomonas aeruginosa* infections

1.2.1 'Traditional' approaches

Antimicrobial chemotherapy is still the cornerstone of treatment for *P. aeruginosa* infections in the clinic. Generally, *P. aeruginosa* strains are susceptible to broad-spectrum penicillins, cephalosporins, monobactams, and carbapenems which all share the same β -lactam core ring with variable substitutions and extensions. Aminoglycosides and fluoroquinolones have also been introduced to clinical practice since the 1980s.¹⁰ The most common combination used for *P. aeruginosa* infections is intravenous therapy with piperacillin or ceftazidime (β -lactam antibiotic) with an aminoglycoside which has been effective for the last two decades.¹⁰ However, the emergence of resistance against this treatment, particularly in intensive care and patients with chronic disease, has called for alternatives.²⁵ β -lactam is a class of antibiotic targeting penicillin-binding proteins which are enzymes that contribute to the synthesis of peptidoglycan, the vital constituent of bacterial cells, which leads to autolytic processes within the cell.²⁶ In response to this selective pressure, the pathogen releases a β -lactamase enzyme that hydrolyses the β -lactam ring and deactivates the antibiotic. Recently, two new cephalosporins – ceftazidime-avibactam and ceftolozane-tazobactam – combined with β -lactamase inhibitor have been introduced to the clinic; this combination has been effective against this type of resistance.²⁵ On the other hand, the bacterium employs a different resistance strategy against aminoglycosides which have a bactericidal effect by inhibiting protein synthesis essential for survival. These strategies are exemplified by the production of aminoglycoside-modifying enzymes (AMEs) and modification of the target of aminoglycosides with different mutational strategies.²⁷ Another strategy to combat MDR strains is the revival of old polypeptide drugs, colistin and polymyxin B, whose use was abandoned for many years because of their neurotoxic and nephrotoxic side effects.

Nevertheless, the vital need for more active therapy has led to their relaunch in clinical practice. These cationic polypeptide antibiotics work by disrupting the outer cell membrane by interacting with anionic lipopolysaccharide (LPS) molecules leading to the displacement of calcium (Ca^{2+}) and magnesium (Mg^{2+}) and neutralisation of the lipopolysaccharide, thereby increasing the permeability of the bacterial membrane and leakage of cell contents.²⁸ Despite the novelty of the mechanism of action of these antibiotics, a *P. aeruginosa* isolate from a high-risk clone has shown new resistant isoforms to these antibiotics which emphasises the urgency of finding alternatives.²⁹

1.2.2 The ‘modifications of current classes’ approach

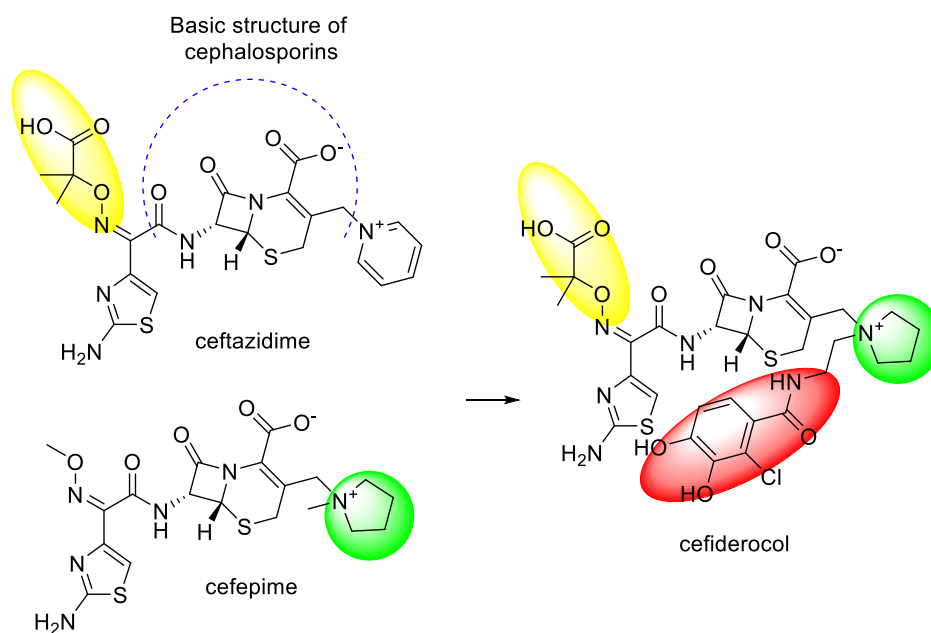


Figure 1-3: **The ‘modification of current classes of antimicrobial drugs’ approach.** The design of cefiderocol, a new member of the cephalosporin family, by employing cephalosporin core with side chains similar to ceftazidime and cefepime. The aminothiazole ring and carboxy propyl-oxyimino group (highlight in yellow) block recognition and inhibit hydrolysis by β -lactamases. A catechol 2-chloro-3,4-dihydroxybenzamide moiety (highlight in red) functions as the siderophore mimic. a pyrrolidine ring (highlight in green) confers zwitterionic properties, similar to those of cefepime, which enhance water solubility of the molecule.³⁰

All the recent improvements in the field are associated with modifications of analogues of current classes of antimicrobial drugs that share the basic chemical structures and mode of action. For example, cefiderocol is a new member of the cephalosporin family and shares its side chains with ceftazidime and cefepime which block recognition and inhibit hydrolysis by β -lactamases. Its novelty is due to the extension of one side chain by a catechol 2-chloro-3,4-dihydroxybenzamide moiety which enables ferric ion binding to create a cefiderocol–iron ion complex. Active iron transport systems then facilitate the transport of the complex across the outer membrane to the periplasmic space where dissociation occurs releasing the cefiderocol moiety to bind to penicillin-binding proteins. This strategy reduces the resistance associated with cell membrane permeability in addition to the ability to overcome resistance to β -lactamase in the first place. In *in vitro* assays, cefiderocol is more potent than ceftazidime-avibactam and ceftolozane-tazobactam against different MDR strains, including the strain highly resistant to carbapenem. In clinical studies, this antibiotic seems to address the problem of the highest priority strain (carbapenem-resistant strain) at least at present. A completed phase II clinical trial (ClinicalTrials.gov identifier: NCT02321800) has shown clinical efficacy and safety of intravenous cefiderocol in patients with complicated urinary tract infections. Further phase III clinical trials provided evidence of cefiderocol efficacy in the treatment of serious infections caused by carbapenem-resistant strains (ClinicalTrials.gov identifier: NCT02714595) and the efficacy and safety of intravenous cefiderocol compared to meropenem and linezolid, a synthetic antibiotic in the oxazolidinone class, in patients with hospital pneumonia (ClinicalTrials.gov identifier: NCT03032380). Both studies have resulted in cefiderocol being approved for use in the clinic.

1.2.3 The ‘novel mechanism of action’ approach

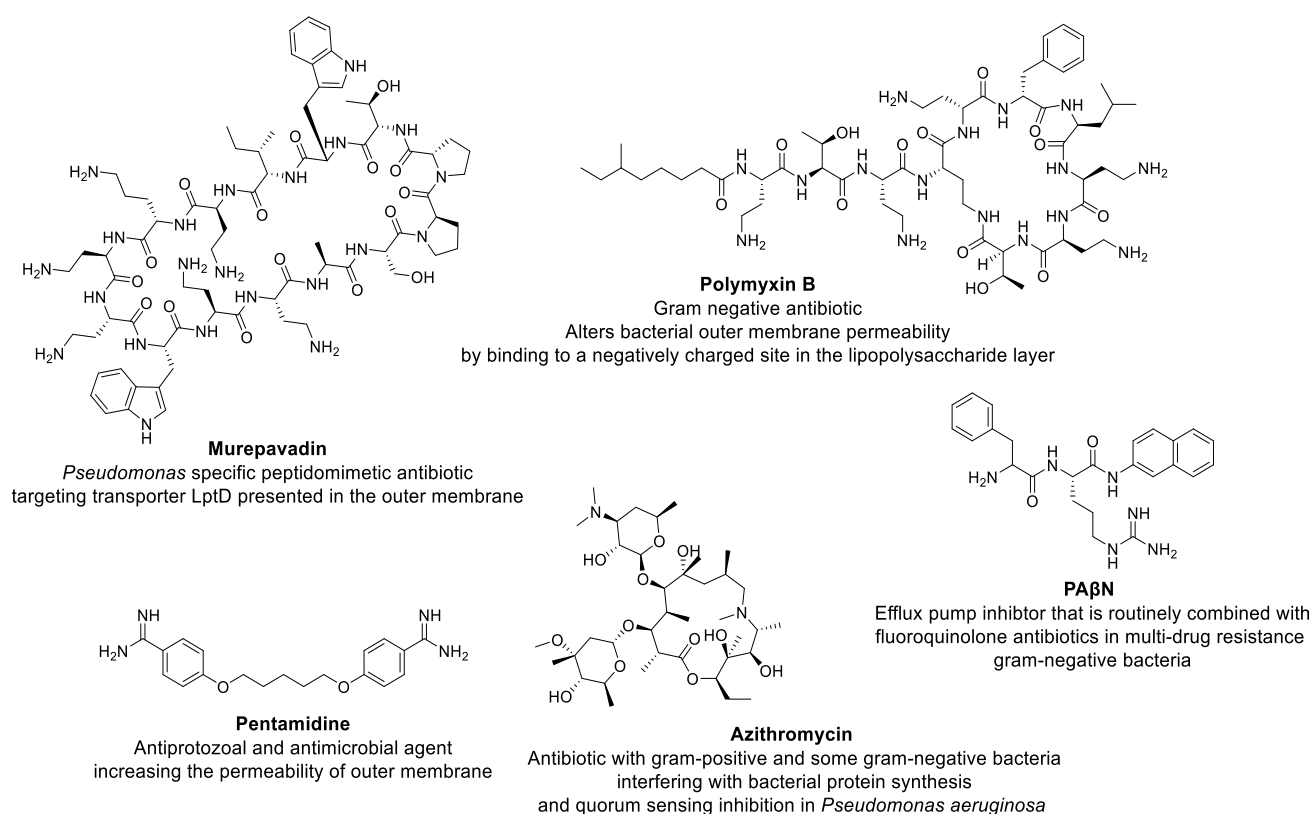


Figure 1-4: **The ‘novel mechanism of action’ approach.** Structure of antibiotics with their novel mechanisms of action.^{31,32,28,33,34}

Murepavadin is another example of the recent progress in this area with a novel mechanism of action (Figure 1-4). This antibiotic is a highly active and selective weapon against *P. aeruginosa* as a 14–amino acid synthetic peptidomimetic. It is the first antibiotic targeting the outer membrane protein transporter LptD which is responsible for transport of lipopolysaccharides from the periplasmic side of the outer membrane to its final location on the cell surface.³¹ Inhibition of this transporter causes alterations to lipopolysaccharide in the outer membrane and ultimately bacterial cell death.³¹ Although the clinical studies of this antibiotic progressed to phase III with two clinical trials targeting 2 and 41 participants (ClinicalTrials.gov identifiers: NCT03582007 and NCT03409679, respectively), both studies were terminated due to an unexpectedly high frequency of renal failure in participants who had

received murepavadin. Due to the high efficacy of this antibiotic against a range of *P. aeruginosa* strains, including carbapenem-resistant, ceftolozane/tazobactam-resistant and colistin-resistant strains, further development of an aerosolised formulation of murepavadin for topical application is ongoing. Recently, preclinical studies on mice demonstrated the efficacy of this formulation for treating *P. aeruginosa* infection in neutropenic lung infection models.³⁵

It is clear from the discussion above that all the current treatments used in clinical settings aim to inhibit cellular viability which has been highly effective over the past decades. However, this type of mechanism imposes selective pressure that fosters the growth of MDR strains of *P. aeruginosa* which are associated with high morbidity and mortality rates. Different strategies have been employed to modulate the permeability, signalling or virulence of *P. aeruginosa* instead of targeting bacterial growth. Vaara and Vaara (1983) introduced the concept of the outer membrane disorganising sensitiser which makes the membrane more permeable to amphiphilic and lipophilic compounds.³⁶ To date, there are three sensitisers (approved anti-protozoal drug pentamidine and the polymyxin B analogues SPR206 and SPR741, (Figure 1-4) in preclinical and clinical studies which employ this concept to work as adjuvant therapy and increase the permeability of fluoroquinolones.²⁵

Furthermore, the use of efflux pump inhibitors has emerged as a potential therapeutic strategy for treatment of *P. aeruginosa* infections. A good example of this strategy is phenylalanine arginyl β -naphthylamide (PA β N) which is a well-studied efflux pump inhibitor (Figure 1-4) that not only impairs antibiotic efflux through competitive inhibition of efflux pumps but also increases the permeability of bacterial outer membranes.³³ This compound has been shown to reduce virulence and increase antibiotic susceptibility of *P. aeruginosa*.³³

The well-known macrolide antibiotic, azithromycin (Figure 1-4), is normally not included in *P. aeruginosa* treatment regimens because of the absence of bactericidal or bacteriostatic

activity against this pathogen. However, several studies have highlighted the benefit of long-term administration of this medication in CF patients.³² It has been administered in a small number of people at concentrations below those needed for growth inhibition but enough to inhibit QS-induced gene expression.³⁷ Only one clinical trial has been established to demonstrate the concept of employing azithromycin as a QS inhibitor in patients and assess its clinical efficacy in preventing or delaying the occurrence of pneumonia in ventilated patients colonised with *P. aeruginosa*. Unfortunately, the study was terminated due to financial issues (ClinicalTrials.gov identifier: NCT00610623).

1.3 *Pseudomonas aeruginosa* resistance and tolerance

P. aeruginosa displays all types of known resistance and tolerance strategies which can be categorised as intrinsic, acquired and adaptive mechanisms. A resistance mechanism is any type of mutation that eliminates the molecular target of the antibiotic or effluxes the drug outside the bacterial cell. In contrast, tolerance is usually derived through physical mechanisms that adapt bacterial populations to environmental stress by employing different strategies such as biofilm formation. This adaptive strategy supports bacterial cells to survive high antibiotic concentrations only if embedded in biofilms. However, when the biofilm is dispersed, planktonic cells will regain their susceptibility to the minimum inhibitory concentration (MIC) dose of the antibiotic which indicates that tolerance is driven by physical barriers rather than mutations in bacterial cells.

1.3.1 Intrinsic resistance

Intrinsic resistance of *P. aeruginosa* comprises all its inherent properties, including low outer membrane permeability, expression of efflux pumps and the production of antibiotic inactivating enzymes that limit the action of current antimicrobial treatments.

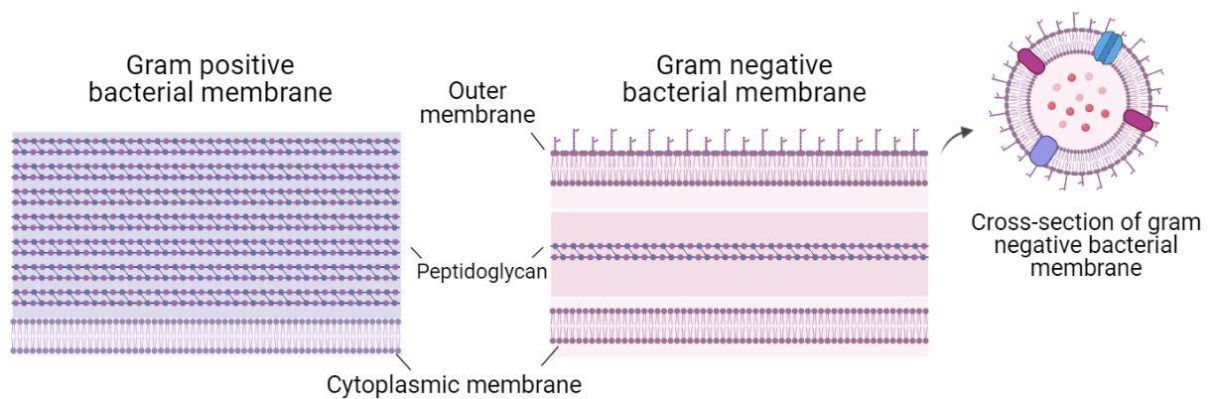


Figure 1-5: **The differences between gram positive and gram negative bacterial membranes.** The cross section illustrating the presence of porins and efflux systems across the membrane.

Decreased permeability. Being a gram-negative bacterium, *P. aeruginosa* is less susceptible to antibiotics than gram-positive bacteria. This is because the structure of a gram-negative bacterium consists of, in addition to an inner lipid membrane and peptidoglycan layer, an outer lipid membrane layer that serves as an impermeable barrier to many small molecules (Figure 1-5).³⁸ Furthermore, the outer membrane of the gram-negative bacterium contains water-filled pores that extend across the membrane and facilitate the uptake of hydrophilic compounds up to a certain size limit. The proteins that form these channels are called porins; generally, there are four classes of porins.³⁹ OprF, the predominant type which is responsible for non-specific uptake of ions and saccharides, has low efficiency for antibiotic permeation. Only 5% of this protein population is open channel which explains the low permeability of this pathogen in comparison to other bacteria. In addition, some porins allow penetration of specific types of molecule, for example, OprB for carbohydrates and OprD for basic amino acids. One of the known resistance mechanisms that could be used by *P. aeruginosa* is reduction of the expression of specific porins, such as OprD which represents the second major porin protein and the gate through which carbapenems enter the bacterium.⁴⁰ The expression of this porin is reduced in the carbapenem-resistant strain which, as mentioned earlier (1.1.1), is categorised

as one of the most critical resistant strains.⁵ The third class of porins is constituted by the ion-regulated gated porins which are responsible for uptake of ion complexes, and the fourth class consists of efflux porins (OprM) which are important components of the efflux pump system.³⁹

Expression of efflux systems. Efflux pumps, when coupled with a low-permeability cell membrane, represent a greater threat of antibiotic resistance in *P. aeruginosa* due to the synergistic effect between these two resistance strategies. Active efflux pumps are used to prevent intracellular accumulation of toxic compounds, including antibiotics. There are different families of efflux pumps, such as resistance-nodulation-division (RND), small multidrug resistance (SMR), multidrug and toxic compound extrusion (MATE) and major facilitator superfamily (MFS), in *P. aeruginosa*.⁴¹ However, the most investigated family is RND due to its key role in antibiotic resistance. *P. aeruginosa* expresses twelve RND efflux pumps, four of which can expel a range of antibiotics and contribute to antibiotic resistance. The MexAB–OprM efflux pump, for example, can expel β -lactams and quinolones, while MexCD–OprJ targets β -lactams only. Quinolones are the substrate for MexEF–OprN and aminoglycosides are expelled by MexXY–OprM. Overexpression of multiple efflux pumps in some clinical isolates of *P. aeruginosa* is the main factor contributing to the development of multidrug resistance in these strains, without affecting the ability of the pathogen to cause severe infections.⁴²

Antibiotic inactivating enzymes. Chemical modification of antibiotics catalysed by *P. aeruginosa* enzymes is one of the major intrinsic mechanisms of drug resistance. A good example of this type of resistance is the β -lactamase enzyme which mediates resistance against different types of β -lactam antibiotics such as penicillin, extended-spectrum cephalosporins, monobactams, and carbapenems. This enzyme is able to break the amide bond of the β -lactam ring, leading to inactivation of β -lactam antibiotics. One successful strategy for combating this type of resistance is combination therapy involving a β -lactam antibiotic with a β -lactamase

inhibitor, such as clavulanate, sulbactam, and tazobactam, which has been developed and applied in clinical practice.⁴³

1.3.2 Acquired resistance

Acquired resistance refers to a susceptible strain becoming resistant through either horizontal transfer of resistance genes to the next generation or mutational changes.⁴⁴ Horizontal transfer of DNA may occur *via* three main mechanisms involving conjugation, transduction and transformation (Figure 1-6).⁴⁵

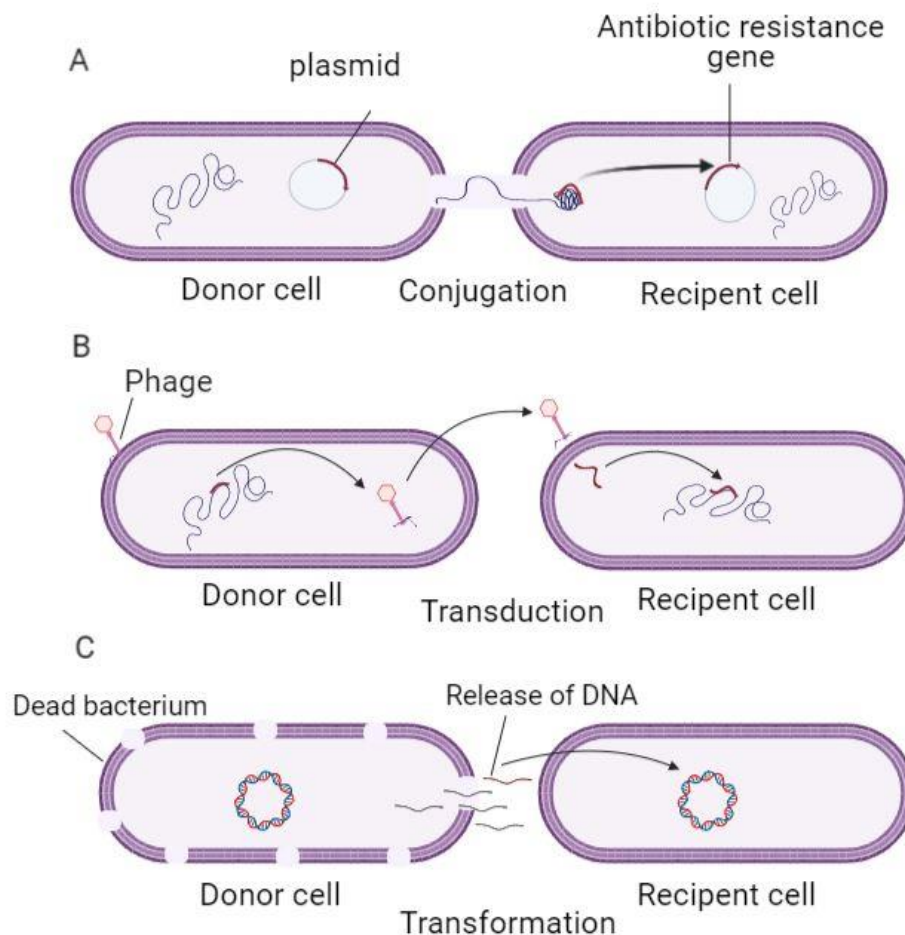


Figure 1-6: **Different mechanisms of horizontal gene transfer.** The horizontal transfer mechanisms include conjugation, transduction and transformation. a) Conjugation is a process that transfers DNA through direct physical contact between donor and recipient cells. b) Transduction is the transfer of DNA from one bacterium to another by bacteriophages. c) Transformation, bacteria take up free fragments of DNA released into the environment and incorporate it into their own genome. Source: Pang Z *et al.*⁴²

Conjugation processes occur through physical contact between the donor cell and the recipient cell, while transduction is transfer of DNA from one bacterium to another by bacteriophages. Transformation is bacterial uptake and incorporation into their own genome of free fragments of DNA of dead cells released into the environment.⁴⁵

The second strategy to acquire resistance in *P. aeruginosa* is by mutational changes which lead to reduced antibiotic uptake, modifications of the antibiotic target, overexpression of efflux pumps and production of antibiotic-inactivating enzymes.⁴² The significance of using the appropriate treatment regimen at sufficient dose is all too apparent as incomplete eradication of the pathogen leads to the acquisition of resistance through one or more of these mechanisms.

1.3.3 Adaptive resistance

In *P. aeruginosa*, the best characterised mechanisms of adaptive resistance are formation of biofilm and generation of persister cells which result in persistent infection and poor prognosis in CF patients.⁴⁶

Biofilm is a highly structured community of bacterial cells enclosed within an extracellular matrix that adheres to abiotic or biological systems. The matrix of extracellular polymeric substance (EPS) that holds the microbial cells together contains mainly polysaccharides, proteins, extracellular DNA (eDNA), and lipids, while 10% of the biofilm is represented by bacterial cells. Biofilm formation depends mainly on the genomic structure of the strain and the environmental conditions which lead to the development of different phenotypes. Biofilm development is regulated by QS systems (for more details see Section 1.5) and an intracellular second messenger molecule known as 3',5'-cyclic diguanylic acid (c-di-GMP). In fact, c-di-GMP has been implicated in numerous cellular functions, including regulation of the cell cycle, differentiation, and coordination of the 'lifestyle transition' from planktonic cells to biofilm and *vice versa*. In general, increases in the level of c-di-GMP in experimental biofilm model

systems promote biofilm formation, whereas decreased levels promote dispersion of the biofilm. The concentration of c-di-GMP is high in biofilm cells (75–110 pmol per mg of total cell extract), whereas planktonic cells contain less than 30 pmol per mg.⁴⁷ Small, non-coding regulatory sRNAs have also been shown to be involved in the regulatory network that determines the switch from the planktonic to the sessile form of growth in various bacterial species.⁴⁸ *In vitro* studies have also shown that iron serves as a signalling molecule for biofilm development and that subinhibitory concentrations of the iron chelator lactoferrin block the ability of *P. aeruginosa* biofilms to mature from thin layers of cells attached to a surface into large multicellular structures. Respiratory secretions and sputum of CF patients contain micromolar concentrations of free iron, making this micronutrient more readily available to inhaled pathogens and creating an appropriate atmosphere to build biofilm.⁴⁹

Biofilm formation is described as a multi-stage process: initially, free floating bacteria adhere to an inert or living surface; these bacteria proliferate and form microcolonies; and mature biofilms emerge from these colonies. In the mature biofilm stage, subpopulations of the bacterial community start to appear with a wide range of metabolic activity, including the periphery subpopulation which is characterised by high physiological activity, whereas the inner part consists of a physiologically less active subpopulation (called dormant cells).⁵⁰ This heterogeneity of the bacterial community leads to different degrees of efficacy of bactericidal antibiotics which depends mainly on the metabolic rate of the cells. For example, β -lactam and aminoglycosides have no activity against non-dividing cells inside the biofilm, while anaerobic conditions impair the activity of quinolones.⁵¹ Current treatment of these types of infections usually decreases the number of bacteria in biofilm but does not completely eradicate them which leads to relapse of biofilm infection.⁵² Several studies have shown the significance of early intervention in treating biofilm infections. However, the tolerance of mature biofilm infections to antibiotics has led to treatment at high concentrations, in some cases up to 1000

times higher than for planktonic cells. These doses cannot be achieved without toxicity *in vivo* by systemic administration.⁵³ This demonstrates the significance of topical administration, such as inhalation therapy, which provides the required concentration to the location of infection. In addition, combination therapy using different classes of antibacterial drugs, as well as the use of adjuvant medication that targets the biofilm formation process, increases the susceptibility of bacterial cells to the antibiotic.

Another reason for relapsed *P. aeruginosa* infections is the occurrence of persister cells. These small subpopulations of dormant cells possess high tolerance to antibiotics due to their reduced metabolism and entry into a dormant state without undergoing genetic changes. Consequently, when antibiotic treatment is terminated, these cells can resume their growth and increase the size of the population which is genetically identical to the original population and equally susceptible to antibiotics.⁵⁴ The fraction of persister cells in biofilms is usually low (1%); however, it is believed that they are responsible for the recalcitrance of chronic infections highly resistant to antibiotics. Many factors and transcriptional regulators stimulate the formation and proliferation of persister cells; these include, but are not limited to, environmental stress and nutritional deficiency as well as the QS signalling molecule *N*-(3-oxododecanoyl)-L-homoserine lactone (3-OC12-HSL) and pyocyanin (see Section 1.5).⁵⁴

1.4 Establishment of *Pseudomonas aeruginosa* infection

Another characteristic of *P. aeruginosa* is the expression and secretion of various virulence factors during the course of an infection as illustrated in Figure 1-7.⁵⁵

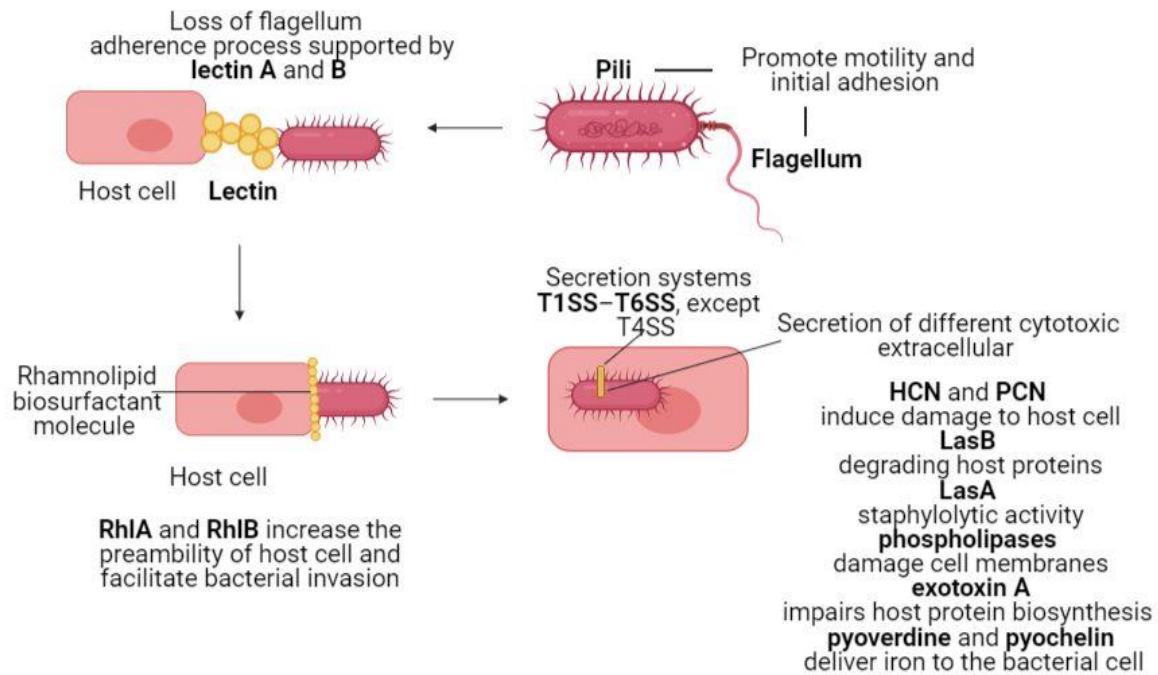


Figure 1-7: **Schematic representation of *P. aeruginosa* infection establishment process and virulence factors secretion.** HCN is hydrogen cyanide, PCN is pyocyanin, RhIA and RhIB, rhamnolipids, LasB is elastase and LasA is protease.

Pili and flagella promote adhesion to the initial infection site as well as the motility of the pathogen for dissemination of the infection.⁵⁶ The adherence process is further supported by lectin A and B which bind to specific carbohydrates on the surface of host cells.⁵⁷

The production of bacterial surfactants, especially rhamnolipids (RhIA and RhIB), increases the permeability of host epithelia, thereby facilitating bacterial invasion.⁵⁸ Rhamnolipid is a surface-active amphipathic biosurfactant molecule. In *P. aeruginosa*, it is employed to modulate swarming motility and affect biofilm architecture. On the other hand, under iron-limiting conditions, rhamnolipid is required for detaching from biofilms and promoting twitching motility.⁵⁹

Secretion systems are another strategy employed by *P. aeruginosa* to release enzymes that hydrolyse complex carbon sources into usable compounds, or to release proteins that capture essential ions such as Fe^{3+} . In *P. aeruginosa*, five of the six secretion systems (T1SS–T6SS, except T4SS which is not found in this species) are dedicated to specific secretion of exoproteins and enzymes. These systems are critical for pathogenicity and environmental adaptation of the pathogen.⁶⁰

Furthermore, secretion of different cytotoxic extracellular products like hydrogen cyanide (HCN) and the redox-active blue pigment pyocyanin (PCN) induces damage to host cells and impairs the growth of competing pathogens.^{61,62} PCN is one of the major virulence factors in this pathogen that contributes to both acute and chronic infections. It is readily recovered in large quantities from the sputum of CF patients who have *P. aeruginosa* infection.⁶¹ It increases cellular oxidative stress by elevating the intracellular levels of reactive oxygen species, especially superoxide and hydrogen peroxide, leading to subsequent cell lysis and damage.⁶³ In addition, pyocyanin contributes to biofilm formation by promoting eDNA binding (a critical element in biofilm formation) to *P. aeruginosa* cells, and consequently influences cell surface properties, physicochemical interaction between cells and aggregation.⁶³

P. aeruginosa secretes various enzymes like elastase (LasB) which is responsible for degrading host proteins,⁶⁴ proteases (LasA) for staphylolytic activity, phospholipases that damage cell membranes,⁶⁵ and exotoxin A that impairs protein biosynthesis in eukaryotic cells.⁶⁶ In addition, the pathogen employs high-affinity uptake systems or siderophores – pyoverdine and pyochelin – which bind to Fe^{3+} and deliver iron to the bacterial cell. However, the absence of freely available iron in the human body causes *P. aeruginosa* to use the iron transport proteins transferrin and lactoferrin as iron source. Therefore, these siderophores need extracellular elastase (LasB) which is responsible for the transferrin-hydrolysing activity of small peptides. This allows the pathogen to overcome iron limitation and facilitate iron acquisition from host

proteins.⁶⁷ Overall, all these virulence determinates contribute to the establishment and maintenance of the infection process.

The release of virulence factors and biofilm establishment and maturation would remain ineffective if they were carried out by a single organism. Hence, these activities need to be coordinated on a population-wide scale, and regulation behaviours mostly involve bacterial cell-to-cell communication systems which are discussed in the following section.⁶⁸

1.5 Quorum sensing networks of *Pseudomonas aeruginosa*

During the last decades, our understanding of bacterial lifestyle has changed drastically. Previously, bacteria were considered unicellular planktonic organisms, while nowadays it is more appreciated that bacterial cells are, in fact, highly communicative and can build organised communities. The generic term QS or cell-to-cell communication is the ability of bacterial cells to produce and secrete (or freely diffuse) small chemical signals called autoinducers into the surrounding environment.⁶⁹ Thus, at high population density, the accumulated signals interact with cognate receptors to set up autoinduction of autoinducer biosynthesis as well as induce transcriptional expression of various target genes, including those encoding the production of virulence factors.⁷⁰ This can modify the nature and dynamics of the pathogen, and bacterial cells act as a community to accomplish tasks that would be impossible to achieve by individual cells.⁷⁰ The first described quorum-sensing system is the *lux* system, responsible for the cell-density dependent control of bioluminescence genes by the marine bacteria *Vibrio fischeri*, and it is considered the paradigm for quorum sensing in most gram negative bacteria.⁶⁸ These bacteria did not synthesise luciferase and therefore did not produce light in the freshly inoculated culture. However, at high cell population densities, the organism produced an extracellular substance that could induce bioluminescence which was subsequently purified, and the structure was confirmed as belonging to that of the *N*-acyl-homoserine lactones (AHL) autoinducers as will be discussed below.⁷¹

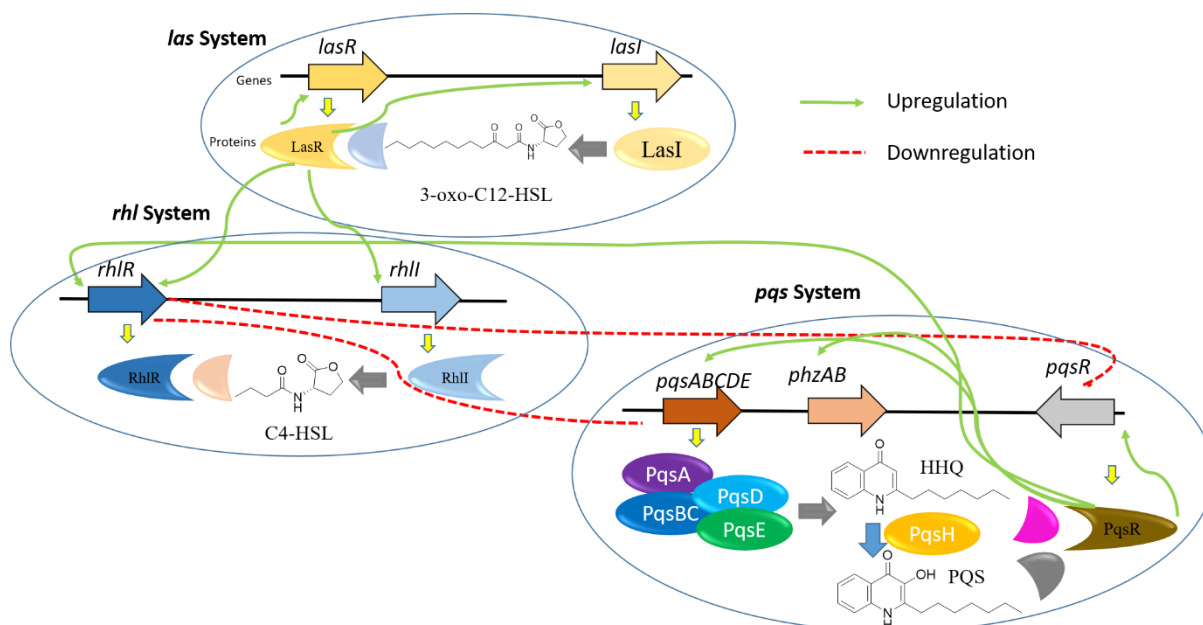


Figure 1-8: **Schematic representation of the interconnected quorum sensing systems in *Pseudomonas aeruginosa* (*las*, *rhl* and *pqs*).** Solid green arrows and dashed red lines indicate upregulation and downregulation, respectively. Oval shapes represent various proteins, chemical structures of quorum sensing signal molecules (QSSMs) are shown, and large coloured arrows represent genes. large grey arrows represent protein expression, and yellow arrows indicate QSSM biosynthesis. Source: Soukarieh *et al.*⁷²

The QS systems in *P. aeruginosa* may be considered as a hierarchical QS network which contains sets of connected systems including *las*, *rhl* and *pqs* (Figure 1-8). This network has highly adaptive mechanisms for responding to external cues of biological stress, which provides the pathogen flexibility in controlling virulence gene expression.⁷³ QS in *P. aeruginosa* may be categorised into two classes according to the chemical structure of the autoinducer: *N*-acyl-L-homoserine lactone (HSL) and alkyl quinoline (AQ) which activate *las*, *rhl* and *pqs* respectively.⁷³

1.5.1 *N*-acyl-L-homoserine lactone-dependent quorum sensing

Two QS systems, *las* and *rhl*, belong to this class as they employ two different *N*-acyl-L-homoserine lactone (AHL) signal molecules, *N*-(3-Oxododecanoyl)-L-homoserine lactone (3-oxo-C12-HSL)⁷⁴ and *N*-butanoyl-L-homoserine lactone (C4-HSL)⁷⁵, respectively. In general,

these two systems employ LuxI-type enzymes (LasI and RhlI) which generate the corresponding autoinducer (AHL). These signal molecules are accumulated in the medium, and at threshold population density, the autoinducer molecules bind to corresponding transcriptional regulator cytoplasmic LuxR-type proteins (LasR and RhlR) which function as AHL receptors. This type of protein is insoluble and its binding to the corresponding AHL stabilises the receptors, enabling dimerisation, DNA binding, and transcription of QS target genes.⁷³ It is worth mentioning that the *las* and *rhl* systems play their more significant roles during the early stages of exponential growth of *P. aeruginosa*, when the cells are more metabolically active.⁷⁶ In addition, these systems are intimately connected, and they regulate the production of multiple virulence factors, including several proteases, exotoxin A, rhamnolipids, HCN, and swarming motility, and contribute to biofilm maturation.^{77,78}

1.5.2 Alkyl quinoline-dependant quorum sensing

Another QS system in *P. aeruginosa* is *pqs* which is a distinct system that produces more than 55 different AQS, including PQS (2-heptyl-3-hydroxy-4(1*H*)-quinolone), its immediate precursor HHQ (2-heptyl-4-hydroxyquinoline) and NHQ (2-nonyl-4-hydroxyquinoline).⁶⁹ PQS and HHQ are regarded as the most prominent autoinducer molecules among AQS.⁶⁹

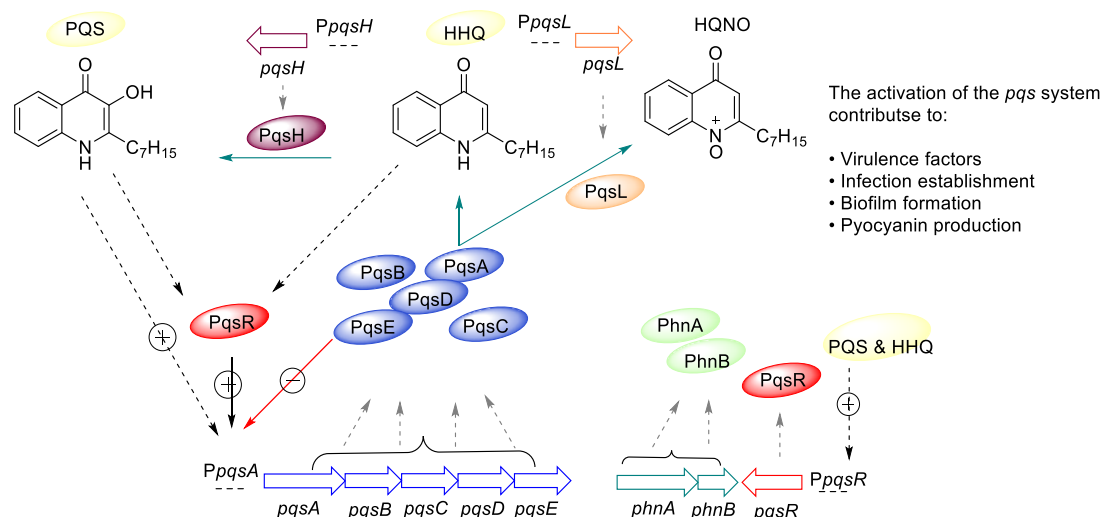


Figure 1-9: **Schematic representation of the *pqs* quorum sensing (QS) system in *Pseudomonas aeruginosa*.** The core of the *pqs* QS system is composed of the *pqsABCDE-phnAB* operon and the *pqsR* gene. Proteins coded by the *pqsABCDE-phnAB* operon synthesise HHQ; the conversion of the latter to PQS is controlled by the *pqsH* gene. Both molecules bind to PqsR, and the complex PqsR–HHQ or PqsR–PQS then activate the *PpqsA* promoter, leading to the transcription of the *pqsABCDE-phnAB* operon which in turn produces the enzymes required for the biosynthesis of HHQ which upon modification by PqsH results in the generation of PQS. The *pqsL* gene is required for biosynthesis of HQNO which does not act as a signal molecule and has no effect on its own biosynthesis. Dashed grey arrows indicate gene expression; solid green arrows represent biosynthesis; the solid black arrow indicates PqsR-dependent activation (+); dashed black arrows indicate PqsR-independent activation (+); and solid red arrows indicate negative regulation (-). Oval shapes represent various proteins and the large coloured arrows represent genes. Source: Rampioni *et al.*⁷⁹

These signal molecules (PQS and HHQ) are the autoinducers that activate PqsR, the key regulatory receptor protein in this system. Hence, HHQ or PQS interacts with PqsR to form the

PqsR–AQ complex which in turn binds to the promoter region of the *pqsABCDE* operon, known as *PpqsA*, and triggers the transcription of the genes required for AQ biosynthesis. These genes produce a range of enzymes, which contribute to the biosynthesis of HHQ as well as a range of different AQ and virulence factors.⁷⁹ The monooxygenase PqsH then catalyses the oxidization of HHQ to PQS under aerobic conditions.^{80,81} PqsL is an additional monooxygenase which together with PqsABCD synthesise 2-heptyl-4-hydroxyquinoline *N*-oxide (HQNO) and other AQ *N*-oxides (Section 1.5.3).

AQs produced by activation of this system have a variety of functions, including cell signalling, redox activity and antimicrobial activity.⁸⁰ It is worth mentioning that mutations in the biosynthetic genes *pqsA*, *pqsB*, *pqsC*, or *pqsD* or in the regulatory gene *pqsR* prevent AQ production. However, the mutation in *pqsH* or *pqsL* leads to accumulation of HHQ and HQNO or HHQ and PQS, respectively.^{80,81,82} On the other hand, the mutation in *pqsE* does not affect AQ biosynthesis, which may be due to an alternative thioesterase that replaces the functionality of PqsE thioesterase.⁷⁹

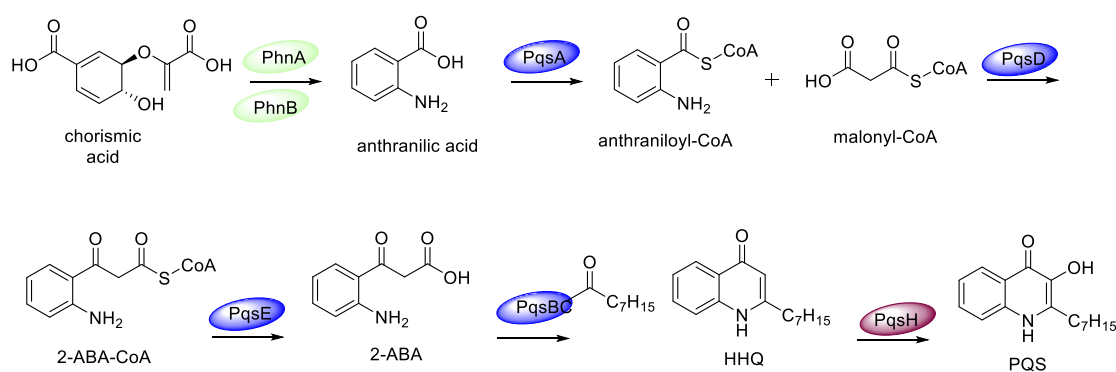


Figure 1-10: Schematic representation of alkyl quinolone biosynthesis. The biosynthesis starts from chorismic acid, the product of the shikimate pathway, converting to anthranilic acid which is activated by PqsA. Different steps mediated *via* PqsBC, PqsD, and PqsE generate HHQ which is converted to PQS *via* PqsH. Oval shapes represent enzymes. Source: Soukarieh *et al.*⁷²

The biosynthesis of HHQ (Figure 1-10) starts with the cellular metabolite, anthranilic acid, which is activated by coenzyme A ligase PqsA to anthraniloyl-CoA. This is followed by PqsD catalysing a Claisen-type condensation reaction using anthraniloyl-CoA and malonyl-CoA to yield 2-aminobenzoylacetyl-CoA (2-ABA-CoA). The thioester of 2-ABA-CoA is cleaved by PqsE thioesterase to obtain the free carboxylic acid 2-aminobenzoylacetate (2-ABA). Then, the heterodimer PqsBC, a β -keto acyl synthase III enzyme, catalyses the condensation of 2-ABA and octanoyl-CoA to form HHQ, which is subsequently oxidised to PQS.⁸⁰

1.5.3 Key effectors of the *pqs* QS system in virulence

PqsE enzyme. Although PqsE seems superfluous for AQ biosynthesis, it emerges as a major effector of the *pqs* QS system as it controls the full expression of virulence biosynthetic genes like pyocyanin, hydrogen cyanide and rhamnolipids, in addition to the transcription of genes involved in biofilm development and resistance-nodulation-cell division (RND) efflux pump coding which are involved in antibiotic resistance.⁸³ Knock-out complementation studies have clearly demonstrated that PqsE can activate PQS-controlled genes in the absence of a functional *pqs* system.^{84,85} Similar experiments have confirmed these findings in different *in vivo* infection models.⁸³ The regulatory function of PqsE is at least partially mediated *via* RhIR.^{84,85} Furthermore, PqsE downregulates the expression of its own operon leading to a negative regulatory loop.^{83,85} Microarray analysis showed that 12.2% of the genes upregulated by PqsE could be classified as secreted factors (toxins, enzymes, and alginate), while 7.3% belonged to adaptation and protection functional classes, highlighting the importance of PqsE in the adaptive behaviour and virulence of *P. aeruginosa*.⁷⁹ However, 29.3% of the PqsE upregulated genes are still unclassified or unknown which limits the understanding of its physiological role.⁷⁹ On the other hand, the crystal structure of PqsE has been determined and key active site

residues have been identified; however, neither the substrate nor the product of PqsE catalysis has been identified, making this target less exploited.⁸⁶

PQS molecule. It is more active than HHQ as a PqsR agonist, with EC₅₀ values of 16.4 ± 2.6 μ M and 3.8 ± 1.6 μ M for HHQ and PQS, respectively. These values were determined in a chromosomal reporter *PpqsA::lux* fusion in a *P. aeruginosa pqsAH* mutant strain.⁸⁷ This strain can neither synthesise endogenous HHQ nor convert exogenously supplied HHQ to PQS which is necessary to provide the absolute measurement of agonistic activity. Although both HHQ and PQS can function as *pqs* system signal molecules, PQS is a multifunctional molecule *via* several PqsR-dependent and PqsR-independent pathways. It regulates the expression of 182 genes; 103 genes are upregulated and 79 genes downregulated in response to exogenous PQS.⁷⁹ The majority (75%) of genes upregulated by PQS are also induced by iron starvation and contribute to iron acquisition, cytotoxicity, modulation of host immune response and biogenesis of outer-membrane vesicles (OMV).⁸⁸ Biogenesis of OMV has many implications for *P. aeruginosa* virulence, one of which relates to overcoming the problem of PQS associated with high lipophilicity and low solubility (1 mg/L) and enhancing PQS bioavailability in biological systems. These vesicles package PQS, which remains biologically active and can reinstate biosynthesis of virulence factors in PQS-deficient mutant strains.⁸⁹ In addition, the hydroxyl group in PQS is essential for iron binding and PQS–iron complex formation. However, this complex is not transported back into the cell and, therefore, does not function as a siderophore. Instead, PQS is found at high concentrations in the outer cell membrane of *P. aeruginosa* within membrane vesicles. The PQS–iron complex in the membrane seems to contribute to accumulation of iron close to the cell which facilitates the work of actual siderophores (pyoverdine and pyochelin).⁹⁰ The benefit of this mechanism is allowing the bacterium to rapidly and efficiently obtain iron without losing siderophores to the surrounding environment.⁹⁰

HQNO molecule. The *N*-oxide of HHQ does not act as a signal molecule and has no effect in promoting its own biosynthesis. However, it has a role mainly during polymicrobial infections by contributing to environmental competition.⁷⁹ An *in vitro* coculture model of polymicrobial infection showed that HQNO and the siderophore of *P. aeruginosa* protect *S. aureus* from antibiotics with mechanism of action targeting cell wall synthesis or protein synthesis.⁹¹ The proposed mechanism is that *P. aeruginosa* causes *S. aureus* to shift from respiration to fermentation growth, leading to a reduction in the latter's growth⁹² and decreased susceptibility to antibiotics.⁹¹ In addition, HQNO induce the formation of Small Colony Variants (SCV) in *S. aureus*. This SCVs constitute a slow-growing subpopulation of bacteria with distinctive phenotypic and pathogenic traits. Phenotypically, SCVs have a slow growth rate, atypical colony morphology and unusual biochemical characteristics, making them a challenge for clinical microbiologists to identify. Clinically, SCVs are better able to persist in mammalian cells and are less susceptible to antibiotics than their wild type strain and can cause latent or recurrent infections.⁹³ On the other hand, HQNO possesses innate antimicrobial activity against *S. aureus* due to its ability to bind and inhibit the activity of cytochrome *b*.^{94,95} Currently, the role played by HQNO in *P. aeruginosa* physiology and the mechanism by which HQNO self-poisoning is avoided have not been determined.⁷⁹

1.6 Targeting quorum sensing as a novel strategy for treatment of *Pseudomonas aeruginosa* infections

The current treatment for *P. aeruginosa* infection targets bacterial viability (it is bactericidal) or bacterial replication (it is bacteriostatic); this promotes the spread of resistant bacterial strains.⁹⁶ On the other hand, the development of anti-virulence drugs which prevent the expression of highly virulent phenotypes without affecting bacterial viability is an attractive and innovative strategy to control bacterial resistance. In contrast to conventional antibiotics, this strategy does not exert selective pressure on bacterial populations and, therefore, it is assumed to be less susceptible to rapid development and spread of resistance.⁹⁷ However, this claim is still controversial in the scientific community and has to be proved or contradicted in future studies.⁹⁸

Most anti-virulence strategies for *P. aeruginosa* target either virulence traits (protein secretion and biofilm formation) or master virulence regulators (c-di-GMP and QS). T3SS secretion system in *P. aeruginosa* is critical for delivery of toxins into host cells. This system is well conserved among pathogens, broadening the application of T3SS inhibitors to multiple pathogens and polymicrobial infections. Another strategy employing biofilm inhibitors, which target carbohydrate-binding lectins, has shown good potency *in vitro* and *in vivo*, but might disrupt host lectins. On the other hand, targeting *P. aeruginosa* pili is an unsuitable strategy because they are not well conserved in all isolates. Global biofilm regulators, such as intracellular cyclic-di-GMP and intercellular QS signalling systems, are appealing as attractive anti-virulence targets.⁶⁰

QS systems in *P. aeruginosa* contribute to the production of virulence factors, such as proteases, lectins, toxins, and biofilm polymers. This has spurred interest in the design of QS

inhibitors as anti-virulence drugs. Several QS inhibitors have been shown to reduce virulence and to aid the clearance of pathogens in both animal and plant infection models.⁸⁸ In addition, different mutagenesis studies of QS in *P. aeruginosa* have shown attenuated pathogenicity and restoration of the susceptibility of conventional antibiotics,⁸⁸ supporting the employment of this strategy to interfere with the production of virulence factors and attenuate bacterial pathogenicity. Several studies that successfully designed QS inhibitors proceeded to *in vivo* studies targeting different regulatory systems in *P. aeruginosa*; these are summarised in Sections 1.6.1, 1.6.2 and 1.6.3.

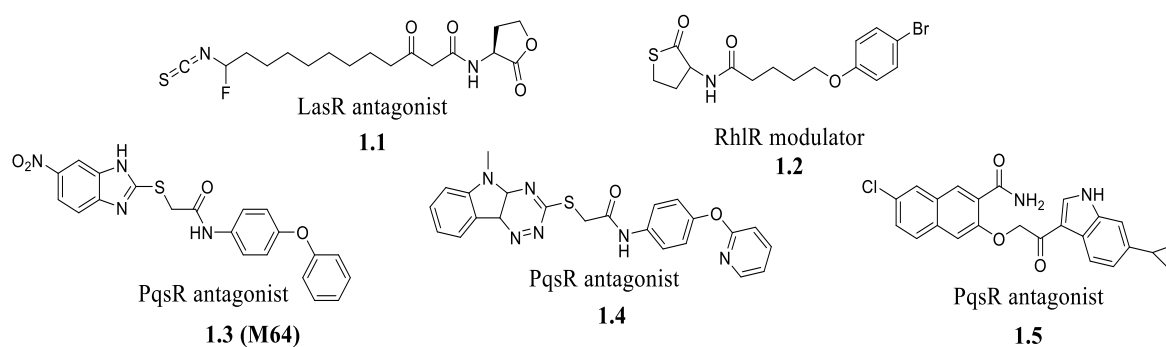


Figure 1-11: **The structures of current successful candidates targeting quorum sensing systems in *Pseudomonas aeruginosa*.** All these candidates have proceeded to *in vivo* studies (except 1.4).^{72,99}

1.6.1 Targeting the *las* system

According to Soukarieh (2018), despite the extensive efforts to target the *las* system, only one candidate, **1.1** (Figure 1-11), has proceeded to preclinical development,⁷² with covalent binding between Cys79 and the isothiocyanate electrophile, leading to inhibition of LasR activity with IC₅₀ of 69 and 154 μ M in two different strains of *P. aeruginosa*.¹⁰⁰

Although, the *las* system does not regulate pyocyanin production directly, its position in the hierarchy of QS systems affects pyocyanin production in indirect ways; therefore, production of pyocyanin in the presence of *las* inhibitors has been investigated. Pyocyanin production in

the *P. aeruginosa* PA14 wild-type strain in the presence of 100 μM of **1.1** was reduced by almost 40% relative to the control. In addition, swarming motility is another important phenotype that is regulated by QS, and it was inhibited by 44% using 20 μM of **1.1**. Moreover, the inhibitory effect was examined in two different disease models: burn wounds in *ex vivo* grown human skin samples and *in vivo* study of *Caenorhabditis elegans*. Results showed that **1.1** increased the survival rate of *C. elegans* over the course of four days and reduced PA14 infections in the burn wound model.¹⁰⁰ However, **1.1** has a lactone group considered a labile functional group and isothiocyanate as a reactive species which could be associated with metabolic issues in biological systems. Nevertheless, the knowledge gained, along with the availability of crystal structures for LasR and LasI, should facilitate future discovery and evaluation of more drug-like molecules.⁷²

1.6.2 Targeting the *rhl* system

The absence of structural information for RhlR and RhlI and the lack of validation of the *rhl* system as a therapeutic target makes the design of RhlR and RhlI inhibitors more difficult, and efforts to exploit this QS system have been limited.⁷² A study targeting this system reported that the RhlR modulator **1.2** (Figure 1-11) could act as an antagonist in the presence of C4-HSL and an agonist in its absence. However, pyocyanin production was reduced, with $\text{IC}_{50} = 8 \mu\text{M}$, biofilm formation was inhibited, and *C. elegans* survival was increased during *P. aeruginosa* PA14 infection at 50 μM ligand concentration.¹⁰¹ A subsequent study explained the effect of **1.2** as an RhlR agonist – it inhibits pyocyanin production through the downregulation of the *pqs* system.¹⁰² However, further investigation of this system is needed as it is not yet clear whether antagonising this system alone would yield a therapeutic benefit.

1.6.3 Targeting the *pqs* system

The *pqs* system could be targeted in different ways through: (i) inhibition of AQ biosynthesis by targeting PqsA, PqsD, and PqsBC enzymes; (ii) inhibition of signal reception by targeting

the PqsR regulatory protein; and (iii) inhibition of the virulence factor effector by targeting PqsE.

However, the validity of PqsBC and PqsE as anti-virulence targets remain to be validated, and only PqsA, PqsD and PqsR have been exploited in different drug discovery programmes.⁷² Despite the attempts to target PqsA and PqsD enzymes, most inhibitors suffer from weak potency or the lack of ability to reduce AQ and pyocyanin production, and as a result, no further progress has been made with these inhibitors.⁷² On the other hand, only two candidates targeted the PqsR receptor are proceeded to preclinical development.

An *in vivo* effect of the first candidate, **1.3**, or as reported in literature **M64**, (Figure 1-11), was investigated by Starkey *et al.* **1.3** binds to the PqsR co-inducer binding domain with $K_D = 5.4$ nM¹⁰³ and antagonises the receptor in two different strains, PAO1-L and PA14, with IC_{50} of 0.32 and 1.22 μ M, respectively.⁹⁹ The substantial reduction of virulence factor production at concentrations of 0.20–0.35 μ M and the impact on PA14 biofilm eradication along with tobramycin were other factors that progressed this antagonist to *in vivo* study in two burn and lung infection models. **1.3** was successful in potentiating the effect of ciprofloxacin and reduced persistence and increased post-infection survival rates in burn and lung infection models in mice.¹⁰³

A recent study introduced **1.4**, which was the result of further optimisation of **1.3**.⁹⁹ This compound showed similar activity in PAO1-L, with IC_{50} of 0.25 ± 0.12 μ M, but better activity in PA14, with IC_{50} of 0.34 ± 0.03 μ M. This candidate is one of the most potent PqsR antagonists reported and shows significant inhibition of *P. aeruginosa* pyocyanin production and *pqs* system signalling in both planktonic cultures and biofilms. However, no *in vivo* study has been established for this candidate.

An extensive structure activity relationship (SAR) study by Spero Therapeutics to optimise **1.3** led to the publication of the most potent candidate, **1.5** in the aryloxyacetoinole series, as a PqsR inhibitor. The **patented** compound is highly potent in inhibiting pyocyanin production, with a stated IC₅₀ in the range of 50–250 nM. In addition, in a murine thigh infection model using PA14, **1.5** was able to reduce PQS and HHQ levels to 50% and 40%, respectively, 12 hours after infection. To date, no further optimisation or development of these compounds has been reported. The available biological data for both candidates provide robust proof of concept for targeting PqsR for attenuating the pathogenicity of *P. aeruginosa* without affecting bacterial growth.

1.7 PqsR receptor as a transcriptional regulator in *Pseudomonas aeruginosa* QS

1.7.1 Validation of PqsR receptor as a therapeutic target in *Pseudomonas aeruginosa* infections

Most studies have focused on the *las* system because of its hierarchical position and ability to control both *rhl* and *pqs* systems. However, spontaneous *lasR* mutants of this pathogen are frequently found in chronic infections in humans questioning its validity as a therapeutic target.¹⁰⁴ In parallel, some studies have shifted the focus towards the *rhl* system which shows a contrasting virulence modulatory effect as mentioned above (Section 1.6.2). The agonist of this system reduces pyocyanin but induces rhamnolipid production, while antagonists have the opposite effect.¹⁰⁵ These findings have made LasR and RhlR less attractive as anti-virulence targets than originally anticipated.

The fact that AQs have been found in sputum, plasma and urine of chronic CF patients infected with *P. aeruginosa* and that their levels correlated with negative prognosis suggest a key role of the *pqs* system in infection. Furthermore, it suggests that AQs could be used as a potential biomarker for the severity of infection,¹⁰⁶ These findings make exploitation of the *pqs* system as an anti-virulence target promising. The PqsABSDE enzymes and the PqsR regulator are key for the biosynthesis of AQ, and hence most of them have been considered as drug targets. The question is which of these drug targets are crucial for attenuating the virulence of *P. aeruginosa* in a wide range of strains.

Among the various anti-virulence strategies, targeting key transcriptional regulator of genes involved in the production of virulence traits appears to hold great promise for future discovery and development of anti-virulence treatments.¹⁰⁷

According to current knowledge, PqsR is a target that controls an array of virulence mechanisms at once, and focusing on this receptor instead of addressing just single factors seems an efficient strategy to reduce pathogenicity.¹⁰⁸

A study established by Xiao *et al.* analysed the survival rate of four groups of thermally injured mice infected with wild-type PA14, *pqsR*, *pqsA* or *pqsH* mutant strains. The result shows that the *pqsH* strain displays wild-type virulence in mice, which indicates fully functional PqsR. In contrast, both *pqsR* and *pqsA* exhibit attenuated virulence strains and a high survival rate of the mouse groups infected with these strains due to reduced AQ production in the *in vivo* model.¹⁰⁹

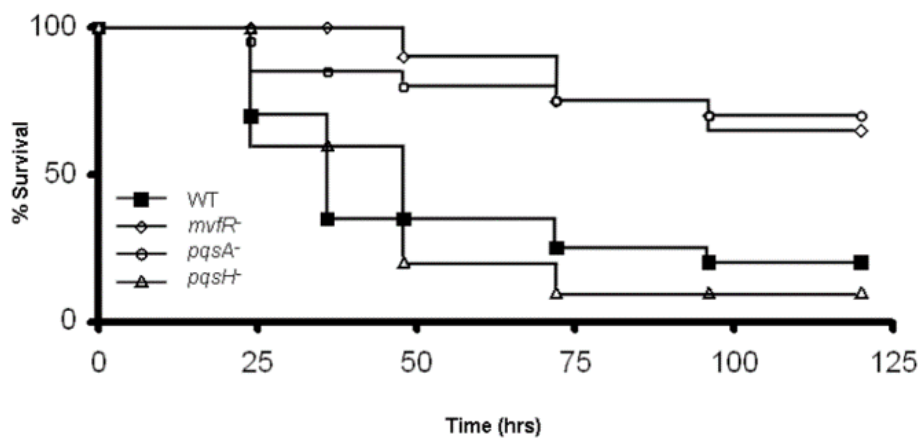


Figure 1-12: **Thermally injured mouse model.**¹⁰⁹ Mice were infected with PA14, (*mvfR*⁻) *pqsR*, *pqsA*⁻ or *pqsH*⁻ mutant strains. The mutant strains are isogenic with PA14. Fifteen mice were used for each experiment. Each experiment was performed twice. Source: Xiao *et al* ¹⁰⁹

Other studies have also shown that this reduction is not only because of the deficiency in AQ production but also due to the loss of *pqsE*¹⁰⁸ and *phnAB* expression,^{81,110} providing further evidence for the significance of this receptor as a therapeutic target for *P. aeruginosa* infections.

Furthermore, the targeting of this receptor with an antagonist in different *in vivo* disease models^{103,111} has provided robust proof of the significance of focusing on PqsR as a therapeutic target.

Starkey *et al.* demonstrate two *in vivo* murine models of acute infection; thermal injury and lung infection. **1.3** exhibits significant *in vivo* therapeutic efficacy against both mammalian infections with an increase in survival rate as shown in Figure 1-13.

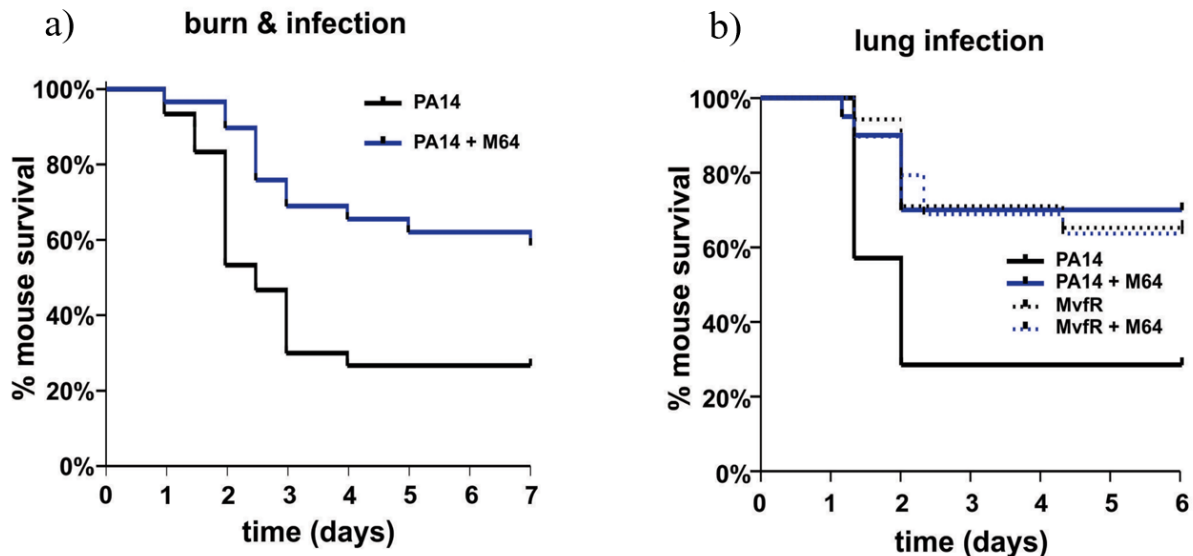


Figure 1-13: **Thermal injured and lung infection mice models.** a) Survival rate of burn and infection mice model following PA14 infection, minus (black, n= 30), and plus (blue, n= 36), **1.3 (M64)** (4 mg/kg). **1.3** was administered by intravenous injection 6 h post-burn and infection, and then twice a day for 6 days post-infection. b) Survival rate of lung infection mice model following PA14 infection, minus (solid black line, n≥10), and plus (solid blue line, n≥10) **1.3** (4 mg/kg); and infection with PqsR⁻ (MvfR⁻), minus (dot black line, n≥10), and plus (dot blue line, n≥10) **1.3** (12 mg/kg). **1.3** was administered by intravenous injection at 2, 4, 8, and 12 h post infection, and then twice a day up to day 4. Differences between PA14 and PA14 + **1.3** (p,0.05) or between MvfR⁻ and + **1.3** (p,0.05) are statistically significant, while differences between MvfR⁻ and MvfR⁻ + **1.3** (p,0.05) or between PA14 + **1.3** and MvfR⁻ + **1.3** (p,0.05) are not statistically significant (Kaplan-Meier method). PqsR⁻ or MvfR⁻ referred to PqsR mutant strain of PA14. Source: Starkey *et al.*¹⁰³

The evidence mentioned above, provide the basis for selecting PqsR as a promising therapeutic target that decreases the pathogenicity of *P. aeruginosa* and improves the efficiency of current antibacterial treatment in resistant strains.

1.7.2 Molecular insight of PqsR receptor.

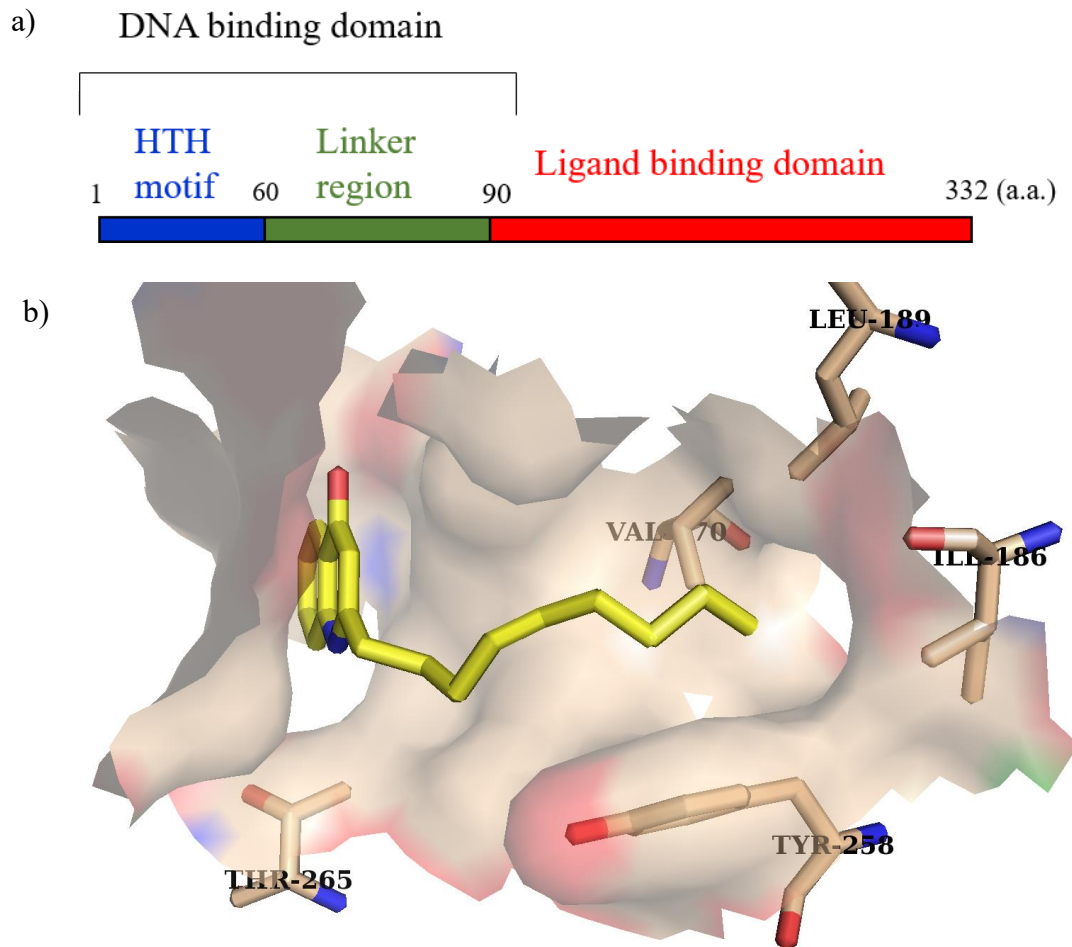


Figure 1-14: **Schematic representation of the PqsR ligand-binding domain.** a) Representative diagram of PqsR domains.¹¹² b) crystal structure of PqsR^{CBD} complexed with PqsR agonist (NHQ; PDB code 4JVD).⁸⁷

PqsR (also known as MvfR) belongs to the LysR-type transcriptional regulator (LTTR) receptor family, which consists of an N-terminal helix-turn-helix (HTH), DNA-binding domain (PqsR^{DBD}). Additionally, LTTR contains a C-terminal that encodes a ligand-binding domain (LBD) known as the co-inducer binding domain (CBD) (PqsR^{CBD}) (Figure 1-14a). PqsR^{CBD} recognises and responds to their cognate autoinducer to mediate their respective regulatory activity.¹¹³ Generally, LTTRs, which are approximately 300 amino acids in length, form homodimeric complexes that bind to specific DNA regions close to the regulated gene. Two

dimers form a tetrameric complex that leads to the bending of the DNA strand. The binding of autoinducer molecules results in an alteration to this bending that facilitates the interaction of RNA polymerase with the promoter region, thereby leading to enhanced transcription of the target genes.¹¹⁴ It is worth to mention, this working model has been proven for similar LTTRs but not specifically for PqsR. However, PqsR exhibits several characteristic features indicating that it works in a similar fashion; for example, specific DNA binding¹¹⁰, enhanced expression of *pqsABCDE* and *phnAB* operons in the presence of autoinducer molecules^{115,109}, and its CBD crystallising as a homodimeric complex.⁸⁷

To our knowledge, no existing work has described the crystal structure for the full length of the PqsR protein. However, the CBD of PqsR (PqsR^{CBD}) has previously been described. Ilangoan *et al.* reported the first crystal structure of PqsR^{CBD} (Figure 1-14b), which showed that the domain is generally hydrophobic and consists of two subdomains (pockets A and B) connected by an antiparallel β -sheet hinge region that provides flexibility to the protein and enables the two domains to rotate relative to each other.⁸⁷ The analysis of the natural substrate (NHQ; PDB code 4JVD) orientation and binding interactions to the binding domain was obtained via a crystal soaking experiment. The results of this experiment showed that the quinolone ring accommodates pocket A, whilst pocket B is accommodated by an aliphatic chain supported by hydrophobic interactions with Tyr²⁵⁸, Leu¹⁸⁹, Ile¹⁸⁶, and Val¹⁷⁰.^{87,116} One special feature about this binding is that all interactions are hydrophobic, with no hydrogen bonding or electrostatic interactions with the oxygen or amino group in the quinolin-4(1*H*)-one ring.⁸⁷

1.8 The design of an anti-virulence development project

Drug discovery is the process through which potential new therapeutic entities are identified by using a combination of computational, experimental, and clinical models. Despite advances in biotechnology and the understanding of biological systems, drug discovery is still a lengthy, costly, and difficult process with a high attrition rate of novel therapeutic discoveries. Drug design is the inventive process of finding new medications based on the knowledge of a biological target and involves the design of molecules that are complementary in shape and charge to the molecular target. In general, drug discovery projects can be initiated by two approaches to identify a novel molecule; a structure-based which relies on the knowledge of the three-dimensional structure of the biomolecular target and a ligand-based which is relies on knowledge of other molecules that bind to the biological target of interest. A previous work by Fadi Soukariéh had undertaken a virtual screen of University of Nottingham Managed Chemical Compound Collection (MCCC), with the PqsR ligand binding domain (LBD) crystal structure (PDB: 4JVI) reported by Ilangovan *et al*⁸⁷ and had identified the following hits with diverse chemical structures (Figure 1-15).

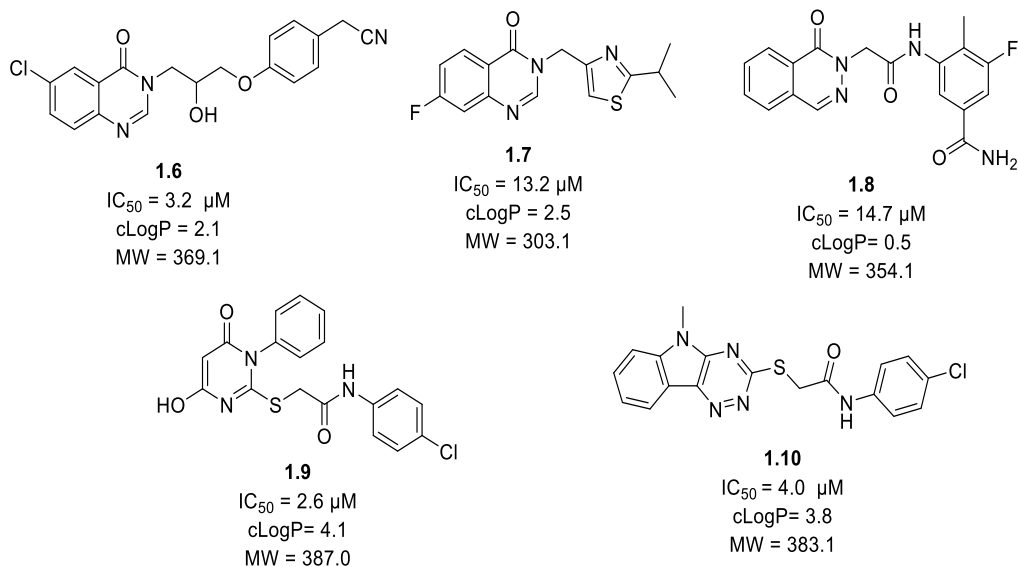
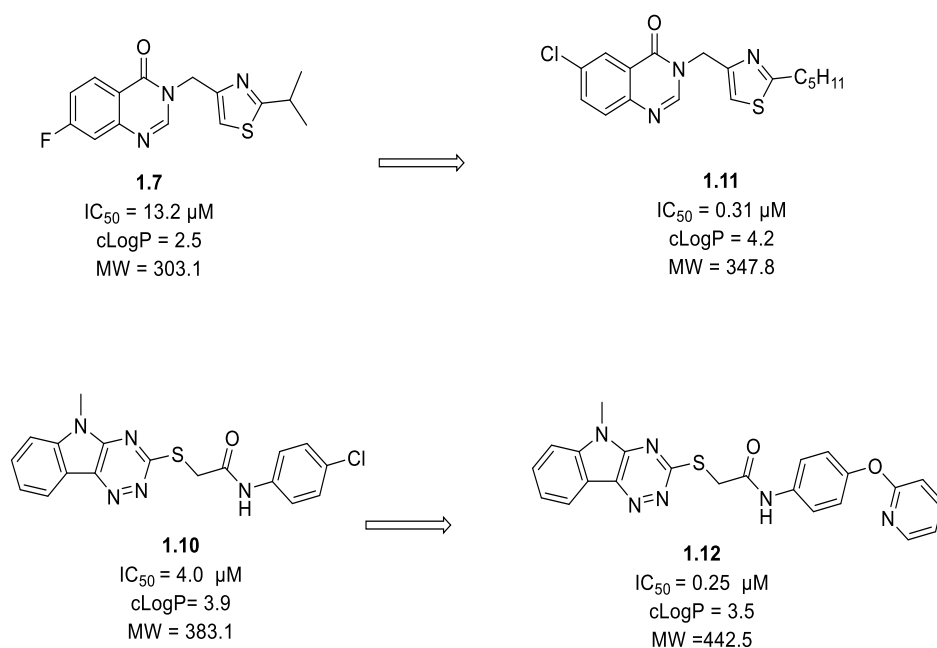


Figure 1-15: **The result of *in silico* virtual screening of MCCC library to identify PqsR inhibitors.** Chemical structures of the five hits that showed inhibition of PqsR activity employing PAO1-L CTX::P_{pqsA}-lux strain. Source: Fadi Soukarieh *et al.*⁹⁹

Grossman *et al.* and Soukarieh *et al.* employed **1.7** and **1.10**, respectively, as hit in two independent studies which provide the field with potent candidates in the sub-micromolar range as shown below.^{99,117}



Compound **1.6** was selected as a hit in this work, as it shows reasonable balance between good activity and low lipophilicity. In addition, the chemical structure of **1.6** is simple and novel with scope for a rapid med chem exploration.

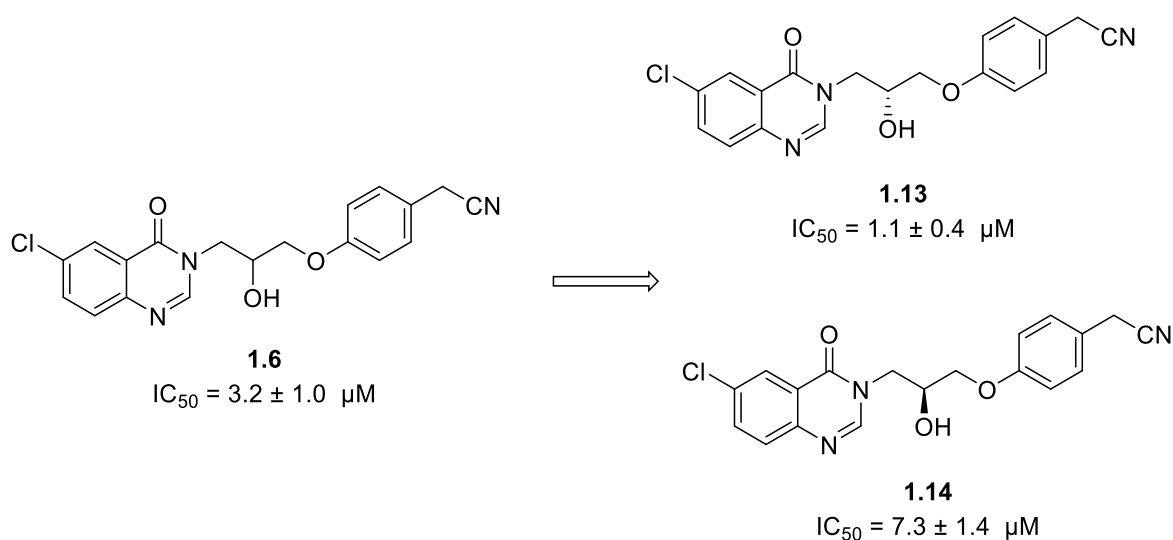


Figure 1-16: The analysis of the biological activity of **1.6** enantiomers in PAO1-L CTX::P_{pgsA}-lux strain. Source: Fadi Soukarieh *et al*, in press.

Further analysis of both enantiomers of **1.6** was established by Soukarieh demonstrating that, the *R* isomer, **1.13** is the more active isomer, ($IC_{50} = 1.1 \pm 0.4 \mu\text{M}$), while the *S* isomer, **1.14** was 7-fold less active (IC_{50} of $7.3 \pm 1.4 \mu\text{M}$) (Figure 1-16).

A SAR study was established for quinazolin-4(3*H*)-one series (chapter 2) which were affected to some extent by the structural features discussed in Section 1.8.1. A hit to lead stage was presented in (Chapter 3) and several candidates were identified with good potency and physicochemical proprieties. In the lead optimization stage, different secondary pharmacological assays as well as cytotoxicity studies were performed to evaluate the selected candidate before proceeding to *in vivo* study. The type of biological assay employed in the literature are discussed below (Section 1.8.2) to provide a general view of the design of the biological work presented in this thesis.

1.8.1 Physicochemical properties of antibacterial compounds

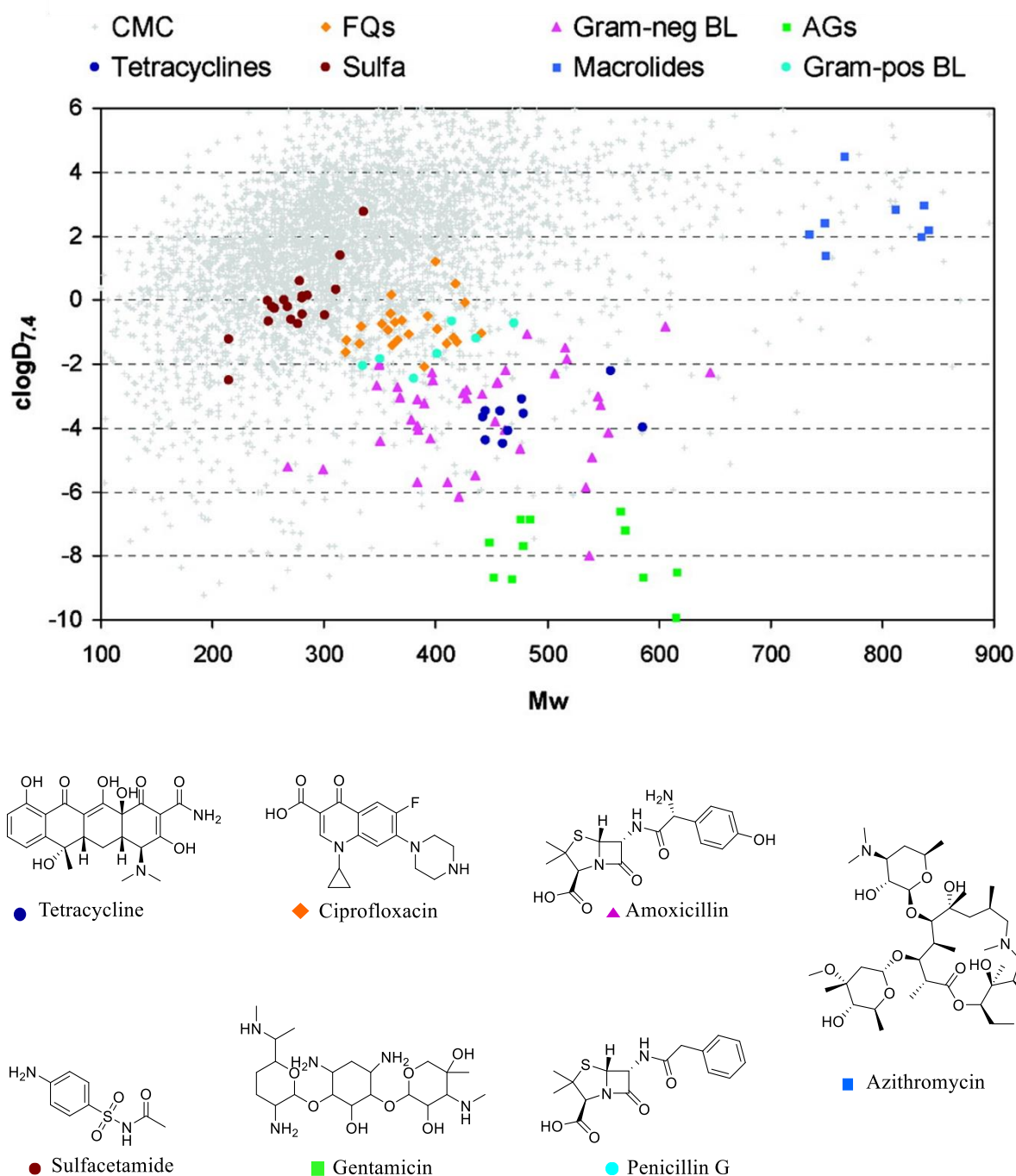


Figure 1-17: Two-dimensional representation of physicochemical properties ($\text{clogD}_{7.4}$ and MW) of a comprehensive medicinal chemistry (CMC) dataset (grey) and major classes of antibacterial drugs (colour). Abbreviations: FQs = fluoroquinolones; Gram-neg BL = gram negative β -lactams; AGs = aminoglycosides; Gram-pos BL = gram positive β -lactams. Source: O'Shea and Moser.¹¹⁸ Structure examples of each class of antibiotic are presented here.

Consideration of the molecular properties of the hit from the early stages of the drug discovery project is more likely to yield a successful candidate with a good pharmacokinetic profile.¹¹⁹ Over the past two decades, the number of failures of small-molecule drug candidates due to poor pharmacokinetic profiles seems to have diminished significantly due to the guidance for the design of new compounds offered by different analyses and rules, such as the Lipinski rules, which direct hit selection to the right property space with molecular weight (MW) less than 500 and cLogP less than 5.^{120,121} However, antibacterial compounds have always been considered exceptions to these rules mainly because they are required to penetrate the pathogen membrane and frequently the human cell membrane (Figure 1-17).¹¹⁸

In general, natural antibacterial compounds tend to shift the property space towards higher polarity and MW. The best example are aminoglycosides. However, this type of antibiotic is not orally bioavailable, and its penetration of the bacterium is due to an active electron transport mechanism that facilitates the drug entry into the cytoplasm *via* a slow, energy dependent, electron transport mediated process¹²²; therefore, no conclusions can be drawn from this type of compound. On the other hand, the physicochemical properties of the synthetic fluoroquinolone antibiotics, are the best example of the desirable unique property space of antibacterial medication. They fulfil the requirements to: (1) achieve gram-negative activity by obtaining high polarity to penetrate bacterial porins and (2) be bioavailable orally by maintaining a reasonable level of lipophilicity to penetrate the lipid membrane.

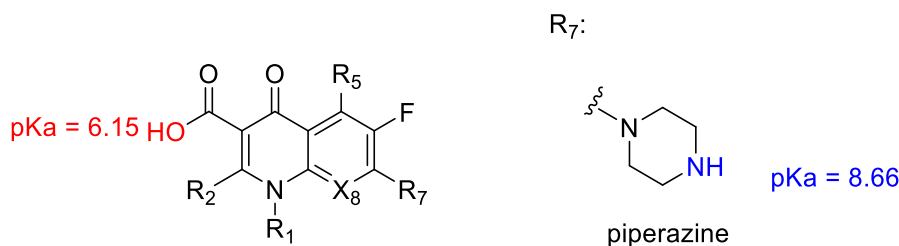


Figure 1-18: The fluoroquinolone antibiotics pharmacophore. The substitution at R₇ is the most influential point on the molecule. The five- or six-membered nitrogen heterocycle at this position has improved antibiotic

activity and pharmacokinetic profile. The most popular heterocycle employed at position 7 is piperazine, which is found in Ciprofloxacin.¹²³

The nature of most fluoroquinolones as zwitterionic compounds leads to a lower cLogD_{7.4} value with a mean of -0.8 in general and cLogP of 1.3. In addition, the pKa value is required to be close to neutral pH 7.4 in order for charged and noncharged species to coexist in the biological environment.¹¹⁸ The experimental pKa values of ciprofloxacin for example are 6.15 for carboxylic acid and 8.66 for piperazine ring which restricts the types of functionality allowed in this type of antibiotic (Figure 1-18).¹²⁴

Consideration of the possible routes of administration of novel candidates is another factor that contributes to the determination of the appropriate property space which affects to some extent the design of the structure–activity relationship study. Systemic oral dosing remains the preferred delivery method for most drug therapies and the ideal route of administration for chronic patients. However, oral bioavailability is a major hurdle in drug development as it requires properties of the compound that allow dissolution and stability in the gastrointestinal tract as well as stability against the first-pass metabolism in the liver. Therefore, it is important to consider the required ~~properties~~ ~~properties~~ of alternative routes of administration in the early stage of the study design. The pulmonary route is an ideal alternative for chronic *P. aeruginosa* lung infections in patients with CF or non-CF bronchiectasis. This route provides a high local concentration of the drug with low systemic exposure which reduces the risk of unwanted systemic adverse effects. The ideal characteristics of a compound for this type of administration are a long residence time in the lungs to increase local efficacy and rapid clearance after systemic absorption. From the perspective of medicinal chemistry, consideration of the molecular properties that contribute to increasing retention time in the lungs is important to guide the design of the study. A previous study suggests that increasing lipophilicity and MW leads to increased retention time in the lungs.¹²⁵ In addition, a review summarised different

efforts to determine the factors required for lung accumulation of different pharmacological classes. Although the investigated drugs, species and experimental models varied, lung accumulation was particularly significant for basic amines with pKa values greater than 8. Most basic amines are amphiphilic, with a large lipophilic group and a hydrophilic group that is ionised at physiological pH 7.4.¹²⁶ *P. aeruginosa* infections start usually in the smaller airways, the bronchioles, and move into the larger airways. Therefore, the optimal deposition for inhaled antimicrobial therapy would be a uniform distribution on the conducting airways.¹²⁷ However, many factors, such as particle size, pharmaceutical formulation, the severity of the disease and the breathing pattern of the patient, affect the extent and site of drug distribution.

1.8.2 Biological evaluation of novel quorum sensing inhibitors

An overview of current biological assays employed in the literature to evaluate a new candidate as quorum sensing (QS) inhibitors in *P. aeruginosa* is presented here (Figure 1-19).

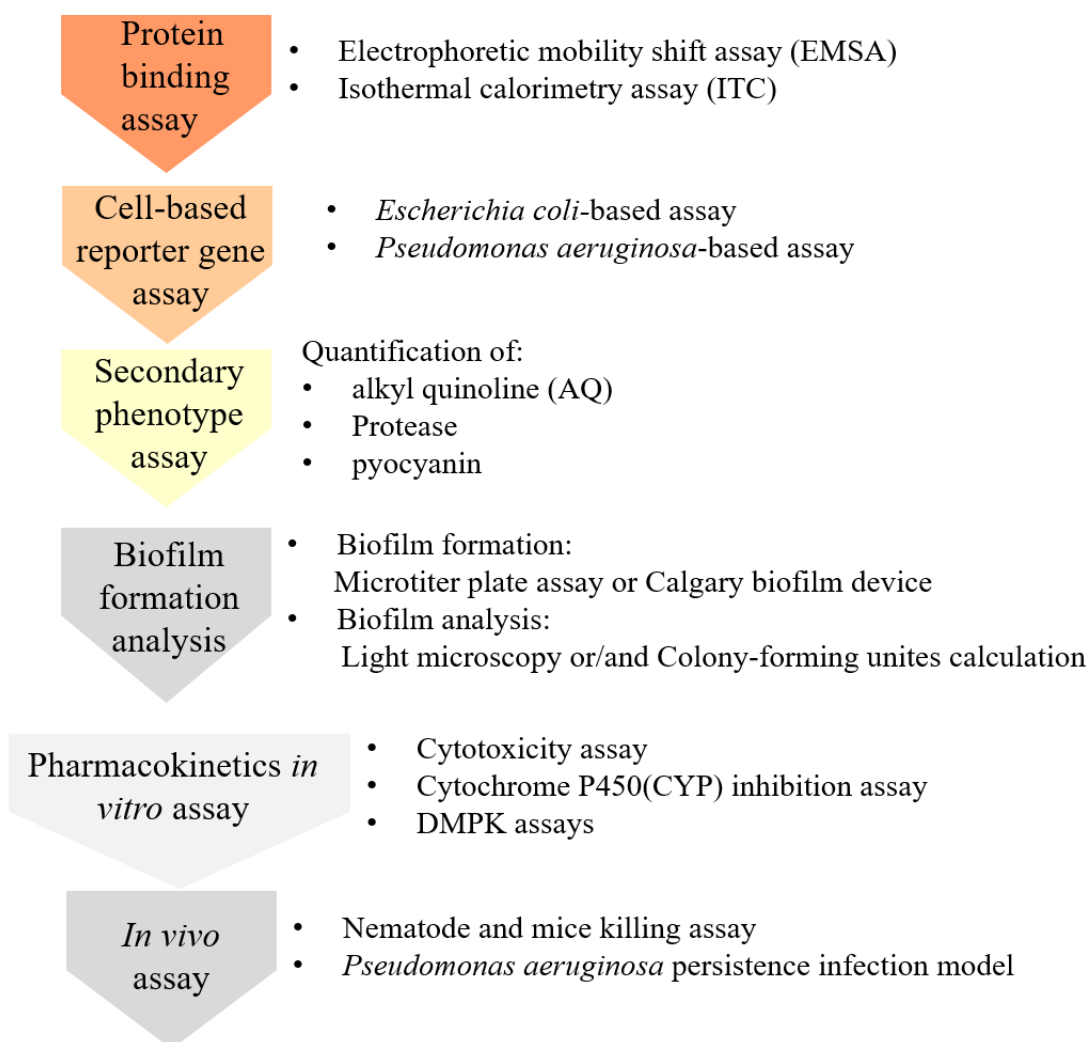


Figure 1-19: The biological assays employed in evaluation of quorum sensing (QS) inhibitors, according to the literature.^{99,103,117,128,129}

Cell-based reporter gene assays. According to the literature, cell-based reporter gene assays are routinely used to assess the activities of putative QS inhibitors in *P. aeruginosa*. In these experiments, a receptor (regulatory protein) of interest is typically expressed in a heterologous species, such as *Escherichia coli* (*E. coli*), that does not produce the corresponding QS signal molecule and carries a plasmid construct encoding a transcriptional fusion of a receptor-

regulated promoter coupled to a reporter gene. Different reporter genes, such as green fluorescent protein (GFP), β -galactosidase or luciferase could be employed in these assays in which the intensity of fluorescence emission is proportional to the level of transcriptional activation by the receptor of interest. However, the limitation of this approach is that these heterologous reporter systems may not accurately represent the cellular environment of the native host. The IC_{50} values of QS inhibitors are substantially higher in the native *P. aeruginosa* background than in *E. coli* reporters.¹³⁰ There are several reasons for this discrepancy, including lower membrane permeability and higher active efflux in *P. aeruginosa* than in *E. coli*, competition with native ligands (autoinducers) for receptor binding in *P. aeruginosa*, and differences in the levels of receptor expression between *P. aeruginosa* and *E. coli*. Therefore, two strains of *P. aeruginosa* were employed in this study to overcome these problems and exclude compounds with permeability issues.¹³¹

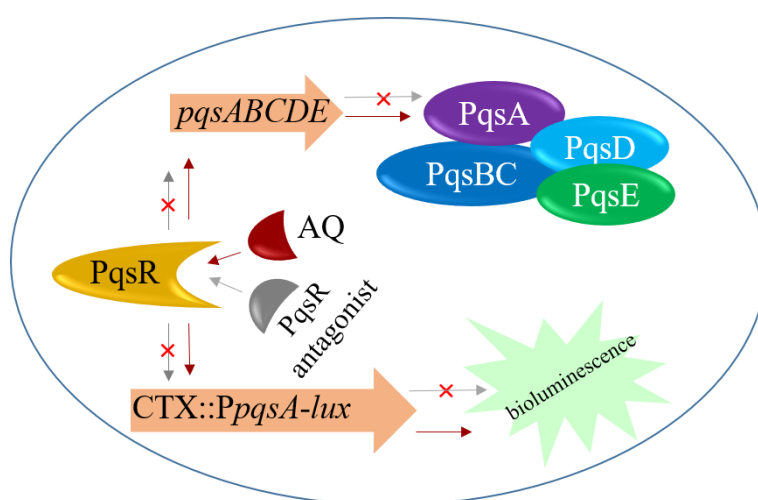


Figure 1-20: Schematic representation of the PAO1-L or PA14 bioreporter strains. The chromosomal transcriptional fusion of *PpqsA-lux* was introduced to report on PqsR activation by HHQ and PQS (AQ). These strains produce AQ signal molecules that activate *PpqsA::luxCDABE* transcription, which results in light emission in the biosensor strain. Compounds antagonising PqsR are expected to reduce bioluminescence relative to untreated samples.¹³¹ Oval shapes represent various proteins and the large orange arrows represent genes. Red small arrows for activation and grey ones for inhibition activity.

These strains, which are PAO1 or PA14 wild-type strains carrying CTX-lux vector fused in the *pqsA* promoter region, were used in a transcriptional fusion assay to evaluate the antagonistic activity of compounds presented in this work.

Since *P. aeruginosa* is not naturally bioluminescent, these strains were designed to emit bioluminescence when the PqsR transcriptionally regulated target is activated by natural ligands, especially PQS and HHQ. However, PqsR is no longer able to activate the *PpqsA* promoter upon interaction with antagonists leading to a reduced bioluminescence output for active compounds. This assay was used as a primary screening assay to determine the inhibitory potency of the highest-scoring compounds in virtual screening (Section 1.8) and the synthesised compounds demonstrated in Chapters 2 and 3. Any compound with a threshold of 10 μ M concentration that led to $\leq 50\%$ bioluminescence density suppression relative to DMSO (0.1%) control values would be classified as a hit. Concentration-response experiments were then conducted to determine the IC_{50} values for the active compound. The initial IC_{50} screen employed the PAO1-L strain, and any candidate with good activity was further analysed using the PA14 strain. This assay provides a rapid and sensitive evaluation based on the detection of bioluminescence to identify an appropriate candidate that can proceed to further biological evaluations.

Protein binding assay. A more direct approach known as electrophoretic mobility shift assay (EMSA) is employed to measure the effect of the putative QS inhibitors on the binding ability of the receptor of interest to the target DNA. In this assay, the purified protein is incubated with the test compound and a short segment of DNA containing a promoter sequence which is recognised by the receptor. The binding of the receptor to DNA is indicated by a shift in the protein band in gel electrophoresis. The advantage of this assay is that it provides a direct measurement of the activity of the compound on the protein regardless of permeability and efflux pump effects. Unfortunately, most QS receptors in *P. aeruginosa*, including PqsR, have

low solubility when isolated *in vitro* and complexed to non-native ligands, making the establishment of this type of assay challenging. On the other hand, Ilangovan *et al.* reported a purification process for the PqsR ligand binding domain (LBD) complexed to native (NHQ) and non-native ligands.⁸⁷ This process could be employed to perform another technique called isothermal calorimetry (ITC) to test whether the putative QS inhibitors directly bind to the domain and measure their affinity. ITC is a quantitative method used to directly detect the heat either released or absorbed during the receptor–ligand binding interaction. Measurement of heat transfer during binding enables accurate determination of binding constants (K_D), stoichiometry, entropy, and enthalpy of the binding reaction in solution, without the need to use reporter genes. This deeper understanding of molecular binding enables more confident decision-making in hit selection and the lead optimisation process. This technique was used to measure the affinity of **1.3** and confirm its binding to PqsR.¹⁰³ Another technique to confirm the bond-interaction with the receptor is determination of the crystal structure which provides qualitative data about the molecular interaction rather than the strength of the bond.

Secondary phenotypic assays. Inhibition of QS systems and the pathoblocker concept are strategies with no clinical proof of concept for their translation as a therapeutic approach. Therefore, secondary phenotypic assays are needed as well as analysis of biofilm formation to prove the concept before the selected candidate proceeds to *in vivo* study. The most common secondary phenotypic assay employed in the literature to evaluate PqsR antagonists is LC MS/MS detection of AQ and pyocyanin production which are robust outputs of *pqs* system activation.^{84,99,100,117}

Biofilm formation analysis. The biofilm formation process is another important virulence trait that needs to be evaluated in PqsR antagonist discovery projects. The *in vitro* biofilm assay consists of two stages: biofilm formation and biofilm analysis. The type of platform selected for biofilm formation affects to some extent the type of data that can be extracted. ~~A~~ Commonly

used assays in this regard are static microtiter plate assays or the Calgary biofilm device. These techniques are suitable for high throughput screening without the need for advanced equipment. However, in microtiter plate assays, a part of the biomass may be of cells sedimented at the bottom of the wells and subsequently embedded by extracellular polymeric substances (EPS).¹³² On the other hand, the Calgary biofilm device overcomes this limitation by assaying at the coverlid composed of pegs that fit into the wells of the microtiter plate containing the growth medium and bacteria. The biofilm formed on the pegs does not result from cell sedimentation but only from sessile development. However, the sonicated biomass does not represent the whole sessile community and the physiological properties of the detached population may not reflect the physiology of sessile cells, as different populations inside the biofilm community could exhibit different adhesive and detachment properties on the material.¹³³ Currently, biofilms grown on glass coverslips under flow conditions and light microscopy are used to evaluate established biofilms.^{117, 134}

Based on the literature, reliable methods of establishing biofilm include continuous flow-cell systems, colony biofilms, drip flow reactors and rotating disc reactors.¹³⁵ The analysis of established biofilm could be achieved by microscopy or the calculation of colony-forming units (CFUs). However, the throughput of these methods is low and they typically require an abiotic surface that produces biofilm, which is structurally very different from those seen *in vivo*.¹³²

Biofilm assays in literature. A previous study by Rahme *et al.*, examined the biofilm treatment with **1.3** which showed that **1.3** can interfere with further biofilm development but does not disrupt a preformed PA14 biofilm.¹³⁶ The formation of biofilm involved the use of a Calgary Biofilm Device in which biofilms were grown on peg lids in microtiter plates. Crystal violet staining and CFU counts were used to quantify biofilm biomass (Figure 1-21a) and viable cells (Figure 1-21b), respectively.

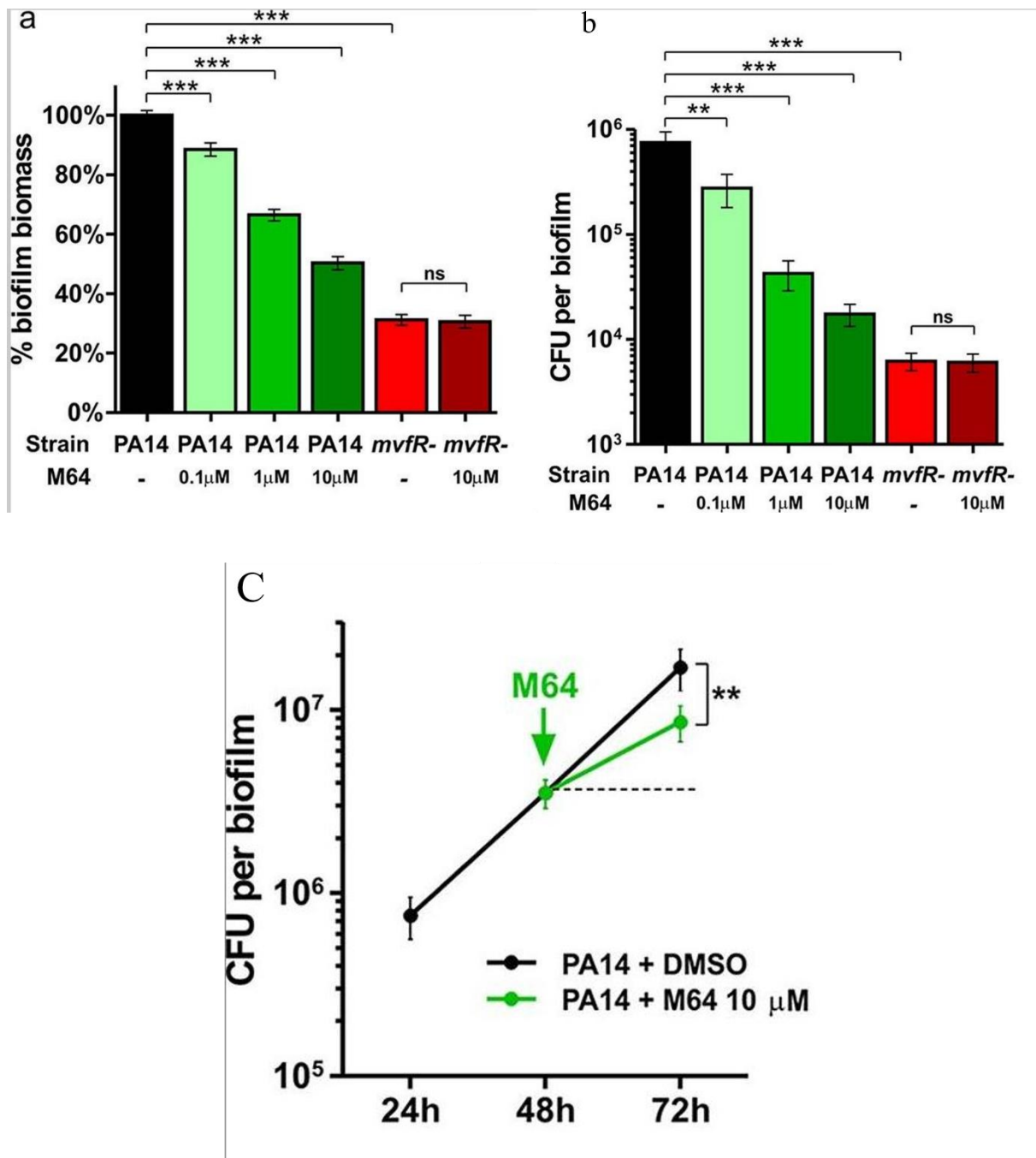


Figure 1-21: **Biofilm formation analysis in the presence or absence of 1.3 candidate.** (a) Biofilm biomass and (b) biofilm viable cells were measured by crystal violet staining or CFU counts, respectively, in the presence or absence of 0.1, 1 or 10 μM **1.3**. c) Biofilm CFUs were quantified before (24 h or 48 h) or after (72 h) treatment with 10 μM **1.3**. Data show the average +/- standard error of the mean (SEM) of at least six replicates. Statistical significance was assessed using the unpaired t-test. Source: Maura and Rahme.¹³⁶

1.3 was added at different concentrations (0.1, 1 and 10 μM) and different time points (24, 48 and 72 h). Treatment with **1.3** reduced the increase in biofilm CFUs that occurred between 48

and 72 h by 50% relative to the control. However, **1.3** did not reduce biofilm CFUs to below the pre-treatment level, indicating that **1.3** alone can interfere with further biofilm development but cannot disrupt a preformed PA14 biofilm (Figure 1-21c).

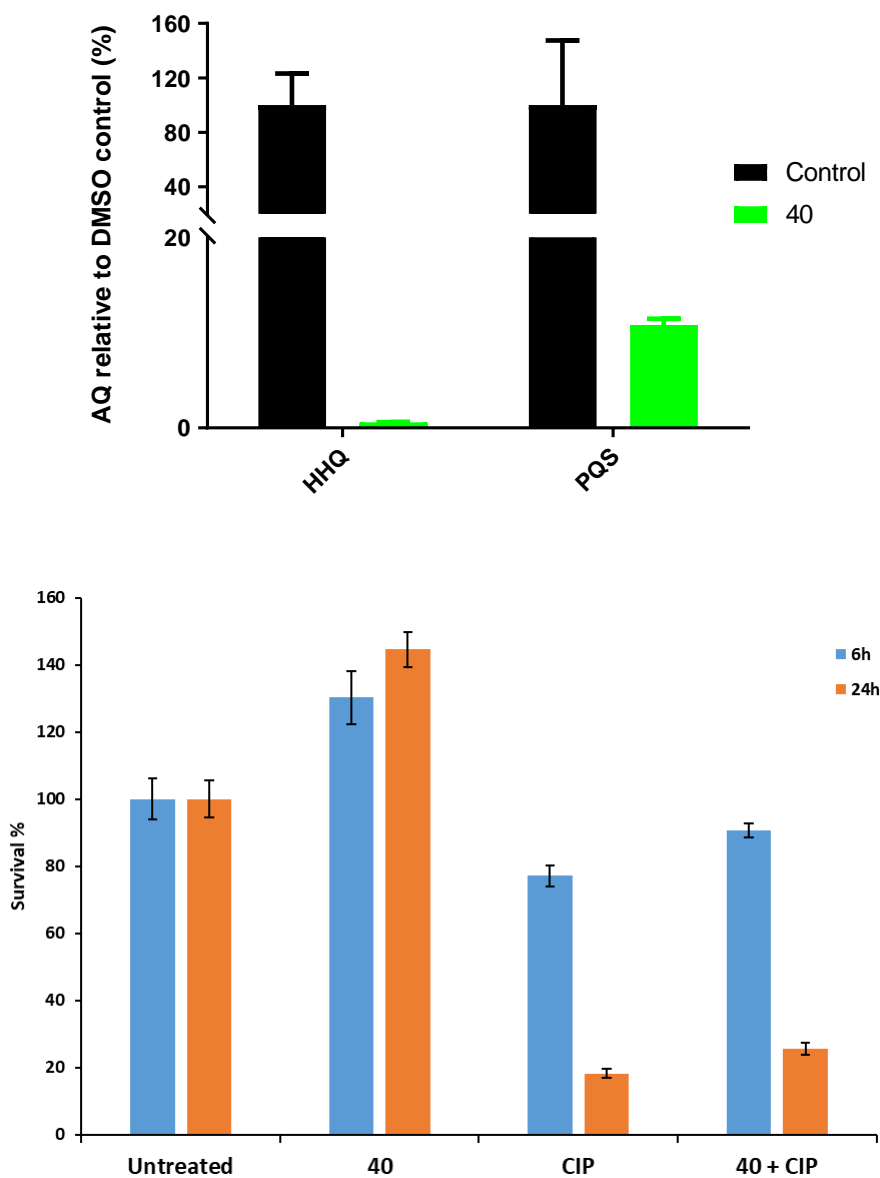


Figure 1-22: **Biofilm formation analysis in the presence or absence of 1.12 (40) candidate.** a) Quantification of AQ concentrations in PAO1-L biofilm cultures treated with **1.12** (10 μ M). Biofilms were grown in M9 minimal medium for 18 h in 24-well glass-bottom plates and supernatants were extracted for AQ analysis. b) PAO1-L biofilm viability quantified after treatment with different conditions for 6 (blue) or 24 h (orange). The concentrations of drugs used were ciprofloxacin 60 μ g/mL (CIP) and **1.12** 10 μ M. Source: Soukarieh *et al.*⁹⁹

Another study that examined the effect of PqsR antagonist on biofilm formation was conducted by Soukarieh *et al*, 2020. This study analysed the inhibitory effect of **1.12** on AQ production in biofilm cultures. The biofilm was grown on round glass coverslips under flow conditions. It was established for 48 h and incubated for a further 6 or 24 h before treatment (**1.12** 10 μ M or/and ciprofloxacin 60 μ g/mL). However, the results obtained from this experiment contradicted the hypothesis since they indicated a slight increase in the viability of samples treated with the PqsR antagonist **1.12** in comparison to the control (Figure 1-22).

The reasons of these conflicting results were not investigated; however, this raises the question of whether biofilm experiments performed in the laboratory are useful for understanding how the novel candidates can inhibit QS and interfere with biofilm formation. Therefore, there is a need to investigate this area in depth and provide the field with experiments reflecting the pathological situation in an *in vivo* system.

From a pharmacokinetic perspective, the ability of a candidate to show metabolic stability and safety in the corresponding *in vitro* assays, such as cytochrome P450 (CYP) inhibition assay, using human liver microsomes and cytotoxicity assays with cultured cells, is critical at this stage of the project before it proceeds to *in vivo* study.

1.9 Project overview and objectives

The work performed in this thesis mainly focuses on attenuating the pathogenicity and resistance of one of the most critical pathogens by designing and developing a range of novel QS inhibitors targeting the transcriptional regulator (PqsR) of the *pqs* system which is distinct to *P. aeruginosa*. Different chemical approaches are employed to synthesise a range of compounds, and the selected candidates are validated through different biological evaluations and molecular structure analysis.

Chapter 2 focuses mainly on an SAR study for the selected hit with a quinazolin-4(3*H*)-one scaffold which is similar to the natural substrate of the receptor. The chemistry to synthesise different analogues is discussed in this chapter as well as the approaches employed to enhance the physicochemical properties of the series.

In chapter 3, the work aimed to expand the SAR further by replacing the quinazolin-4(3*H*)-one moiety with different heterocyclic ring systems; it was concluded that the optimal replacement is the 1-methyl-1*H*-benzo[*d*]imidazol-2-amine ring. Many attempts were established to identify the optimal conditions to synthesise this series by employing different strategies, and the selected pathway was successful in synthesising a range of analogues with different substitutions.

Biological evaluations of the active compounds are presented in the final chapter (4) in an attempt to prove the concept and validate the target as a relevant therapeutic target. Furthermore, a cytotoxicity study of the most active compounds in the work was conducted to investigate the therapeutic-toxicity index of these compounds before proceeding to the *in vivo* study. However, it is critical to establish further pharmacokinetics *in vitro* and *in vivo* assays to evaluate the efficacy and safety of the novel candidate which are beyond the scope of this thesis.

2 Design, Synthesis and Evaluation of Novel quinazolin-4(3H)-one-based PqsR antagonists as Adjuvant Therapies to Treat *Pseudomonas aeruginosa* Infection

2.1 Background of the project

The first step of any drug discovery program aiming to develop a new drug candidate is finding a hit with which to establish a structure–activity relationship (SAR) study. Two previous studies employed a ligand-based design approach using the structures of PqsR agonists.^{87,111} The findings offer insights into the ligand–receptor interaction of PqsR and provide a promising starting point for further drug design.

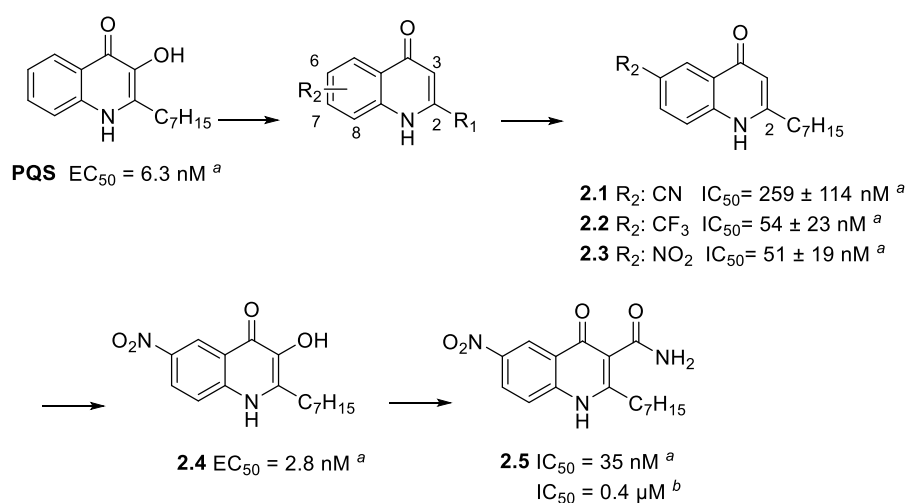


Figure 2-1: Summary of the first SAR study designed to identify a PqsR antagonist 2.5 by employing a ligand-based approach. The inhibition of PqsR activity was measured using β -galactosidase reporter gene assays based on *E. coli*^a or *P. aeruginosa*^b.

The Hartmann laboratory have been a pioneer in the design of PqsR antagonists.¹³⁷ In a pivotal study using a ligand-based drug design approach, Hartmann and co-workers outlined a general SAR for PqsR antagonism by developing structural analogues of PQS.¹¹¹ Notably, they found that an alkyl chain of at least six carbons was required for biological activity, and introducing

electron-withdrawing groups (EWGs) at the 6- position of the quinolone core resulted in strong inhibition of PqsR activity. The antagonistic effect was not only attributable to the nature of the substituents, it was also affected by the substituent position, as substitution of the 7- and 8- positions of the quinolone did not show inhibition. These trends allowed the identification of the first competitive inhibitors of PqsR, with compound **2.3** emerging as the lead compound (Figure 2.1). Compound **2.3** bound to PqsR with $K_D = 7$ nM and $IC_{50} = 51$ nM in an *E. coli* reporter assay. However, a subsequent study showed that **2.3** behaved as a mild agonist of PqsR in a reporter gene assay based on *P. aeruginosa*.¹³⁸ Hartmann and co-workers proposed that **2.3** may be a substrate for the PqsH enzyme, which hydroxylates the 3- position in the final step of PQS synthesis. A small library of compounds was prepared with different functional groups substituting the hydrogen atom in the 3- position to block the reaction site of the PqsH enzyme. Compound **2.5** with a carboxamide functional group was selected as the best candidate from that series, showing good activity in the *P. aeruginosa* reporter gene assay. This compound provided the first proof of concept that PqsR antagonists reduce the mortality caused by *P. aeruginosa* in two *in vivo* models (*Caenorhabditis elegans* and *Galleria mellonella*).¹³⁸

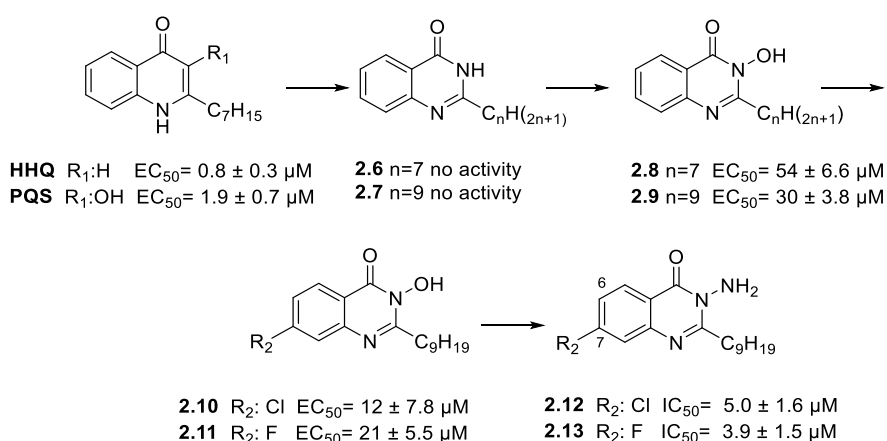


Figure 2-2: Summary of SAR study employing ligand-based approach and novel 2-alkyl-4(3H)-quinazolinone scaffold. The inhibition of PqsR activity was measured by a reporter gene assay based on *P. aeruginosa*. EC₅₀ determined in a *P. aeruginosa* *ApqsA* CTX::P_{pqsA}-lux; IC₅₀ determined in a *P. aeruginosa* CTX::P_{pqsA}-lux.

A study conducted by Williams and co-workers analysed a series of AQs and 2-alkyl-4(3*H*)-quinazolinone (QZN) analogues with either 7 or 9 carbon atoms in the aliphatic side chain.⁸⁷ The SAR study revealed that the QZN core in **2.6** and **2.7** was devoid of both agonist and antagonist activity, while hydroxylation at R₁ of both analogues led to weaker agonist activity compared to PQS (**2.8** and **2.9**). Interestingly, halogenation at the R₂ position with chlorine or fluorine improved the agonistic activity (**2.10** and **2.11**). Replacing the OH at R₁ with its isostere NH₂ resulted in good antagonistic activity, with IC₅₀ values of 5 and 3.9 μM for 7- Cl **2.12** and 7- F **2.13** analogues, respectively.

According to these two previous studies, the most important structural features for achieving antagonistic activity was the introduction of strong EWGs at the 6- position of the quinolin-4(1*H*)-one core or at the 7- position of the quinazolin-4(3*H*)-one core. In addition, these studies revealed that substitution of the 3- position has a role beyond blocking the metabolic hotspot, as it appears that converting the hydroxyl to an amino group in **2.12** and **2.13** results in antagonistic activity. These findings affect, to some extent, the design of the SAR study presented in this chapter.

2.2 Hit characterization

As discussed in Section 1.8, a virtual screening experiment was established by Soukariéh employing the crystal structure of PqsR^{LBD} followed by biological analysis of the top scoring compounds to evaluate their activity through measuring the IC₅₀s. Compound **1.6** was selected as a hit for this project and further analysis of both enantiomers demonstrated that, the *R*-isomer, **1.13** is more active enantiomer.

Subsequently, a work presented by Sou *et al.* analysed the pharmacokinetic properties of **1.13** and **2.12** using intratracheal pulmonary administration in rats model to predict their therapeutic potential and suitability as drug candidates.

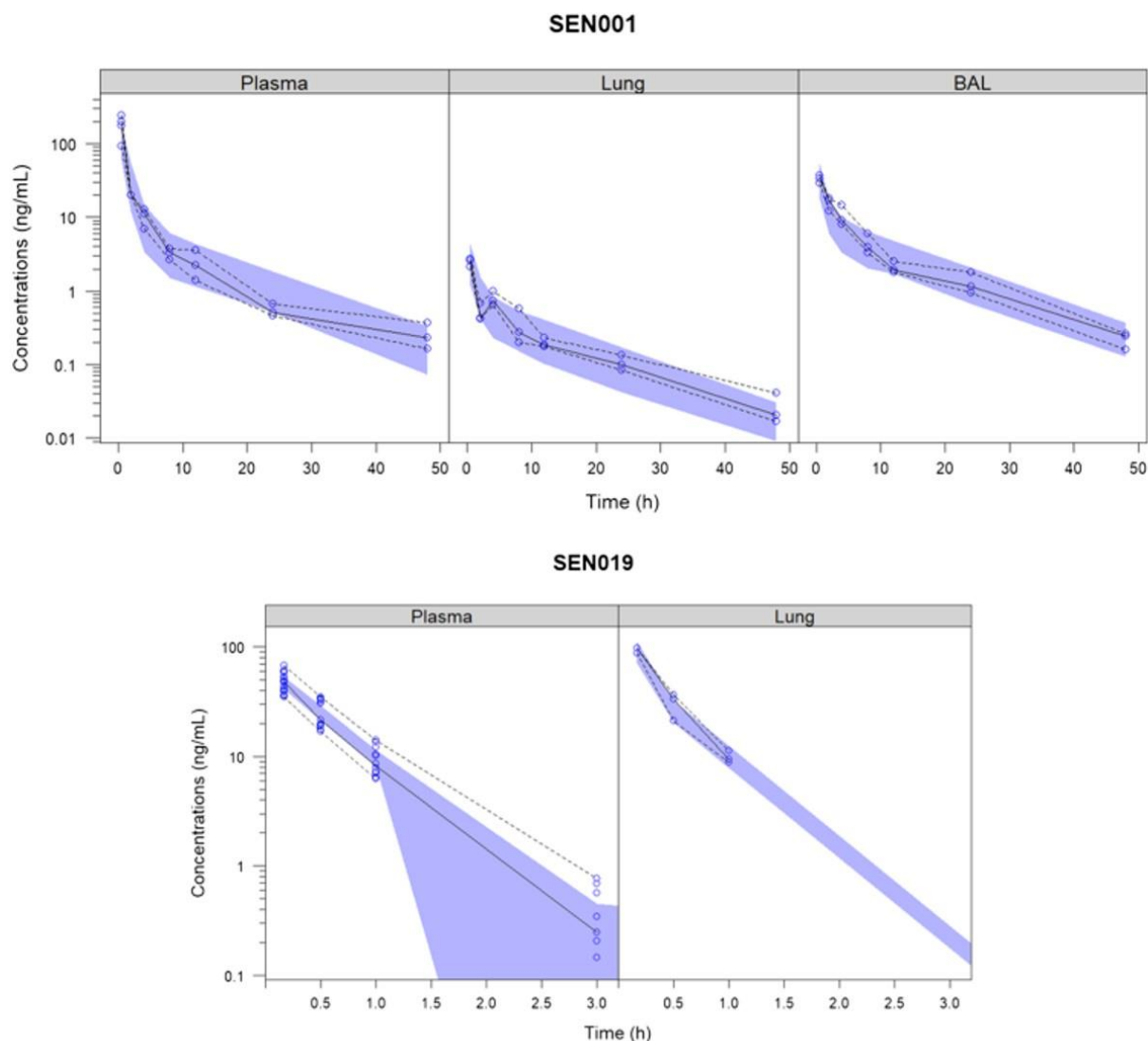


Figure 2-3: Pharmacokinetic analysis in *in vivo* model. **2.12** (SEN001) and **1.13** (SEN019) were administered into rats *via* intratracheal administration. Blood, lung, and (bronchoalveolar lavage (BAL) for **2.12** only) samples were collected at determined time points, and the concentration of both compounds were analysed by LC-MS. Source: Sou *et al.*¹³⁹

The compounds were given *via* intratracheal administration to the lungs at doses of 0.07 mg/kg and 0.12 mg/kg of body weight, respectively. The selection of doses was restricted by the aqueous solubility and availability of the tested compounds. Samples were collected from blood, lung, and (bronchoalveolar lavage for **2.12** only) at determined time points, and the samples were analysed by LC-MS. The results showed that, both compounds (**1.13** and **2.12**) were rapidly cleared from the lung to the plasma, as demonstrated by the rapid appearance of the compounds in plasma shortly after administration (Figure 2-3). However, the plasma

concentration of **2.12** declined steadily over the sampling period while the plasma concentration of **1.13** declined more rapidly and was below 1 µg/mL after 3 h.¹³⁹

Furthermore, the solubility determination showed that **1.13** and **2.12** were poorly water-soluble, 20 µg/mL and < 1 µg/mL, respectively. However, the addition of PP2% formulation improved the solubility of the compounds significantly and increased the amount of solubilized compounds to more than 180 µg/mL. This formulation is a mixture of polyethylene glycol400 (PEG400) 2% + polysorbate 80 (PS80) 2% w/w in water. Another advantage of PP2% formulation that it does not cause any detectable acute toxicity to the lungs of the animals, as shown by histological examination of the terminal lung samples. Therefore, PP2% was used to deliver solubilized drugs for IT administration in the PK studies.¹³⁹

These results highlight the importance of designing novel PqsR antagonists with enhanced water solubility and an increased residence time in the lung to enable local efficacy in combination with rapid clearance after systemic absorption to reduce the risk of adverse systemic reactions.

2.3 Rationale of the design

This study aimed to analyse the effect of slight modifications of the original structure (**1.6**) on the pharmacological activity and to explore the essential pharmacophore for antagonistic activity (Figure 2-4).

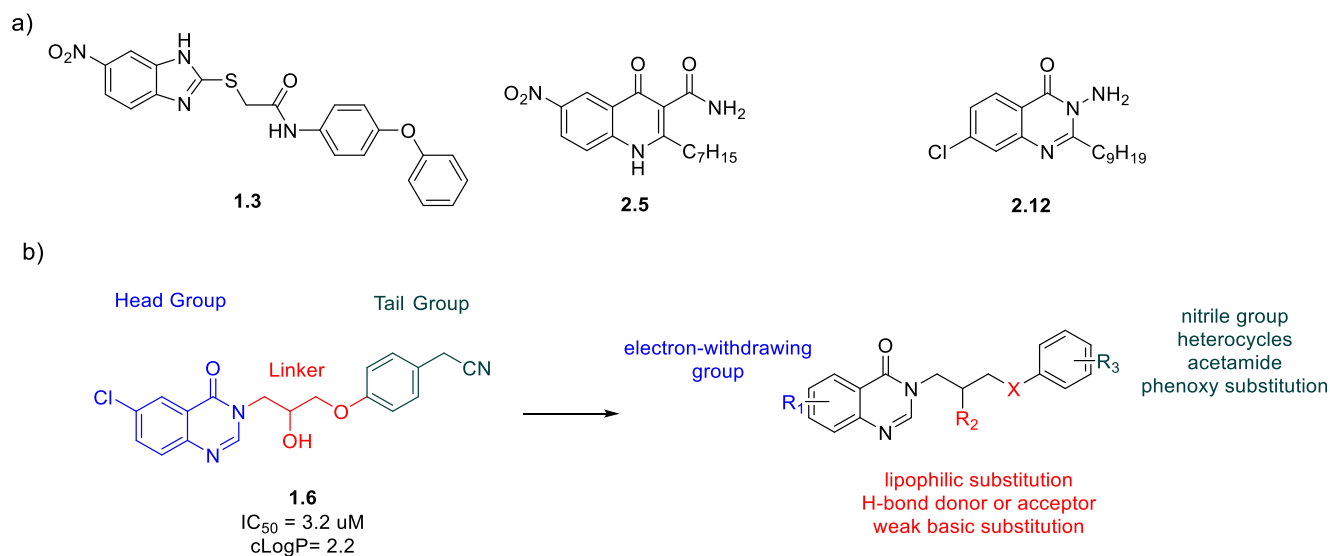


Figure 2-4: a) Chemical structures of the previously identified antagonists **1.3**, **2.5** and **2.12**. b) Chemical structure of hit compound **1.6**, the SAR study design and the investigated functional groups in this study.

The main core of **1.6** is the quinazolinone ring, which is a class of fused heterocycles that are of considerable interest owing to their diverse biological properties.¹⁴⁰ This privileged structure in drug development and discovery can be found in more than 200 naturally occurring alkaloids with a wide range of pharmacological applications including antibacterial, anti-inflammatory, antifungal and antimalarial activities.¹⁴⁰ The quinazolinone ring is stable towards oxidation, reduction and hydrolysis inspiring medicinal chemists to explore this scaffold in the search for new potential medicinal agents.¹⁴⁰ In addition, the similarity of **1.6** to the natural ligands of PqsR (quinolin-4(1*H*)-one) and to the structure of the previously identified antagonists **2.5** and **2.12** (with a quinolin-4(1*H*)-one or quinazolin-4(3*H*)-one core) together support the selection of **1.6** as an ideal hit to initiate a SAR study in an attempt to improve the potency and the

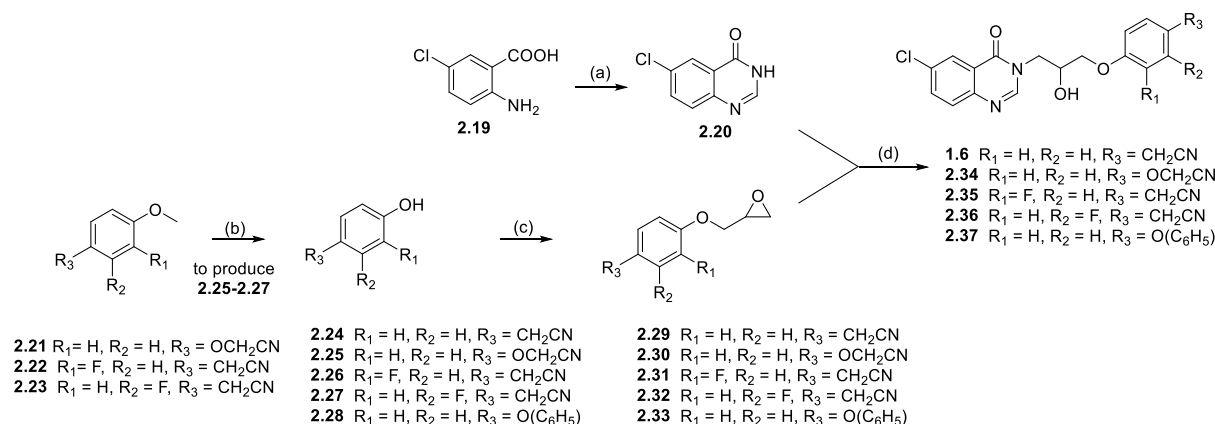
physiochemical properties of this compound. Previous studies demonstrated that the *R* isomer of **1.6 (1.13)** was poorly water-soluble and had a short retention time in the lung,¹³⁹ which guided our study design to focus on enhancing the hydrophilicity of the compound by introducing weakly basic functional groups in order for charged and noncharged species to coexist in the biological environment, as previously discussed (1.8.1).¹²⁶ Furthermore, it was shown that substitution with **electron withdrawing groups** (EWGs) on the phenyl ring of the quinazolin-4(3*H*)-one core **are** important to improve antagonistic activity; however, the position of the substitution should be carefully considered. Therefore, it is important to probe the effect of substituting different positions of the phenyl ring with different EWGs to identify the optimal substituent and position. In addition, the linker was investigated by replacing the secondary alcohol with different substituents to determine the type of interaction provided by this functional group. Importantly, the position of the nitrile functional group on the phenyl ring were also probed. Furthermore, different types of nitrile bioisosteres, as well as heterocycles, were employed to increase the overall polarity or ionization of the compound to enhance its water solubility and probe biological activity. Finally, as an inspiration from the literature, the published compound **1.3** containing a diphenyl ether functional group showed π - π stacking interactions with the side chain of Tyr²⁵⁸.^{112,103} Therefore, an attempt was made to modify the acetonitrile functional group by replacing this functional group with a phenoxy substitution at the *para* position.

2.4 Results and discussion

2.4.1 Synthesis of 2-(4-(3-(6-chloro-4-oxoquinazolin-3(4*H*)-yl)-2-hydroxypropoxy)phenyl) acetonitrile, **1.6** and its analogues

The route used to prepare **1.6** and its analogues (**2.34-2.37**) is shown in Scheme 2-1, which employed two building blocks: 4-(3*H*)-quinazolinone **2.20** and epoxides **2.29-2.33**.

Scheme 2-1: Synthesis of compounds **1.6** and its analogues (**2.34-2.37**).



Reagents and conditions: a) Formamide, 150°C, 16 h, 99%. b) BBr₃, DCM, rt, 16 h, 80%. c) (±) epichlorohydrin, Cs₂CO₃, CH₃CN, reflux, 16 h, 28%. d) Cs₂CO₃, TBAI, CH₃CN, reflux, 16 h 46%.

The 4-(3*H*)-quinazolinone **2.20** was prepared according to the method described by Vi Niementowski in 1895.¹⁴¹ The reaction was carried out by condensing different substituted 2-aminobenzoic acids with formamide to form the substituted quinazolinone cores. The yield of this reaction was very high, leading to a clean product with water as a side product.¹⁴²

The second building block required to synthesise **1.6** and **2.34-2.37** was 2-(phenoxy)methyl oxirane **2.29-2.33**, which was synthesised by employing either a two-step synthesis for some analogues or a one-step for others. The phenol as a starting material for analogues **2.25-2.27** was either commercially unavailable or very expensive and therefore anisoles **2.21-2.23** were used in the first step. The ether demethylation is synthetically challenging, as it is a stable group

and can be activated only if it is an aryl-alkyl ether by using an acid with a nucleophilic counterion, such as HBr or HI. However, using strong acids in this specific case could hydrolyse the nitrile functional group present in the starting material, converting it to carboxylic acid. An alternative approach is to use a strong Lewis acid, such as BBr_3 .¹⁴³ The oxygen atom in **2.21-2.23** will attack the empty p orbital of the boron, and the methyl attached to the resulting oxonium ion can be attacked by Br^- in an $\text{S}_{\text{N}}2$ reaction. The workup with water led to the phenols **2.25-2.27**.¹⁴³

Epoxide preparation. The epoxides were prepared by reacting a range of phenols with (\pm)-epichlorohydrin in basic conditions through an expected $\text{S}_{\text{N}}2$ reaction to produce racemic epoxides.

4-(3H)-quinazolinone alkylation. The reaction to synthesise **1.6** and **2.34-2.37** consisted of two steps and proceeded *via* an *in situ* epoxide ring-opening at the less substituted carbon atom by adding a catalytic amount of tetrabutylammonium iodide (TBAI). The second step was a substitution reaction in which the nitrogen atom at position 3 of the QZN attacked the electrophilic alkyl iodide to furnish the final product (Figure 2-5).

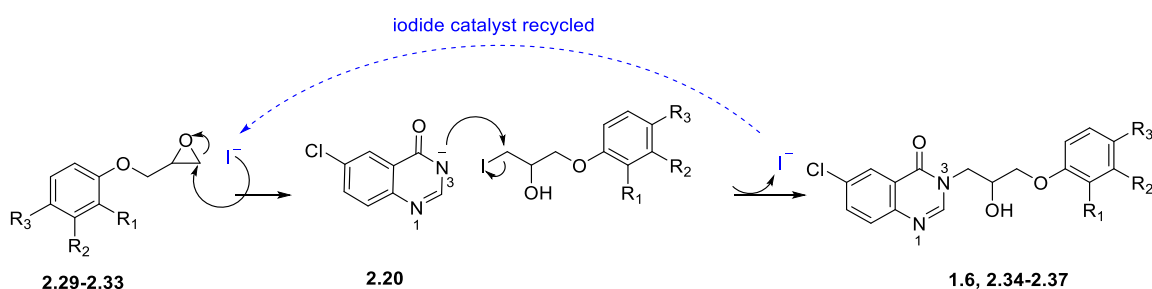
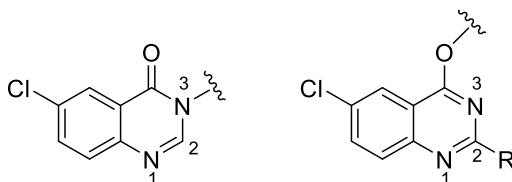


Figure 2-5: Alkylation of 4 (3H)-quinazolinone ring. The reaction uses a catalytic amount of tetrabutylammonium iodide (TBAI).

In an unsymmetrical epoxide, two ring-opening products can be formed corresponding to the reaction of the nucleophile at the two different carbons of the ring. However, in basic

conditions, the nucleophile typically reacts at the carbon atom bearing the greater number of free hydrogen atoms.¹⁴⁴ This carbon is highly reactive and is considered to be a hard electrophile because epoxides possess significant angle strain, and the bonds of an epoxide are weaker than those of cyclic ethers with larger rings or open-chain ethers. However, employing TBAI led to epoxide ring opening and provided the corresponding alkyl halide which is considered as a soft electrophile. This decreased the reactivity of the electrophile and enhanced the selectivity ratio to produce the desired regioisomer. Most literature reports two sites of possible alkylation: N³, O or a mixture of both products, which depends on the electronic and steric nature of the C₂ substituents and the reaction conditions.¹⁴⁵



The selectivity of OH-alkylation can be directed by using specific conditions, such as the Mitsunobu reaction,¹⁴⁶ or specific reagents, such as BOP¹⁴⁷, POCl₃ or HCCP.¹⁴⁸ Otherwise, the regioselectivity mainly depends on the alkylating agent, substrate, reaction solvent and other reaction conditions.¹⁴⁹

The ¹³C NMR spectra (Figure 2-6) showed that the same chemical shift of the carbonyl group in the 4 (3*H*)-quinazolinone ring of **2.20** as in the product 2-(4-(3-(6-chloro-4-oxoquinazolin-3(4*H*)-yl)-2-hydroxypropoxy)phenyl)acetonitrile **1.6**, with shifts of 160.28 ppm and 159.99 ppm, respectively. This evidence proves that the OH-alkylation did not take place in this reaction.

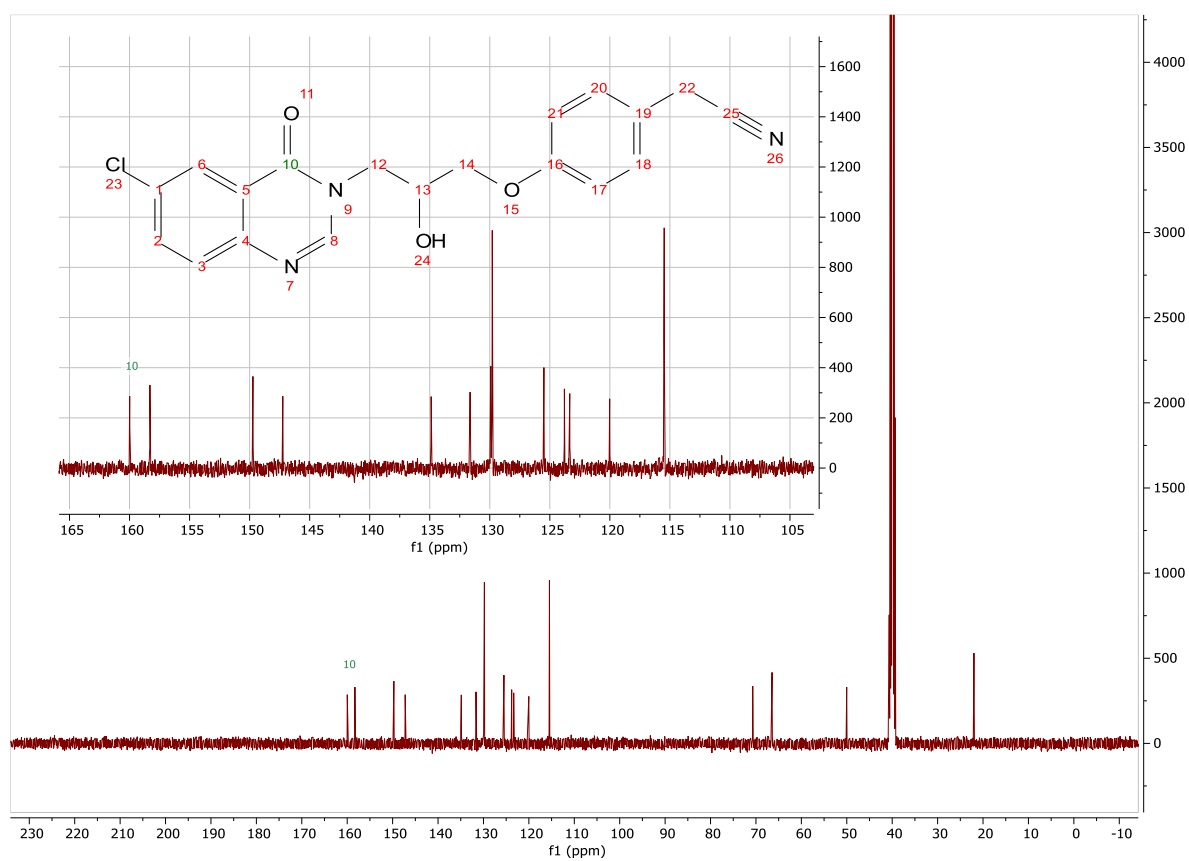
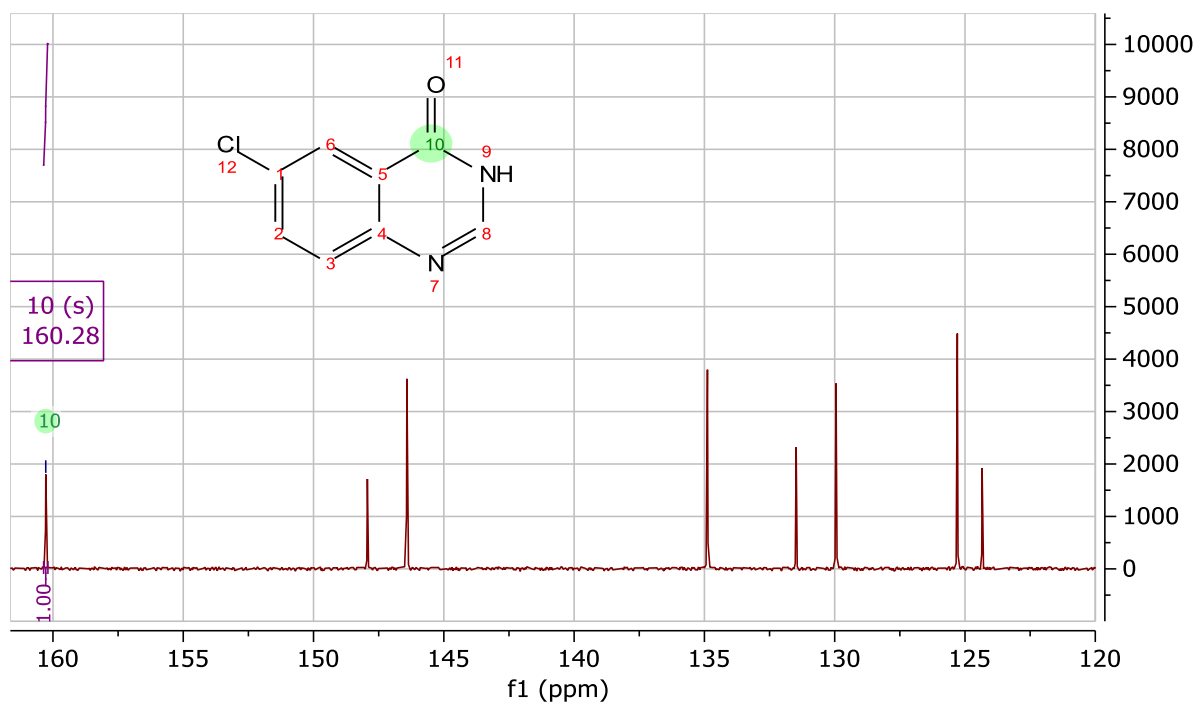
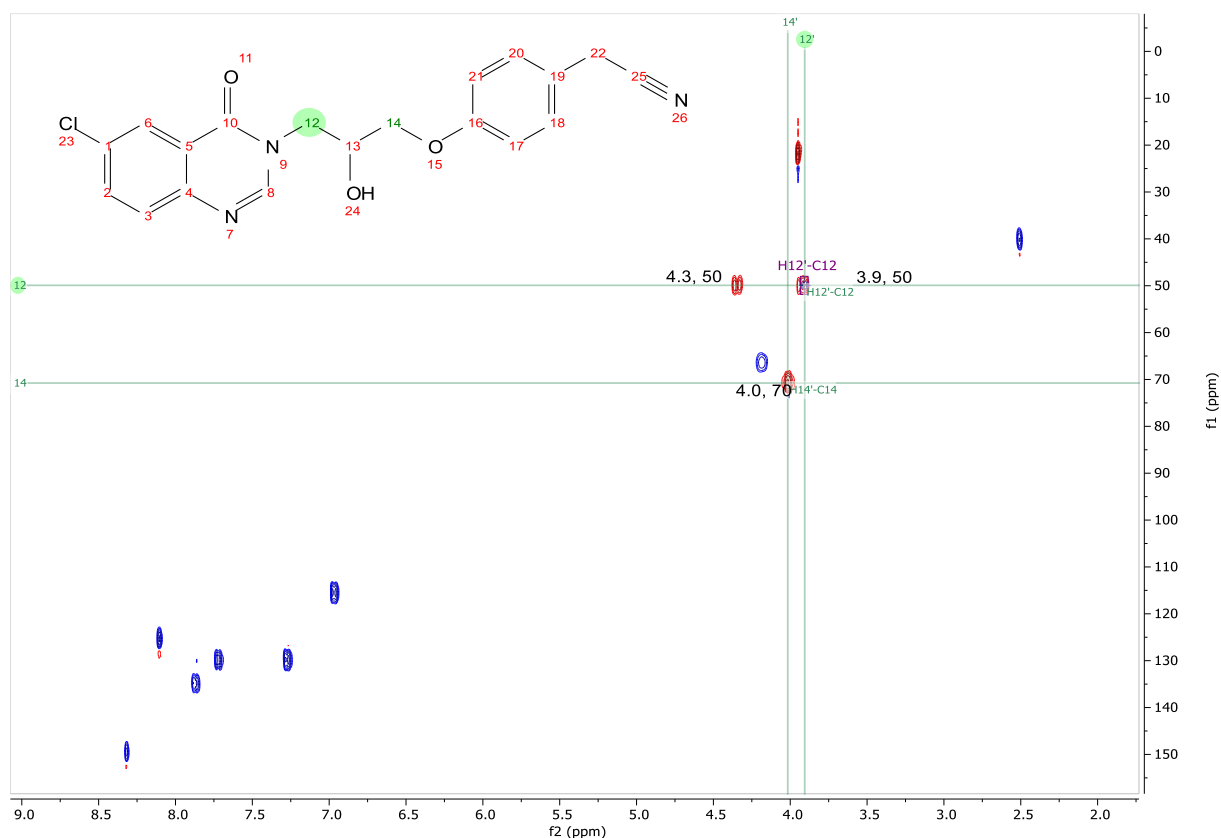


Figure 2-6: The ^{13}C NMR spectra of 4 (3H)-quinazolinone ring of **2.20** (above) and 2-(4-(3-(6-chloro-4-oxoquinazolin-3(4H)-yl)-2-hydroxypropoxy)phenyl)acetonitrile **1.6** (below) with an enlarged section of the aromatic region, in $\text{DMSO-}d_6$ solvent at 100.66 MHz.

A heteronuclear single quantum correlation (HSQC) experiment was used with the resulting two-dimensional (2D) spectrum showing one axis for proton (^1H) and the other for a heteronucleus (an atomic nucleus other than a proton), which is in this case ^{13}C . The spectrum implies that carbon 13, which is attached to nitrogen appears at 50 ppm and couples to two protons appearing in different regions, 4.35 ppm and 3.87 ppm. Further analysis was established employing a heteronuclear multiple-bond correlation (HMBC) experiment to determine the site of alkylation. This experiment detects heteronuclear correlations over longer ranges of approximately 2–4 bonds. The characteristic peak of the carbonyl group (160 ppm) was coupled with proton appear at 4.35 ppm, indicating that N^3 rather than N^1 was the site of alkylation as shown in (Figure 2-7).



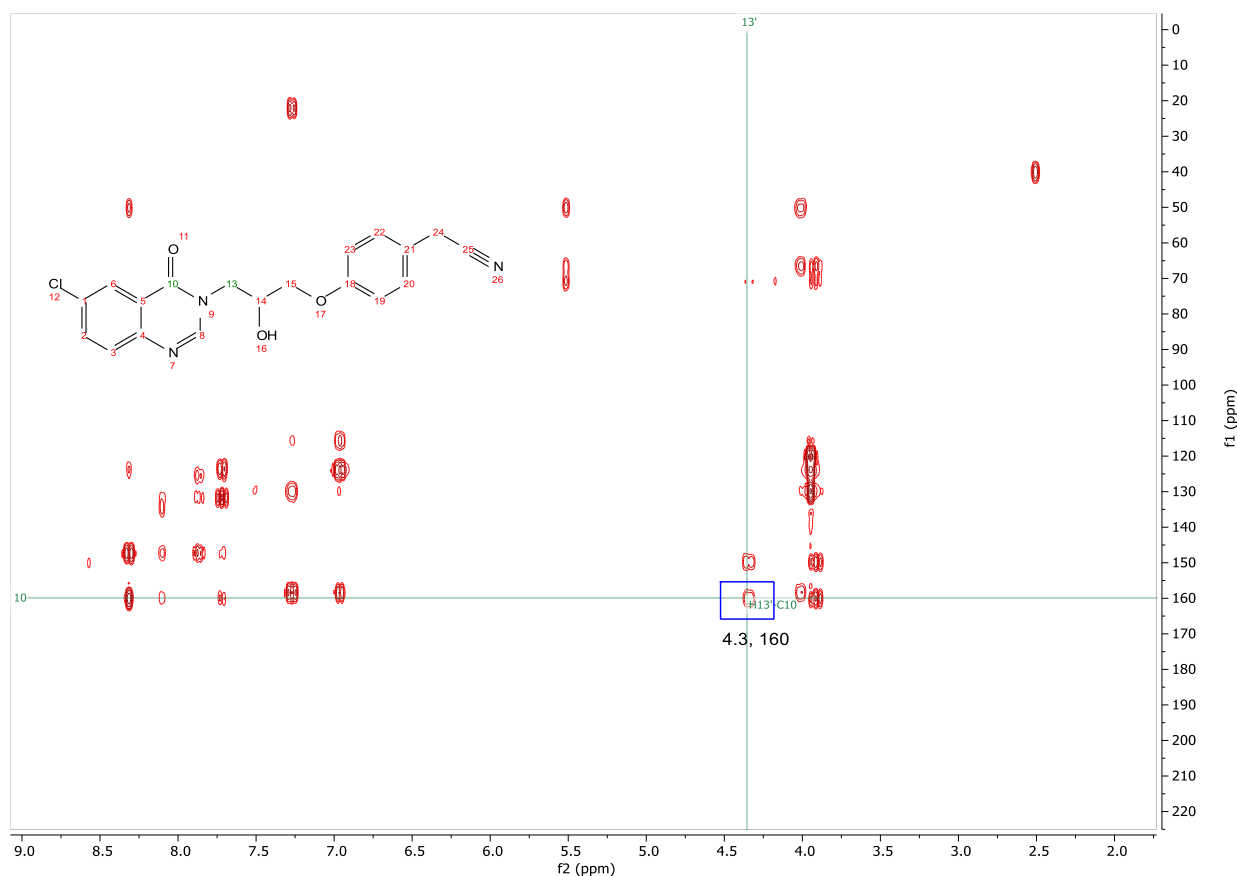
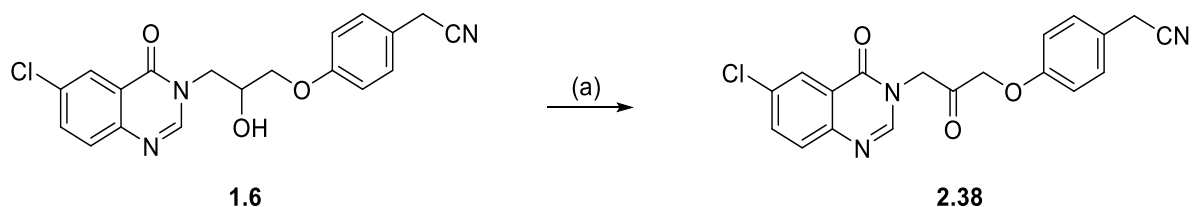


Figure 2-7: 2D NMR analysis of 2-(4-(3-(6-chloro-4-oxoquinazolin-3(*H*)-yl) -2-hydroxypropoxy) phenyl) acetonitrile, **1.6**. The heteronuclear single quantum correlation (HSQC) spectrum (above) and the heteronuclear multiple-bond correlation (HMBC) spectrum (below), in DMSO-*d*₆ solvent.

2.4.2 Oxidizing the hydroxyl functional group in 2-(4-(3-(6-chloro-4-oxoquinazolin-3(*H*)-yl)-2-hydroxypropoxy) phenyl) acetonitrile, **1.6**

Scheme 2-2: Oxidation of a secondary alcohol to a ketone functional group.

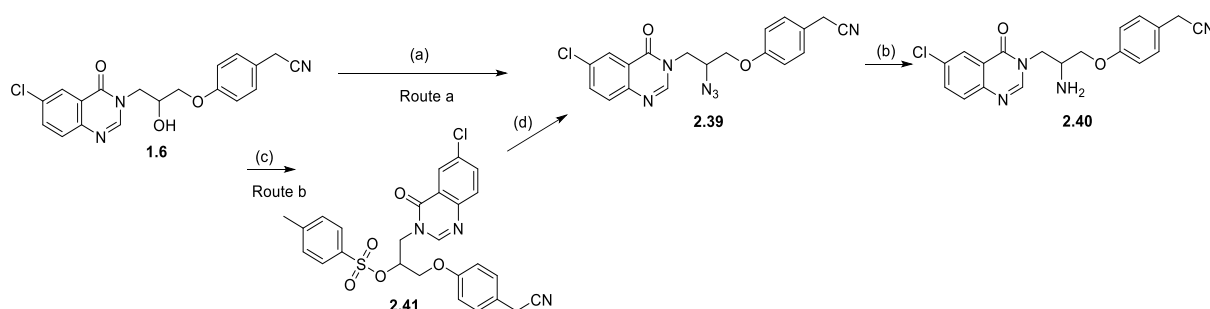


Reagents and conditions: a) Dess–Martin periodinane, DCM, rt, 16 h, 76%.

There are a variety of oxidizing methods and reagents that can be used for secondary alcohol oxidation, such as chromates, Swern oxidation, or Dess–Martin periodinane (DMP) reagent. DMP oxidation is preferable in comparison to other oxidation reagents due to its mild reaction conditions such as room temperature and a neutral pH.¹⁵⁰ This reaction also avoids the use of toxic chromium reagents and does not require a large excess of oxidizing reagent or co-oxidants. The reaction of the hypervalent iodine-containing reagent with secondary alcohol in **1.6** was efficient to afford ketone **2.38** (Scheme 2-2), with acetic acid and the mono-acetoxyiodinane as easily removed side products.¹⁵⁰

2.4.3 Synthesis of 2-(4-(2-amino-3- (6-chloro-4-oxoquinazolin-3(4*H*)-yl) propoxy) phenyl) acetonitrile **2.40** and its analogues

Scheme 2-3: Synthesis of **2.40**.



Reagents and conditions: a) triphenylphosphine (Ph_3P), di-isopropyl azodicarboxylate (DIAD), di-phenyl phosphoryl azide (DPPA), THF, 45°C, 16 h, 30%.¹⁵¹ b) Ph_3P , NH_4OH , THF: H_2O , rt, 16 h, 25%. c) Tosyl chloride, NEt_3 , DMAP, DCE: 5% THF, rt, 16 h, 82%. d) NaN_3 , DMF, 60°C, 16 h, 65%.

Two different well-known reactions were employed to furnish **2.40**. The Mitsunobu reaction was used to substitute the hydroxyl group with azide **2.39**. The azide was subsequently reduced to the primary amine through the Staudinger reaction to give **2.40**. This product **2.40** was employed in subsequent reactions to either alkylate or form amides.

Mitsunobu reaction 2.39. The Mitsunobu reaction was employed to furnish an S_N2 product in a one-pot synthesis by activating the alcohol into a better leaving group, which then underwent nucleophilic substitution (S_N2) by azide anion as the nucleophile.

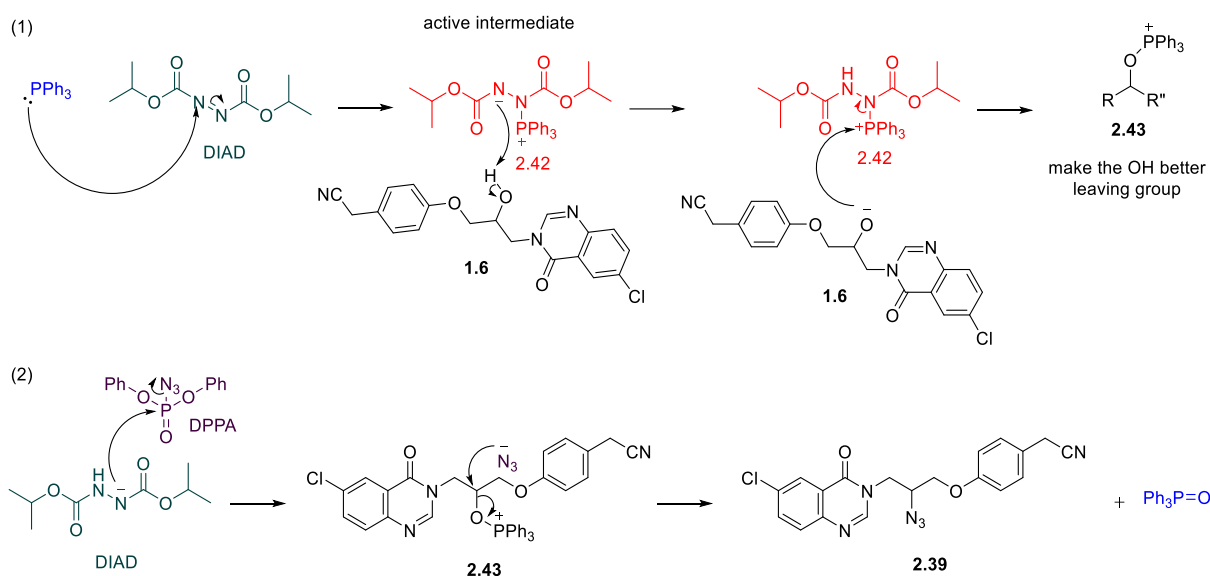


Figure 2-8: **Mechanism of Mitsunobu reaction.** The reaction employs **1.6**, PPh₃, DPPA and DIAD to furnish the azide moiety in **2.39**.

Two reagents (PPh₃ and DIAD) were mixed for 30 minutes to form an active intermediate **2.42**, as shown in Figure 2-8. Subsequently, **1.6** was added and the active intermediate **2.42** deprotonated the alcohol, generating the alkoxide ion which immediately attacked the positively charged phosphorus atom, forming a strong bond. In the second step, DPPA was added, which was attacked by the second basic nitrogen anion, thereby liberating the azide as a nucleophilic anion. Finally, the azide attacked the electrophilic carbon in a normal S_N2 reaction, leading to the displacement of the phosphorus derivative of the alcohol by azide moiety **2.39**. The whole process took place in one operation. The four reagents (DIAD, PPh₃, DPPA and the substrate) were all added to one flask, generating two side products—phosphine oxide and the reduced azo diester with two NH bonds replacing the N=N double bond.

An alternative approach was used by transforming the hydroxyl group in **1.6** into a good leaving group and subsequent substitution with the desired nucleophile. The alcohol was

treated with *p*-toluenesulfonyl chloride and base to form sulfonate ester **2.41**, which was obtained in good yield. Subsequently, the product was reacted with NaN₃ to produce **2.39** in good yield and purity. The advantage of this approach was to avoid the generation of phosphine oxide (a side product from the Mitsunobu reaction), which interferes with the desired product in the chromatographic separation process.

Staudinger reaction 2.40. The azide moiety can be reduced to the primary amine by several methods such as catalytic hydrogenation, LiAlH₄ reduction or the Staudinger reaction. However, the first two reduction methods are not chemo-selective, and they could affect different labile functional groups present within the compound. Catalytic hydrogenation using 10 wt% palladium on carbon, for example, can hydrogenate the aryl chloride¹⁵² in **2.39**, while LiAlH₄¹⁵³ can also reduce the nitrile functional group present in the starting material to an amine. Therefore, the Staudinger reaction provides the optimal condition to afford the desired primary amine moiety with high chemo-selectivity.

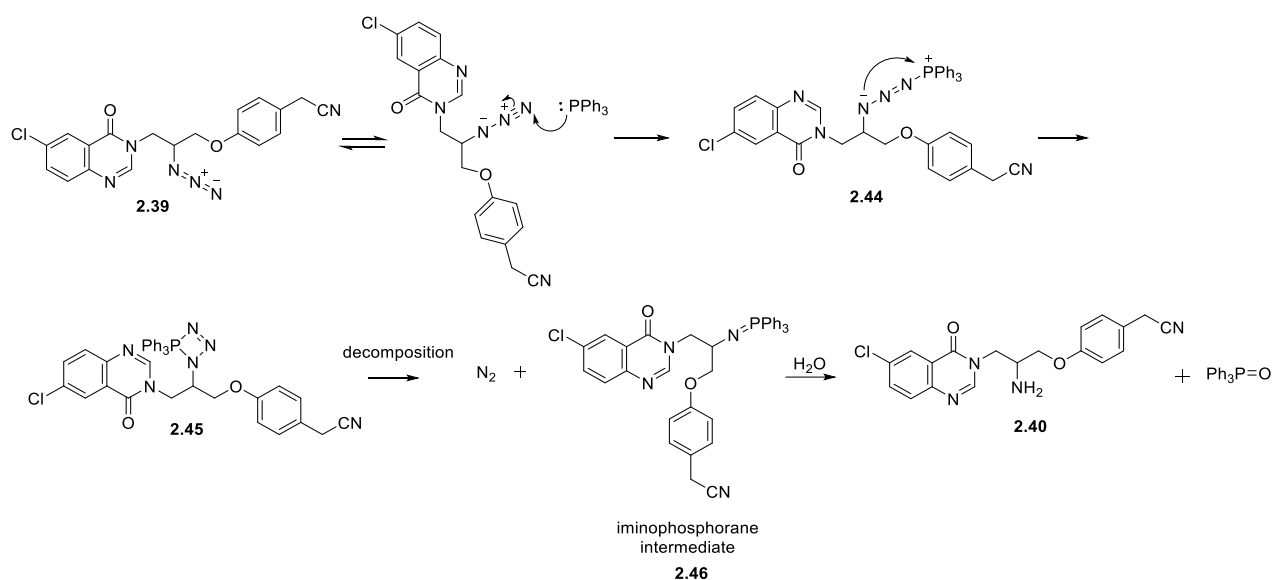
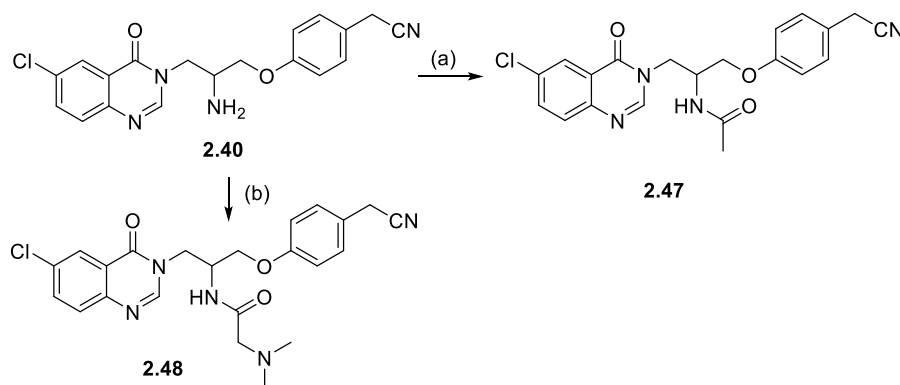


Figure 2-9: **Mechanism of Staudinger reaction.** The reaction employs **2.39** to furnish the amine moiety in **2.40**.

Mechanistically, the first step of this reaction is nucleophilic addition of triphenylphosphine leading to the formation of the 4-membered ring intermediate **2.45**, which is not stable due to angle strain and therefore is rapidly decomposed. The side product of this reaction is nitrogen gas, which means that this reaction will be thermodynamically favourable due to an increased reaction entropy. Following that, decomposition yields the corresponding iminophosphorane intermediate **2.46**, similar to the Wittig ylide. A water molecule then attacks the phosphorus atom in **2.46**, and a series of proton transfer steps take place to form the final primary amine **2.39**, with triphenylphosphine oxide as a by-product.

Scheme 2-4: Amide bond formation in **2.47** and **2.48**.



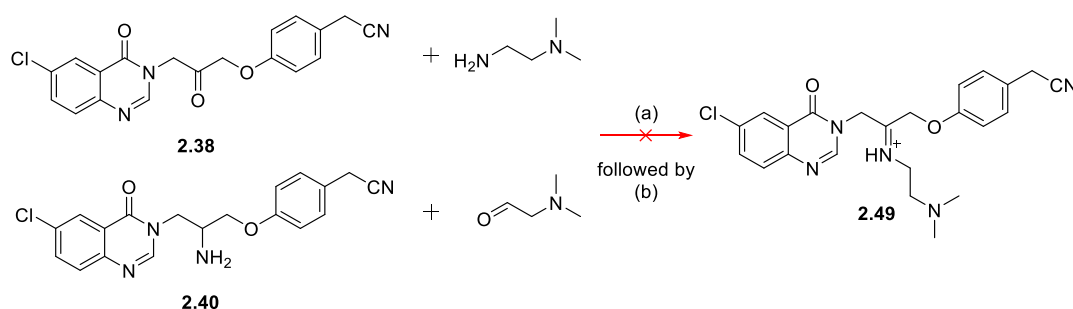
Reagents and conditions: a) $(\text{CH}_3\text{CO})_2\text{O}$, rt, 3 h, 95%. b) $(\text{CH}_3)_2\text{NCH}_2\text{COOH}$, PyBrop, Et_3N , DMF, rt, 4 h 59%.

Amide bond formation is one of the most important reactions in organic chemistry, and the design and synthesis of innovative coupling reagents have been an area of intense investigation.¹⁵⁴ In this work, amide bond formation was achieved by employing a robust and classical method using acid anhydrides. The desired anhydride was readily reactive with the secondary amine at room temperature. In theory, this reaction does not require a base, as the addition generates a carboxylate anion *in situ* and no coupling would be obtained. Another strategy used here is coupling the amine to the desired carboxylic acid. The leaving group, in this case, is the hydroxyl anion, which is a poor leaving group and therefore carboxylic acid

needs to be activated by a coupling reagent. A one-pot coupling condition was employed here using a phosphonium reagent called bromo tri-(pyrrolidino) phosphonium hexafluorophosphate (PyBrop), which is a more efficient peptide coupling reagent for secondary amine groups when compared to benzotriazol-1-yl-oxy-tris-(dimethylamino)-phosphonium hexafluorophosphate (BOP) and benzotriazol-1-yl-oxy-tris-pyrrolidino-phosphonium hexafluorophosphate (PyBop).¹⁵⁵ This may be because of the formation of *in situ* acyl bromide, which has less steric hindrance than the acyl benzotriazole generated by BOP or PyBop coupling reagents.¹⁵⁵

Amine alkylation 2.50. In general, the alkylation of amines can be obtained *via* nucleophilic addition to aldehydes or ketones, followed by reductive amination or S_N2 reaction with an alkyl halide.

Scheme 2-5: Synthesis of imine functional group in **2.49**.

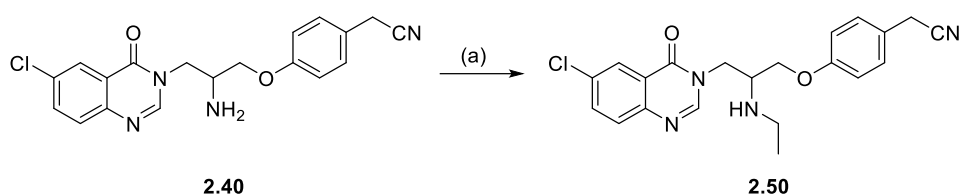


Reagents and conditions: a) MeOH with 10% acetic acid, 40°C, 16 h. b) 2-picoline-borane complex or sodium borohydride NaBH₄.

The first attempt to synthesise **2.49** was to employ a reductive amination reaction by reacting **2.38** with the primary amine *N*¹, *N*¹-dimethylethane-1,2-diamine or **2.40** with 2-(dimethylamino) acetaldehyde in acidic conditions to form imine intermediate **2.49**, which was planned to subsequently reduce by an appropriate reducing agent, such as 2-picoline-borane complex or sodium borohydride. However, the nucleophilic addition did not take place, and no product was detected from this reaction.

The formation of imines is reversible and generally takes place under acid or base catalysis or with heat.¹⁵⁶ To drive the reaction to completion, different strategies were employed by adding the reducing reagent to produce the amine as the imine formed, removing the water from the reaction, and increasing the heat. Unfortunately, all of these strategies failed to produce the required product. The reduction of the starting material **2.38** to **1.6** (reduction of the ketone to alcohol) was the only reaction that occurred in this condition.

Scheme 2-6: Synthesis of **2.50**.

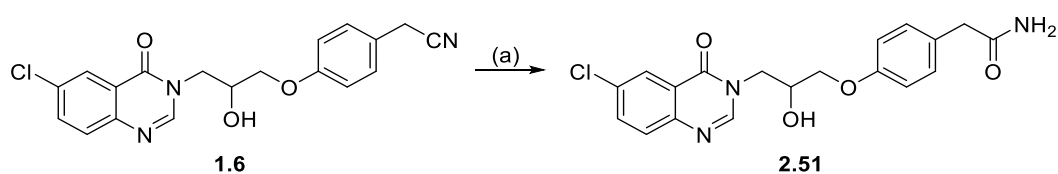


Reagents and conditions: a) C₂H₅I, Cs₂CO₃, CH₃CN, 60°C, 16 h, 65%.

A further attempt to alkylate the amino functional group in **2.40** with alkyl iodide was employed to directly alkylate the amine and produce **2.50**. This was the only successful strategy that provided a simple alkylation. However, the biological analysis of this compound did not show promising results; therefore, the synthesis effort was directed to different series of analogues.

2.4.4 Nitrile hydrolysis in **1.6** to synthesis 2-(4-(3-(6-chloro-4-oxoquinazolin-3(4H)-yl) -2-hydroxypropoxy) phenyl) acetamide **2.51**

Scheme 2-7: Synthesis of amide moiety in **2.51**



Reagents and conditions: a) Cs₂CO₃, DMSO:30% H₂O₂, rt, 30 min, 96%.

Preparation of the Amide 2.51. The hydrolysis of a nitrile group to an amide is one of the critical transformations in organic chemistry, as amides can undergo further hydrolysis to furnish carboxylic acids. Therefore, the selection of the proper reagent and conditions to hydrolyse the nitrile to an amide is important to obtain the desired product. One specific condition is to use a weakly basic condition of 30% hydrogen peroxide in DMSO.¹⁵⁷ The mechanism and kinetics of the reaction were investigated by Wiberg (1953), demonstrating that this reaction involves the oxidation-reduction of hydrogen peroxide with simultaneous hydrolysis of the nitrile.¹⁵⁷

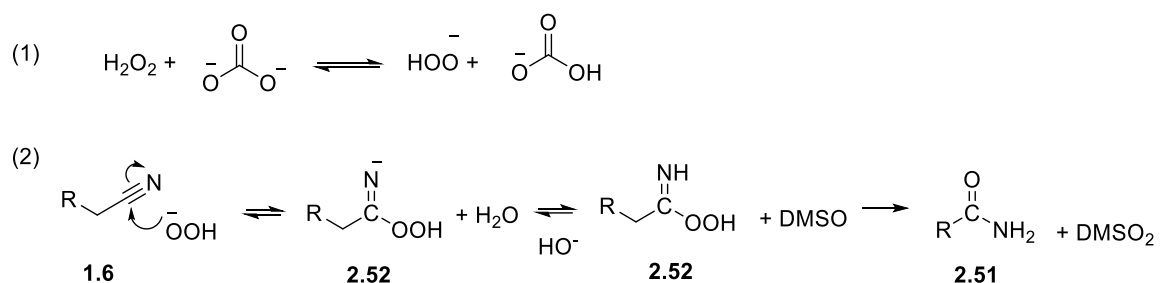
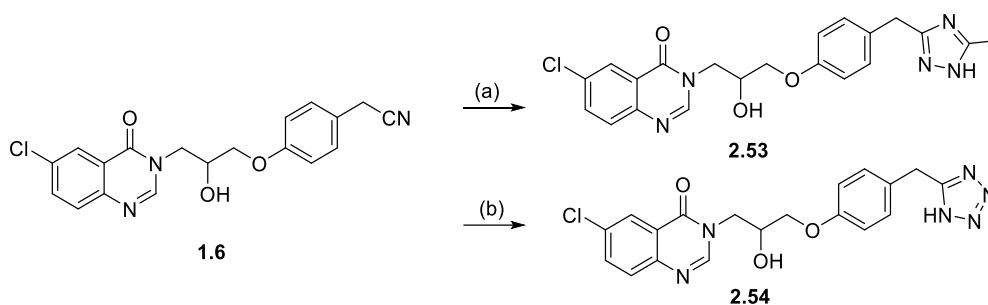


Figure 2-10: Mechanism of nitrile hydrolysis with alkaline hydrogen peroxide.

The hydrogen peroxide first reacts with the **carbonate** to generate hydroperoxide anion, which attacks the electrophilic carbon of the nitrile and forms peroxycarboximidic acid intermediate, **2.52**. After a proton transfer, this intermediate, **2.52** undergoes oxidation-reduction with DMSO to afford the amide **2.51** and dimethyl sulfone (DMSO₂) (Figure 2-10). Notably, adding DMSO to this reaction as a solvent or as an additive significantly increases the reaction rate.¹⁵⁷

2.4.5 Modification of the nitrile group to different heterocycles

Scheme 2-8: Synthesis of 3-methyl-1*H*-1,2,4-triazole and 1*H*-tetrazole heterocycles.



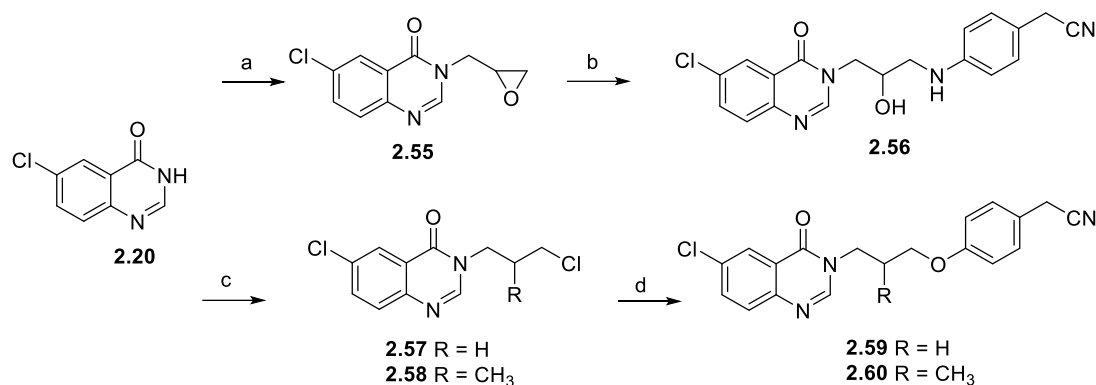
Reagents and conditions: a) Acetyl- hydrazide, sodium methoxide, CH₃OH, 80°C, 16 h, 15%.¹⁵⁸ b) NaN₃, Et₃N·HCl, DMF, 130°C, 16 h, 75%.¹⁵⁹

By considering the carbon of the nitrile as an electrophile functional group, two different nucleophiles were used, leading to internal cyclisation and producing two different heterocycles: 3-methyl-1*H*-1,2,4-triazole **2.53** and 1*H*-tetrazole **2.54**. As the acetonitrile group was attached to an electron-withdrawing group (phenyl), the cycloaddition of acetyl hydrazide or NaN₃ took place at a sufficient rate, followed by internal cyclisation to furnish the corresponding heterocycles.

2.4.6 Different approaches for linker modifications

Here, two different approaches were applied to modify the linker of **1.6**: 1) replacing the oxygen with an amine functional group, 2) substituting the hydroxyl moiety with a methyl or hydrogen.

Scheme 2-9: Synthetic route approaches for linker modifications.



Reagents and conditions: a) (\pm) epichlorohydrin, Cs₂CO₃, TBAI, CH₃CN, reflux, 16 h, 38%. b) 4-aminobenzyl nitrile, Cs₂CO₃, CH₃CH₂OH, microwave, 125°C, 30 min, 47%. c) 1-bromo-3-chloro-2-propane for **2.57** and 1-bromo-3-chloro-2-methylpropane for **2.58**, Cs₂CO₃, TBAI, CH₃CN, reflux 16 h, 70–72%. d) 4-hydroxyphenylacetonitrile, Cs₂CO₃, TBAI, CH₃CN, reflux 16 h, 40–49%.

First, to replace the oxygen with nitrogen in **2.56**, the synthesis pathway previously used for **1.6** synthesis (Scheme 2-1) was slightly modified to a new route (Scheme 2-9). The new route starts with chlorine displacement in (\pm) epichlorohydrin by deprotonated QZN. Subsequently, the epoxide was ring opened by 4-aminobenzyl nitrile under microwave irradiation to furnish the final product **2.56**.

Additionally, QZN reacted with 1-bromo-3-chloro-2-propane or 1-bromo-3-chloro-2-methylpropane to produce two intermediates, **2.57** and **2.58**, respectively, which were later reacted with 4-hydroxyphenylacetonitrile. The principle of the chemical behaviour of this reaction depends on many influencing factors. a) the strength of the covalent bond and b) the stability of the corresponding halide anions. Except for the C-F bond, all of the C-halogen

bonds are weaker than the C-C and C-H bonds, and the increase in electronegativity is in direct proportion to the strength of the covalent bond. This makes the C-Br bond more susceptible to breakage than the C-Cl bond. Another reason to direct the chemo-selectivity of this substitution toward the C-Br bond is the stability of the halide anions, which mainly depends on the charge distribution over the halide anion. The stability of the charge distribution is in direct proportion to the size of the halide, which makes the bromide anion more stable and the substitution with C-Br more favourable. Therefore, the substitution by activated QZN was expected to be at the C-Br bond. This was in agreement with the molecular weight of the intermediates detected by LC-MS. Subsequently, the chlorine was displaced by 4-hydroxyphenylacetonitrile in SN2 mechanism to furnish the final compounds (**2.59** and **2.60**) in high yield.

2.5 Molecular analysis

2.5.1 Isothermal calorimetry titration (ITC) of PqsR^{CBD} with 1.13

An important element of drug discovery projects is the confirmation of direct binding to the receptor and one approach of achieving this, is by determination the thermodynamic signature of a molecule. Notably, ITC is the gold standard for this purpose.¹⁶⁰ ITC experiments measure the heat evolved (ΔH) when a drug interacts with its target. Additionally, it measures the Gibbs free energy ($\Delta G_{binding}$) associated with binding that is related to the affinity of this interaction. Gibbs energy (ΔG), enthalpy of reaction (ΔH), and entropy of reaction (ΔS) are related *via* the following equation: $\Delta G = \Delta H - T\Delta S$. A negative ΔG value will favour ligand-protein interaction, whilst a ΔG value of -10 kJ/mol is sufficient to complete a reaction. Therefore, to increase the binding affinity of the candidates, ideal contributions from both enthalpy and entropy are required.¹⁶¹ However, the simultaneous optimisation of these elements is challenging since enthalpic optimisation can often be offset by a loss in the entropic contribution. Entropy is generally based on the hydrophobic effect and increasing ligand lipophilicity will simply optimise this parameter. In contrast, optimising enthalpy is difficult due to its dependence on establishing productive electrostatic and van der Waals interactions. The critical point here is employing incorrectly positioned polar groups that not obtaining further interaction with the receptor. This can frequently be offset by the entropic penalty associated with the desolvation energy without gaining further improvement of the enthalpy element. The energy required to desolvate a polar group is ~ 8 kcal/mol, which is 10 fold higher than the energy required to desolvate a non-polar group.¹⁶²

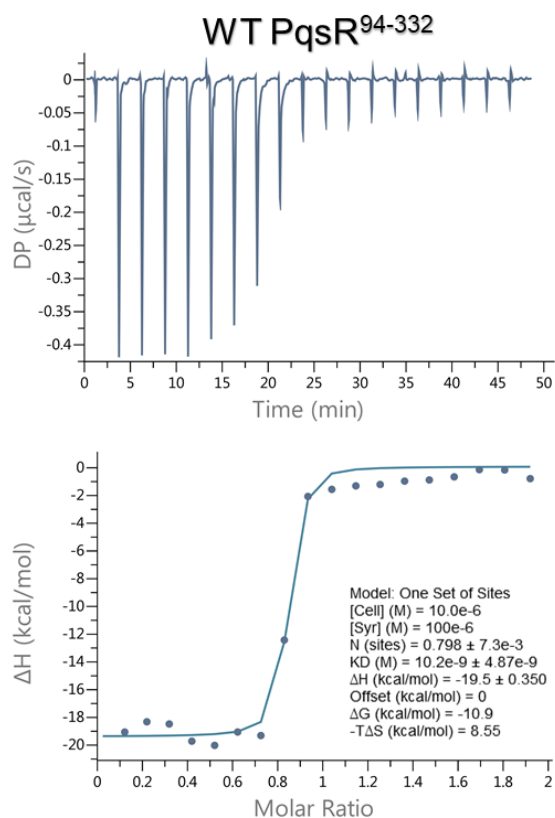


Figure 2-11: **ITC binding data of 1.13**. The experiment employed 100 μM of **1.13** and 10 μM PqsR^{CBD} in two independent experiments. This work was carried out by William Richardson (work in press).

ITC experiment was obtained successfully for **1.13** with PqsR^{CBD} to determine the K_D value and evaluate the binding affinity to the protein. This experiment confirmed that **1.13** binds to PqsR^{CBD} with high affinity (dissociation constant (K_D) = 10 nM) and $\Delta G = -10.9$ kcal/mol.

2.5.2 Crystal structure of PqsR^{CBD} complexed with PqsR antagonists **1.13** and **2.34**.

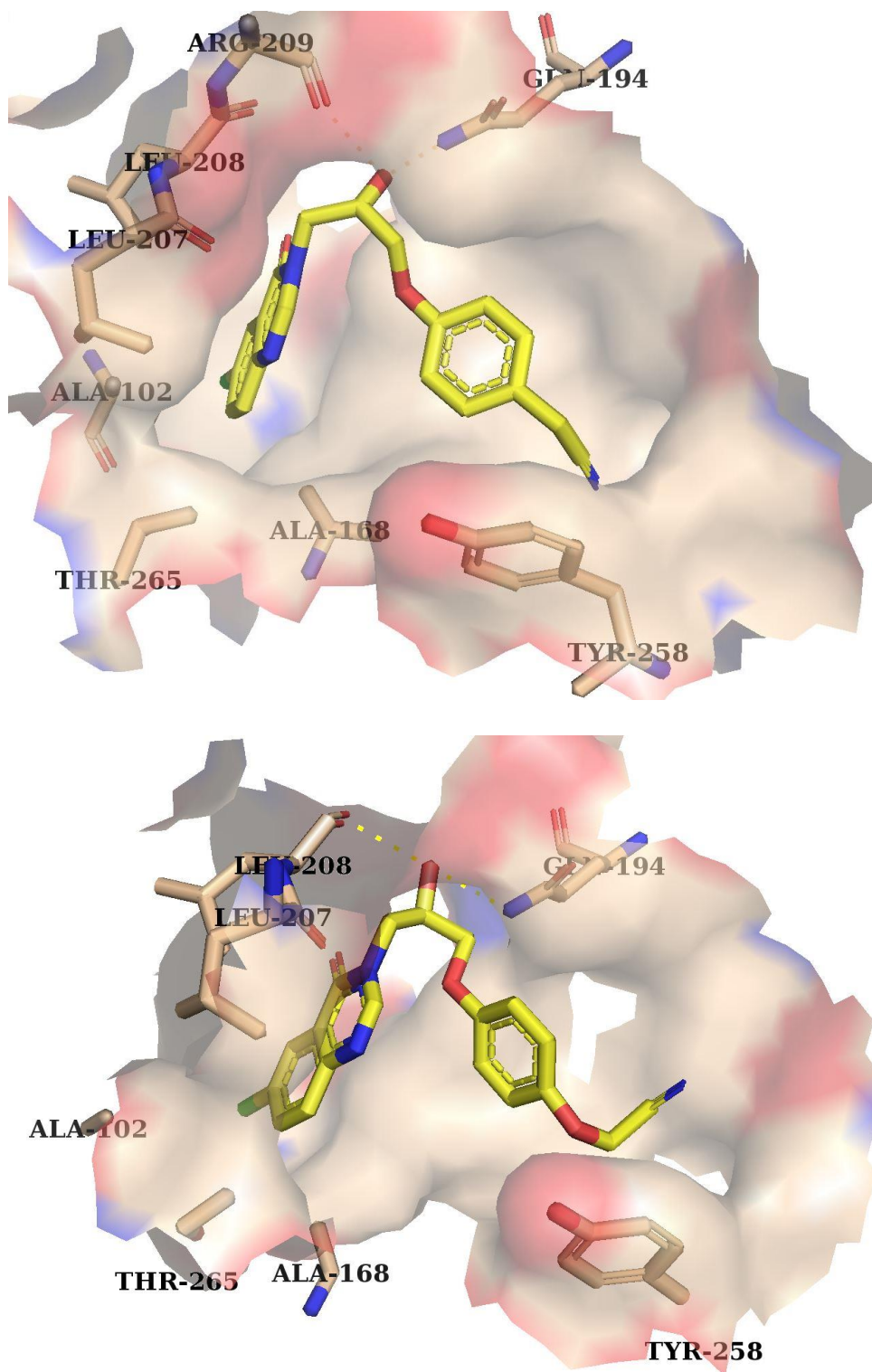


Figure 2-12: Schematic representation of the crystal structure of PqsR^{CBD} complexed with PqsR antagonist; **1.13** (above) and **2.34** (below). Hydrogen bonds are shown as dotted lines. The racemic mixture of **2.34** was soaked, and the *R* enantiomer was observed. This work was carried out by William Richardson (work in press).

To gain a detailed insight into the molecular interaction of the antagonists belonging to the 4-(3*H*)-quinazolinone series with PqsR^{CBD}, the mode of binding of **1.13** and **2.34** was determined by obtaining the co-crystal structure with the PqsR^{CBD} domain employing crystal soaking experiments. As previously discussed (1.7.2), PqsR^{CBD} comprises of a deep pocket (A pocket) which usually accommodates the quinolone part of the autoinducer, as shown with the NHQ crystal structure, while the superficial pocket (B pocket) contains the aliphatic side chain.⁸⁷

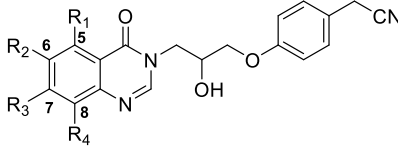
The ligand-bound complex revealed that the quinazolinone ring inserted deeply into the hydrophobic pocket A in a similar manner to NHQ, whilst the *para*-phenyl acetonitrile faced Tyr²⁵⁸ in pocket B. The quinazolinone moiety of **1.13** and **2.34** was surrounded by aliphatic residues (Ala¹⁰², Ala¹⁶⁸, Ile²⁰⁷, Ile²⁰⁸) while the hydroxyl group establishes hydrogen bonding interactions with Glu¹⁹⁴ and Arg²⁰⁹ or Gln¹⁹⁴ and Leu²⁰⁸, respectively. Overall, both compounds maintained the same conformation and electrostatic interaction with the protein residues.

2.6 Structure–activity relationship analysis

2.6.1 Analysing the optimal position of electron-withdrawing substitution on the quinazolin-4(3*H*)-one core

In all of the natural ligands and the PqsR antagonists presented in this chapter, the quinolin-4(1*H*)-one or quinazolin-4(3*H*)-one core was conserved. Therefore, the attempt here was to explore the SAR by substituting the quinazolin-4(3*H*)-one core with EWGs at the R₁-R₄ positions, as presented in Table 2-1.

Table 2-1: **SAR study of quinazolin-4(3*H*)-one core (2.61-2.68).** The inhibition of PqsR activity was initially measured in the PAO1-L CTX::P_{pqsA}-lux strain of *P. aeruginosa* at 10 μM. NA, not active at 10 μM. All compounds resulting in a greater than 50% inhibition of activity were further analysed by concentration-response curves measured in the PAO1-L CTX::P_{pqsA}-lux strain. The asterisk (*) indicates that this parameter was predicted using ChemDraw 19.0.1.28 (<http://www.chemaxon.com>). The sign (\$) indicates that the synthesis and biological evaluation was carried out by Fadi Soukarieh.

						
Compound	R ₁	R ₂	R ₃	R ₄	IC ₅₀ (μM) PAO1-L CTX::P _{pqsA} -lux	cLogP*
^{\$} 2.61	Cl	H	H	H	NA	1.9
^{\$} 2.62	H	Cl	Cl	H	NA	2.6
^{\$} 2.63	H	H	Cl	H	6.7 ± 0.3	1.9
^{\$} 2.64	H	H	H	Cl	NA	1.9
^{\$} 2.65	H	Cl	H	Cl	NA	2.6
^{\$} 2.66	H	NO ₂	H	H	0.5 ± 0.1	1.0
^{\$} 2.67	H	H	NO ₂	H	NA	1.0
^{\$} 2.68	H	CF ₃	H	H	0.6 ± 0.1	2.2

Values reported as Mean ± SEM of n = 3.

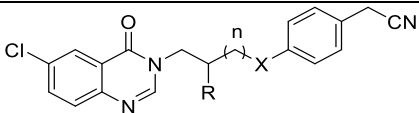
This analysis demonstrated that the introduction of a chlorine atom at the C₅-R₁ or C₈-R₄ position (compounds **2.61** and **2.64**, respectively) led to a loss of potency as well as the di-substituted compounds **2.62** and **2.65**. In addition, the C₇-R₃ chlorine analogue **2.63** had a 2-fold loss of activity indicating that the substitution at the C₆-R₂ is the optimal position. It is noteworthy, that the 7-nitro substituted derivative **2.67**, as opposed to **2.63**, was completely inactive which is likely due to the size of the nitro group compared to the chlorine atom. Furthermore, R₂ was substituted with a stronger EWG functional group such as CF₃ (**2.68**) or NO₂ (**2.66**), with Hammett constant 0.54 and 0.78, respectively in comparison to 0.23 for Cl substitution.¹⁶³ The inhibitory potency of **2.68** and **2.66** was enhanced 6- or 7.5- fold, respectively, compared to **1.6**, which confirmed the importance of the electron-withdrawing effect on that position.

This finding suggests that the EWG creates localised electron-deficient sites, thereby forming a stronger interaction with electron-rich aromatic side chains of amino acids present in the recognition site of the receptor. However, the lack of an electron-donating groups (EDGs) substituent at the C₆-R₂ position in this study limited the ability to make a proper comparison or draw this conclusion. Another possible interpretation is that these moieties (Cl, NO₂ and CF₃) form H-bonds with the receptor, which is consistent with previously reported findings.⁸⁷ Cl in position C₆-R₂ was maintained for all the future SAR analyses. The nitro group, in general, has been extensively associated with mutagenicity and genotoxicity issues,¹⁶⁴ while the trifluoromethyl moiety slightly increased the lipophilicity of the compound.

2.6.2 Amino propan-2-ol linker investigation

Here, the SAR investigation efforts focused on determining the type of interactions formed by the linker by varying the substituents at the R position while the head and tail moieties were fixed corresponding to those of **1.6**. The optimal length of the linker was also investigated, as shown:

Table 2-2: **SAR study of amino propan-2-ol linker.** The inhibition of PqsR activity was initially measured in the PAO1-L CTX::*P_{pqsA}-lux* strain of *P. aeruginosa* at 10 μ M. NA, not active at 10 μ M. All compounds resulting in a greater than 50% inhibition of activity were further analysed by concentration-response curves measured in PAO1-L CTX::*P_{pqsA}-lux*. The asterisk (*) indicates that this parameter was predicted using ChemDraw 19.0.1.28 (<http://www.chemaxon.com>). Compounds **2.70** and **2.72** were not synthesised. The sign (\$) indicates that the synthesis and biological evaluation was carried out by Fadi Soukarieh. The sign (£) indicates that the biological evaluation was carried out by Fadi Soukarieh.

					
Compound	R	X	n	IC ₅₀ (μ M)	
				PAO1-L CTX:: <i>P_{pqsA}-lux</i>	cLogP*
£1.6	OH	O	1	3.2 \pm 1.0	1.9
£2.40	NH ₂	O	1	2.4 \pm 0.2	2.0
2.59	H	O	1	NA	3.1
2.60	CH ₃	O	1	NA	3.5
§2.69	F	O	1	NA	3.3
£2.38	=O	O	1	4.3 \pm 1.3	2.3
2.56	OH	NH	1	NA	1.6
2.70	NH ₂	NH	1	-	1.7
§2.71	OH	O	2	NA	2.3
2.47	NH(CO)CH ₃	O	1	NA	2.0
2.48	NH(CO)CH ₂ N(CH ₃) ₂	O	1	NA	2.2
2.50	NHCH ₂ CH ₃	O	1	NA	2.9

2.72	NHCH ₂ CH ₂ N(CH ₃) ₂	O	1	-	2.9
------	--	---	---	---	-----

Values reported as Mean \pm SEM of n = 3.

All the lipophilic substituents (**2.59**, **2.60** and **2.69**) lead to the loss of activity, while replacing the hydroxyl with the isosteric H-donor or/and acceptor group **2.40** slightly enhanced the inhibitory potency. Interestingly, oxidising the hydroxyl to the ketone **2.38** maintained similar activity to the original hit ($IC_{50} = 4.3 \pm 1.3 \mu M$), which was likely due to the lone pairs of the carbonyl oxygen still acting as a H-bond acceptor. Additionally, the optimal linker length was investigated by introducing an additional carbon in **2.71**, which led to the loss of activity. Taken together, these results confirmed that there is a H-bond interaction between the molecule at the R position and the binding domain, and the position of this substituent is critical for biological activity. The co-crystal structure of **1.13** and **2.34** with PqsR provided further evidence consistent with this finding.

The design of a di-basic compound was applied here in order to find a compound with ionizable basic functional groups in neutral pH 7.4 which could lead to an increase in the retention time of the compound in the lung.

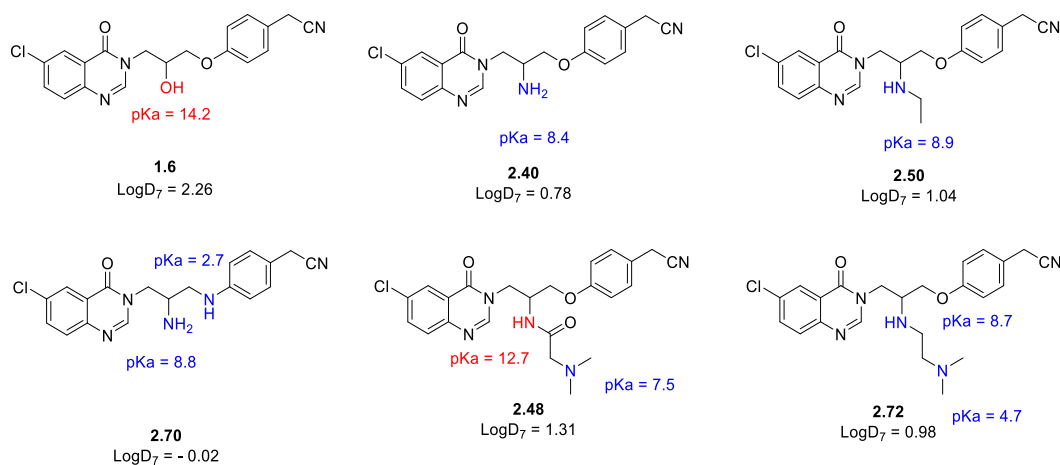


Figure 2-13: analogues that contain acidic (in red) or basic (in blue) functional groups. The parameters (pKa and LogD₇) were predicted using ChemDraw 19.0.1.28 (<http://www.chemaxon.com>).

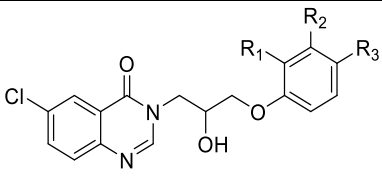
The strategy applied here is by replacing the hydroxyl in **1.6** with the amine in **2.40**, this would convert the weak acid functional group in **1.6** to a base in **2.40** with pKa 8.4. this base can be ionized in neutral pH 7.4. Furthermore, the alkylation of the amino functional group in **2.50** slightly enhanced the basicity. Similarly, replacing the O atom at the X position with nitrogen, then substituting the R position with amino group to produce **2.70** will enhance the basicity as well as provide other weak basic functional group in the molecule. In addition, link the amino group in compound **2.40** with acyl or alkyl chain containing a dimethyl amino group at the end of the side chain (**2.48** or **2.72** respectively) will provide the desired basic functional group with other weak acidic, **2.48** or basic, **2.72** functional group in the molecule as shown in Figure 2-13.

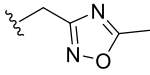
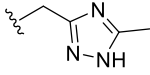
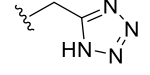
The synthesis of **2.48** and **2.72** proved very challenging, and many attempts were made to synthesise these molecules. First, replacing the oxygen atom with nitrogen at the X position lead to inactive compound **2.56**; therefore, no further chemical reaction was carried out for this molecule to convert the hydroxyl to an amino functional group (compound **2.70**). Second, a simple alkyl chain (ethyl) was linked to the amine at the R position to test the activity of the compound before coupling with an alkyl chain containing a dimethyl amino group at the end of the side chain. Unfortunately, the biological activity was lost in the resulting compound **2.50**, and compounds containing an amide linker **2.47** and **2.48**, also proved inactive. These results are in agreement with the previous conclusion: H-bonding at the R position is critical for the inhibitory potency of the molecule. Regardless of the effect of the different linkers, this strategy was not further examined, and the hydroxyl was considered as the optimal substituent at the R position.

2.6.3 Analysing the substituents on the 2-(4-hydroxyphenyl) acetonitrile ring

As the manipulation of the substitution on the quinazolin-4(3H)-one core as well as in the linker group did not show any improvement in potency, a series of modifications were introduced to the aromatic phenyl ring in **1.6** to explore the SAR of this region (Table 2-3).

Table 2-3: **SAR study of 2-(4-hydroxyphenyl) acetonitrile ring of 1.6.** The inhibition of PqsR activity was initially measured in the PAO1-L CTX::P_{pqsA}-lux strain of *P. aeruginosa* at 10 μM. NA, not active at 10 μM. All compounds showing a 50% or greater inhibition of activity were further analysed by concentration-response curves in PAO1-L CTX::P_{pqsA}-lux. The asterisk (*) indicates that this parameter was predicted using ChemDraw 19.0.1.28 (<http://www.chemaxon.com>). The sign (\$) indicates that the synthesis and biological evaluation was carried out by Fadi Soukarieh. The sign (£) indicates that the biological evaluation was carried out by Fadi Soukarieh.

					
Compound	R ₁	R ₂	R ₃	IC ₅₀ (μM) PAO1-L CTX::P _{pqsA} -lux	cLogP
^{\$} 2.73	H	H	CN	NA	2.3
^{\$} 2.74	H	CN	H	NA	2.3
^{\$} 2.75	H	CH ₂ CN	H	NA	2.1
^{\$} 2.76	H	H	CH ₂ CH ₂ CN	2.9 ± 1.2 ^a	2.4
[£] 2.34	H	H	OCH ₂ CN	4.5 ± 0.7 ^a	1.8
[£] 2.35	F	H	CH ₂ CN	2.2 ± 0.2 ^a	2.3
[£] 2.36	H	F	CH ₂ CN	6.4 ± 0.7 ^a	2.3
^{\$} 2.77	H	H	CH ₂ (CO)OH	NA	2.0
2.51	H	H	CH ₂ (CO)NH ₂	NA	1.1
^{\$} 2.78	H	H	(CO)CH ₂ CH ₃	NA	2.8

2.79	H	H		1.9 ± 0.0^a	2.1
2.53	H	H		NA	2.4
2.54	H	H		NA	2.1
2.37	H	H	O(C ₆ H ₅)	NA	4.3

Values reported as Mean \pm SEM of n = 3^a.

The SAR exploration of 2-(4-hydroxyphenyl) acetonitrile was initiated by finding the optimal length and position of the nitrile functional group. The aromatic nitriles in **2.73** and **2.74** with *para*- and *meta*- benzonitrile respectively, exhibited loss of activity. In addition, the analogue with *meta*- acetonitrile substitution **2.75** lost biological activity which proved the importance of the acetonitrile group at *para*- position. Extending the chain length by an extra methylene group or introduction of an ether bond between the phenyl and acetonitrile group in **2.76** or **2.34**, respectively maintained the activity. A further attempt to enhance the potency was rationalised by the crystal structure of **1.13** with PqsR (2.5.2) and achieved by introducing a fluorine atom at the *ortho*- (**2.35**) or *meta*- position (**2.36**) in order to gain a hydrogen bond interaction with the Tyr²⁵⁸ side chain. Unfortunately, **2.35** did not gain further potency, while the activity of **2.36** was reduced 2-fold.

Another approach focused on finding an appropriate bioisostere for the nitrile moiety that could maintain the activity and prevent the possibility of cyanide ions release during metabolism in biological systems.¹⁶⁵ The unique structural characteristic of the nitrile group with linear shape enables the moiety to fit readily into binding site sub-pockets of the receptor.¹⁶⁶ In addition, as a hydrogen bond acceptor, the lone pair of electrons on the nitrogen atom can form hydrogen

bond (HB) interactions with various protein residues.¹⁶⁶ Thus, this moiety has traditionally been considered as a bioisostere of carbonyl, hydroxyl and carboxyl groups.¹⁶⁶ In this study, the nitrile moiety was modified to a carboxylic acid **2.77**, an amide **2.51** and a ketone **2.78**, and all modifications led to the complete loss of inhibitory potency. These results indicate that the geometry and rigidity of the acetonitrile moiety, the length, and the lone pairs of the nitrogen are critical for activity.

Subsequently, different heterocycles were substituted on the *para*- position to replace the acetonitrile moiety and to enhance the physicochemical properties of the compound. The 1,2,4-oxadiazole ring in **2.79** was the best replacement for the acetonitrile moiety, with similar activity to the original hit **1.6**, while the 1,2,4-triazole **2.53** and tetrazole **2.54** analogues showed a loss in the activity. In addition, extending the *para*-position of the phenyl ring with a bulky phenoxy group **2.37** led to a loss of the activity and therefore the acetonitrile moiety at the *para*- position was conserved for all future SAR studies.

2.6.4 The analysis of **1.6** enantiomer activity.

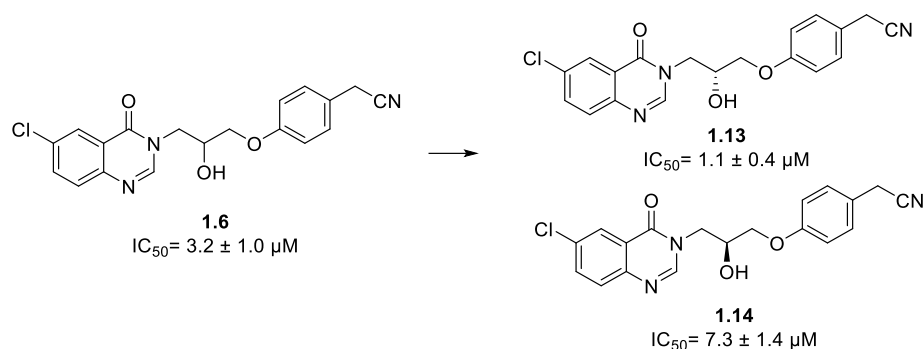


Figure 2-14: **Biological evaluation of 1.6 (racemic), 1.13 (R) and 1.14 (S).** The inhibition of PqsR activity was initially measured in the PAO1-L CTX::P_{pqsA}-lux strain of *P. aeruginosa* at 10 μM . **1.6** and **1.13** showed greater than 50% inhibition of activity and therefore further analysis by concentration-response curves measured in the PAO1-L CTX::P_{pqsA}-lux strain.

Although the two enantiomers of any chiral drug are identical in their NMR, IR and physical properties, 50% of chiral marketed drugs are a single enantiomer. This is because living systems are also chiral, and the two enantiomers of a chiral drug can behave very differently *in vivo*.¹⁶⁷ For example, one enantiomer may be responsible for the therapeutic effects of the drug whereas the other is inactive and/or contributes to side effects.¹⁶⁷ Owing to the FDA regulations for the development of new stereoisomeric drugs, it is critical at this stage of the project to determine the activity of both enantiomers.¹⁶⁸ As discussed before (Section 1.8), Soukariéh analysed the activity of the enantiomers of **1.6**. The analysis demonstrated that, the *R* isomer, **1.13** is the more active enantiomer, with slightly better potency (**1.13**, $IC_{50} = 1.1 \pm 0.4 \mu M$), while the *S* isomer, **1.14** was 7-fold less active (IC_{50} of $7.3 \pm 1.4 \mu M$).

2.7 Conclusion and future work

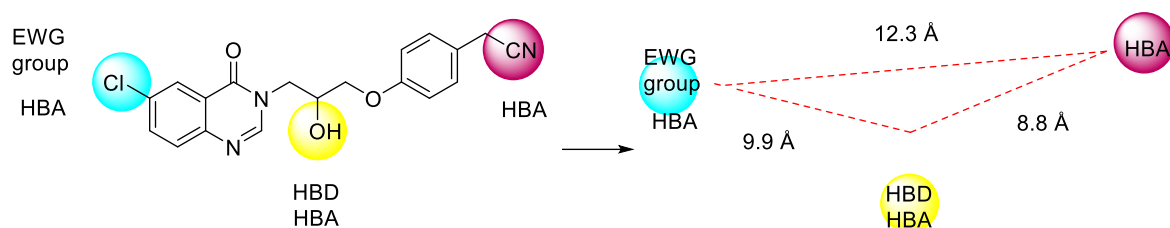


Figure 2-15: **Pharmacophore of quinazolin-4(3H)-one series.**

The SAR analysis of the original hit **1.6** showed that the hydroxyl functional group in the linker interacts with the binding site as a hydrogen bond donor or acceptor which is critical for biological activity. The co-crystal structure of **1.13** with PqsR (Figure 2-12) demonstrates the pharmacophore that is essential for PqsR antagonistic potency (Figure 2-15). The chlorine atom, which has an electron-withdrawing effect on QZN is essential for activity. In addition, other EWGs such as nitro or trifluoromethyl enhanced the inhibitory potency 6- or 7.5- fold, respectively. Thus, the chlorine atom or QZN may act as a hydrogen bond acceptor for the protein residue in the receptor. On the other hand, the role of the acetonitrile group in binding to the receptor is not clearly defined. The lipophilic interaction provided by this moiety, as well as the hydrogen bonding with the lone pair of N, could be why this moiety is critical for the activity. In addition, the acetonitrile moiety is sp hybridised and it could act as an electron-deficient pi system in π - π interaction with electron-rich aromatic ring (Tyr²⁵⁸) presents in the receptor.¹⁶⁹ This interaction was not provided by the bioisosteres of the nitrile functional group (carbonyl, hydroxyl and carboxyl groups), however the 1,2,4-oxazole ring was able to maintain this type of interaction.

Previous work indicated that any simple modification of the quinazolin-4(3H)-one series led to the loss, decrease or maintenance of biological activity similar to that of the original hit **1.6**. For this reason, a limited SAR for this series was carried out. The only modifications that

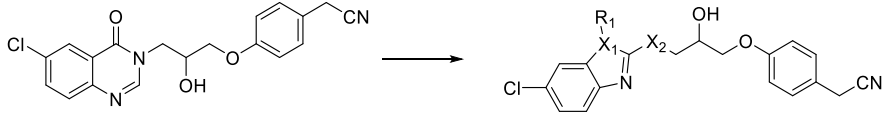
maintained similar or better activity were: 1) replacing the chlorine atom with a stronger EWG, enhancing the inhibitory potency by 6-fold and 7.5-fold in **2.73** and **2.75**, respectively; 2) introducing a hydrogen bond donor or acceptor at the hydroxyl position, which was critical for activity and; 3) introducing a 1,2,4-oxazole ring in **2.87**, which was the only analogue that maintained activity similar to that of the nitrile moiety. Finally, the triazole analogue **2.53** and the tetrazole analogue **2.54** lost activity, which could have been due, in part to cell permeability issues.¹⁷⁰ The focus of this project was to investigate scaffolds that probe the receptor to examine the molecular basis of PqsR receptor–ligand binding and inhibitor interactions. A deeper understanding of these interactions will support target-based antivirulence drug development that exploits PqsR as a virulence modulator in *P. aeruginosa*.

3 Hit to lead Optimisation of Novel 1*H*-benzo[*d*]imidazole based PqsR Inhibitors as Adjuvant Therapy to Treat *Pseudomonas aeruginosa* Infections

3.1 Background and aim of the project

In the previous chapter, a SAR study based on the quinazolin-4(3*H*)-one (QZN) scaffold as PqsR antagonists in *P. aeruginosa* was established. This study identified that introduction of an electron-withdrawing group to the 6- position of the quinazolin-4(3*H*)-one ring as well as the hydrogen bonding of the hydroxyl moiety within the linker group are ~~is~~ critical for inhibitory activity ~~as well as hydrogen bonding with the linker~~. The SAR analysis of **1.6** as a hit was limited, as any small modification in the molecular structure led to a loss of activity. Therefore, another study was established to replace the quinazolin-4(3*H*)-one core with different heterocyclic ring systems (Table 3-1). **An inspiration from the literature (compound 1.3), replacing the quinazolin-4(3*H*)-one ring with the 1-methyl-1*H*-benzo[*d*]imidazol-2-amine ring 3.1 enhanced activity 15- fold in comparison to 1.6. While replacing the quinazolin-4(3*H*)-one ring with benzo[*d*]oxazol-2-amine 3.2 and benzo[*d*]thiazol-2-amine 3.3 led to a loss of the inhibitory activity.** This confirms that the benzimidazole chemotype may be interacting with the receptor in a unique fashion relative to other heterocycles. In fact, this is the only ring that has a methyl substitution (**3.1**, R₁ = Me) which provides a key lipophilic interaction in the ligand binding site as eventually shown by X-ray crystallography. However, replacing the amine functional group in the linker with thiol moiety **3.4** lead to loss the activity. Compound **3.1** was an ideal hit with lead-like properties to start a SAR study. However, the synthesis of the 1-alkyl-1*H*-benzo[*d*]imidazol-2-amine ring proved challenging, especially with bulky substitutions, and therefore this chapter aims to find an appropriate synthetic route that provides a range of **3.1** analogues with reasonable yield and high purity.

Table 3-1: **The initial SAR study conducted by Soukarieh and it aimed to investigate different heterocycles replacing the QZN core in 1.6.** The inhibition of PqsR activity was measured initially in the PAO1-L CTX::P_{pqsA}-lux strain of *P. aeruginosa* at 10 μM concentration. Compounds showing inhibition of activity by 50% or more were further analysed by concentration-response curve measured in PAO1-L CTX::P_{pqsA}-lux and PA14 CTX::P_{pqsA}-lux strains. NA, not active at 10 μM concentration. NT, not tested in PA14 CTX::P_{pqsA}-lux strains. The asterisk (*) indicates that this parameter was predicted using ChemDraw 19.0.1.28 (<http://www.chemaxon.com>). The sign (\$) indicates that the synthesis and biological evaluation was carried out by Fadi Soukarieh.

						
	X ₁	X ₂	R ₁	IC ₅₀ (μM) PAO1-L CTX::P _{pqsA} -lux	IC ₅₀ (μM) PA14 CTX::P _{pqsA} -lux	cLogP *
^{\$} 3.1	N	NH	CH ₃	0.21 ± 0.04 ^a	0.20 ± 0.00 ^a	3.2
^{\$} 3.2	O	NH	-	NA	NT	3.0
^{\$} 3.3	S	NH	-	NA	NT	3.7
^{\$} 3.4	N	S	CH ₃	NA	NT	3.5

Values reported as Mean ± SEM of n = 6 ^a

The most potent and efficacious PqsR inhibitor reported to date is **1.3**, as identified by Rahme and colleagues (Figure 3-1).¹⁰³ In fact, the discovery of this compound was through the use of phenotypic high-throughput screening (HTS) of a library with over 280,000 compounds, followed by SAR analysis and biological evaluation of HAQ and pyocyanin production in the presence of 10 and 1 μM of the compounds. Indeed, the result from HTS showed that from the 17 successful compounds, eight shared a benzamide- benzimidazole scaffold which indicates the preference of this scaffold over other chemical families present in the library.

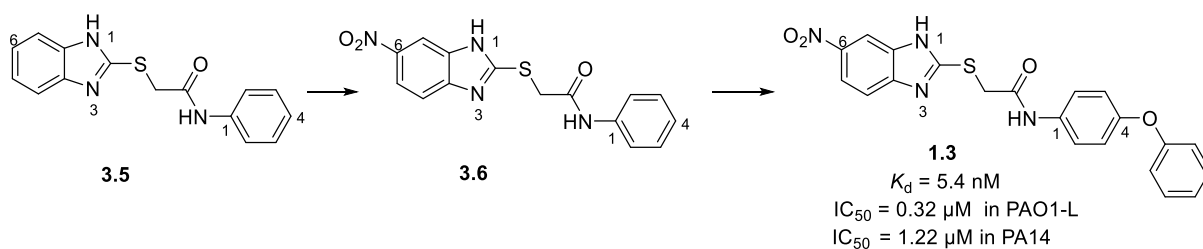


Figure 3-1: **Summary of SAR study conducted by Rahme and colleagues.**¹⁰³ It started with **3.5** by adding an electron withdrawing group to give **3.6**, the potency of HHQ and PQS inhibition was increased. Benzamide-benzimidazole derivatives containing a phenoxy substituted benzamide ring (**1.3**) was the best candidate in that series.¹⁰³ The study did not report IC_{50} values to make clear comparison however, the IC_{50} of **1.3** was determined in our lab by Ruiling Liu and the results reported.⁹⁹

Consistent with previous findings, the key features for antagonistic activity, identified from this study, are a strong electron-withdrawing group (nitro) in the 6- position of the benzimidazole ring, and a hydrophobic extension in the 4- position of the benzamide with the phenoxy group as an ideal substitution. The thioether linker was preserved in all analogues without further investigation.¹⁰³

3.2 Rationale of the design

The benzimidazole moiety is an important heterocycle which has a wide spectrum of physiological and pharmacological properties. It is the basic part of the vitamin B₁₂ structure as well as being considered a structural isostere of naturally occurring nucleotides.¹⁷¹ In addition, this nucleus is present in several FDA-approved agents and serves as a central core in marketed proton pump inhibitors, anthelmintics, anticancer agents, and vasodilators.¹⁷¹ According to PqsR inhibition, **1.3** with the benzamide-benzimidazole scaffold was the first compound that showed *in vivo* efficacy against acute and chronic infections in mice with nanomolar range activity against the PAO1-L strain.¹⁰³ This study provides new insight into the interaction between PqsR and the benzimidazole scaffold at the molecular level.¹¹² Furthermore, the initial SAR exploration discussed above demonstrated that replacing the

quinazolin-4(3*H*)-one ring with benzo[*d*]oxazol-2-amine **3.1** or benzo[*d*]thiazol-2-amine **3.2** led to a loss of the activity, while the 1-methyl-1*H*-benzo[*d*]imidazol-2-amine ring **3.1** enhanced activity 15-fold in comparison to **1.6**. This evidence supports the selection of **3.1** as an ideal hit to establish a SAR study aiming to enhance the potency and the physiochemical properties of the hit compound.

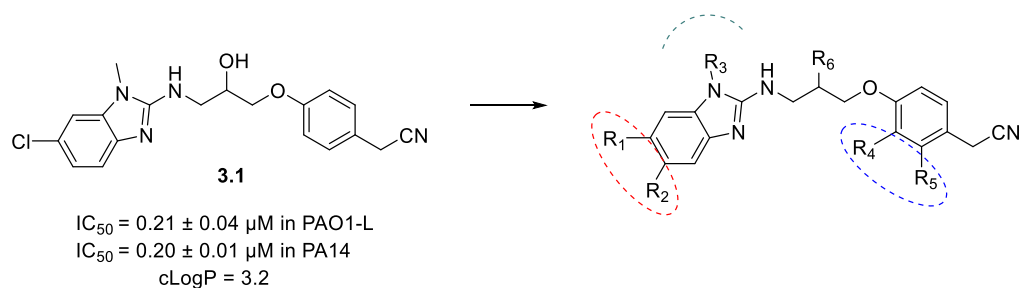


Figure 3-2: **The chemical structure of hit compound 3.1 and the design of the SAR study.** The aim of this study is to explore groups R_1 to R_6 .

The design strategy focused on three aspects: i) exploration of receptor-ligand interactions to build SAR; ii) exploration of the steric and lipophilic requirement for the key R_3 substituent; and iii) introduction of polar solubilising functional groups to enhance the drug-like properties of the series.

3.3 Results and discussion

3.3.1 Synthesis overview

Although the benzimidazole ring system is a privileged substructure among bioactive compounds,¹²⁴ the synthesis of 2-aminobenzimidazole is still challenging. Different synthetic strategies have been accordingly optimised in this study to obtain products with varied substitutions, with high yield and high purity.

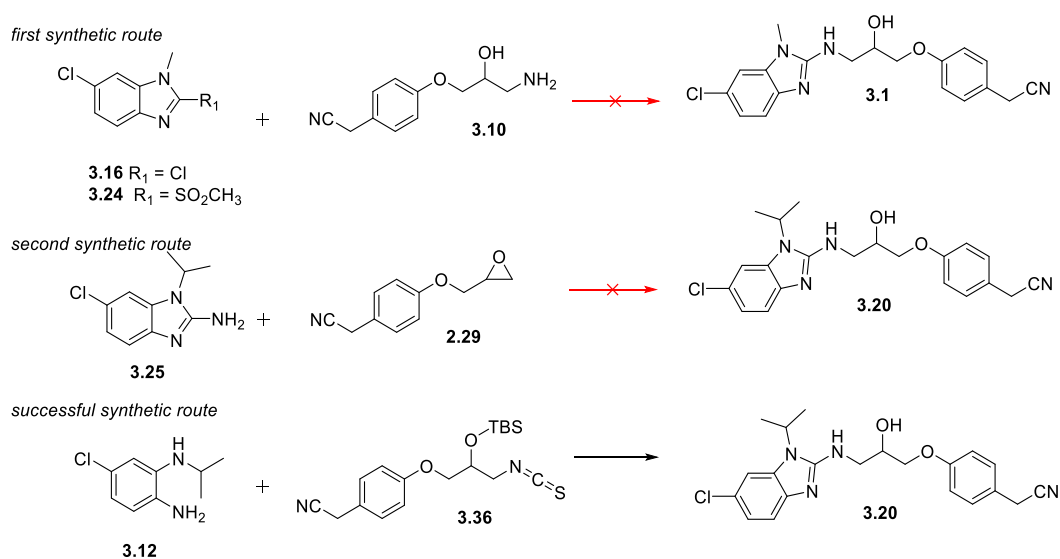
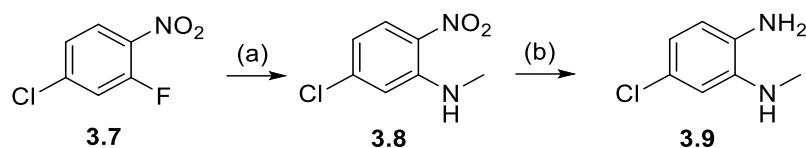


Figure 3-3: The synthetic routes employed in this project to synthesise the 2-aminobenzimidazole scaffold.

Three different synthetic routes were carried out in this chapter to furnish **3.1** or **3.20** employing different functional groups: 1-aminopropan-2-ol in **3.10**, epoxide in **2.29**, and isothiocyanate moiety in **3.36** (Figure 3-3).

Preparation of benzene-1,2-diamine starting material.

(Scheme 3-1): preparation of 4-chloro-*N*¹-methylbenzene-1,2-diamine **3.9**.



Reagent and condition: a) methylamine, MeOH, reflux, 16 h, 93%. b) Zn, NH₄Cl, 10% CH₃COOH; MeOH, rt, 1h, 90-95%.

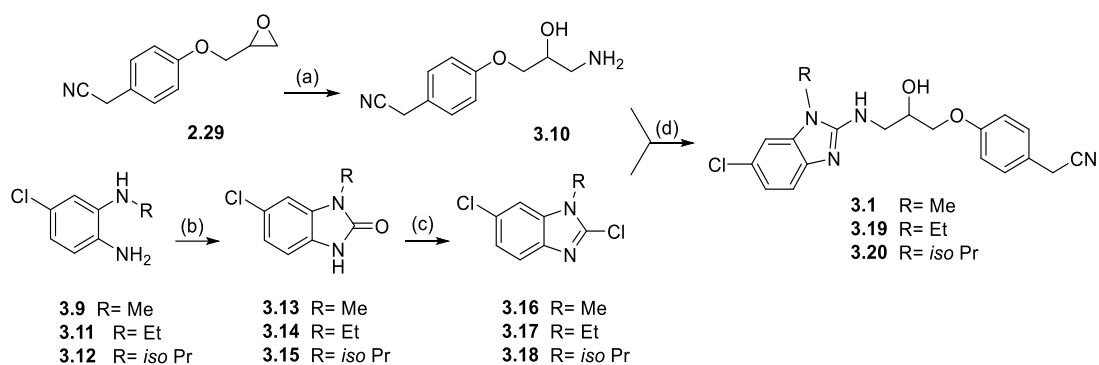
Practically, most syntheses of benzimidazoles start with benzene derivatives possessing nitrogen-containing functions *ortho*- to each other **3.9**. 1-Fluoro-2-nitrobenzene is the immediate precursor to furnish **3.8** as an intermediate. The preparation of this scaffold was initiated by substituting the fluorine atom in **3.7** with methylamine in order to furnish **3.8**.¹⁷²

The type of reaction shown here is the addition–elimination mechanism. The amine adds to the carbon atom attached to the fluorine atom and the negative charge is delocalised through the aromatic ring and stabilised by the nitro group presented on the *ortho*- position to the fluorine atom. Following this, the negative charge will move again toward the tetrahedral carbon intermediate and push the electrons to the fluorine atom as a leaving group. The presence of an electron-withdrawing group in *ortho*- or *para*- position to the leaving group is critical for this type of reaction.

Subsequently, the nitro group was reduced to the amine using a metal reducing reaction with Zn as an electron transfer reagent and proton source (AcOH, NH₄Cl) in order to furnish the benzene-1,2-diamine moiety **3.9**. The selection of these conditions over the more common method of nitro reduction (catalytic hydrogenation) was for a chemo-selectivity issue, as catalytic hydrogenation could remove the chlorine atom present in the scaffold in addition to reducing the nitro functional group.¹⁷³

3.3.2 The first synthetic route employing amino functional group in **3.10**

(Scheme 3-2): preparation of **3.1** and **3.19**, **3.20**. (This scheme was conducted by Fadi Soukarieh).

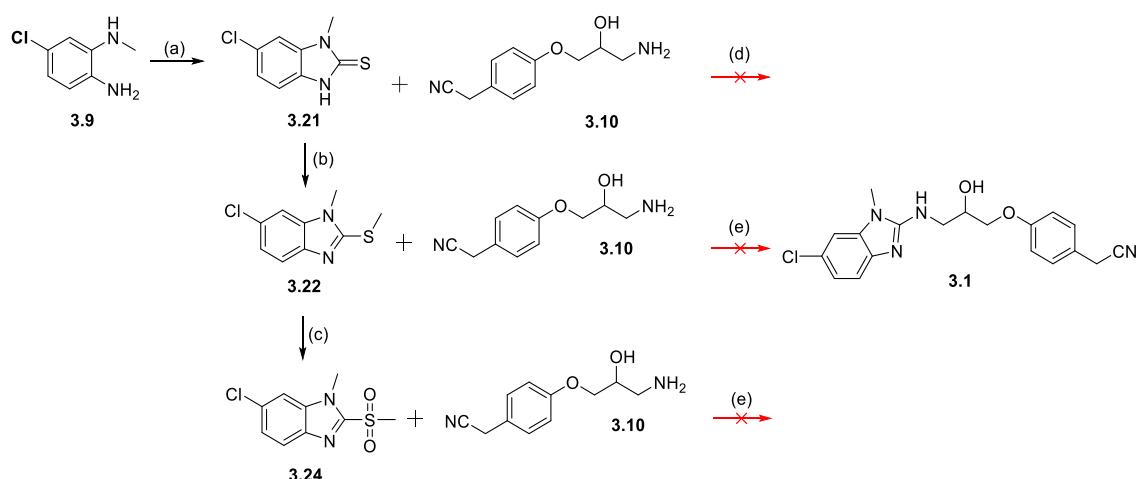


Reagent and condition: a) NH_3/MeOH , rt, 16 h, 80%. b) CDI, DCM, 50°C , 3h. c) POCl_3 , neat, 90°C , 16h. d) MW, Et_3N , EtOH, 180°C , 3h. 10-25%.

The first approach to prepare **3.1** was by coupling two intermediates: 2,6-dichloro-1-alkyl-1*H*-benzo[*d*]imidazole **3.16** and 1-amino-3-propan-2-ol **3.10**.

*Preparation of 1H-benzo[*d*]imidazole series (3.1 and 3.19, 3.20).* 2,6-Dichloro-1-methyl-1*H*-benzo[*d*]imidazole **3.16** was reacted with 2-(4-(3-amino-2-hydroxypropoxy) phenyl) acetonitrile **3.10** to furnish the final product under microwave irradiation, as shown in Scheme 3.2 to give 2-(4-(3-((6-chloro-1-methyl-1*H*-benzo[*d*]imidazol-2-yl) amino)-2-hydroxypropoxy) phenyl) acetonitrile, **3.1**. In addition, the same strategy was applied to synthesise **3.19** and **3.20** analogues. However, this strategy was not efficient enough to synthesise a library of analogues for the SAR study, as the yield was poor (10-25% purified yield) for the successful reactions hence for bulkier analogues the synthesis strategy was modified.

(Scheme 3-3): preparation of **3.1** employing **3.10** & **3.21**, **3.22** and **3.24**.



Reagents and conditions: (a) CS₂, Et₃N, EtOH, rt, 16 h, 83%. (b) CH₃I, NaOH, MeOH, (C₂H₅)₂O, rt, 16 h, 56%. (c) oxone, MeOH, H₂O, rt, 16 h, 42%. (d) Et₃N, HgCl₂, DCM 0° C, 30 min then rt for 16h. (e) MW, Et₃N, MeCN, 150°C, 4h.

*Preparation of thiourea **3.21**, methyl thiol **3.22** & sulfonyl methane **3.24**.* By maintaining the 1-aminopropan-2-ol moiety in **3.10** as a nucleophile, an alternative approach was adopted by changing the chlorine leaving group in **3.16** to a more stable conjugate base, such as the sulfonyl-methane moiety **3.24**, which can stabilise the resulting negative charge by delocalisation over the two oxygen atoms.

The synthesis started with substituted benzene-1,2-diamine moiety **3.9** reaction with carbon disulphide to furnish the thiourea **3.21**. Compound **3.21** was then alkylated by methyl iodide in basic conditions to afford **3.22**. It is noteworthy that the electrophilic carbon of methyl iodide is considered a soft electrophile because its orbitals are diffuse, and it is uncharged giving the chemo-selectivity toward thiol alkylation over the nitrogen. This is because, thiol is considered a soft nucleophile as it is a large atom with diffuse high-energy electrons. However, the nitrogen is considered a hard nucleophile and its reaction is dominated by charges and electrostatic effects. The interaction here is dominated by the polarisable orbital interaction making the thiol alkylation more favourable.

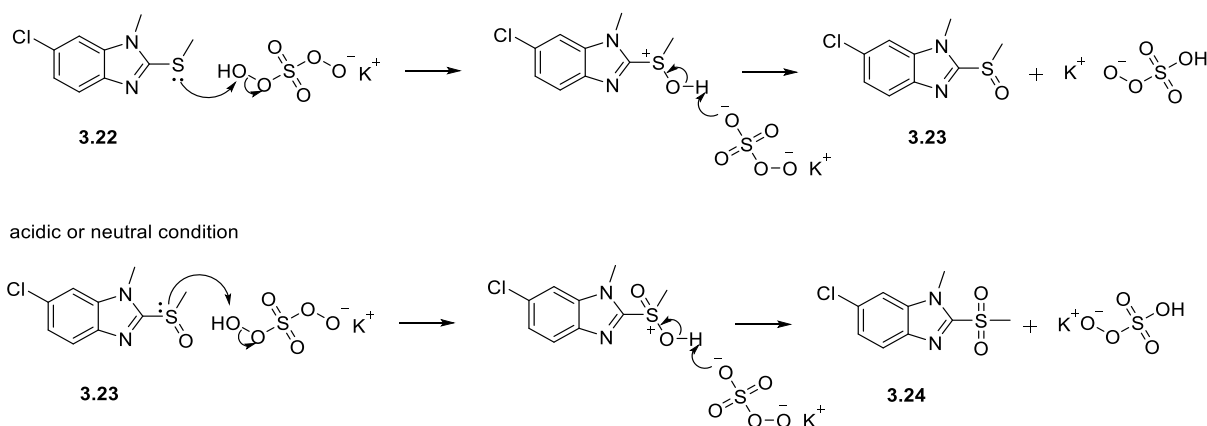


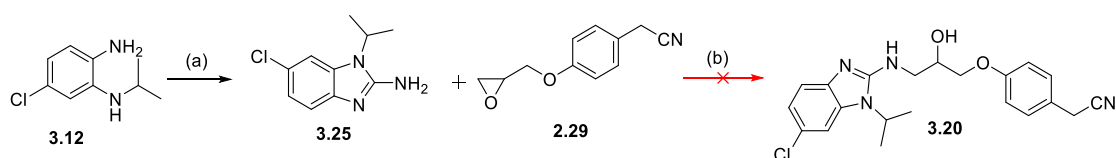
Figure 3-4: **The mechanism of sulfide oxidation.** Sulfide in **3.22** was oxidized to sulfoxide **3.23** and subsequently to sulfone **3.24**.

The following step was to oxidise the sulphur atom with Oxone to furnish the sulfonyl-methane moiety **3.23**. Oxone is a stable mixture of potassium peroxymonosulfate, potassium hydrogen sulfate, and potassium sulfate ($\text{KHSO}_5 \cdot \frac{1}{2} \text{KHSO}_4 \cdot \frac{1}{2} \text{K}_2\text{SO}_4$) which is considered an alternative to hydrogen peroxide with high selectivity to sulfides in the presence of other functional groups.¹⁷⁴ It is the salt of peroxy-acid which has an extra oxygen atom between the carbonyl group and its acidic hydrogen; therefore, it is less acidic than carboxylic acids because its conjugate base is no longer stabilised by delocalisation into the carbonyl group. However, it is electrophilic at the extra oxygen, because the nucleophilic attack at the electrophilic oxygen generates carboxylate_sulfonate, which is a good leaving group. The first step of sulfide oxidation to sulfoxide **3.23** is the sulfur atom attacking the terminal oxygen of the peroxide group followed by the breakage of the peroxide bond, resulting in the formation of an alkoxy anion and a protonated sulfoxide. Proton exchange yields the sulfoxide and the alcohol corresponding to the peroxide. This is faster and the rate-determining step of the reaction. Following that, the oxidation of sulfoxide to sulfone in neutral condition follows the same mechanism described in the first step, as described in Figure 3-4.¹⁷⁵

Preparation of 1H-benzo[d]imidazole 3.1. The coupling of the amine functional group was investigated with the three moieties (thione, methyl thiol and sulfonyl-methane) in **3.21**, **3.22** and **3.24**, respectively. According to the literature, a similar substrate was employed with a thiourea moiety to displace the thione with a primary amine using a basic condition in the presence of mercury (II) chloride, resulting in different asymmetrical *N,N*-disubstituted guanidine with a good yield.¹⁷⁶ The same condition was applied here to displace the thione moiety in **3.21** with the primary amine of **3.10**. Unfortunately, the reaction did not work, and no product was obtained. Moving to displace the methyl thiol **3.22** or sulfonyl-methane **3.24** with the primary amine in basic conditions, refluxing the two building blocks or using microwave irradiation did not enhance the efficiency of the coupling reaction.

3.3.3 The second synthetic route employing epoxide moiety in 2.29

(Scheme 3-4): synthesis of 6-chloro-1-isopropyl-1*H*-benzo[*d*]imidazol-2-amine.



Reagents and conditions: (a) BrCN, MeOH, H₂O, 60°C, 3 h, 85% (b) MW, EtOH, 150°C, 30 min.

Preparation of 6-chloro-1-isopropyl-1H-benzo[d]imidazol-2-amine 3.25. The strategy of synthesis was modified further by preparing the 6-chloro-1-isopropyl-1*H*-benzo[*d*]imidazol-2-amine **3.25** employing 1,2 diamino benzene **3.12** with cyanogen bromide.¹⁷⁷

The synthesis proved a straightforward process carried out in a protic solvent to stabilise the generated bromide ion and generate the 1*H*-benzo[*d*]imidazol-2-amine scaffold in good yield. Following this, **3.25** was refluxed with the epoxide moiety in basic condition using Et₃N as a base and EtOH as a solvent. Following the reaction using LC-MS showed the formation of peak with desired MW (399.1) with a different retention time *t_R* (2.18) while the retention time

t_R of **3.20** is 2.23. In addition, the retention factor R_f of the TLC showed that the product was more polar than the previously prepared **3.20**.

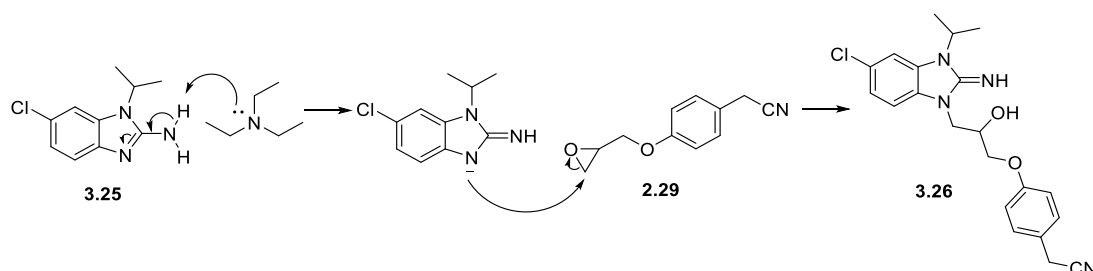


Figure 3-5: Proposed mechanism of the guanidine moiety synthesis in **3.26**.

This result indicates that the other regioisomer with a guanidine moiety, 2-(4-(3-(5-chloro-2-imino-3-isopropyl-2,3-dihydro-1H-benzimidazol-1-yl)-2-hydroxypropoxy) phenyl) acetonitrile **3.26** was synthesised. The proposed mechanism of this reaction is illustrated in Figure 3-5. In addition, this reaction was carried out in neutral and acidic conditions to investigate the effect of these conditions on the regioisomer selectivity. Unfortunately, all the conditions produced the undesired product **3.26** according to TLC and LC-MS analysis in comparison to **3.20**.

The first evidence to support this hypothesis was analysing the biological activity of **3.26** in comparison to DMSO as a negative control and **3.20** as a positive control at 10 μM concentration (Figure 3-6). This analysis showed that the product of the reaction mentioned above is not active which confirmed that different regioisomer was synthesised.

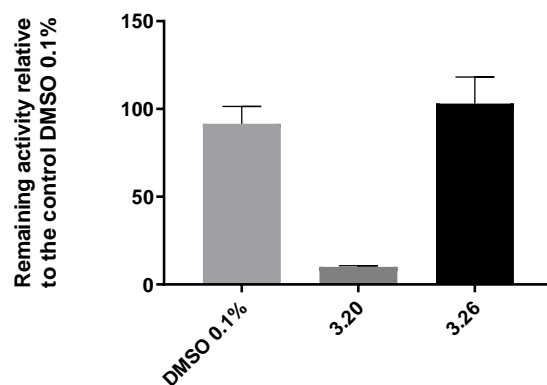


Figure 3-6: measuring the remaining activity of **3.26** and **3.20** as a positive control at 10 μ M concentration in cell-based reporter gene assay employing PAO1-L CTX::*P_{pqsA}-lux* strain.

Furthermore, the comparison between ^{13}C NMR spectra of the previously synthesised compound, 2-(4-(3-((6-chloro-1-isopropyl-1*H*-benzo[*d*]imidazol-2-yl) amino)-2-hydroxypropoxy) phenyl) acetonitrile, **3.20** and the product of this reaction, **3.26** showed that the peaks of some carbons in the aromatic regions appear in different positions as shown in Figure 3-7. This confirms that a different regioisomer of **3.20** was synthesised.

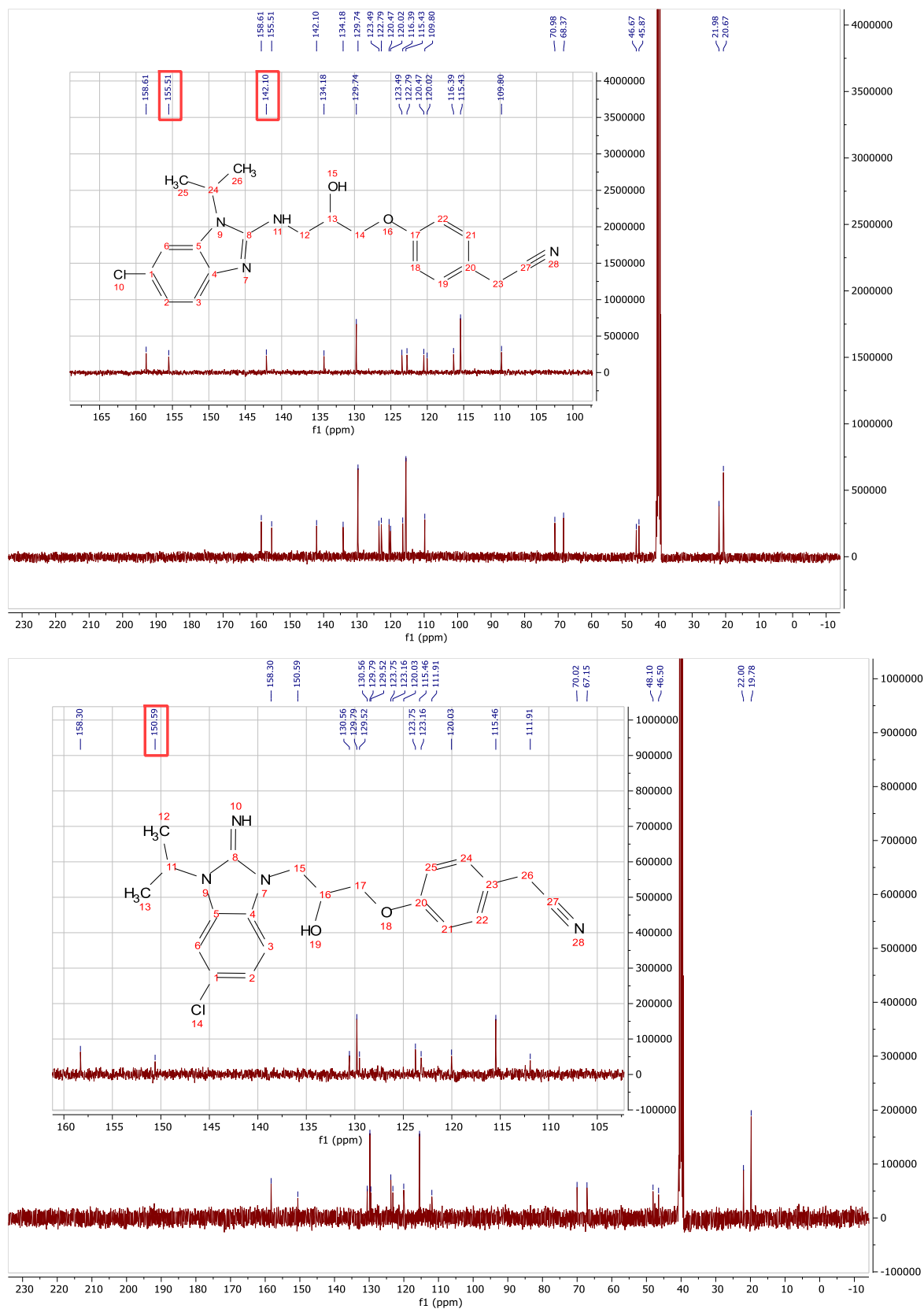
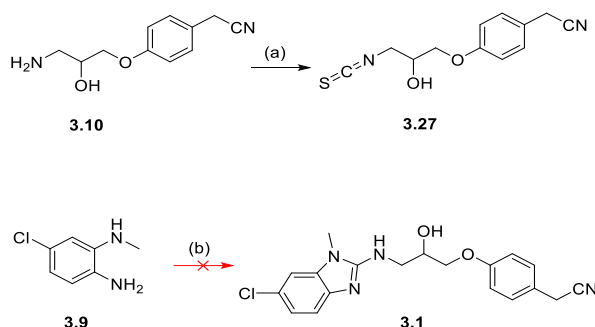


Figure 3-7: The ¹³C NMR spectra of 2-(4-(3-((6-chloro-1-isopropyl-1*H*-benzo[*d*]imidazol-2-yl) amino)-2-hydroxypropoxy) phenyl) acetonitrile, **3.20** (above) and 2-(4-(3-(5-chloro-2-imino-3-isopropyl-2,3-dihydro-1*H*-benzo[*d*]imidazol-1-yl)-2-hydroxypropoxy) phenyl) acetonitrile **3.26** (below) with enlarged section of the aromatic region, in DMSO-*d*₆ solvent at 100.66 MHz.

3.3.4 The third synthetic route employing isothiocyanate moiety.

Finally, the focus was directed to a more promising pathway employing isothiocyanate moiety **3.27** which was reacted with 1,2-diaminobenzene **3.9** followed by cyclisation to the benzimidazole ring.

(Scheme 3-5): the initial synthetic design employing isothiocyanate **3.27**.

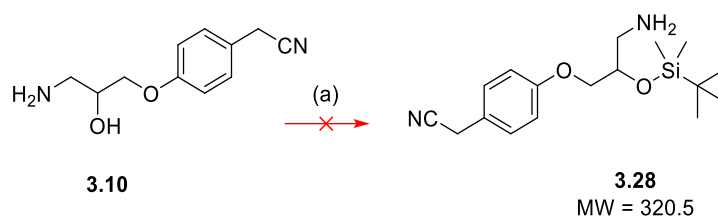


Reagent and conditions: (a) thio-CDI, DCM, inert atmosphere, rt, 16 h, 55%. (b) **3.27**, EtOH, 70 °C, 16 h.

Preparation of isothiocyanate 3.27. The preparation of isothiocyanate moiety was successful by reacting the amino functional group in **3.10** with thio-CDI to produce the required compound **3.27**.¹⁷⁸ Subsequently, the generated intermediate **3.27** refluxed with benzene-1,2-diamine **3.9** in ethanol. However, no product was detected from this coupling. The critical issue in this step was the presence of hydroxyl as a nucleophile and the carbon of isothiocyanate as an electrophile, which could lead to the internal cyclisation of the compound and as a result the coupling did not take place in the next step.

Protection of hydroxyl functional group. Therefore, the alcohol was protected by employing Corey's condition.¹⁷⁹ It was reported that the use of *tert*-butyl dimethyl silyl chloride (TBDMS-Cl) reacting with alcohol was not successful, even with elevated temperature or using excess reagent (TBDMS-Cl). However, using 2.5 equivalent of imidazole resulted in enhancement of the efficiency of the reaction with various alcohols to produce a range of silyl ethers.¹⁷⁹

(Scheme 3-6): Protection of hydroxyl functional group in **3.10**.



Reagent and conditions: a) TBDMS-Cl, imidazole, DMF, rt, 16 h.

The LC-MS detection of the product showed that the MW of the compound is 349 instead of the expected MW 321, which means a side reaction could have occurred. The R_f of the TLC and t_R in the LC-MS hints that the product is more lipophilic than expected. In addition, the ^1H NMR of the product showed that there is an extra peak of around 8 ppm in the aromatic region; the expectation of this finding is that the hydroxyl group was protected with *tert*-butyl dimethyl silane, as well as the amino group interacting with the solvent **3.29**. The proposed mechanism of this reaction is illustrated in Figure 3-8. It is worth mentioning that changing the solvent to DCM or MeCN diminished the efficiency of the reaction and no product was detected, which is in agreement with recent work reported by Patschinsk *et al.*¹⁸⁰ This work demonstrated the catalytic activity of DMF over other polar solvents such as DCM and chloroform, even in the presence of highly active catalysts.

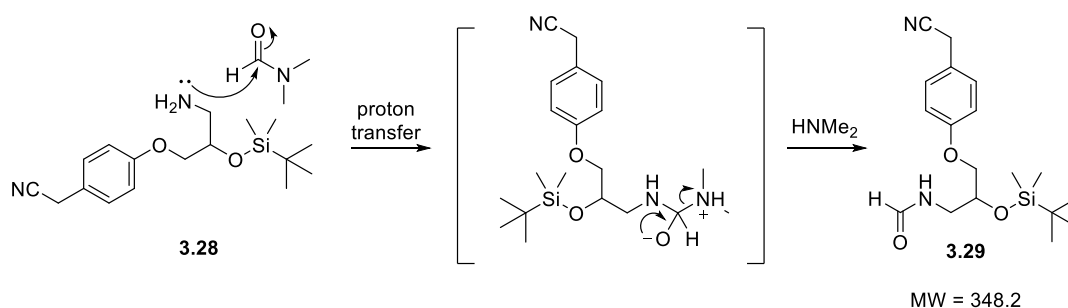


Figure 3-8: **The proposed mechanism of the side reaction with DMF.**

Therefore, it was important to open the epoxide moiety in **2.29** with a reagent that cannot undergo further reaction. Sodium azide, which is a very well-known amine synthon, is a

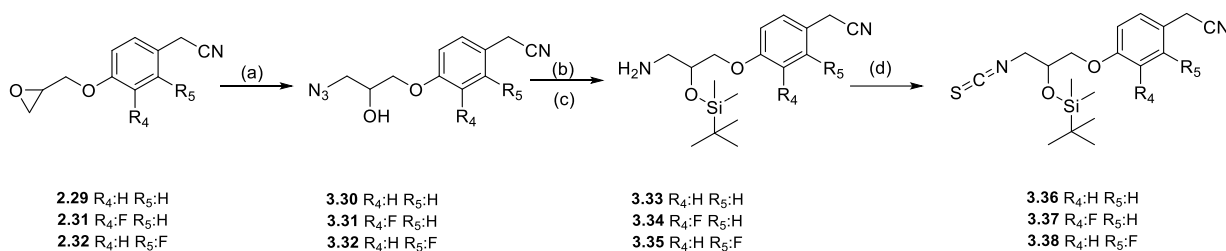
reagent of choice and it could act as temporary protecting group in a subsequent alcohol protection reaction. Afterwards, the azide is reduced to the amine, employing the Staudinger reaction, which then was reacted with thio-CDI to afford the isothiocyanate moiety as proved by ^{13}C -NMR (see the appendix).

3.3.5 The design of the final synthetic route of 2-aminobenzimidazole series

To sum up, all the findings from the previous approaches led to the design of the synthetic route illustrated in this section.

Preparation of isothiocyanate intermediate. The successful synthetic scheme started by opening the epoxide ring with NaN_3 in a protic solvent in the presence of NH_4Cl .¹⁸¹ Following that, the hydroxyl functional group was protected with *tert*-butyl dimethyl silane.¹⁷⁹ The azide moiety was then reduced to the corresponding amine using the Staudinger reaction which produced a cleaner reaction mixture than catalytic hydrogenation. The generated amine was reacted with thio-CDI to afford the desired isothiocyanate moiety (Scheme 3-7).

(Scheme 3-7): synthesis of isothiocyanate intermediate **3.36** - **3.38**.

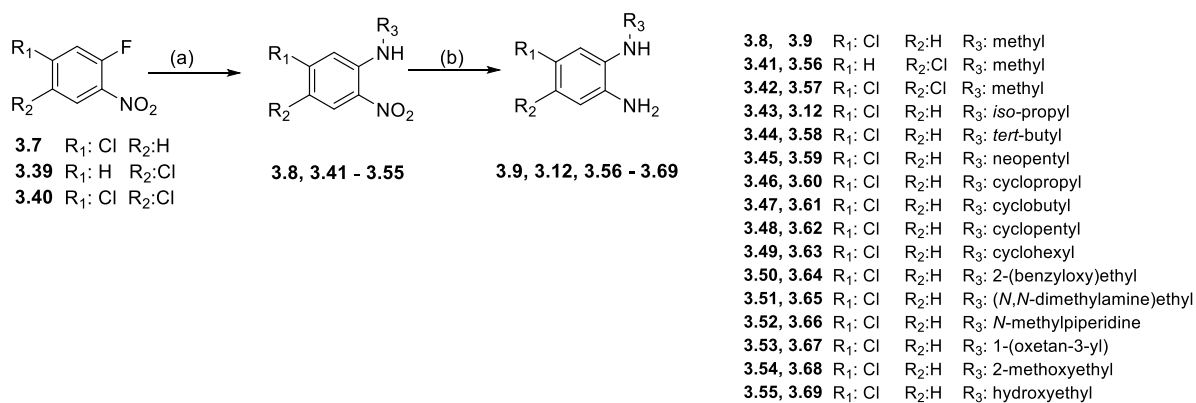


Reagent and conditions: a) NaN_3 , NH_4Cl , EtOH 40°C, 16 h, 99%. b) TBDMS-Cl, imidazole, DMF, rt, 16 h, 84%. c) PPh_3 , 10% H_2O ; THF, rt, 16h, 90%. d) thio-CDI, DCM, inert atmosphere, rt, 16 h, 25%.

Preparation of benzene-1,2-diamine 3.9 analogues. The synthesis of all benzene-1,2-diamine intermediates **3.12** and **3.58-3.71** followed the same procedure, for compound **3.9** (Scheme 3-8). The synthetic pathway was initiated by substituting the fluorine atom in 1-fluoro-2-

nitrobenzene with different amines, followed by reducing the nitro functional group to the corresponding amine.

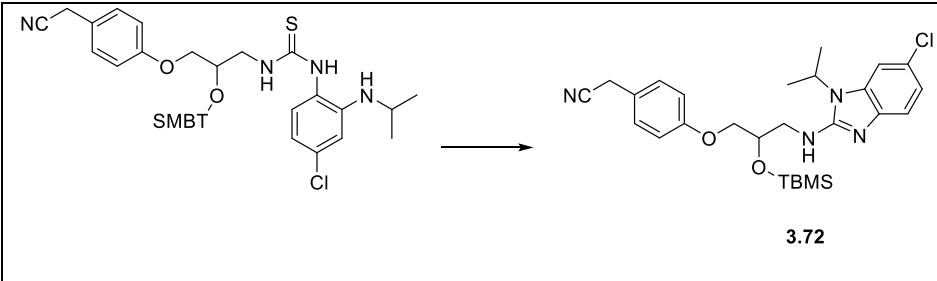
(Scheme 3-8): synthesis of benzene-1,2-diamine intermediates, **3.9**, **3.12** and **3.56-3.69**.



Reagent and conditions: a) Different amines, MeOH, reflux, 16 h, 95%. b) Zn, NH₄Cl, 10% CH₃COOH in MeOH, rt, 1h, 95%.

The cyclisation of thiourea moiety. Later on, the isothiocyanate moiety was reacted with various substituted 1,2-diaminobenzenes.¹⁷⁸ Depending on the literature, different conditions were examined to find out the best method to activate the sulfur and cyclise the thiourea moiety in the compound and furnish the 2-aminobenzimidazole scaffold, as shown in Table 3-2.

Table 3-2: **The most common methods for thiourea cyclisation.** They were reviewed from <https://www.reaxys.com> and the yields of the test reactions were estimated according to TLC and LC-MS analysis.

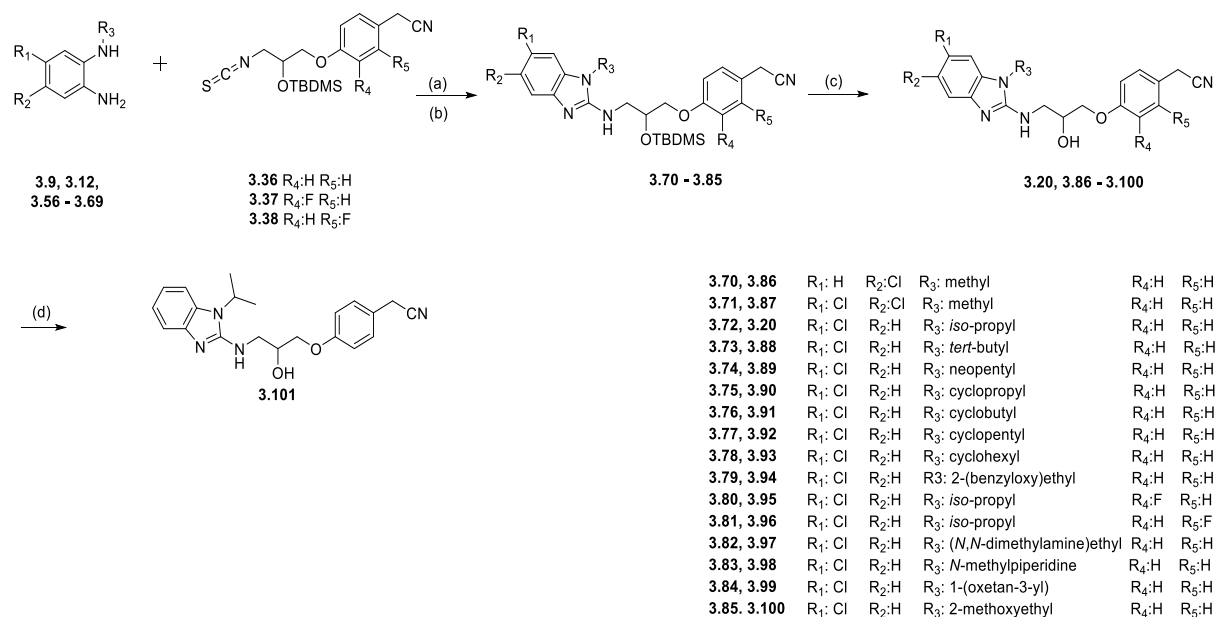
			
	Coupling reagent	Temperature °C	Solvent
1	<i>N,N'</i> -Di- <i>iso</i> propyl carbodiimide (DIC)	80	DMF
2	1,1'-Carbonyldiimidazole (CDI)	80	DMF
3	1-Ethyl-3-(3-dimethylaminopropyl) carbodiimide (EDCI)	70	THF
4 ¹⁸²	EDCI	rt	THF
5 ¹⁸²	CH ₃ I	rt	EtOH
6 ¹⁸³	HgO, S	70	EtOH
7 ¹⁸⁴	Benzotriazol-1-yl oxy tris (di-methyl amino) phosphonium hexafluorophosphate (BOP), 1,8-diazabicyclo [5.4.0] undec-7-ene (DBU)	rt	CH ₃ CN
8	Acetic acid	90	EtOH

Entry 1 was selected as the best condition to provide ring closure of thioureas by sulfur activation with DIC with a good yield observed from LC-MS analysis.

The deprotection of the silyl group. Finally, the deprotection of the silyl group was examined under two different conditions: TBAF in anhydrous THF under inert atmosphere, or 10% TFA in MeOH at room temperature. The first condition seems to be rather harsh, as the LC-MS detection of the reaction mixture did not show either the starting material or the desired product. The second condition was successful to show the desired product with a good yield, although the reaction was carried out over a long time (48h).

(Scheme 3-9 illustrates the final synthetic route to synthesise the 2-aminobenzimidazole scaffold with different substitutions on the benzimidazole or the phenyl ring.

(Scheme 3-9): General Synthesis of 2-aminobenzimidazole analogues, **3.20**, **3.86 – 3.101**.

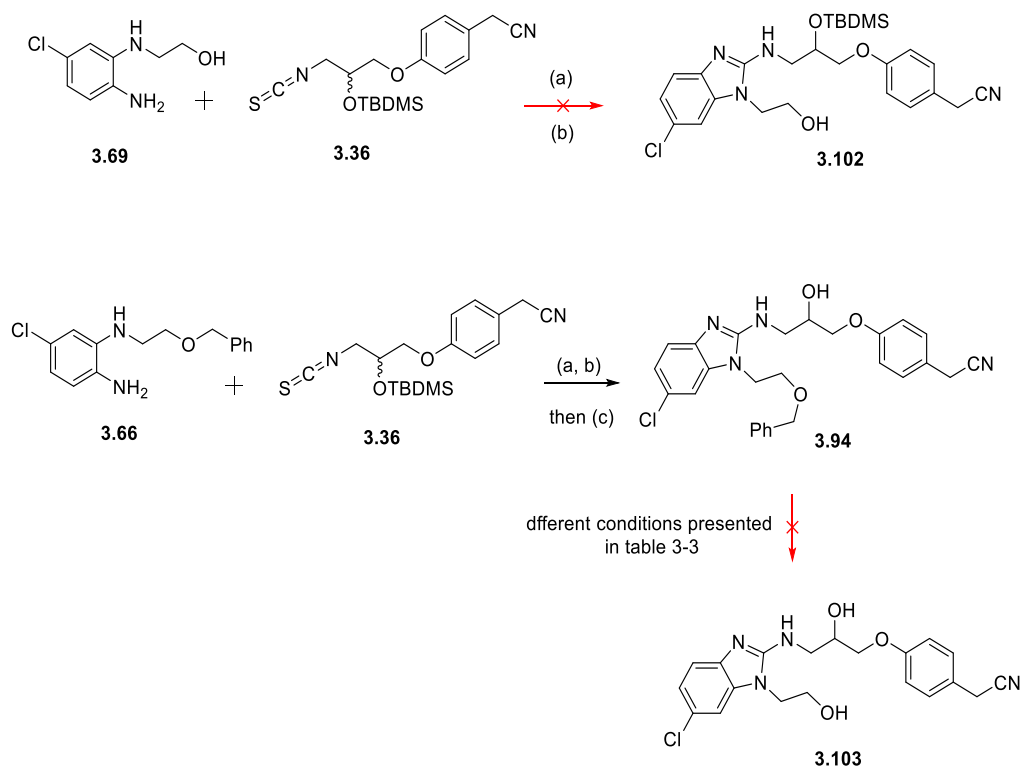


Reagent and conditions: a) EtOH, reflux, 16 h. b) DIC, Et₃N, DMF, reflux, 16 h, 65%. c) 10 % TFA in MeOH, rt, 48h 60%. d) **3.20**, 10% Pd on activated carbon (20% w/w), H₂, MeOH, rt, 16 h, 95%

Synthesis of 3.101 analogue. Employing **3.20** under catalytic hydrogenation with 10% Pd led to substituting the chlorine in R₁ with hydrogen and produce **3.101** analogue.

Synthesis of 3.103 analogue. The synthesis of **3.103** was challenging and there were many attempts carried out to synthesise this analogue, summarised in the following (Scheme 3-10).

(Scheme 3-10): different synthetic routes to synthesis **3.103**.

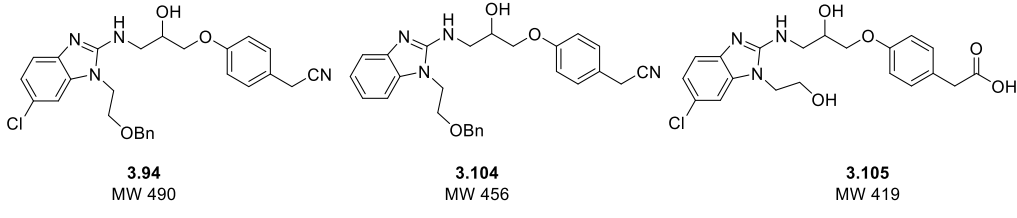


Reagent and conditions: a) EtOH, reflux, 16 h. b) DIC, Et₃N, DMF, reflux, 16 h, 65%. c) 10 % TFA in MeOH, rt, 48h 60%.

The initial attempt to synthesise **3.103** failed with **3.69** as a starting material, which has an unprotected hydroxyl group that could interfere with the coupling process, and therefore this alcohol should be protected.

3.94 was prepared successfully according to the general procedure illustrated in (Scheme 3-8). However, the deprotection of the benzyl group was challenging and a series of hydrogenolytic conditions were examined to furnish **3.103** (Table 3-3).

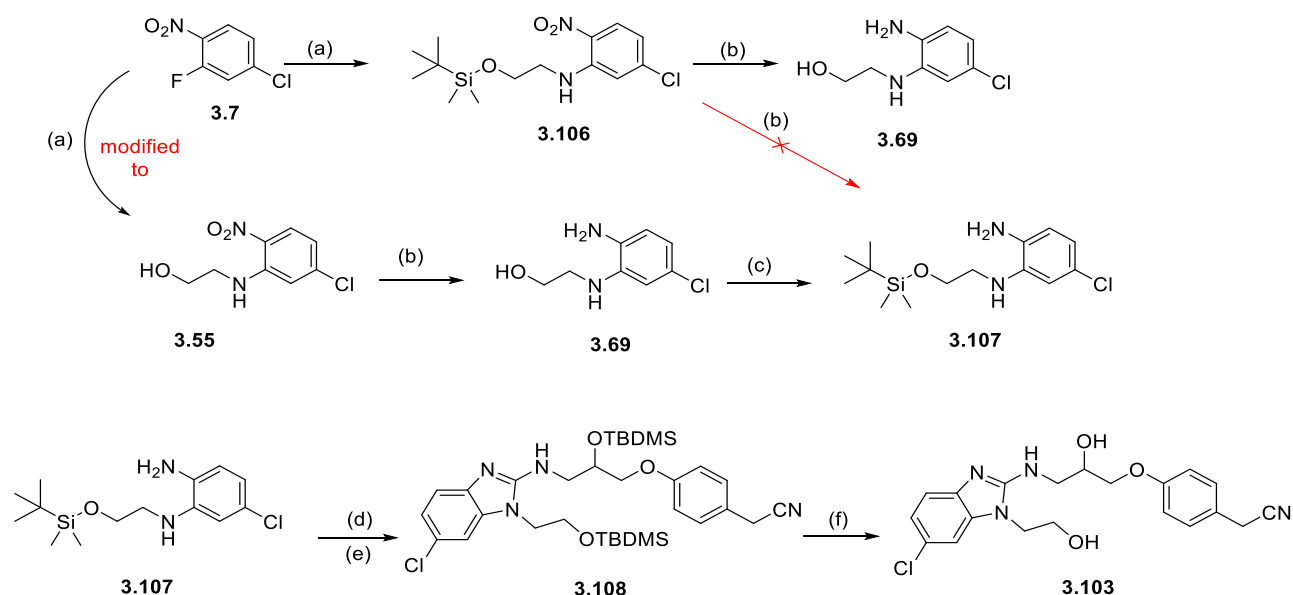
Table 3-3: **Different conditions were applied to remove the benzyl group.** The progress of the reactions was monitored by TLC and LC-MS analysis.

					
	Catalyst ^a or Scavenger ^b	H ₂ source	Solvent	Temperature °C	product
1	Pd ^a	Balloon of H ₂	MeOH	rt	3.104
2	-	4 M HCl	dioxan	rt	3.105
3	Triisopropyl silane ^b	solvent	TFA	60	3.105
4	Triisopropyl silane ^b	solvent	50% TFA/MeOH	rt, until reflux	3.94
5	Zn ^a	HCO ₂ NH ₄	MeOH	rt	3.94
6	Pd ^a	HCO ₂ NH ₄	MeOH	rt	3.105

The initial attempt at using a catalytic amount of 10% Pd on activated carbon (20% w/w) in MeOH under hydrogen led to substitution of the chlorine on the aryl halide with a hydrogen atom **3.104**. Application of strongly acidic conditions is reported in the literature as an efficient strategy in the ~~hydrogenolysis~~-hydrolysis of the *O*-benzyl group. However, the conditions in entry 2 and 3 (Table 3-3) led to hydrolysis of the nitrile functional group to give the carboxylic acid **3.105**. The role of triisopropyl silane in this reaction was to irreversibly scavenge the resulting reactive benzyl cation.¹⁸⁵ On the other hand, reducing the concentration of TFA to 50% led to reduced efficiency of the reaction, and no product was obtained. Furthermore, using ammonium formate (entry 5 and 6) with Zn or Pd afforded the starting material **3.94** or **3.105**, respectively.

Another approach to synthesise **3.103** using *tert*-butyl dimethyl silyl as a protection group was employed. This approach started by fluorine atom displacement in **3.7** with 2-((*tert*-butyl dimethyl silyl) oxy) ethan-1-amine and was subsequently reduced, employing acidic conditions. The silyl group is labile to these conditions (AcOH and zinc) and as a result the hydroxyl group was deprotected **3.69**. Therefore, the synthetic design was modified as illustrated in (Scheme 3-11).

(Scheme 3-11): synthesis of starting materials employed in **3.103** preparation.



Reagent and conditions: a) 2-((*tert*-butyl dimethyl silyl) oxy) ethanamine for **3.106** and 2-aminoethan-1-ol for **3.55**, MeOH, reflux, 16 h, 95%. b) Zn, NH₄Cl, 10% CH₃COOH in MeOH, rt, 1h, 95%. c) TBDMS-Cl, imidazole, DMF, rt, 16 h, 81%. d) **3.36**, EtOH, reflux, 16 h. e) DIC, Et₃N, DMF, reflux, 16 h, 65%. f) 10 % TFA in MeOH, rt, 48h 60%.

The last synthetic route was successful and provided the desired product after deprotection of the silyl group in the last step of the synthetic procedure (Scheme 3-11) using 10% TFA in methanol.

In conclusion, a synthetic procedure of 2-aminobenzimidazole series was developed here to furnish a range of analogues in good yield. The successful strategy was achieved by treating the substituted benzene-1,2-diamine with various isothiocyanates to afford substituted

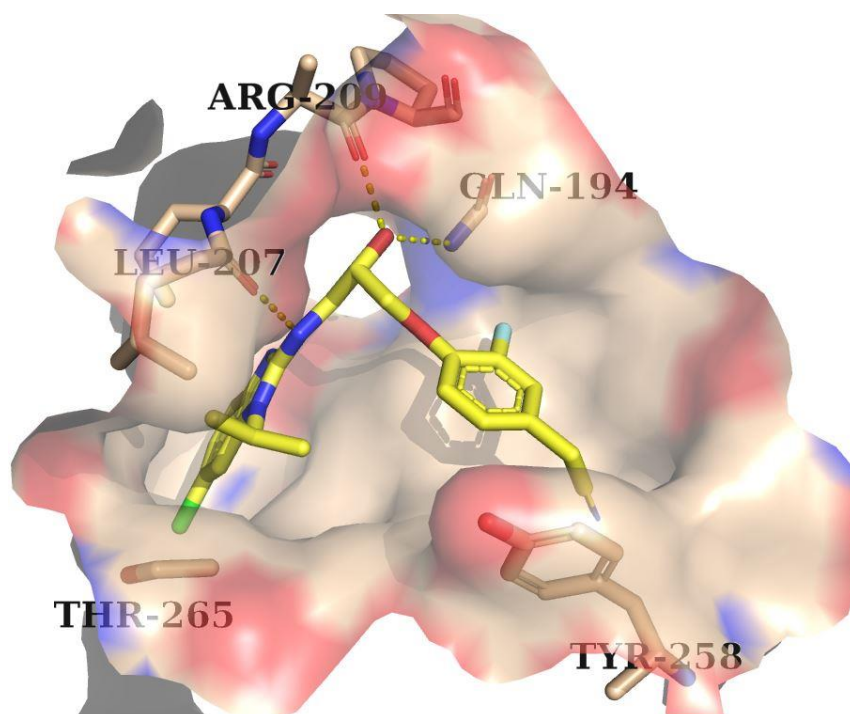
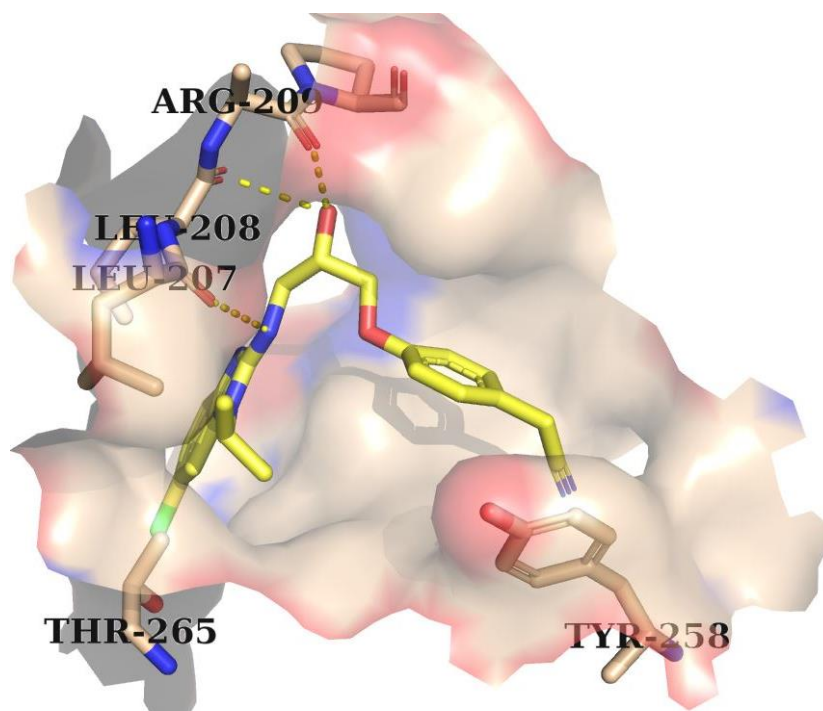
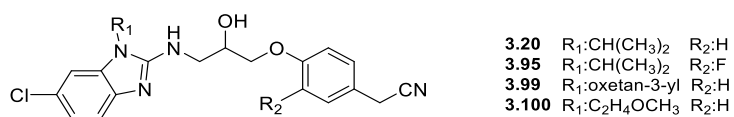
thioureas, following by adding DIC as a coupling reagent to aid ring closure and TFA to deprotect the silyl group. This procedure was employed to synthesis large quantity of **3.20** (200 mg) with high purity ($\geq 95\%$) in order to provide further *in vitro* and *in vivo* assays.

3.4 Molecular analysis

Unfortunately, employing the ITC experiment to evaluate the binding of 1*H*-benzo[*d*]imidazole series was not an ideal method due to solubility issues. Therefore, the cell-based assay was employed as an alternative method to evaluate the potency of the compounds and their ability to penetrate the bacterial cell wall and avoid efflux pump systems. However, it is difficult to determine the K_D and $\Delta G_{binding}$ of the synthesised compounds as well as the effect of employing different functional groups on binding by cell-based assay. In addition, cell-based assays are not sufficient to prove the direct binding of the synthesised compounds to PqsR^{CBD} which limits the biological analysis presented in this work.

A good alternative approach to prove the direct binding to PqsR^{CBD} is determining the ligand crystal structure complex by employing a soaking experiment to identify the binding site of the ligand and the main interactions with the receptor. Determining the crystal structure ligand-protein complex is an important form of analysis in medicinal chemistry that can provide qualitative data on the binding geometry and key compound-amino acids interaction within the binding domain of PqsR.

3.4.1 Crystal structure of PqsR^{CBD} complexed with active compounds belonging to the 2-amino benzimidazole series



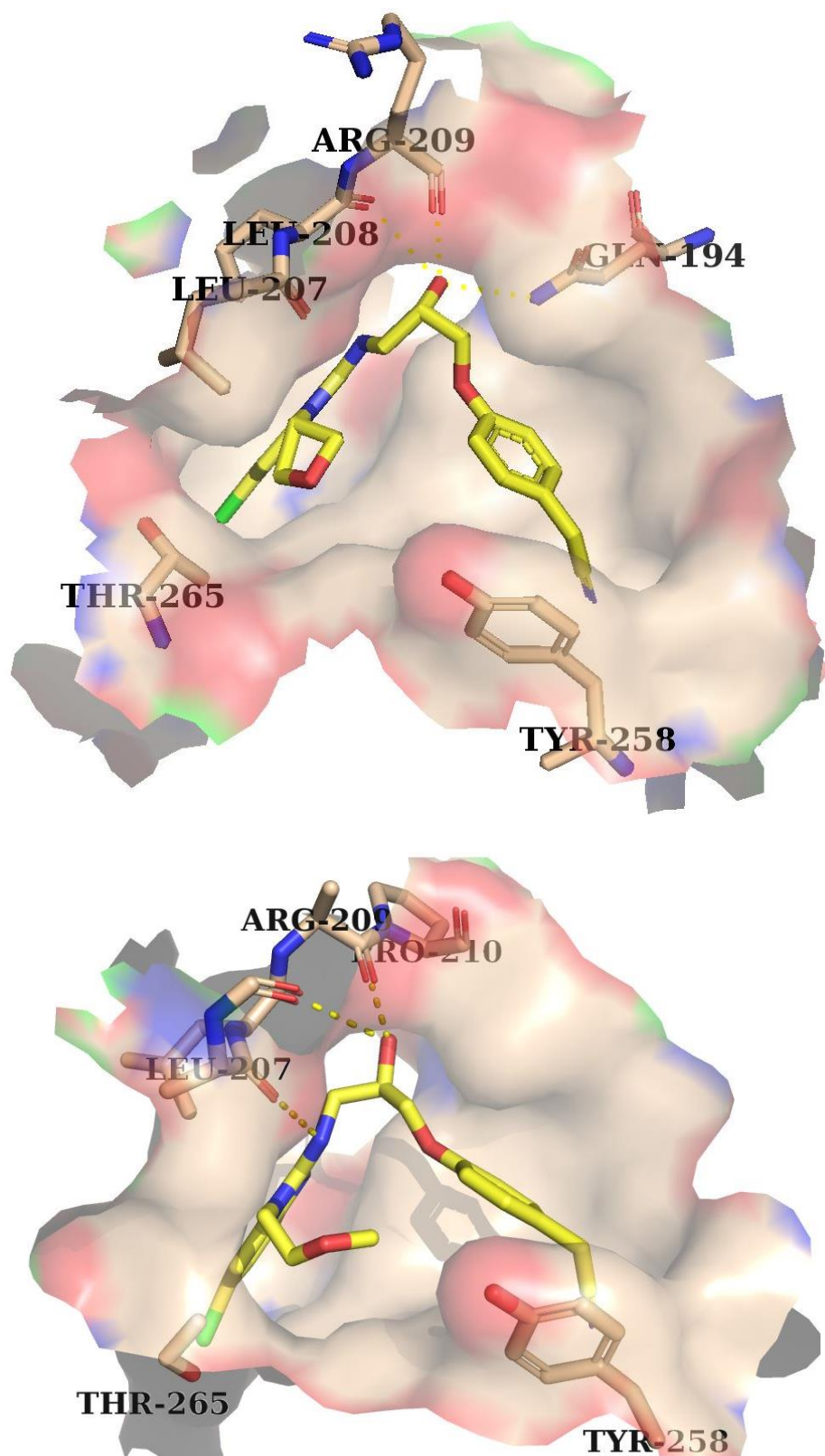


Figure 3-9: Schematic representation of the crystal structure of PqsR^{CBD} complexed with PqsR antagonists (yellow sticks): **3.20**, **3.95**, **3.99** and **3.100**, sequentially from the top, binding to PqsR^{CBD} with hydrogen bonds shown as a dotted line. The racemic mixture of the above compounds was soaked, and the *S* enantiomer was observed. This work was carried out by William Richardson (work in press).

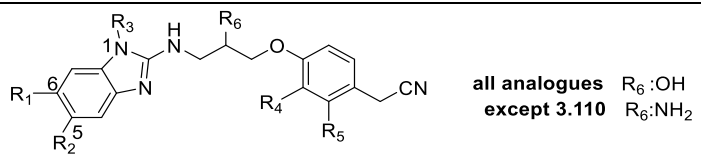
All of the investigated analogues in the 1*H*-benzo[*d*]imidazole series adopted a similar binding mode to the 4-(3*H*)-quinazolinone series, with the benzimidazole moiety buried within pocket A whilst the *para*-phenyl acetonitrile faced Tyr²⁵⁸ in pocket B (Figure 3-9). The chlorine atom at position 6 pointed to the Thr²⁶⁵ residing in pocket A with a 4 Å distance. Additionally, the hydroxyl and the secondary amine in the linker exhibited hydrogen bonding with the backbones of Arg²⁰⁹, Leu²⁰⁷ and Leu²⁰⁸. Moreover, the isopropyl substitution at *N*¹ in the benzimidazole ring had a hydrophobic interaction with the lipophilic residues (Leu²⁰⁷, Leu²⁰⁸, Ile²³⁶ and Ile²⁶³) surrounding that part of the binding pocket. This lipophilic interaction and H-bonding of the secondary amine in the linker accounted for the enhancement of inhibitory potency for this series when compared to 4-(3*H*)-quinazolinone series. The design strategy of **3.95** was to obtain further hydrogen bonding or lipophilic interaction with the Tyr²⁵⁸ by adding a fluorine atom at the R₄ position. Additionally, oxygen atom insertion into the alkyl chains of **3.99** and **3.100** aimed to decrease lipophilicity and obtain more hydrogen bonding with the backbone of the hydrophobic residues surrounding that area. Unfortunately, the crystal structures (Figure 3-9) indicated that neither the fluorine atom nor the oxygen atom established any further interactions with the receptor. However, a comparison of the biological activity of **3.20** and **3.95** suggested that the insertion of a fluorine atom could enhance π - π stacking interaction with Tyr²⁵⁸, which leads to a 2.6-fold increase in activity.

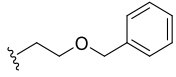
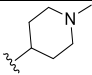

3.5 Structure activity relationship analysis

3.5.1 SAR study of 2-aminobenzimidazole series

An intensive SAR study was established to enrich the initial SAR reported at the beginning of this chapter (3.1), which showed that the 1-methyl-benzo[*d*]imidazole ring is the optimal replacement of the quinazolin-4(3*H*)-one ring, while the 2-amino group proved a better linking group than sulfur.

Table 3-4: **Summary of SAR study of 2-aminobenzimidazole series.** The inhibition of PqsR activity measured initially in PAO1-L CTX::P_{pqsA}-lux strain of *P. aeruginosa* at 10 μM concentration. Any compounds showed inhibition of activity by 50 % or less was further analysed by concentration-response curve measured in PAO1-L CTX::P_{pqsA}-lux and PA14 CTX::P_{pqsA}-lux strains. NA, not active at 10 μM concentration. NT, not tested in PA14 CTX::P_{pqsA}-lux strains. All the active compounds in this series did not show any effect on the bacterial growth. The asterisk (*) indicates that this parameter was predicted using ChemDraw 19.0.1.28 (<http://www.chemaxon.com>). The sign (\$) indicates that the synthesis and biological evaluation was carried out by Fadi Soukarieh.

								
	R ₁	R ₂	R ₃	R ₄	R ₅	IC ₅₀ (μM) PAO1-L CTX::P _{pqsA} -lux	IC ₅₀ (μM) PA14 CTX::P _{pqsA} -lux	cLogP*
[§] 3.1	Cl	H	CH ₃	H	H	0.21 ± 0.04 ^a	0.20 ± 0.01 ^a	3.2
3.86	H	Cl	CH ₃	H	H	NA	NT	3.2
3.87	Cl	Cl	CH ₃	H	H	NA	NT	3.8
[§] 3.109	CF ₃	H	CH ₃	H	H	1.5 ± 0.3 ^b	NT	3.4
[§] 3.19	Cl	H	C ₂ H ₅	H	H	0.13 ± 0.03 ^a	0.08 ± 0.01 ^a	3.7
3.20	Cl	H	CH(CH ₃) ₂	H	H	0.14 ± 0.05 ^a	0.09 ± 0.01 ^a	4.0
3.88	Cl	H	C(CH ₃) ₃	H	H	0.22 ± 0.01 ^a	0.23 ± 0.01 ^a	4.4
3.89	Cl	H	CH ₂ C(CH ₃) ₃	H	H	0.38 ± 0.01 ^b	0.55 ± 0.01 ^b	5.1

3.90	Cl	H	cyclo-propyl	H	H	0.06 ± 0.03^a	0.07 ± 0.01^a	3.8
3.91	Cl	H	cyclo-butyl	H	H	0.16 ± 0.01^a	0.25 ± 0.10^a	4.1
3.92	Cl	H	cyclo-pentyl	H	H	0.44 ± 0.1^a	0.55 ± 0.02^a	4.7
3.93	Cl	H	cyclo-hexyl	H	H	0.75 ± 0.4^a	1.4 ± 0.1^a	5.2
3.94	Cl	H		H	H	1.05 ± 0.2^b	NT	4.9
3.95	Cl	H	CH(CH ₃) ₂	F	H	0.05 ± 0.02^a	0.12 ± 0.02^a	4.1
3.96	Cl	H	CH(CH ₃) ₂	H	F	0.06 ± 0.03^a	0.12 ± 0.04^a	4.1
3.101	H	H	CH(CH ₃) ₂	H	H	0.77 ± 0.2^b	1.04 ± 0.2^b	3.3
^s 3.110	Cl	H	CH(CH ₃) ₂	H	H	0.50 ± 0.3^b	NT	4.1
3.97	Cl	H	C ₂ H ₄ N(CH ₃) ₂	H	H	NA	NT	3.3
3.98	Cl	H		H	H	NA	NT	3.3
3.99	Cl	H		H	H	0.15 ± 0.01^a	0.32 ± 0.08^a	2.6
3.100	Cl	H	C ₂ H ₄ OCH ₃	H	H	0.18 ± 0.04^a	0.12 ± 0.04^a	3.1
3.103	Cl	H	C ₂ H ₄ OH	H	H	0.18 ± 0.05^a	0.29 ± 0.03^a	2.4

Values reported as Mean \pm SEM of n = 6^a or n = 3^b.

Exploration of the SAR for the R₁ and R₂ substituents demonstrated that the introduction of a chlorine atom at the 5-position (compounds **3.86**, **3.87**) or a trifluoromethyl group at the 6-position **3.109** led to loss or decrease of activity, which could be due to a steric limitation in the binding pocket. Therefore, for all future SAR, R₁= Cl was maintained. Exploration of the R₃ position proved very enlightening and the optimal substitutions in the R₃ position were the ethyl **3.19** and isopropyl **3.20** substituents. Furthermore, substitution at the R₃ position with cyclo-alkanes showed a two-fold increase in activity over **3.1** with the cyclopropyl derivative **3.90** being optimal. However, further increase in steric bulk (**3.91** – **3.94**) led to a decrease in activity, indicating the steric limitation of this recognition site in the receptor. Evidence for this

SAR was demonstrated through obtaining the co-crystal structure of **3.20** with PqsR (Section 3.4.1 3.4.1). Finally, we aimed to introduce a fluorine atom at R₄ and R₅ in order to gain a further hydrogen bond interaction with the Tyr²⁵⁸ sidechain, and the biological evaluation of these compounds (**3.95** & **3.96**) showed a slight two-fold increase in activity compared to **3.20**.

The other aim of this study was to enhance the physicochemical properties of the series by employing different strategies. Firstly, removing the lipophilic chlorine atom from the benzimidazole ring **3.101** led to a 10-fold decrease in activity. Furthermore, polar functional groups were introduced in the R₃ position to enhance the overall physical properties including increasing water solubility. We found that any nitrogen-containing alkyl groups (**3.97** & **3.98**), which is considered as a basic functional group with calculated pK_a = 9 led to complete loss of the inhibitory activity. Interestingly, replacing the hydroxyl group **3.20** with an amino group **3.110** gave a 7-fold reduction in activity. This finding could also be associated with permeability issues or substrate to a specific efflux mechanism.¹⁷⁰ On the other hand, oxygen-containing alkyl chains (**3.99**, **3.100** and **3.103**) maintained biological activity with a corresponding reduction in lipophilicity. In light of the SAR study, **3.20** was chosen for further pharmacological evaluation.

3.5.2 Comparison between **3.20** and **1.3**

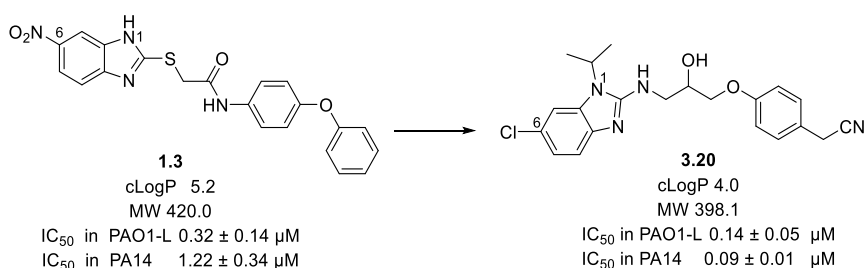
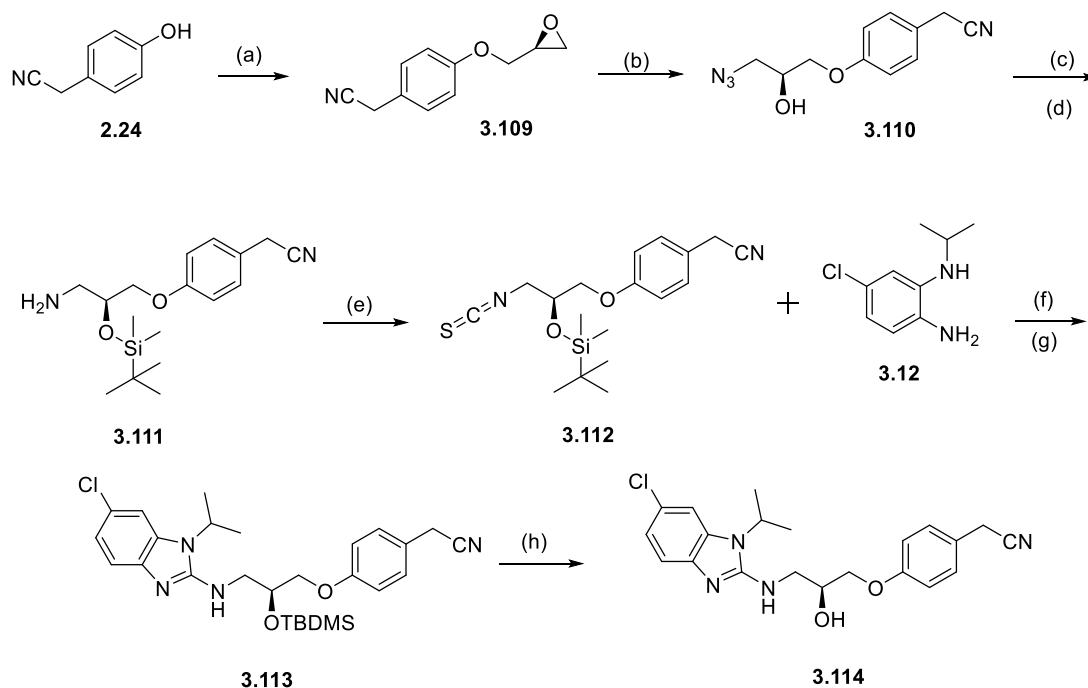


Figure 3-10: **The improvement of potency of 3.20 in comparison to 1.3.** **1.3** is the well-known PqsR antagonist from the literature with promising results in preclinical studies.

1.3 is a well-known PqsR antagonist with promising results in preclinical studies.^{103,112} The SAR of this antagonist provides the key structural features important for activity, including hydrogen bonding and the π - π interaction of the thioactamide and phenoxy group, respectively. The 1*H*-benzo[*d*]imidazole series interacted with the receptor in a similar manner to **1.3** with additional lipophilic interaction with the alkyl chain presented in *N*¹. The presence of an electron withdrawing group at position 6 in this series seems important for activity, as removing the chlorine atom in **3.101** led to a 10 fold decrease in activity in comparison to **3.20**. This is in agreement with **1.3**, where a substituent in position 6 (a nitro group), has been shown to be superior in terms of potency over methyl, methoxy, and the non-substituted benzimidazole ring. However, there are no derivatives for the current SAR study with electron donating groups such as hydroxyl or methoxy substitution on position 6 of **3.20** to draw clear conclusions about the role of the chlorine atom in the binding of this series. **1.3** is higher in calculated lipophilicity to **3.20** by almost one log unit, which could refer to the presence of thioether in the linker and additional aromatic ring in the tail. Furthermore, the low activity of **1.3** in PA14 could be due to that, **1.3** a substrate to a specific ~~reflux~~ efflux pump presented in PA14 or ~~less preamble~~ has lower permeability which leads to a decrease in the activity of the compound.¹⁸⁶ On the other hand, the 1*H*-benzo[*d*]imidazole series represented by the active compounds **3.1**, **3.20**, **3.90**, **3.95**, **3.96**, **3.99**, **3.100** and **3.103** managed to show similar activity in both strains with a 2-fold difference. Therefore, **3.20** is considered as more promising candidate with better potency and lipophilicity to proceed further with secondary pharmacological assays.

3.5.3 Analysis of **3.20** enantiomers activity

Synthesis. (Scheme 3-12): Synthesis of (*S*)-2-(4-(3-((6-chloro-1-isopropyl-1*H*-benzo[*d*]imidazol-2-yl) amino)-2-hydroxypropoxy) phenyl) acetonitrile, **3.114**.



Reagents and conditions: a) (*S*)-(+)-glycidyl nosylate, Cs₂CO₃, CH₃CN, reflux, 16 h, 87%. b) NaN₃, NH₄Cl, EtOH, 40°C, 16 h, 99%. c) TBDMS-Cl, imidazole, DMF, rt, 16 h, 84%. d) PPh₃, 10% H₂O; THF, rt, 16h, 90%. e) thio-CDI, DCM, inert atmosphere, rt, 16 h, 25%. f) EtOH, reflux, 16 h. g) DIC, Et₃N, DMF, reflux, 16 h, 65%. h) 10 % TFA in MeOH, rt, 48h, 60%.

Here, a synthesis of enantiopure epoxide is presented employing the single enantiomer of glycidyl nosylate as a starting material to produce the desired enantiomerically pure product in high enantiomeric excess. In this case, employing the pure enantiomer of epichlorohydrin as the starting material to synthesis **3.109** is not ideal. This is because epichlorohydrin, in theory, has two electrophilic centres in the molecule, resulting in two possible stereochemical outcomes from this reaction (Figure 3-11).

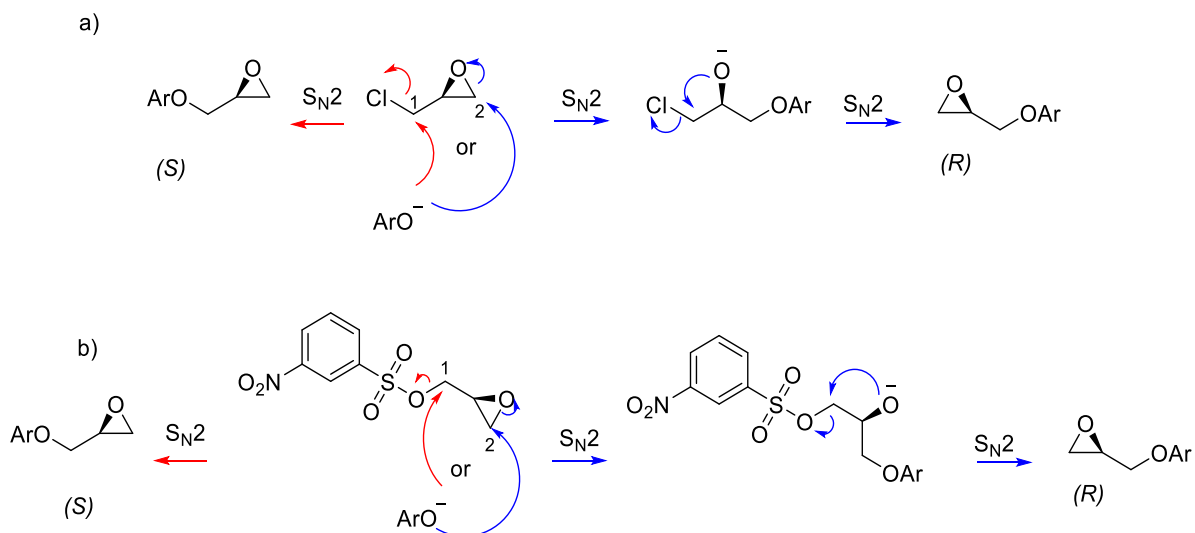


Figure 3-11: **Theoretical mechanism of epoxide synthesis.** The reaction employs pure enantiomer of epichlorohydrin or glycidyl nosylate to furnish the required enantiomer. Two electrophilic centres in the molecule, resulting in two possible stereochemical outcomes. The alkylation of the first electrophilic centre showed in red arrow whereas the blue one for the alkylation of the second electrophilic centre.

Therefore, employing the single enantiomer of glycidyl nosylate as a starting material was more efficient to produce the desired enantiomerically pure product in high enantiomeric excess. The driving force of the selectivity here is the stability of the conjugate base making position 1 more electrophilic and more favourable in this reaction, as shown above.

Following this, analytical chiral high performance liquid chromatography (HPLC) was employed to separate the final product (racemic compound **3.20**) into enantiomerically pure isomers: **3.114** (*S* isomer) and **3.115** (*R* isomer). ~~The principle of this technique depends on the differences in the affinity of each isomer to the column, and therefore each isomer is eluted at different times.~~ The separation of **3.20** showed that the (*S*) enantiomer **3.114** has a lower affinity for the stationary phase, and therefore was eluted from the column first, followed by the (*R*) enantiomer **3.115** with enantiomeric excess (ee) 96.9 % and 96.1 %, respectively ([more details in experimental chapter](#)).

Biological evaluation. The activity of the racemic **3.20** and both enantiomers, **3.114** and **3.115** were evaluated in cell based assay employing PAO1-L *PpqsA::lux* and PA14 *PpqsA::lux* strains.

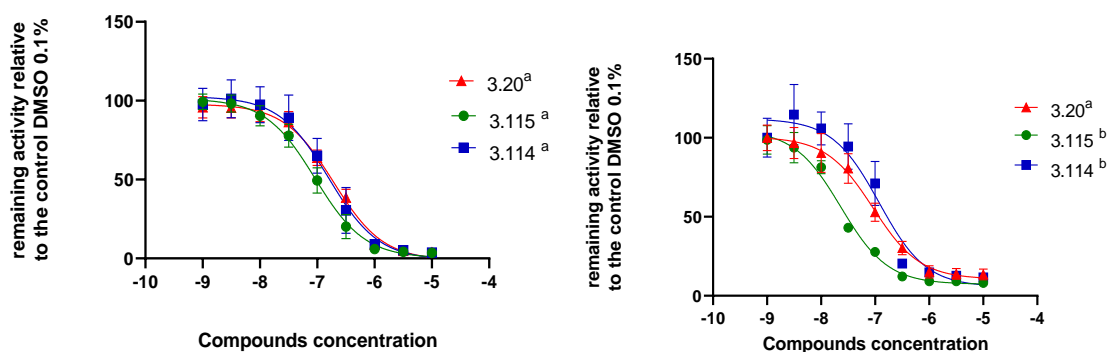


Figure 3-12: **Concentration-response curve of 3.20 and both enantiomers 3.114 and 3.115.** The inhibition of PqsR activity measured in a) PAO1-L *PpqsA::lux*. and b) PA14 *PpqsA::lux* strains. The error bars indicate the SEM of the mean of one or two biological experiments. n = 6^a or n = 3^b biological replicates.

The result showed that both enantiomers **3.114** & **3.115** are equally active within the limit of the biological assay in PAO1-L *PpqsA::lux*. However, the analysis of enantiomers activity in PA14 *PpqsA::lux* strain showed that **3.115** is 4.5- and 5-fold more active than **3.20** and **3.114**, respectively with IC₅₀ = 23 nM ± 2.4.

3.6 Conclusion and future work

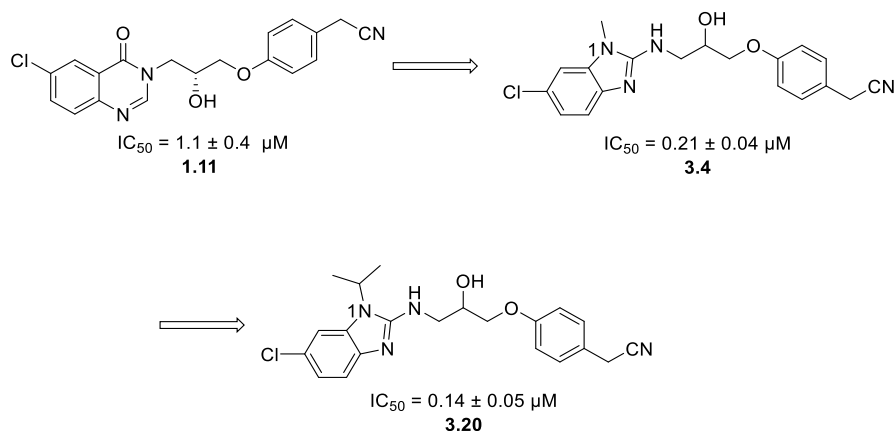


Figure 3-13: The improvement in activity of benzimidazole series by replacing the quinazolin-4(3H)-one scaffold by 1-methyl-1H-benzo[d]imidazol-2-amine ring. IC_{50} measured in PAO1-L *PpqsA::lux*.

The work presented in this chapter demonstrated a hit to lead optimisation study that employed **1.13** as the hit compound, replacing the quinazolin-4(3H)-one scaffold with different heterocycles. The 1-methyl-1H-benzo[d]imidazol-2-amine ring **3.1** has been found as an optimal heterocycle that provides a key lipophilic interaction with the receptor at the N^1 position. The pharmacophore presented here emphasise that the antagonistic activity required the general structural features presented in the previous SAR study (Chapter 2), **1.3** and the current study which is including; EWG on the heterocycle ring, hydrogen bonding with the linker, as well as the π - π interaction with Tyr²⁵⁸. However, some analogues (**3.19**, **3.20**, **3.90**, **3.91**, **3.95**, **3.96**, **3.99**, **3.100** and **3.103**) presented in this study displayed similar or better activity compared to **1.3** against PAO1-L and an enhanced inhibition against PA14 with IC_{50} values in sub-micromolar range. In light of the SAR study presented in this chapter, **3.20** was chosen for further pharmacological evaluations in order to prove the concept. Furthermore, cytotoxicity assays will be established for the most active compounds in the series to support them proceeding to further study.

4 Biological Characterisation of PqsR Inhibitors based on Crystal Structure and *In Vitro* Studies, and their Effect on Quorum Sensing in *Pseudomonas aeruginosa*.

4.1 Overview

The development of novel candidates with specific targets generally follows the same workflow regardless of the target's nature. This work was started by *in silico* virtual screening of the PqsR ligand-binding domain (LBD) crystal structure PDB: 4JVI using the University of Nottingham Managed Chemical Compound Collection (MCCC). Virtual screening was complemented by a whole-cell biosensor reporter assay (Section 1.8.2) to confirm the activity of the highest-scoring compounds. Five hits were identified and **1.6** was selected as the ideal hit to establish a SAR study. Furthermore, another SAR study was performed by replacing the quinazolin-4(3*H*)-one core in **1.6** with a 1*H*-benzo[*d*]imidazole ring lead to produce a range of potent PqsR antagonists in the sub-micromolar range.

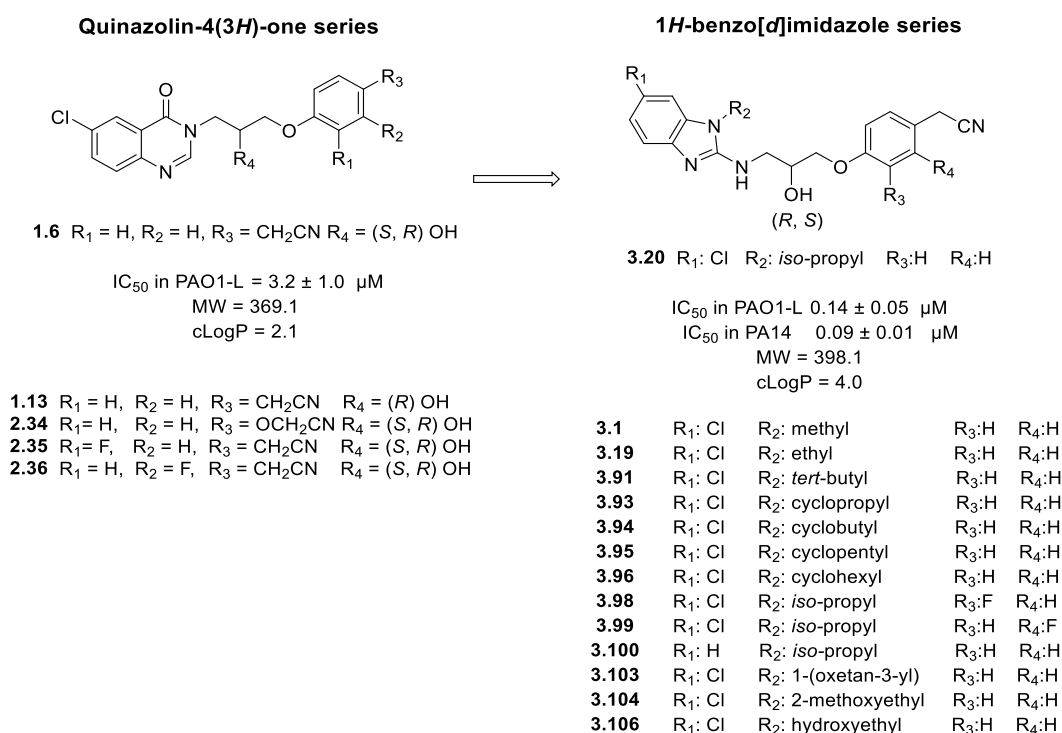


Figure 4-1: Structures of the active compounds in quinazolin-4(3H)-one and 1H-benzo[d]imidazole series. These compounds employed in various biological analysis presented in this chapter.

The synthesised compounds in both series were evaluated using the aforementioned biosensor reporter assay (Section 1.8.2). Moreover, the crystal structures of key compounds in both series were generated to determine the key interactions with PqsR^{CBD}.

In this chapter, the active compounds were further tested against a mCTX::Pkm-lux PAO1-L strain to subtract potential undesired bias by unspecific interactions with the *lux* operon or with the bioluminescence metabolism (Section 4.2.1). In addition, **3.20** was selected as the lead candidate, and further phenotypic pharmacological evaluations were established to prove the concept and confirm the mechanism of action for this novel lead candidate and its analogues. Finally, once the activity of the candidate was confirmed, the relevant compound was studied regarding its ability to repress the pathogenicity of different phenotypes of *P. aeruginosa*. The next step is to evaluate, **3.20** in relevant *in vivo* infection models to investigate the attenuation of virulence and determination the pharmacokinetic and pharmacodynamic properties.

4.2 Primary *in vitro* assays

4.2.1 The CTX::*Pkm*-lux PAO1-L strain

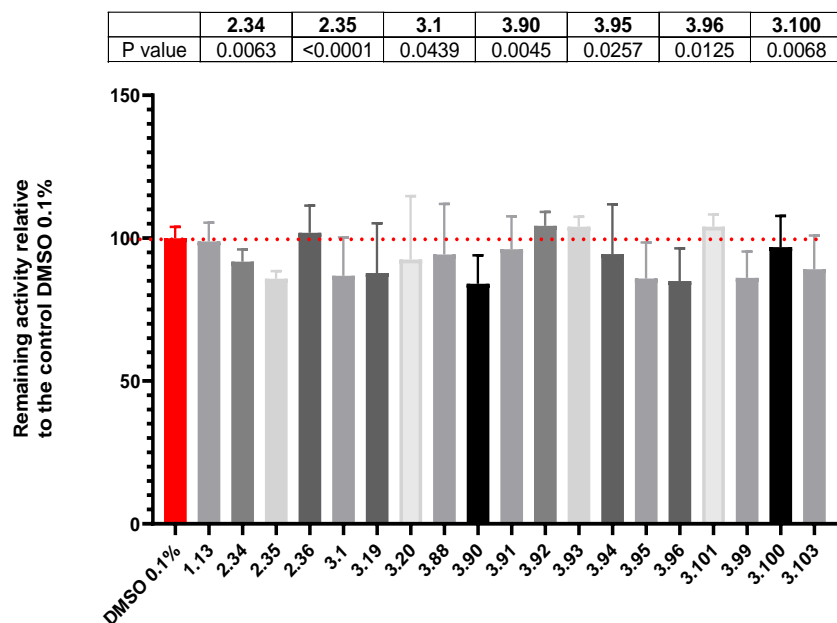


Figure 4-2: **The active compounds presented in Chapters 2 and 3.** 10 μ M concentration of the active compounds were screened against the CTX::*Pkm*-lux PAO1-L strain to detect any potential non-specific interactions with the *lux* operon. Statistical significance was assessed using the unpaired t-test for each column in relative to control (DMSO 0.1%) with P value for significantly different values shown in the graph. The data shown are based on $n = 6$.

An assay was performed in parallel to the concentration-response assay mentioned in chapters 2 and 3 to guide the selection of active compounds by verifying the efficacy of the active compounds using the CTX::*Pkm*-lux PAO1-L strain. This strain is a constitutive reporter control strain that helps to detect and subtract any potential bias from non-specific interactions with the *lux* operon itself rather than the desired interaction with the targeted protein. All active compounds were incubated with this strain at 10 μ M concentration. The results demonstrated that **1.13** and **3.20** did not significantly inhibit *lux* gene expression (Figure 4-2). This confirmed that the measured IC_{50} mainly reflected the impact on the PqsR protein rather than the effect

on the *lux* gene. On the other hand, some active compounds (**2.34**, **2.35**, **3.1**, **3.90**, **3.95**, **3.96** and **3.99**) in both series inhibit *lux* gene expression with percentage ranged between 5 and 15%.

4.2.2 Growth measurement

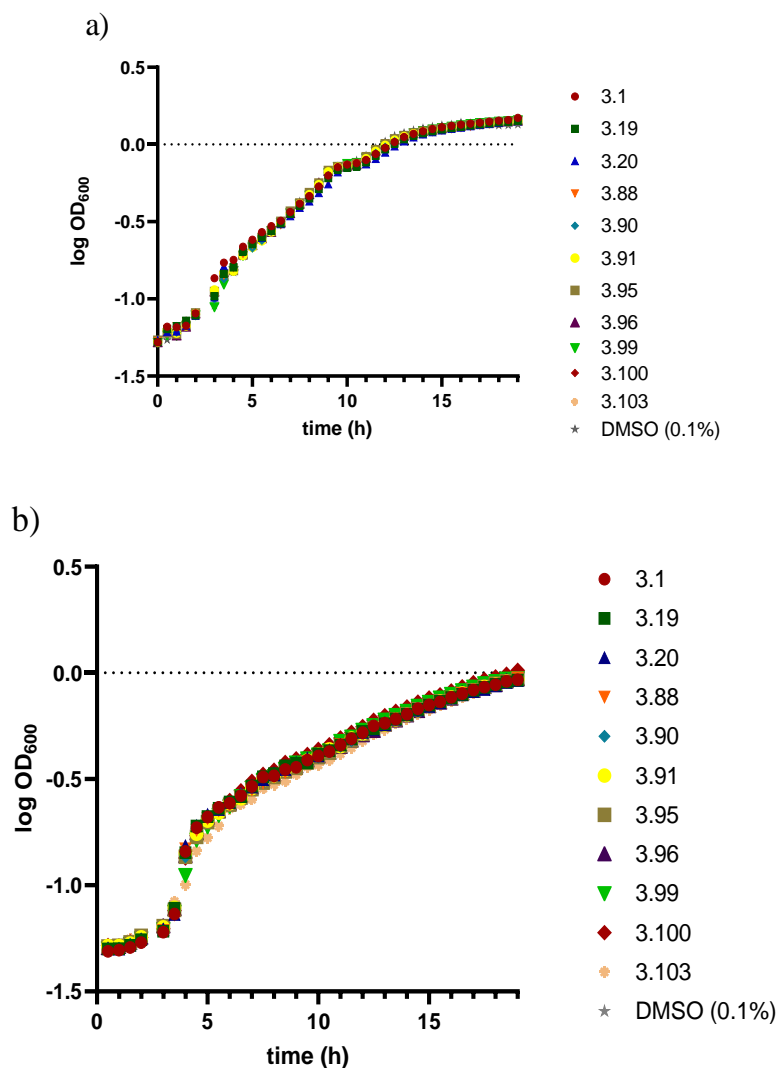


Figure 4-3: **Growth curves of *P. aeruginosa* in the presence or absence of the active compounds.** (a) PAO1-L CTX::P_{pqsA}-*lux* and (b) PA14 CTX::P_{pqsA}-*lux* in the presence of 10 μ M concentration of nanomolar-range active compounds or DMSO control.

The main objective of this work was to identify an antivirulence candidate that antagonises PqsR^{CBD} without affecting bacterial growth. Therefore, it was critical to prove the concept by measuring the impact of the active compounds on bacterial viability overnight. Figure 4-3

showed that all the active compounds with nanomolar range activity did not interfere with bacterial growth at 10 μ M concentration, which is the highest concentration used in this experiment, in comparison to DMSO (0.1%) control. The initial evaluation of the synthesised compounds provided clear evidence of the compounds' activity in both series involving *pqs* system inhibition rather than affecting the *lux* gene. Additionally, it has been proven that all active compounds did not affect the growth of bacteria, which leads to classify the compounds as antivirulence candidates. However, reducing light emission in the primary screening could be due to the *pqs* system being hampered at different levels, including HHQ and PQS biosynthesis as well as transport and signal perception. Therefore, the primary screening alone is not sufficient to prove the molecular interaction with PqsR. As such, there remains a need to prove the direct binding of the novel compounds with PqsR and the concept of this novel therapeutic strategy via secondary *in vitro* assays.

4.3 Secondary *in vitro* assays

Antagonising PqsR is a novel mechanism of action used to combat the virulence of *P. aeruginosa* that requires additional in-depth investigations. At this stage of the project, it is important to prove the concept of this novel strategy by measuring the secondary metabolites of the *pqs* system in the presence and absence of inhibitors. Such analyses are crucial to determine the effect of antagonising PqsR on *pqs* system activity and the pathogenicity of the bacteria in general. Additionally, as mentioned in Section 1.1.4, it is critical to determine the activity range of inhibitors against different isolates of *P. aeruginosa* (including the most resistant strains) and prove the applicability of targeting PqsR receptor as a core protein that is essential for the pathogenicity in a wide range of strains of this bacterium.

4.3.1 Pyocyanin signal quantification

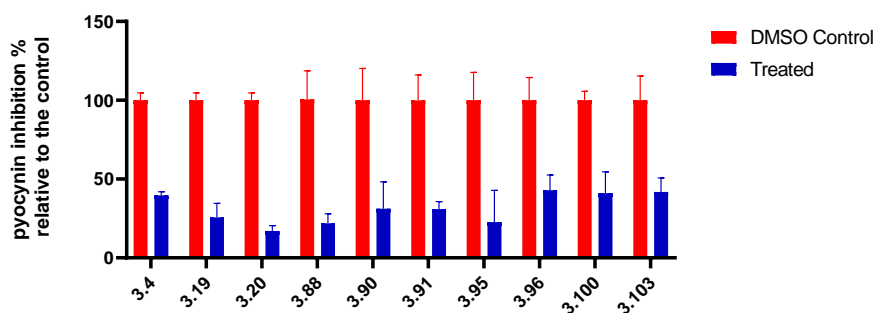


Figure 4-4: **Pyocyanin production quantification.** This occurred in the presence of the nanomolar-range active compounds in the series at 3 fold IC_{50} concentration relative to the DMSO negative control. The data shown are based on $n = 9$.

Pyocyanin has emerged as an important virulence factor that is produced by *P. aeruginosa* and strongly regulated by the *pqs* system.¹⁸⁷ Therefore, the measurement of pyocyanin production provides an indirect readout of *pqs* QS system activity. The most active compounds with $IC_{50} \leq 200$ nM in the 2-aminobenzimidazole series were screened against pyocyanin production in the PAO1-L wt strain (Figure 4-4). All of the compounds inhibited pyocyanin production to 50% or less when used at concentration equivalents to three fold of their IC_{50} values. Compounds **3.20** and **3.88** showed a significant effect on pyocyanin production, with an approximately 80% reduction relative to the control. On the other hand, the weakest effects were associated with **3.96** and **3.100, 3.103** with approximately 50% reduction relative to the control.

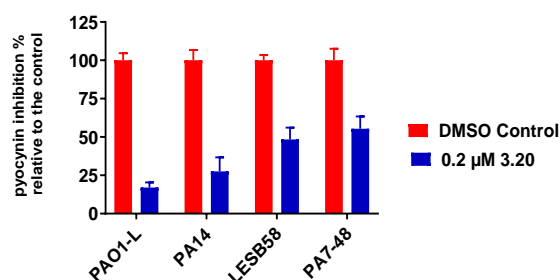


Figure 4-5: **Pyocyanin production quantification.** This occurred in the presence and absence of **3.20** at 200 nM concentration in different genomic classes of *P. aeruginosa*. The data shown are based on n = 9. This analysis was carried out by Eduard Vico Oton.¹⁸⁸

P. aeruginosa is generally considered as an opportunistic pathogen but there are several widespread clones that appear to have become more specialised pathogens, particularly in cystic fibrosis patients, including the Liverpool epidemic strain (LES) which is found mainly in the UK,²⁴ DK2 in Denmark,¹⁸⁹ and AUST-02 in Australia¹⁹⁰. In general, The population of *P. aeruginosa* can be divided into three main groups: PAO1, PA14 and the highly divergent PA7.¹⁹¹ PAO1 is considered as the major reference for genetic and functional studies in most laboratories while PA14 is a clinical isolate which considered as a more virulent strain than PAO1.

Therefore, further analysis was established to determine the spectrum of **3.20** and its activity against different genomic classes of *P. aeruginosa*. This compound is considered as the most active compound based on pyocyanin inhibition analysis. The analysis was performed to quantify pyocyanin production in the presence of 200 nM concentration of the selected candidate. **3.20** successfully inhibited different isolates of *P. aeruginosa*—even the most antibiotic resistance strain (PA7-48¹⁹¹)—and the degree of inhibition was highly dependent on the pathogenicity of the strain (Figure 4-5).

4.3.2 Alkyl quinolone signal quantification

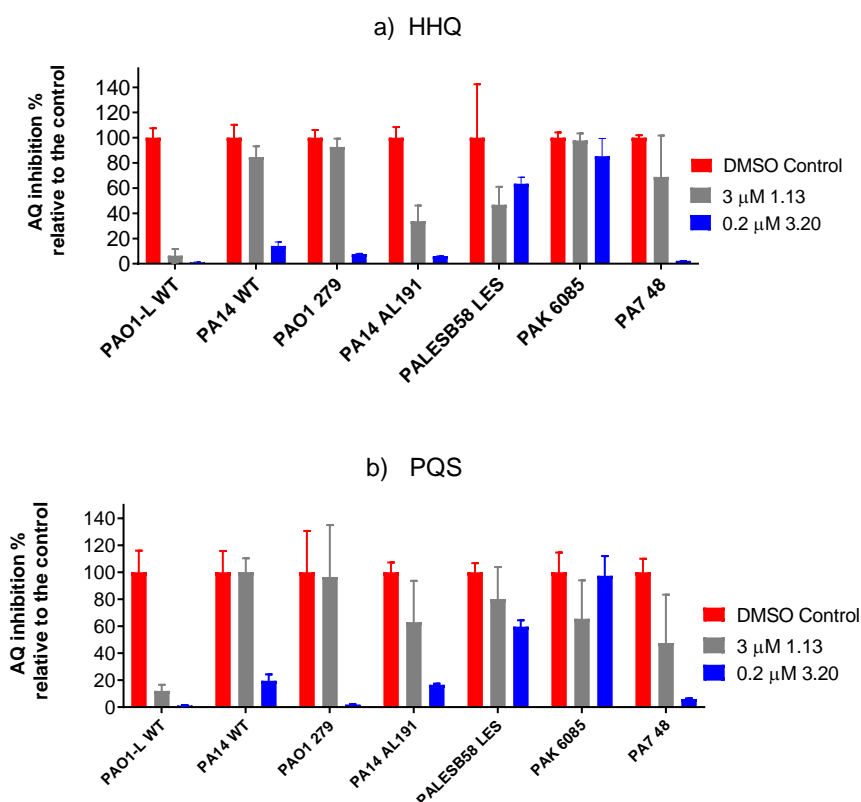


Figure 4-6: **AQ production quantification.** This occurred in the presence of 3 μM of **1.13** or 0.2 μM of **3.20** relative to DMSO (negative control) in different genomic classes of *P. aeruginosa*. a) HHQ and b) PQS. The data shown are based on $n = 9$. This analysis was carried out by Eduard Vico Oton.¹⁸⁸

Previous discussions regarding the AQ biosynthetic pathway and *pqs* gene production (Sections 1.5.2 and 1.5.3) emphasised that AQ production measurements are a direct reflection of *pqs* system activity and thus serve as a useful tool for determining the efficiency of PqsR inhibitors. Additionally, previous studies have suggested that PQS is a multifunctional molecule that functions via several PqsR-dependent and PqsR-independent pathways and directly contributes to iron acquisition¹⁹² and microvesicle formation.¹⁹³ The quantitative measurement of major AQ (HHQ and PQS) production using the LC-MS/MS technique is useful for evaluating the effectiveness of this strategy. The analysis involved different genomic classes of *P. aeruginosa* with the presence of 3 μM of **1.13** and 200 nM of **3.20**. Although both

compounds demonstrated significant reductions of HHQ and PQS in PAO1-L WT, **1.13** generally had little to no impact on the AQ production of other strains. On the other hand, **3.20** showed significant inhibition of the tested strains, with the notable exceptions of the LES and PAK strains.

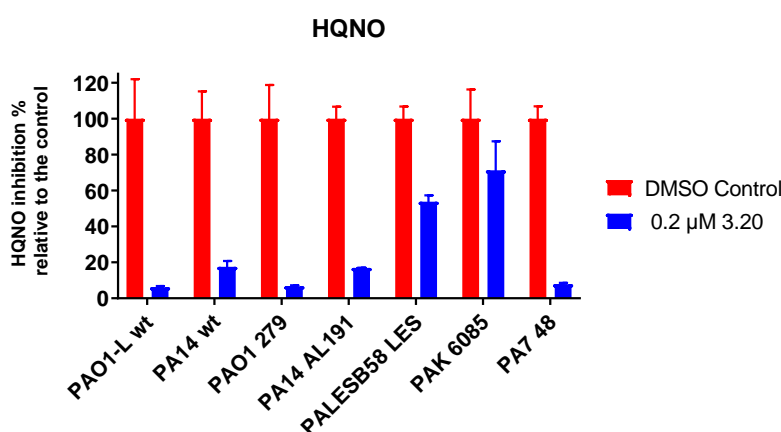


Figure 4-7: HQNO production quantification in the presence of 0.2 μM of **3.20** relative to DMSO (negative control) for different genomic classes of *P. aeruginosa*. The data shown are based on n = 9. This analysis was carried out by Eduard Vico Oton.¹⁸⁸

Moreover, regarding HQNO, the *pqs* system by-product promoting the environmental competition of *P. aeruginosa* in polymicrobial infections was also analysed in the presence and absence of **3.20**. Notably, **3.20** showed a significant reduction in HQNO expression over the tested strains, except for LES and PAK. This result is in agreement with AQ production analysis, which could be due to the high pathogenicity of these strains^{24,194} or the presence of a special efflux pump mechanism¹³⁰ that targeted **3.20**. Taken together, these results prove the concept of attenuating the pathogenicity of *P. aeruginosa* by targeting the PqsR receptor and indicate the potential of **3.20** as a wide spectrum antivirulence therapy against different isolates of *P. aeruginosa*.

4.4 Biofilm formation analysis

The most challenging strategy employed by resistance strains of any bacterial species is biofilm formation. This strategy significantly reduces the sensitivity of bacteria to antibacterial agents and radiation, making this a serious threat to public health.¹⁹⁵ Therefore, when analysing the effect of QS inhibitors on the biofilm formation process, the strategy used and the time of intervention are critical in the early stages of a drug discovery project. There are four possible antibiofilm strategies: prevention, weakening, disruption and direct killing. Moreover, QS inhibitors must be clinically useful to disrupt established biofilm to be eradicated via traditional antibiotics or phagocytosed and killed by the immune system. In-depth investigations of three-dimensional biofilm are important in determining the effect of PqsR antagonists on this parameter.

However, based on literature, conflicting results were obtained by different methods employed for biofilm formation and analysis as discussed in (Section 1.8.2) and the reasons were not investigated. This raises the question of whether biofilm experiments performed in the laboratory are useful for understanding how the novel candidates can inhibit QS and interfere with biofilm formation. Much of the existing knowledge regarding chronic infection comes from studying bacteria growing in test tubes with nutrient conditions that differ from pathological conditions, regardless of the significant differences between *in vitro* biofilms grown in the laboratory and *in vivo* biofilms. Additionally, as a research community, single-species cultures are routinely examined. However, in reality, the majority of chronic infections caused by polymicrobial communities and the interactions between different species may critically influence various factors associated with chronic infection (e.g., virulence, biofilm nature and antimicrobial resistance).¹⁹⁶

Therefore, Harrison and Diggle developed a version of the model that uses small sections of pig bronchiole to better represent *P. aeruginosa* biofilm during the long periods of relatively quiescent chronic infection that characterise CF.¹⁹⁷ The *ex vivo* pig lung (EVPL) model is a tractable model for studying *P. aeruginosa* growth and virulence that uses a bio-surface area (lung tissue) to establish biofilm in an artificial sputum medium (ASM). This media has an advantage over complex commercially available laboratory media by providing nutritional conditions similar to CF sputum, which demonstrates the level of PQS and QS signalling seen in CF patients. Previous work using this model showed that adding an unrealistic amount of iron led to the siderophore gene being switched off in experiments, thereby confirming the significance of designing an experiment reflecting the pathological situation in an *in vivo* system.

Additionally, ASM gives some complexity for the model when examining the ability of a compound to penetrate the media, which simulates the viscous condition of chronic lung infection and the ability to penetrate biofilm, tissue and bacterial cells. Other advantages of employing lung tissue instead of abiotic surfaces include this assay providing the ability to analyse histopathological changes in tissue that occur in the presence or absence of quorum sensing inhibitors (QSIs). Furthermore, cell-free suspensions of homogenised tissue could be assayed for a range of bacterial virulence factors such as QS signals, protease, pyocyanin and the siderophores pyoverdine and pyochelin. A key advantage of EVPL is that it provides the opportunity to study bacterial virulence factor production, growth, and cell-cell interactions in a spatially structured environment. The spatial structure of the tissue is retained, and microbes can be visualised within the tissue by conventional or confocal microscopy.

On the other hand, this model still has limitations and further work is needed to address these. The initial work with this model involved evaluating the effect of **3.20** on biofilm formation and acknowledged the high variance in the data presented in the replicates of one experiment

and from one experiment to another. In the published protocol of the *ex vivo* model, bacterial cells were loaded by touching a sterile 29G insulin needle to the top of a colony on a Luria broth (LB) plate and then lightly touching the tissue with the needle.¹⁹⁷ However, this strategy will not transfer a constant amount of bacterial load to each plate and variable data will be produced as a result. Therefore, the final concentration of bacterial load should be normalised in all well plate cells with an appropriate dosage that avoids the overgrowth of bacterial cells in each plate and simultaneously produces stable and long-lived infections. To overcome this issue, it was recommended to resuspend a colony in ASM and grow it to a specific optical density (OD) before adding a constant volume to each plate.

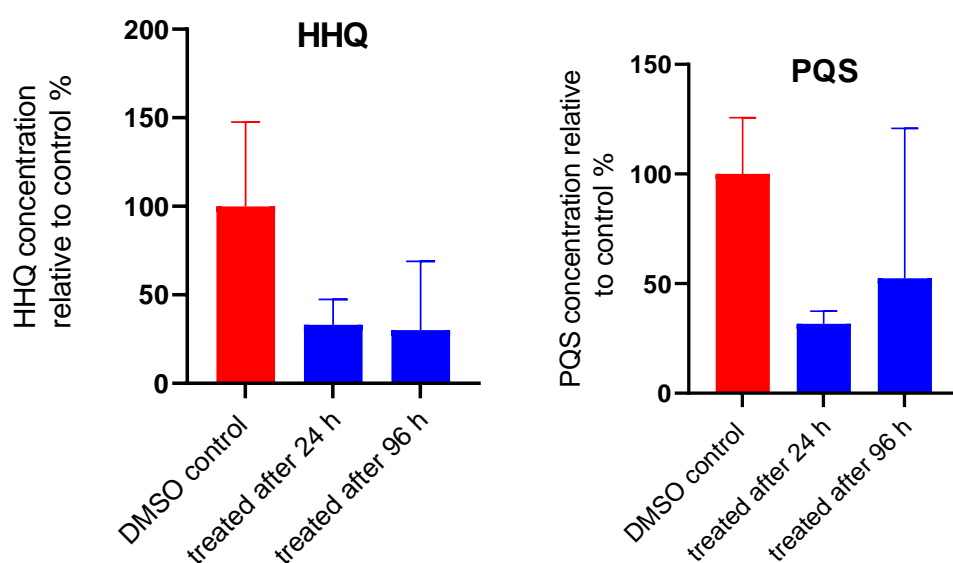


Figure 4-8: **The provisional data obtained from an *ex vivo* pig lung model.** The biofilm was established for two time points (24 and 96h) before treatment with 0.2 μ M of **3.20**. The *ex vivo* pig lung assay and supernatant preparation was carried out by the author. The AQ was extracted and quantified according to the protocol presented in the experimental section by Nigel Halliday. The data shown are based on n = 3.

The handling and processing of lung tissue have been addressed, which will facilitate the establishment of various types of analyses and investigations. The ability to process lungs in batches and easily cut several dozen regular cubes of tissue from each lung will facilitate high-throughput screening. Furthermore, this method can provide an in-depth investigation of one

candidate by using different species of *P. aeruginosa* in a single experiment. The time of intervention (before or after biofilm establishment) with QS antagonists and the final concentration of the candidate must also be considered. Additionally, the treatment of infection with PqsR antagonist alone or in combination with an optimal concentration of different classes of antibiotics could be investigated. The initial results of this model indicate that the PQS and HHQ concentrations inside the biofilm decreased with 0.2 μ M of **3.20** (relative to the control) without affecting the number of CFUs (data not shown). However, further optimisation and standardisation of this assay was terminated early due to the unexpected pandemic effect of (Covid-19). This assay was designed to evaluate the following: a) Bacterial cell growth by employing the PAO1-L CTX::P_{pqsA-lux} strain to evaluate the growth of bacteria after treatment with **3.20** alone, antibiotics alone, or **3.20** and antibiotics combined; b) the production of virulence factors such as AQ, protease, pyocyanin and the siderophores pyoverdine and pyochelin; c) biofilm analysis performed with different therapeutic intervention points (before, during and after the biofilm formation process); d) the histopathological analysis of infected tissue in order to evaluate the efficacy of **3.20** alone, antibiotic alone or **3.20** and antibiotics combined in restoring the histology of normal non-infected tissue in comparison to non-treated tissue.

Future work with this model could address changes in nutritional and oxygen levels within biofilm communities established on EVPL and how these factors affect the growth and virulence production of *P. aeruginosa*. Additionally, a comparison between treating an infection on lung cubes obtained from healthy pigs or genetically engineered pig lung that expresses human CF mutations could also be obtained using this method. Finally, the establishment of biofilm with multispecies microbes is an important condition that needs to be investigated in this model. All of these considerations should be accounted for ~~in~~ any novel antivirulence drug development project before proceeding with an *in vivo* study.

4.5 Cytotoxicity study

Assessing the toxicity of a novel candidate is crucial in the early stage of a drug discovery project to predict any undesirable toxicological effects, determine the candidate therapeutic index and avoid any financial issues associated with proceeding with a candidate to preclinical and clinical studies.¹⁹⁸ Here, the effects of four represented candidates (i.e., **3.20**, **3.90**, **3.95** and **3.96**) were investigated on A549 adenocarcinomic human alveolar basal epithelial cell line, which represents the site of most *P. aeruginosa* infections.⁸ The analysis employed a sensitive fluorometric assay (resazurin reduction assay) that is widely applied in drug discovery projects. This assay depends on the ability of living cells to reduce resazurin to the fluorescent compound resorufin, which reflects the rate of the metabolic process and the number of living cells.¹⁹⁹

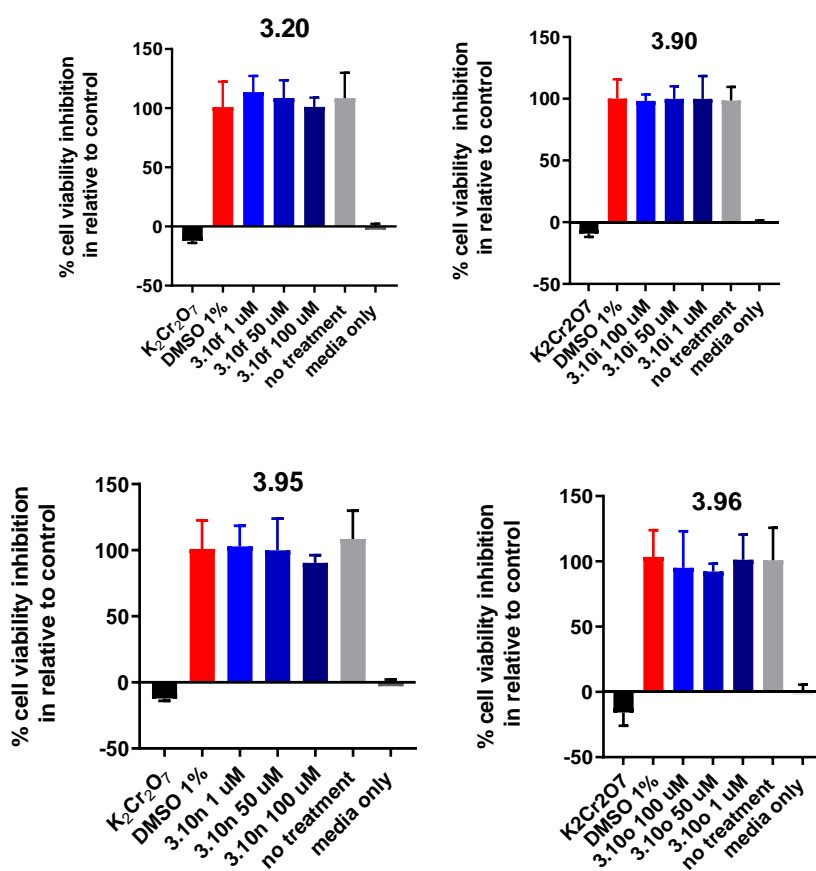


Figure 4-9: **Cytotoxicity study of the active compounds in benzimidazole series.** The Resazurin reduction assay of **3.20**, **3.90**, **3.95** and **3.96** in three concentrations in comparison to 1% DMSO (negative control) and potassium dichromate reagent (positive control) that killed the cells. The data shown are based on n = 9.

The results obtained (Figure 4-9) indicate that all studied compounds (**3.20**, **3.90**, **3.95** and **3.96**) are non-toxic at concentrations up to 100 μM , which indicates a wide therapeutic index for all compounds. However, further preclinical analyses are needed to confirm the safety and efficacy of this candidate in biological systems.

4.6 Conclusions and future work

The initial investigations and secondary phenotype pharmacological assays presented in this chapter confirmed that **3.20** binds to PqsR as a transcriptional regulator of the *pqs* system and that the antagonising effect of this compound leads to the inhibition of AQ production and pyocyanin without affecting the viability of bacteria. However, the next stage in this work involved evaluating the effect of this compound in a pathological model to determine the effect of **3.20** on the pathogenicity of *P. aeruginosa* and the ability to prevent or disrupt the biofilm formation process obtained in an *ex vivo* model. The selection of experimental and nutritional conditions is critical to providing the field with a reliable biological assay that reflects a similar clinical situation of pathogenicity and gene expression. This will support the progress of QSI discovery projects and provide an in-depth understanding of how complex QS network systems are interconnected.

Before progressing **3.20** to preclinical study, it is important to determine the stability of the candidate through *in vitro* plasma and hepatic stability assays to predict the stability and bioavailability of the compound in an *in vivo* system and determine the metabolites. The site of metabolic attack could be protected by applying the medicinal chemistry strategy to enhance the metabolic stability and bioavailability of the compound.

Additionally, during preclinical studies, it is important to evaluate the stability of the compound in the lung (by measuring the residence time) and the rate of systemic clearance since pulmonary administration is the targeted route of administration. In this context, the target is long residence time and rapid systemic clearance to reduce the frequency of administration and side effects of the medication. This objective could be achieved by modifying the design of the chemical structure or the pharmaceutical formulation to extend the residence time in the lung.

5 General Discussion and Future Work

5.1 Antivirulence drugs in the clinic

After the golden age of using traditional antibiotics for the treatment of bacterial infections, the evolution and spread of antibiotic resistance resulted in the need to seek alternatives. A novel concept has emerged that focuses on pathoblockers or disarming the virulence weaponry of pathogens instead of directly killing them. The discovery of antivirulence compounds with a novel mechanism of action requires a profound understanding of the respective pathogenic mechanisms in combination with modern medicinal chemistry strategies to develop highly effective therapies. The pathoblocker approach could be achieved through several strategies, as among these is the interference with QS to disrupt bacterial communication and biofilm formation. This strategy—known as quorum quenching (QQ)—could be achieved by: 1) Interfering with the production or perception of autoinducers via QSIs; 2) Scavenging autoinducers using quorum quenching antibodies or macromolecules such as cyclodextrins; 3) Using extracellular hydrolysis of autoinducers using QQ enzymes.²⁰⁰ The scope of this work primarily focuses on the first strategy by designing molecules that antagonise the transcriptional regulator PqsR and inhibit the synthesis of AQs (the autoinducer molecules for the *pqs* system). This system is the dominant QS in chronic *P. aeruginosa* infections and it is involved in antibiotic-tolerant and multi-drug resistant mechanisms.¹⁰⁶ In addition, the PqsR knockout strains of *P. aeruginosa* are significantly less virulent in *in vivo* infection models.¹⁰⁹ Also, the production of virulence factors such as pyocyanin and biofilm formation were drastically diminished.^{108,109} Furthermore, the rate of persister cell formation decreased, which makes bacterial populations more susceptible to antibiotic treatment.¹⁰³

Although substantial progress has been achieved in antivirulence approaches, all current evidence supporting the hypothesis of QSI approach primarily depends on *in vitro* and *in vivo* studies. While the clinical proof of concept for QSI strategy applicability remains pending. Thus, the first clinical evaluation of QSI must select therapeutic indications and patient groups carefully to avoid failure at that stage. Currently, there is a limited number of known QSIs of natural and synthetic origin in the literature.²⁰¹ To date, the only compound identified as a QSI in *P. aeruginosa* based on clinical observation is azithromycin, with only one terminated clinical trial (Clinicaltrials.gov identifier: NCT00610623).

Therefore, it remains difficult to estimate whether QSI could be used as a prophylaxis for immunosuppressed or high-risk patients, as a monotherapy treatment or in combination with conventional antibiotics. Furthermore, predicting the propensity of bacteria to develop resistance to QSI drugs is also difficult because bacterial transmission and colonisation dynamics are complex, differ among species and are incompletely understood.¹⁰⁷ For example, the hierarchy quorum sensing network in *P. aeruginosa* could overcome the inhibition of the *pqs* system and activate an alternative pathway to maintain the pathogenicity of bacteria in long-term treatment.⁷³ Additionally, the narrow spectrum of PqsR antagonists could limit the efficacy of this approach in polymicrobial infections or lead to the domination of another microbial species at the infection site. The scientific community (i.e., academic groups and the pharmaceutical industry) must provide the field with more potent candidates and more robust biological assays to analyse the activity of the candidates and predict their effect in more complex systems at the early stages of antivirulence development projects.

It becomes evident that the majority of PqsR antagonists identified to date function as useful probes for mechanistic studies for further drug development, rather than lead-like compounds.⁷² Therefore, more effort needs to be directed toward the design of drug-like molecules with favourable physicochemical properties. Following previous efforts, the work

performed in this thesis provides the field with a novel (SAR) analysis of two different series with quinazolin-4(3*H*)-one and 1*H*-benzo[*d*]imidazole derived scaffolds. **3.20** the lead candidate in this work showed a nano-molar range activity in two representative strains of *P. aeruginosa*. In addition, **3.20** inhibited the HHQ, PQS and HQNO production in different isolates of *P. aeruginosa* with the exception of PAK which is practically unaffected. These results support the proceeding of this candidate for further biological evaluation as a promising candidate that successfully proves the concept and provides the field with a wide spectrum PqsR antagonist.

5.2 The pharmacophore of PqsR antagonists

The pharmacophores of PqsR antagonists with quinazolin-4(3*H*)-one and 1*H*-benzo[*d*]imidazole scaffolds in this study are consistent with previous studies.^{87,99,103} Most of the PqsR antagonists maintain the structural features highlighted in (Figure 5-1), which provide the ideal geometry to fit the receptor and maximise the van der Waals interactions.

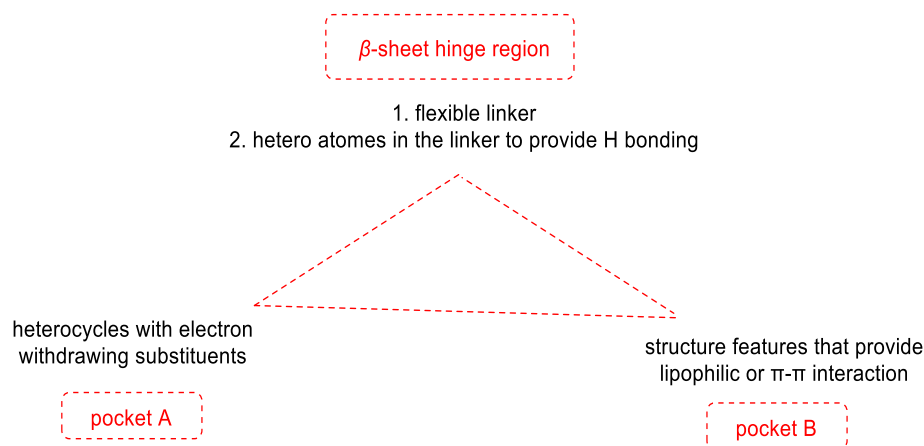


Figure 5-1: **The pharmacophore of PqsR antagonists.**

Generally, the structural features for antagonistic activity include: 1) The fused heterocycle ring system, which is likely to improve the parameters of research compounds by decreasing the number of heavy atoms and the lipophilicity of the scaffold; 2) A flexible linker that contains heteroatoms that provide hydrogen bonding with the hinge region of PqsR^{CBD}. Since H-bond interactions are highly sensitive to both distance and angle, the well-placed hydrogen bond between the linker and the receptor is critical for activity, as concluded by the SAR studies presented in this work; 3) A structural feature that provides lipophilic or π - π interactions residing in pocket B.

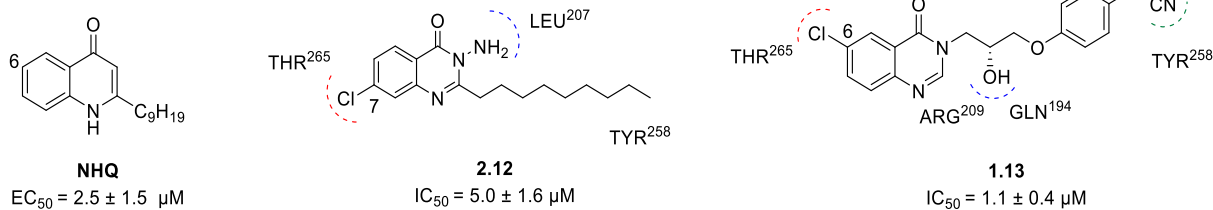


Figure 5-2: The key interactions of NHQ, **2.12**⁸⁷ and **1.13** and the improvement of antagonistic activity. EC_{50} determined in a *P. aeruginosa* $\Delta pqsAH$ CTX::P_{pqsA}-lux strain. IC_{50} determined in a *P. aeruginosa* PAO1-L CTX::P_{pqsA}-lux strain.

NHQ mainly interacts with PqsR^{CBD} via lipophilic interactions.⁸⁷ On the other hand, the binding of **2.12** featured a hydrogen bond between the backbone oxygen of Leu²⁰⁷ and the 3-amino hydrogen atoms. Additionally, the chlorine atom in position 7 can occupy a vacant sub pocket in the receptor and slightly change the conformation of the receptor.⁸⁷ Furthermore, **1.13** maintains the interaction with Thr²⁶⁵; even though, the chlorine position was moved to position 6. Additionally, although the interaction with Leu²⁰⁷ was lost in **1.13**, the hydroxyl moiety maintains H-bonding with two amino acids in the hinge region and the acetonitrile facing the Tyr²⁵⁸, which enhances the antagonistic potency 5 fold in comparison to **2.12**.

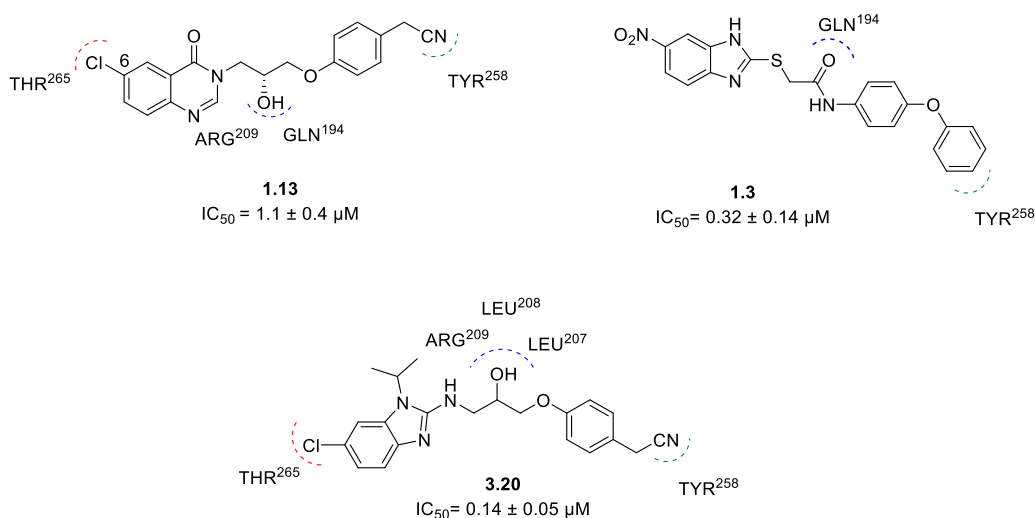


Figure 5-3: The key interactions of **1.13**, **1.3** and **3.20**, and the improvement of antagonistic activity. IC_{50} determined in a *P. aeruginosa* PAO1-L CTX::P_{pqsA}-lux strain.

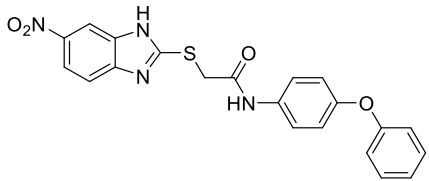
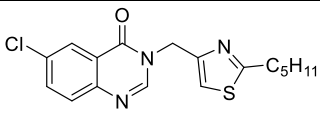
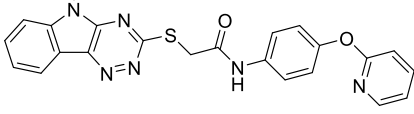
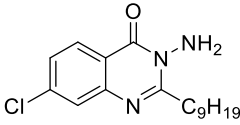
Consistent with previous findings, compounds presented in this work accommodate the receptor in a similar fashion to **1.3**. The quinazolin-4(3*H*)-one in **1.13** or 1-alkyl-1*H*-benzo[*d*]imidazol-2-amine core in **3.20** inserts deeply into the hydrophobic pocket whilst the hydroxyl moiety creates hydrogen bonding with the amino acids in the hinge region. Upon comparing **1.13** and **3.20**, the enhancement of the antagonistic activity could be due to the additional hydrogen bond obtained by the secondary amine present in the linker within **3.20**. Additionally, the lipophilic interaction between the alkyl substitutions in the 1*H*-benzo[*d*]imidazol-2-amine series and lipophilic amino acids contributes to increasing the potency of the compounds. Unravelling the precise interactions of the receptor showed that the hydroxyl in **1.13** creates H-bonding with the Arg²⁰⁹ and Gln¹⁹⁴, whilst the hydroxyl in **3.20** creates H-bonding with Arg²⁰⁹ and Leu²⁰⁸. Additionally, the secondary amine in **3.20** creates additional H-bonding with Leu²⁰⁷. Furthermore, it was reported that the benzimidazole core in **1.3** shows hydrophobic contacts with Ile¹⁴⁹ and Ile^{236,112} which could explain the 8 fold drop in IC₅₀ value after replacing quinazolin-4(3*H*)-one in **1.13** with a 1-isopropyl-1*H*-benzo[*d*]imidazol-2-amine core in **3.20**.

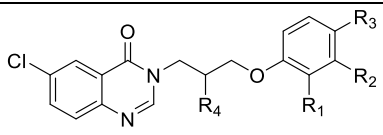
All the analysed compounds presented in this work occupied the PqsR^{CBD} domain in a similar manner to **2.12**, **1.3** and the natural ligand (NHQ), thereby demonstrating that these antagonists are competitive inhibitors to AQ ligands. However, it has been found that moving from the lipophilic interactions of natural ligands to electrostatic interactions converts agonistic activity to antagonistic activity.⁸⁷ Moreover, increasing the strength of these interactions with the receptor leads to enhanced antagonistic potency, as demonstrated in this work. The activity of PqsR antagonists is largely governed by intermolecular van der Waals attractive forces, H-bonding interactions and repulsive forces (e.g., hydrophobic effects) that help to drive a molecule from an aqueous environment into the hydrophobic cavity of PqsR^{CBD}.

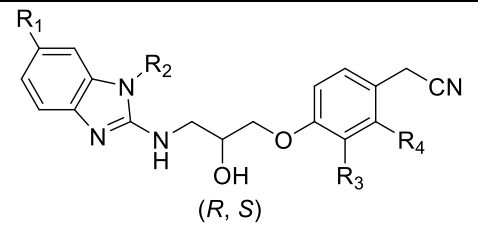
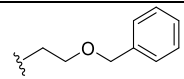
5.3 Physicochemical properties analysis

The drug development process targets the selectivity and potency of the candidate to the pharmacodynamic target as well as efficient delivery to the target site, which is achieved through maintaining proper physicochemical properties. Furthermore, the physicochemical properties determine the absorption, distribution, metabolism, excretion and toxicity properties to some extent, and ultimately affect the pharmacological activity of the drug molecule. Therefore, modifying the chemical structure and building a-SAR analysis for candidates is critical to identifying the optimal balance between activity and physicochemical properties. A better understanding of the antibacterial property space is one of the many parameters essential to improving the future success rate of identifying of novel antibacterial drugs, especially indispensable compounds with activity against multi-drug-resistant gram-negative pathogens that are becoming more prevalent in nosocomial and community-based infections. The polarity of gram-negative antibacterials drugs is increasing substantially in comparison to other drugs in the comprehensive medicinal chemistry data set.¹¹⁸ This parameter is reflected in the relative polar surface area (tabulated surface contributions of polar atoms in a molecule with regard to their binding pattern²⁰² divided by total surface area, relPSA %), hydrogen bond donor (HBD) and hydrogen bond acceptor (HBA), which are analysed in this study. Additionally, it is crucial to analyse the molecular weight (MW) and lipophilicity (the logarithm of the octanol-water distribution coefficient, clogP), since all of these parameters are primarily affected by the chemical structures of the molecules. The targeted physicochemical space of antibacterial drugs has slightly shifted to more polar and larger MW molecules when compared to other therapeutic categories of oral drugs¹¹⁸; therefore, it was crucial to enhance the polarity of both series presented in this work. The physicochemical proprieties analyses of current PqsR antagonists in the literature as well as the active compounds in the quinazolin-4(3*H*)-one and

1*H*-benzo[*d*]imidazole series are presented in this section whilst considering the ideal space of antibacterial drugs as a reference point. The ideal space of antibacterial drugs was defined based on the analysis of 64 anti-infective drugs launched from 1983–2002 and summarised as follows: MW is 456 Da, cLogP is 1.6, relPSA is 24.6%, HBD is 2.4 and HBA is 5.2.¹⁶¹ A study by O’Shea and Moser (2007) defined the proper space of synthesised antibacterial drugs with gram-negative activity represented by fluoroquinolone class as follows: MW is 371 Da, cLogP is 1.3, relPSA is 25.1%, HBD is 2.1 and HBA is 6.5.¹¹⁸ On the other hand, natural antibiotics (e.g., aminoglycosides) occupy a space with very high polarity (cLogP -2.9) with MWs between 400 and 600 Da. Analysing the physicochemical ~~properties proprieties~~ of the PqsR published in the literature and the active compounds identified in this work is critical to defining the current situation and guiding future projects.

a)	Structure	IC ₅₀ (μM)	MW	cLogP
1.3		0.32 ± 0.14	420.0	5.2
1.11		0.31 ± 0.15	347.8	4.2
1.12		0.25 ± 0.12	442.5	3.5
2.12		5.0 ± 1.6	321.8	5.9

							
b)	R ₁	R ₂	R ₃	R ₄	IC ₅₀ (μM)	MW	cLogP
1.6	H	H	CH ₂ CN	(<i>S</i> , <i>R</i>) OH	3.2 ± 1.0	369.1	1.9
1.13	H	H	CH ₂ CN	(<i>R</i>) OH	1.1 ± 0.4	369.1	1.9
2.34	H	H	OCH ₂ CN	(<i>S</i> , <i>R</i>) OH	4.5 ± 0.7	385.8	1.8
2.35	F	H	CH ₂ CN	(<i>S</i> , <i>R</i>) OH	2.2 ± 0.2	387.8	2.3
2.36	H	F	CH ₂ CN	(<i>S</i> , <i>R</i>) OH	6.4 ± 0.7	387.8	2.3

							
c)	R ₁	R ₂	R ₃	R ₄	IC ₅₀ (μM)	MW	cLogP
3.1	Cl	CH ₃	H	H	0.21 ± 0.04	370.8	3.2
3.109	CF ₃	CH ₃	H	H	1.5 ± 0.3	404.4	3.4
3.19	Cl	C ₂ H ₅	H	H	0.13 ± 0.03	384.9	3.7
3.20	Cl	CH(CH ₃) ₂	H	H	0.14 ± 0.05	398.9	4.0
3.91	Cl	C(CH ₃) ₃	H	H	0.22 ± 0.01	412.9	4.4
3.92	Cl	CH ₂ C(CH ₃) ₃	H	H	0.38 ± 0.01	426.9	5.1
3.90	Cl	cyclo-propyl	H	H	0.06 ± 0.03	396.9	3.8
3.91	Cl	cyclo-butyl	H	H	0.16 ± 0.01	410.9	4.1
3.92	Cl	cyclo-pentyl	H	H	0.44 ± 0.1	424.9	4.7
3.93	Cl	cyclo-hexyl	H	H	0.75 ± 0.4	439.0	5.2
3.94	Cl		H	H	1.05 ± 0.2	491.0	4.9
3.95	Cl	CH(CH ₃) ₂	F	H	0.05 ± 0.02	416.9	4.1


3.96	Cl	CH(CH ₃) ₂	H	F	0.06 ± 0.03	416.9	4.1
3.101	H	CH(CH ₃) ₂	H	H	0.77 ± 0.2	364.4	3.3
3.99	Cl		H	H	0.15 ± 0.01	412.9	2.6
3.100	Cl	C ₂ H ₄ OCH ₃	H	H	0.18 ± 0.04	414.9	3.1
3.103	Cl	C ₂ H ₄ OH	H	H	0.18 ± 0.05	400.9	2.4

Table 5-1: Structures of compounds employed in physicochemical ~~properties~~ properties analysis presented in this chapter. a) various PqsR antagonists presented in the literature and b) active compounds in the quinazolin-4(3*H*)-one and c) 1*H*-benzo[*d*]imidazole series. IC₅₀ determined in a *P. aeruginosa* PAO1-L CTX::*P_{pqsA}-lux* strain.

Notably, the candidate must reach the biophase and cross several bio-membranes in planktonic and eukaryotic cells. This process requires a balance between two contradictory parameters: lipophilicity and polarity. Lipophilicity is a key molecular descriptor influencing a variety of drug and candidate properties. This property essentially reflects the key event of molecular desolvation in transferring from aqueous phases to cell membranes and to protein binding sites, which are mostly hydrophobic. If lipophilicity is too high, there is an increased likelihood of poor solubility, poor metabolic clearance and binding to multiple targets (drug promiscuity), which leads to pharmacologically based toxicology. Another molecular descriptor that could evaluate the lipophilicity of compounds is relPSA %. Increasing the polarity by balancing between low cLogP and high relPSA % (as shown in Figure 5-4) is the ideal space for antibacterial drugs.

5.3.1 Lipophilicity analysis

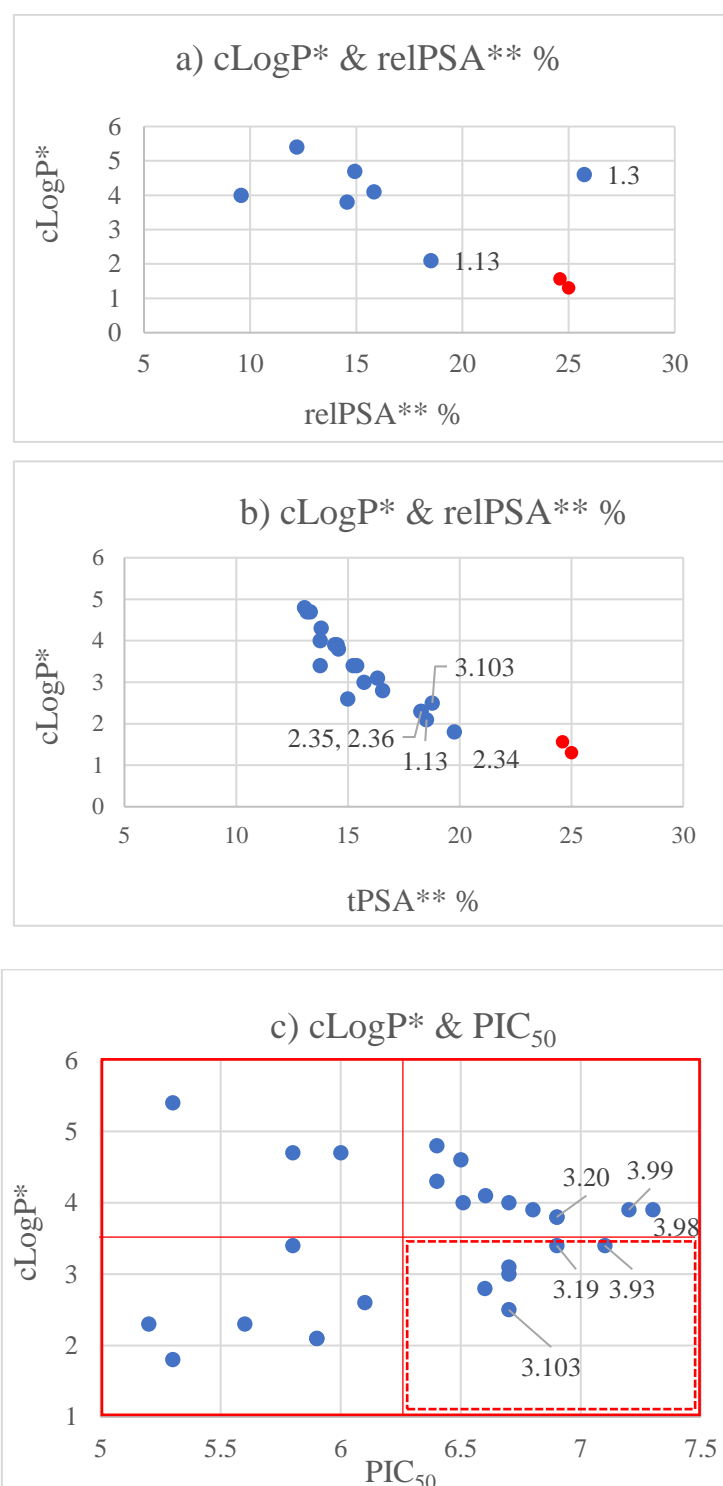


Figure 5-4: **Illustration of cLogP* values plotted against relPSA** %.** a) PqsR antagonists presented in the literature, in addition to **1.13** and **3.20**. b) Active compounds in the quinazolin-4(3*H*)-one and 1*H*-benzo[*d*]imidazole series. c) Illustration of cLogP values plotted against the PIC₅₀ of active compounds in the quinazolin-4(3*H*)-one and 1*H*-benzo[*d*]imidazole series. Red spots indicate the reference points of antibacterial drugs' ideal space, as defined in the literature.^{118,161} The asterisk (*) indicates that this parameter was predicted

using ChemDraw 19.0.1.28 (<http://www.chemaxon.com>). The asterisks (**) indicates that this parameter was predicted using SwissADME website (<http://www.swissadme.ch>).

The only candidate that has a relPSA value similar to the reference point is **1.3**; however, the cLogP of this candidate is 2.5 fold higher. The **1.13** hit of quinazolin-4(3*H*)-one series was the strongest candidate positioned within the high probability zone of the ideal space. Similarly, analysing the polarity of the active compounds in the quinazolin-4(3*H*)-one and 1*H*-benzo[*d*]imidazole series (Figure 5-4b) showed that **2.34** is better than **1.13** at balancing between low cLogP and high relPSA. Additionally, **3.103** is the only compound from the 1*H*-benzo[*d*]imidazole series that fits within the zone of quinazolin-4(3*H*)-one compounds. Notably, lipophilicity is a crucial factor that drives potency. Since PqsR^{CBD} is generally lipophilic, it is essential to plot the activity versus the cLogP to remove this effect and determine the potent compounds with optimal physicochemical space. Leeson and Springthorpe introduced lipophilic ligand efficiency (LLE) (or LiPE) as a parameter to evaluate the quality of research compounds by linking potency and lipophilicity to estimate drug-likeness.¹²¹ Additionally, LLE provides readily determined guideposts that are useful in decision making during the lead optimisation stage, especially in the absence of ITC data. This expression is defined as the difference of log P (or log D) and the negative logarithm of potency measures (pIC₅₀). LLE describes the contribution of lipophilicity to potency and can be used in conjunction with log P, log D or clog D. For **3.95**, $LLE = (7.3 - 3.9) = 3.4$, whilst **3.103** $LLE = (6.7 - 2.5) = 4.2$. This implies that even though **3.95** is the most potent compound in the present work, **3.103** is better in terms of balancing between potency and lipophilicity. The optimal target range for LLE is generally considered to be between 5 and 7.¹⁶¹ Unfortunately, the compounds presented in the literature and this work fail to fit in that range.

5.3.2 Molecular weight analysis

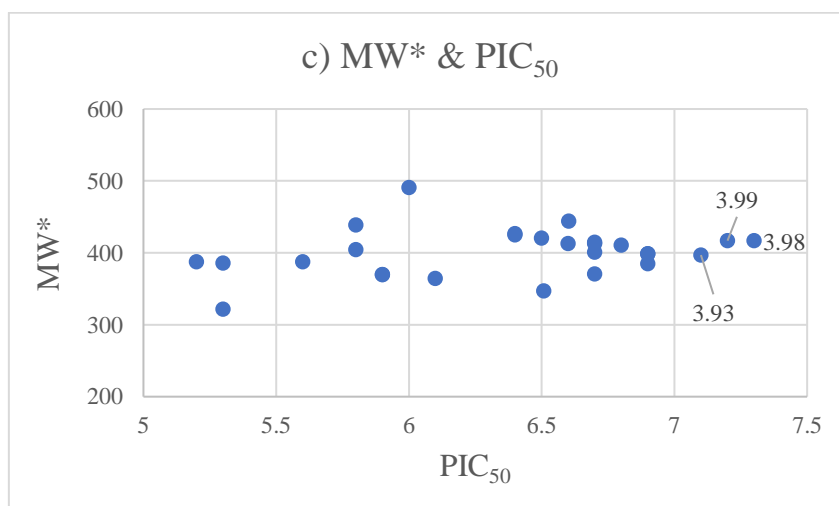
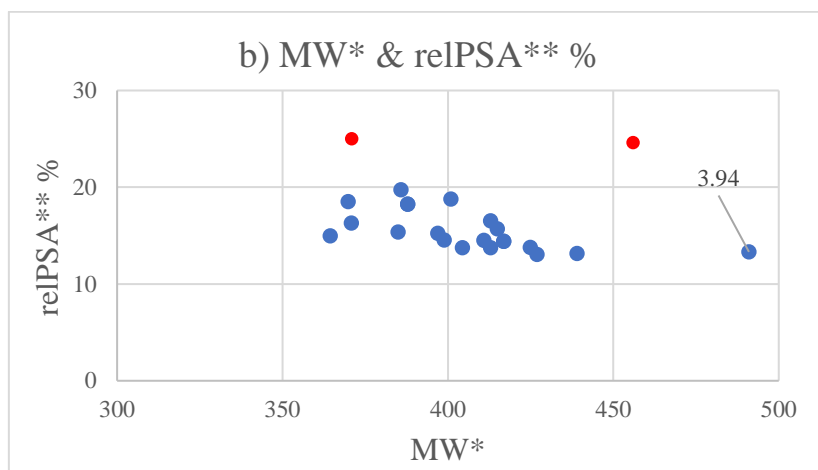
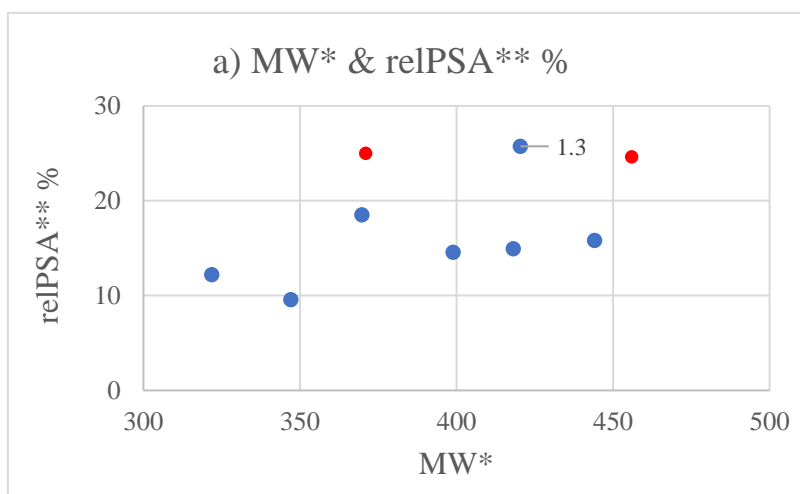


Figure 5-5: **Illustration of MW* values plotted against relPSA* %.** a) PqsR antagonists presented in the literature. b) Active compounds in the quinazolin-4(3*H*)-one and 1*H*-benzo[*d*]imidazole series. c) Illustration of MW values plotted against PIC₅₀. The red spots are the reference points of antibacterial drugs' ideal space, as defined in the literature.^{118,161} The asterisk (*) indicates that this parameter was predicted using ChemDraw 19.0.1.28 (<http://www.chemaxon.com>). The asterisk (**) indicates that this parameter was predicted using SwissADME website (<http://www.swissadme.ch>).

Another characteristic of antibacterial drugs is their high MW, especially in antibacterial drugs of natural origin. An increase in MW could increase the lipophilicity or relPSA, which are contraindicated proprieties to each other. To define the optimal space (i.e., high relPSA and high MW), these two parameters were plotted against each other (Figure 5-5a and Figure 5-5b). The results indicate that the compounds in both groups did not occupy the targeted space and that **1.3** is the only candidate that achieved relPSA and MW values similar to the reference points. On the other hand, the range of MW for the most potent compounds in the [quinazolin-4\(3*H*\)-one and 1*H*-benzo\[*d*\]imidazole](#) series was between 400 and 420 Da, with a relPSA range between 14 and 15% (Figure 5-5c).

3.94 showed the highest number of C atoms with one micromolar activity. Additionally, the restriction of conformation into the active conformer plays a role in driving potency since it appeared in comparison to the *iso* propyl **3.20** and cyclopropyl analogue **3.90**, with an approximately 2 fold enhancement in potency. This could be driven by conformational entropy—which is more favourable in **3.90**—by decreasing the loss of conformational freedom.

5.3.3 Hydrogen bond donor and acceptor analysis

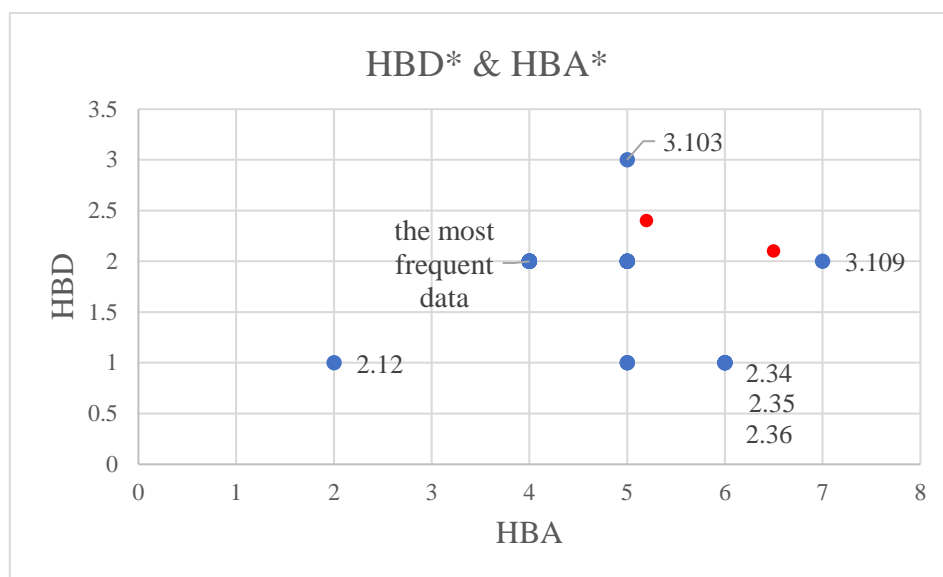


Figure 5-6: Illustration of the number of hydrogen bond donor* plotted against the number of hydrogen bond acceptor* in PqsR antagonists presented in the literature and active compounds in the quinazolin-4(3*H*)-one and 1*H*-benzo[*d*]imidazole series. The red spots are the reference points of antibacterial drugs' ideal space, as defined in the literature.^{118,161} The asterisk (*) indicates that this parameter was predicted using SwissADME website (<http://www.swissadme.ch>).

The number of HBD and HBA are additional parameters that describe property requirements and define the targeted space of the candidates. Nitrogen and oxygen are the most common heavy atoms that can act as both (HBD and HBA) with functional groups such as OH and NH₂. The mean of HBD and HBA of 64 anti-infective drugs were 2.4 and 5.2, respectively. To some extent, these parameters affect the lipophilicity and relPSA % of the molecules as well as the ligand-protein interaction. **3.109** has the highest number of HBA, whilst **3.103** has the highest number of HBD in comparison to the reference point.

The anti-infective drugs generally possessed the highest mean MW, lowest mean lipophilicity, highest HBA, and highest O and N atom counts in comparison to other therapeutic category drugs¹⁶¹. Thus, the design of antivirulence candidates should be directed to this space.

5.4 Conclusions and future work

The work presented in this thesis further promotes the progression of PqsR antagonists by providing the field with potent compounds with sub-micromolar potency and acceptable physicochemical properties. These *pqs* inhibitors can be used as tools to unravel the current knowledge behind the role of the *pqs* system in certain complicated mechanisms such as bacterial biofilms.

The PqsR antagonists presented here were obtained from *in silico* screening followed by *in vitro* validation and further chemical optimisation. Two SAR studies were established for the quinazolin-4(3*H*)-one and 1*H*-benzo[*d*]imidazol-2-amine series. The first study (Chapter 2) found that the *R* enantiomer **1.13** had a reasonable micromolar IC₅₀ value in PAO1-L, with cLogP 2.1. The SAR analysis of **1.13** as a hit was limited since any small modification to the molecule led to a loss of activity. However, **2.34** was the only analogue in the series that exhibited slightly enhanced polarity, with a 4 fold decrease in potency. Further chemical optimisation (outlined in Chapter 3) led to the discovery of another series with a 1*H*-benzo[*d*]imidazol-2-amine scaffold. The synthetic strategy of benzo[*d*]imidazol-2-amine series was optimised in this work leading to synthesis **3.20** in large quantity (100-200 mg) with high purity (≥ 95%) sufficient for further *in vitro* and *in vivo* assays. Although the quinazolin-4(3*H*)-one core is almost 3 fold more polar than the 1*H*-benzo[*d*]imidazole ring (regardless of the alkyl substitution in *N*¹), this replacement leads to a 5 fold enhancement of antagonistic potency.

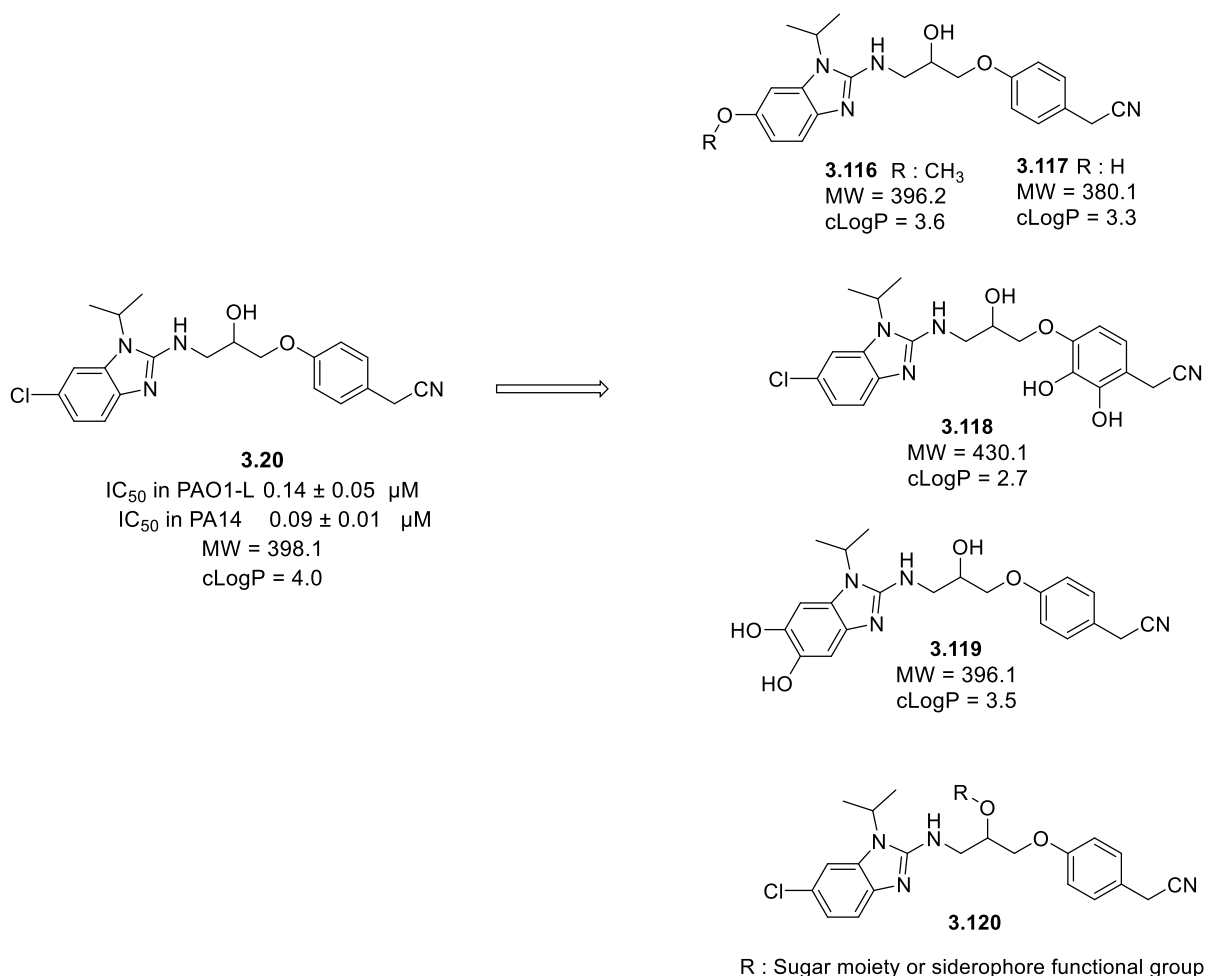


Figure 5-7: The design of future work to support the current SAR study and improve the activity of the series.

Further investigation of the series could be performed by replacing the chlorine atom in **3.20** with methoxy **3.116** or hydroxy moiety **3.117** in order to probe the effect of H-bond donor on the binding as well as enhance the lipophilicity of the compound. Another optimization strategy could be applied to enhance the accumulation of the PqsR antagonists inside the bacterial cells, especially the resistance strains, by introducing a microbial siderophore functional group such as catechol, in **3.118** and **3.119**. These compounds are likely to chelate iron in the extracellular environment and form iron–siderophore complex which is recognized by high-affinity receptor proteins in the bacterial cell wall. These proteins utilize active transport to internalize the iron.²⁰³ In addition, linking the molecule to a sugar moiety, different siderophore or siderophore

mimic functional groups, **3.120** could be an effective strategy to enhance the uptake and release the free PqsR antagonist, **3.20** inside the bacterial cell. The last two strategies could enhance the accumulation of the compound as well as the potency.

Additionally, in rich media (LB) and aerobic conditions, using **3.20** as a lead candidate (200 nM concentration) inhibited the production of pyocyanin in all strains. At this concentration, the AQ production of PAO1-L WT was close to the production detected in a $\Delta pqsR$ mutant.¹⁸⁸ The inhibition was also significant in clinical isolates.¹⁸⁸ On the other hand, **1.13** demonstrated a significant reduction of HHQ and PQS in PAO1-L WT and little to no impact on the AQ production of other strains. Additionally, upon comparing the IC₅₀ values of **3.20** to the previously reported PqsR antagonist in the literature (**1.3**), it was evident that **3.20** successfully exhibited a wide spectrum of potency against different phenotypes of *P. aeruginosa* with PAK CF isolate (one of the more resistant strains) as an exception. It is worth mentioning that the action of phenylalanine arginyl β -naphthylamide (an efflux pump inhibitor) has been observed to increase the action of **3.20** against a PAK CF isolate.¹⁸⁸

Furthermore, there is a need to investigate the effect of **3.20** on biofilm assay as well as *in vivo* studies to determine the compound's efficacy in a biological system. Additionally, the effect of **3.20** should be investigated in aerobic and anaerobic settings to examine the relevance of *pqs* inhibition under these conditions. A biological evaluation of **1.3** has proven that it can significantly decrease the number of persister cells in a culture, which is highly relevant to the clinical environment.¹⁰³ Persisters cells are dormant, non-dividing cells that exhibit multidrug tolerance and survive under antibiotic treatment. Consequently, when the course treatment is completed, these cells can resume their growth and increase the size of the bacterial population. Therefore, it remains critical to assess the effect of **3.20** over persister cells in future work to prove this concept.

Additionally, various pharmacokinetic models involving solubility, permeability across an artificial membrane, hERG inhibition and cytochromes P450 (CYPs) enzyme inhibition need to be established to evaluate the safety and stability of this novel compound. Furthermore, different pharmaceutical formulations could be employed to increase the half-life of the candidate in desired sites whilst also increasing its accumulation within bacterial cells.

However, the lack of methodological standardisation in assessing QSI candidates including the use of single laboratory-adapted *P. aeruginosa* strains and abiotic surface biofilm that may be distinct from relevant clinical infections is the major challenge in this field. Therefore, it remains critical to employ different laboratory strains as well as clinical isolates to test the spectrum of the candidate's activity. In addition, there is a need to provide the field with reliable biological assays that represent a chronically infected human lung with a similar clinical situation of pathogenicity and gene expression. This will support the progress of QSI discovery projects and provide an in-depth understanding of how complex QS network systems are interconnected and work.

6 Experimental

6.1 Chemistry

6.1.1 Reagents and instruments

Chemical Synthesis. Chemicals and solvents were purchased from commercial sources (typically, Sigma Aldrich, Alpha Aesar, Fisher Scientific, Acros Organics, or Fluorochem), and used without further purification. Anhydrous solvents were purchased from Sigma Aldrich and used without further distillation. All reactions involving air- or moisture- sensitive reagents were performed under nitrogen atmosphere. all compounds were dried under high vacuum either at rt or within an oven at 40 °C.

Nuclear magnetic resonance. ^1H -NMR and ^{13}C -NMR were obtained at RT using a Bruker AV(III) HD 400 NMR spectrometer, spectrometer operated at 400 MHz and equipped with a 5 mm BBFO β probe, recording ^1H and ^{13}C NMR at 400.25 MHz and 100.66 MHz respectively; or a Bruker AV(III) 500 NMR spectrometer equipped with a 5 mm dual $^1\text{H}/^{13}\text{C}$ helium-cooled cryoprobe, recording ^1H and ^{13}C NMR at 500.13 MHz and 125.77 MHz respectively. The samples were prepared in deuterated solvent; DMSO- d_6 . The data was processed using iNMR (version 5.5.7) referencing spectra to residual solvents and the chemical shifts (δ) were recorded in ppm relative to trimethylsilan (TMS) and coupling constants (J) were recorded in Hz. Abbreviations used in the description of spectra are: s (singlet), br (broad), d (doublet), dd (doublet of doublets), t (triplet), q (quartet), sp septet and m (multiplet). The spectra were analysed using Topspin 3.0 and MestReNova 14.1.1-24571 softwares and the assignment of the peaks are CH_{Ar} for aromatic region and CH_{Al} for aliphatic region.

Mass spectrometry. LC-MS data was recorded on a Shimadzu UFLCXR HPLC system coupled to an Applied Biosystems API2000 electrospray ionization mass spectrometer (ESI-MS). The column used was a Phenomenex Gemini-NX 3 μm 110 Å C-18, 50 x 2 mm

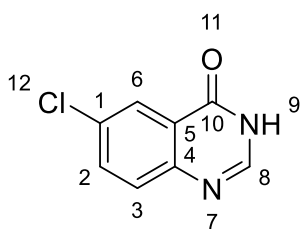
thermostated at 40 °C. The flow rate was 0.5 mL / min of a solvent system of increasing gradient of acetonitrile (5-95%) in water, each containing 0.1% formic acid. UV detection was at 220 nm and 254 nm. m/z values are reported in Daltons to one decimal place and retention times (t_R) are provided in minutes to two decimal places.

Chromatography. Thin-layer chromatography (TLC) was performed, UV light and standard TLC stains were used to visualise the Merck Silica gel 60 Å F254 plates. Compounds were purified via column chromatography using either a Thompson pump or normal phase Interchim Purifl ash pre-packed cartridges consisting of 50 µM silica, or a glass column using Merck Geduran silica gel 60 Å (230-240 µm). Column size selected was generally 40-60 times the loading amount.

The compounds presented in this chapter are novel unless they referred to the literature with an agreement in $^1\text{H-NMR}$ and $^{13}\text{C-NMR}$. The HRMS analysis was carried out by Dr. Fadi Soukarieh for the purpose of publication.

6.1.2 Experimental of chapter 2

6-Chloroquinazolin-4(3H)-one (2.20).¹¹⁷

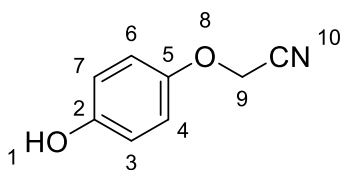


A solution of 5-chloroanthranilic acid (20 g, 0.11 mol) in Formamide (45 mL) was refluxed and stirred at 150 °C for 16 h, forming a brown precipitate. The reaction mixture was cooled to room temperature and left to stand for 1 h, then the precipitate filtered and concentrate *in vacuo*. Brown microcrystals (21 g, 100 %). ¹H NMR (400 MHz, DMSO-*d*₆) δ 12.37 (br s, 1H, NH), 8.13 (s, 1H, C₈H), 8.00 (d, *J* = 2.5 Hz, 1H, C₆H), 7.80 (dd, *J* = 8.8, 2.5 Hz, 1H, C₂H), 7.66 (d, *J* = 8.8 Hz, 1H, C₃H). ¹³C NMR (101 MHz, DMSO-*d*₆) δ 160.3, 147.9, 146.4, 134.7, 131.4, 129.8, 125.2, 124.3. LCMS *m/z* calc for C₈H₅ClN₂O⁺ [M+H]⁺ : 181.0, found 180.8 with *t*_R 2.25 min.

General procedure (2.A) for preparation (2.25-2.27).

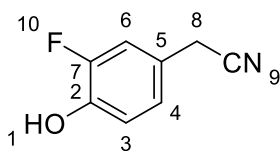
To a solution of different methoxides in DCM at 0 °C was treated with dropwise of BBr₃ (1M in DCM, 10 mL/g). The mixture was allowed to warm to rt and stirred overnight. H₂O (10 mL) was added dropwise to the mixture which then stirred for 30 min at rt. The organic layer was concentrated *in vacuo* to the dryness and the residue was dissolved in ethyl acetate and washed with water. The organic phase was concentrated *in vacuo* to afford the desired product as a colourless oil which was used in the next step without further purification.

2-(4-Hydroxyphenoxy) acetonitrile (2.25) ²⁰⁴



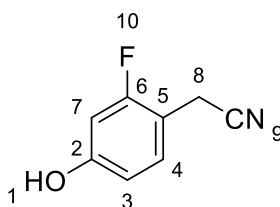
The title compound was prepared in the manner similar to the general procedure (2.A) by utilizing 2-(4-hydroxyphenoxy) acetonitrile **2.21** (1g, 6mmol) as the starting material. Brown oil (0.8g, 80 %). ¹H NMR (400 MHz, DMSO-*d*₆) δ 6.81 (m, 2H, *CH*_{Ar}), 6.75 (m, 2H, *CH*_{Ar}), 5.03 (s, 2H, *C*₉*H*). ¹³C NMR (101 MHz, DMSO-*d*₆) δ 151.4, 148.9, 116.9, 116.2, 68.0.

2-(3-Fluoro-4-hydroxyphenyl) acetonitrile (2.26)



The title compound was prepared in the manner similar to the general procedure (2.A) by utilizing 2-(3-fluoro-4-methoxyphenyl) acetonitrile **2.22** (5g, 0.03mol) as the starting material. Brown oil (3.2g, 70 %). ¹H NMR (400 MHz, DMSO-*d*₆) δ 9.95 (s, 1H, *OH*), 7.14 (dd, *J* = 12.3, 1.9 Hz, 1H, *CH*_{Ar}), 7.03 – 6.87 (m, 2H, *CH*_{Ar}), 3.91 (s, 2H, *C*₈*H*). ¹³C NMR (101 MHz, DMSO-*d*₆) δ 151.2 (d, *J* = 242.7 Hz), 144.8 (d, *J* = 12.6 Hz), 124.8 (d, *J* = 3.5 Hz), 122.6 (d, *J* = 7.8 Hz), 119.7, 118.5 (d, *J* = 4.2 Hz), 116.6 (d, *J* = 19.2 Hz), 21.8.

2-(2-Fluoro-4-hydroxyphenyl) acetonitrile (2.27).



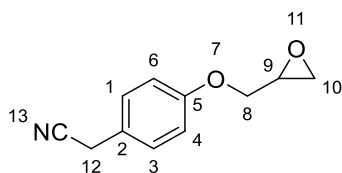
The title compound was prepared in the manner similar to the general procedure (2.A) by utilizing 2-(2-fluoro-4-methoxyphenyl) acetonitrile **2.23** (5g, 0.03mol) as the starting material. Brown oil (4.1g, 86 %). ¹H NMR (400 MHz, DMSO-*d*₆) δ 10.02 (s, 1H, *OH*), 7.23 (t, *J* = 8.9 Hz, 1H, *CH*_{Ar}), 6.67 – 6.57 (m, 2H, *CH*_{Ar}), 3.88 (s, 2H, *C*₈*H*). ¹³C NMR

(101 MHz, DMSO-*d*₆) δ 160.9 (d, *J* = 243.3 Hz), 159.2 (d, *J* = 11.9 Hz), 131.3 (d, *J* = 5.5 Hz), 118.9, 112.3 (d, *J* = 3.0 Hz), 108.6 (d, *J* = 17.3 Hz), 103.4 (d, *J* = 21.6 Hz), 16.6.

General procedure (2.B) for preparation (2.29-33).

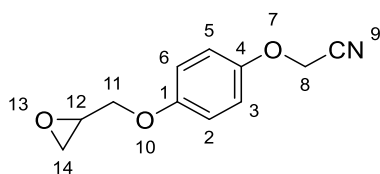
To a stirred solution of different phenols (1eq) in MeCN (50 mL), was added Cs₂CO₃ (2 eq), then epichlorohydrin (1.2 eq). The reaction mixture was heated at 85 °C for 16h. The mixture was filtered and purified using column chromatography eluting the desired compound with 80:20 Petroleum Ether: Ethyl Acetate.

2-(4-Oxiran-2-ylmethoxy) phenyl) acetonitrile (2.29)



The title compound was prepared in the manner similar to the general procedure (2.B) by utilizing 4-hydroxyphenylacetonitrile **2.24** (20g, 0.15mol) as the starting material. White solid (7g, 25 %). ¹H NMR (400 MHz, DMSO-*d*₆) δ 7.30 – 7.24 (m, 2H, CH_{Ar}), 7.02 – 6.95 (m, 2H, CH_{Ar}), 4.33 (dd, *J* = 11.3, 2.7 Hz, 1H, CH_{Al}), 3.95 (s, 2H, C₁₂H), 3.83 (dd, *J* = 11.3, 6.5 Hz, 1H, CH_{Al}), 3.33 – 3.30 (m, 1H, CH_{Al}), 2.85 (t, *J* = 4.7 Hz, 1H, CH_{Al}), 2.71 (dd, *J* = 5.1, 2.7 Hz, 1H, CH_{Al}). ¹³C NMR (101 MHz, DMSO-*d*₆) δ 158.1, 129.7, 123.8, 119.9, 115.4, 69.4, 50.1, 44.2, 22.0.

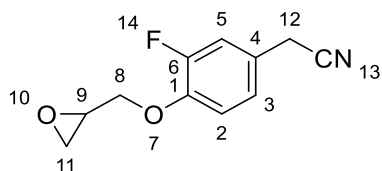
2-(4-(2-cyanoethyl)phenoxy) oxirane (2.30)



The title compound was prepared in the manner similar to the general procedure (2.B) by utilizing 2-(4-hydroxyphenoxy) acetonitrile **2.25** (0.8g, 5mmol) as the starting material. White solid (0.6g, 54 %). ¹H NMR (400 MHz, DMSO-*d*₆) δ 7.10 – 6.86 (m, 4H, CH_{Ar}), 5.10 (s, 2H, C₈H), 4.29 (dd, *J* = 11.4, 2.7 Hz, 1H, CH_{Al}), 3.80 (dd, *J* = 11.4, 6.6

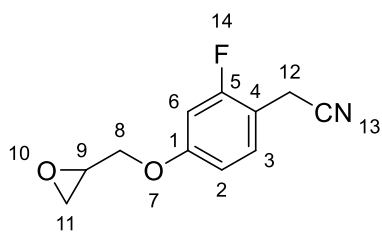
Hz, 1H, CH_{Al}), 3.33 – 3.28 (m, 1H, CH_{Al}), 2.84 (dd, $J = 5.1, 4.2$ Hz, 1H, CH_{Al}), 2.70 (dd, $J = 5.1, 2.7$ Hz, 1H, CH_{Al}). ^{13}C NMR (101 MHz, DMSO- d_6) δ 154.1, 151.0, 117.2, 116.6, 116.0, 69.8, 54.6, 50.2, 44.2.

2-(3-Fluoro-4-(oxiran-2-ylmethoxy) phenyl) acetonitrile (2.31)



The title compound was prepared in the manner similar to the general procedure (2.B) by utilizing 2-(3-fluoro-4-hydroxyphenyl) acetonitrile **2.26** (3.2g, 0.01mol) as the starting material. White solid (1.5g, 35 %). 1H NMR (400 MHz, DMSO- d_6) δ 7.27 – 7.17 (m, 2H, CH_{Ar}), 7.16 – 7.10 (m, 1H, CH_{Ar}), 4.42 (m, 1H, CH_{Al}), 3.97 (s, 2H, $C_{12}H$), 3.92 (m, 1H, CH_{Al}), 3.43 – 3.36 (m, 1H, CH_{Al}), 2.87 (m, 1H, CH_{Al}), 2.77 – 2.68 (m, 1H, CH_{Al}). ^{13}C NMR (101 MHz, DMSO- d_6) δ 151.9 (d, $J = 245.8$ Hz), 146.0 (d, $J = 10.5$ Hz) 124.9 (d, $J = 4.2$ Hz), 119.5, 116.6 (d, $J = 21.0$ Hz), 116.0 (d, $J = 1.5$ Hz), 70.6, 49.9, 44.1, 21.9.

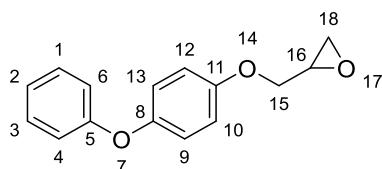
2-(2-Fluoro-4-(oxiran-2-ylmethoxy) phenyl) acetonitrile (2.32)



The title compound was prepared in the manner similar to the general procedure (2.B) by utilizing 2-(2-fluoro-4-hydroxyphenyl) acetonitrile **2.27** (4.1g, 0.02mol) as the starting material. White solid (2g, 36 %). 1H NMR (400 MHz, DMSO- d_6) δ 7.37 (t, $J = 8.8$ Hz, 1H, C_3H), 6.96 (d, $J = 2.6$ Hz, 1H, C_6H), 6.86 (dd, $J = 8.8, 2.6$ Hz, 1H, C_2H), 4.38 (dd, $J = 11.5, 2.6$ Hz, 1H, $C_{Al}H$), 3.96 (s, 2H, $C_{12}H$), 3.86 (dd, $J = 11.5, 6.6$ Hz, 1H, CH_{Al}), 3.37 – 3.30 (m, 1H, CH_{Al}), 2.90 – 2.81 (m, 1H, CH_{Al}), 2.71 (dd, $J = 5.1, 2.7$ Hz, 1H, CH_{Al}). ^{13}C NMR (101 MHz, DMSO- d_6) δ 161.1 (d, $J = 226.9$ Hz), 159.7 (d, $J = 8.7$ Hz), 131.4

(d, $J = 5.1$ Hz), 118.8, 111.7 (d, $J = 3.6$ Hz), 110.9 (d, $J = 15.3$ Hz), 102.8 (d, $J = 24.5$ Hz), 69.9, 49.9, 44.1, 16.6.

2-((4-Phenoxyphenoxy) methyl) oxirane (2.33)

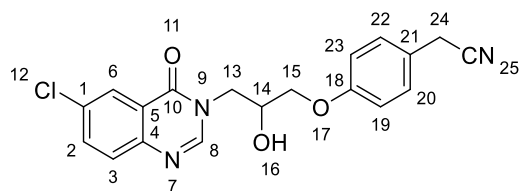


The title compound was prepared in the manner similar to the general procedure (2.B) by utilizing 4-phenoxy phenol **2.28** (2g, 0.01mol) as the starting material. White solid (0.6g, 23 %). ^1H NMR (400 MHz, DMSO- d_6) δ 7.32 (t, $J = 9.6, 8.7$ Hz, 2H, CH_{Ar}), 7.06 (t, $J = 7.3$ Hz, 1H, CH_{Ar}), 6.99 (d, $J = 6.6, 3.8$ Hz, 4H, CH_{Ar}), 6.92 (t, $J = 8.7, 7.2$ Hz, 2H, CH_{Ar}), 4.27 – 3.75 (m, 4H, CH_{Al}), 3.44 (s, 1H, CH_{Al}). ^{13}C NMR (101 MHz, DMSO- d_6) δ 158.4, 155.4, 150.0, 130.3, 123.03, 121.1, 117.8, 116.3, 68.76, 51.11, 44.21.

General procedure (2.C) for preparation (1.6, 2.34-2.37).

To a stirred solution of 6-chloroquinazolin-4(3H)-one **2.20** (1eq) in MeCN, a mixture of different epoxides (**2.29-2.33**) (1.2 eq), Cs_2CO_3 (2 eq) and TBAI (0.1 eq) was added. The reaction mixture was heated at 100 °C for 16 h. The mixture was filtered, concentrated *in vacuo* and purified using column chromatography eluting the desired compound with 80:20 Ethyl Acetate: Petroleum Ether.

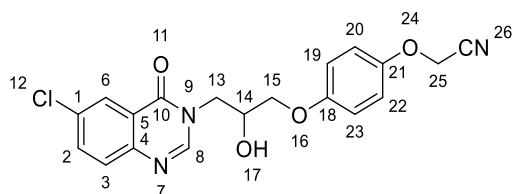
2-(4-(3-(6-Chloro-4-oxoquinazolin-3(4H)-yl)-2-hydroxypropoxy) phenyl) acetonitrile (1.6)



The title compound was prepared in the manner similar to the general procedure (2.C) by utilizing 2-(4-oxiran-2-ylmethoxy) phenyl)

acetonitrile **2.29** (7.3g, 0.039 mol) as the starting material. The mixture was filtered and purified using column chromatography eluting the desired compound with 80:20 Ethyl Acetate: Petroleum Ether. Yellow solid (3.2 g, 24 %). ¹H NMR (400 MHz, DMSO-*d*₆) δ 8.32 (s, 1H, C₈H), 8.11 (d, *J* = 2.5 Hz, 1H, C₆H), 7.88 (dd, *J* = 8.8, 2.5 Hz, 1H, C₂H), 7.73 (d, *J* = 8.8 Hz, 1H, C₃H), 7.32 – 7.23 (m, 2H, CH_{Ar}), 7.03 – 6.93 (m, 2H, CH_{Ar}), 5.52 (d, *J* = 5.6 Hz, 1H, OH), 4.35 (dd, *J* = 13.4, 3.8 Hz, 1H, C₁₅H), 4.19 (ddd, *J* = 9.1, 5.6, 3.8 Hz, 1H, C₁₄H), 4.08 – 3.95 (m, 2H, C₁₃H), 3.95 (s, 2H, C₂₄H), 3.95 – 3.87 (m, 1H, C₁₅H). ¹³C NMR (101 MHz, DMSO-*d*₆) δ 159.9, 158.3, 149.7, 147.2, 134.8, 132.0, 129.9, 129.7, 125.4, 123.7, 123.3, 120.0, 115.8, 70.7, 66.4, 50.0, 22.0. LCMS *m/z* calc for C₁₉H₁₇ClN₃O₃⁺ [M+H]⁺: 370.1, found 369.9 with *t*_R 2.68 min. HRMS *m/z* calc for C₁₉H₁₇ClN₃O₃⁺ [M + H]⁺: 370.1 found 370.1. Purity of the compound was confirmed to be >95% by LCMS using a long method run.

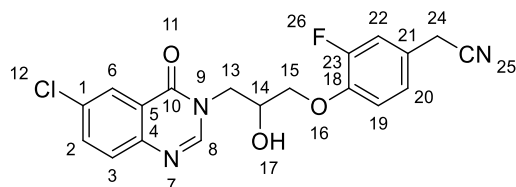
2-(4-(3-(6-Chloro-4-oxoquinazolin-3(4*H*)-yl)-2-hydroxypropoxy) phenoxy) acetonitrile (2.34)



The title compound was prepared in the manner similar to the general procedure (2.C) by utilizing 2-(4-(oxiran-2-ylmethoxy) phenoxy) acetonitrile **2.30** (0.6 g, 3 mmol) as the starting material. White solid (0.3 g, 26 %). ¹H NMR (400 MHz, DMSO-*d*₆) δ 8.32 (s, 1H, C₈H), 8.10 (d, *J* = 2.5 Hz, 1H, C₆H), 7.85 (dd, *J* = 8.7, 2.5 Hz, 1H, C₂H), 7.71 (d, *J* = 8.7 Hz, 1H, C₃H), 7.07 – 6.97 (m, 2H, CH_{Ar}), 7.00 – 6.91 (m, 2H, CH_{Ar}), 5.51 (d, *J* = 5.6 Hz, 1H, OH), 5.10 (s, 2H, C₂₅H), 4.40 – 4.31 (m, 1H, C₁₅H), 4.23 – 4.12 (m, 1H, C₁₃H), 3.99 (dd, *J* = 5.6, 1.8 Hz, 2H, C_{13,14}H), 3.91 (dd, *J* = 13.5, 8.6 Hz, 1H, C₁₅H). ¹³C NMR (101 MHz, DMSO-*d*₆) δ 159.9, 154.3, 150.9, 149.6, 147.1, 134.8, 131.6, 129.8, 125.4, 123.3, 117.2, 116.6, 116.1, 71.1, 66.5, 54.6, 50.0. LCMS *m/z* calc for C₁₉H₁₆ClN₃O₄⁺

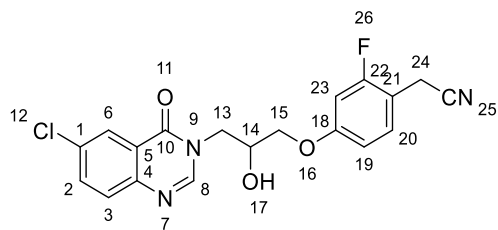
[M+H]⁺: 386.0, found 386.4 with *t*_R 2.66 min. Purity of the compound was confirmed to be >95 % by LCMS using a long method run.

**2-(4-(3-(6-Chloro-4-oxoquinazolin-3(4*H*)-yl)-2-hydroxypropoxy)-3-fluorophenyl)
acetonitrile (2.35)**



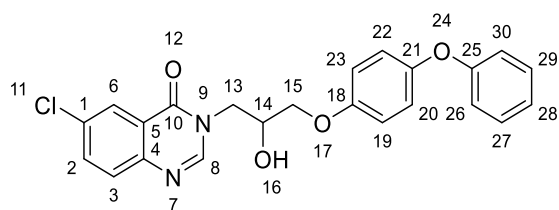
The title compound was prepared in the manner similar to the general procedure (2.C) by utilizing 2-(3-fluoro-4-(oxiran-2-ylmethoxy) phenyl) acetonitrile **2.31** (0.18 g, 8 mmol) as the starting material. White solid (90 mg, 24 %). ¹H NMR (400 MHz, DMSO-*d*₆) δ 8.31 (s, 1H, C₈H), 8.15 – 8.05 (m, 1H, C₆H), 7.87 (ddd, *J* = 9.0, 6.5, 2.5 Hz, 1H, C₂H), 7.72 (dd, *J* = 9.0, 6.5 Hz, 1H, C₃H), 7.27 – 7.19 (m, 2H, CH_{Ar}), 7.14 (dd, *J* = 9.0, 1.9 Hz, 1H, CH_{Ar}), 5.56 (d, *J* = 5.6 Hz, 1H, OH), 4.34 (dd, *J* = 13.4, 3.7 Hz, 1H, C₁₅H), 4.21 (d, *J* = 10.3 Hz, 1H, C₁₃H), 4.10 (dd, *J* = 5.6, 2.6 Hz, 2H, C_{13,14}H), 3.98 (s, 2H, C₂₄H), 3.92 (dd, *J* = 13.4, 8.5 Hz, 1H, C₁₅H). ¹³C NMR (101 MHz, DMSO-*d*₆) δ 160.0, 154.0 (d, *J* = 247.3 Hz), 147.2, 146.4, 134.9 (d, *J* = 10.2 Hz), 131.6 (d, *J* = 2.7 Hz), 129.9 (d, *J* = 19.7 Hz), 125.3 (d, *J* = 1.5 Hz), 124.3, 123.3, 119.5, 116.4, 116.0, 72.1, 66.4, 50.1, 21.9. LCMS *m/z* calc for C₁₉H₁₅ClFN₃O₃⁺ [M+H]⁺: 388.0, found 388.3 with *t*_R 2.68 min. Purity of the compound was confirmed to be >95 % by LCMS using a long method run.

**2-(4-(3-(6-Chloro-4-oxoquinazolin-3(4*H*)-yl)-2-hydroxypropoxy)-2-fluorophenyl)
acetonitrile (2.36)**



The title compound was prepared in the manner similar to the general procedure (2.C) by utilizing 2-(2-fluoro-4-(oxiran-2-ylmethoxy) phenyl) acetonitrile **2.32** (0.2, 10 mmol) as the starting material. White solid (93 mg, 25 %). ^1H NMR (400 MHz, DMSO- d_6) δ 8.31 (s, 1H, C₈H), 8.11 (d, $J = 2.4$ Hz, 1H, C₆H), 7.87 (dd, $J = 8.7, 2.4$ Hz, 1H, C₂H), 7.72 (d, $J = 8.7$ Hz, 1H, C₃H), 7.36 (t, $J = 8.8$ Hz, 1H, CH_{Ar}), 6.95 – 6.88 (m, 1H, CH_{Ar}), 6.83 (dd, $J = 8.5, 2.5$ Hz, 1H, CH_{Ar}), 5.54 (d, $J = 5.6$ Hz, 1H, OH), 4.32 (dd, $J = 13.4, 3.6$ Hz, 1H, C₁₅H), 4.18 (ddt, $J = 13.9, 9.1, 5.6$ Hz, 1H, C₁₄H), 4.13 – 3.99 (m, 2H, CH_{Al}), 3.99 – 3.88 (m, 3H, CH_{Al}). ^{13}C NMR (101 MHz, DMSO- d_6) δ 161.1 (d, $J = 226.9$ Hz), 159.9, 159.7 (d, $J = 8.7$ Hz), 149.6, 147.2, 134.8, 131.4 (d, $J = 5.1$ Hz), 129.9, 125.3, 123.3, 118.8, 111.7 (d, $J = 3.6$ Hz), 110.9 (d, $J = 15.3$ Hz), 102.8 (d, $J = 24.5$ Hz), 71.1, 66.3, 49.9, 16.6. LCMS m/z calc for C₁₉H₁₅ClFN₃O₃⁺ [M+H]⁺: 388.0, found 388.3 with t_R 2.71 min. Purity of the compound was confirmed to be >95 % by LCMS using a long method run.

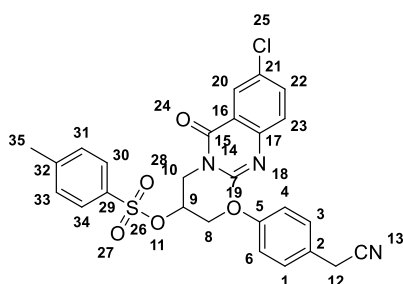
6-Chloro-3-(2-hydroxy-3-(4-phenoxyphenoxy) propyl) quinazolin-4(3H)-one (**2.37**)



The title compound was prepared in the manner similar to the general procedure (2.C) by utilizing 2-((4-phenoxyphenoxy) methyl) oxirane **2.33** (0.6 g, 24 mmol) as the starting material. White solid (85 mg, 24 %). ^1H NMR (400 MHz, DMSO- d_6) δ 8.33 (s, 1H C₈H), 8.11 (d, $J = 2.5$ Hz, 1H C₆H), 7.88 (dd, $J = 8.7, 2.5$ Hz, 1H C₂H), 7.73 (d, $J = 8.7$ Hz, 1H C₃H), 7.35 (t, $J = 9.7, 6.0, 2.3$ Hz, 2H, CH_{Ar}), 7.08 (t, $J = 7.4$ Hz, 1H, CH_{Ar}), 6.99 (d, $J = 1.7$ Hz, 4H, CH_{Ar}), 6.95 – 6.90 (m, 2H, CH_{Ar}), 5.51 (d, $J = 5.6$ Hz, 1H OH), 4.35 (dd, $J = 13.4, 3.7$ Hz, 1H, C₁₅H), 4.23 – 4.14 (m, 1H, C₁₄H), 4.08 – 3.97 (m, 2H,

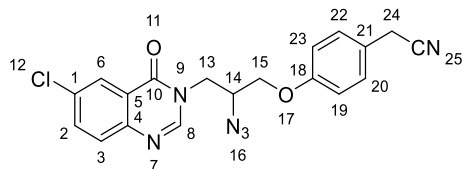
$C_{13}H$), 3.92 (dd, $J = 13.4, 8.6$ Hz, 1H, $C_{15}H$). ^{13}C NMR (101 MHz, DMSO- d_6) δ 159.9, 158.4, 155.2, 150.1, 149.7, 147.2, 134.8, 131.6, 130.3, 129.9, 125.4, 123.3, 121.2, 118.0, 116.3, 115.9, 71.1, 66.5, 50.0. LCMS m/z calc for $C_{23}H_{19}ClN_2O_4^+$ $[M+H]^+$: 423.1, found 423.4 with t_R 3.27 min. Purity of the compound was confirmed to be >95 % by LCMS using a long method run.

Preparation of 1-(6-chloro-4-oxoquinazolin-3(4H)-yl)-3-(4-(cyanomethyl) phenoxy) propan-2-yl 4-methylbenzenesulfonate (2.41)



To a stirred solution of 2-(4-(3-(6-chloro-4-oxoquinazolin-3(4H)-yl)-2-hydroxypropoxy) phenyl) acetonitrile **1.6** (1 g, 3 mmol) in DCE: 5% THF, was added, *p*-toluenesulfonyl chloride (1.5 gm, 8 mmol), NEt_3 (0.8 g, 8 mmol), DMAP (0.3 g, 3 mmol). The mixture was stirred for 16 h at rt. The mixture was purified using column chromatography eluting the desired compound with 40:60 Ethyl Acetate: Petroleum Ether. White solid (0.8 g, 57 %). LCMS m/z calc for $C_{26}H_{22}ClN_3O_5S^+$ $[M+H]^+$: 524.1 found 524.1 with t_R 3.11 min.

Preparation of 2-(4-(2-azido-3-(6-chloro-4-oxoquinazolin-3(4H)-yl) propoxy) phenyl) acetonitrile (2.39)



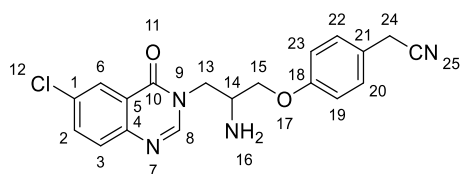
Method A: to a stirred solution of 2-(4-(3-(6-chloro-4-oxoquinazolin-3(4H)-yl)-2-hydroxypropoxy) phenyl) acetonitrile **1.6** (2 g, 5 mmol) in anhydrous THF (100 mL), the Ph_3P (2 g, 8 mmol) was added under anhydrous condition at rt. After 5 min the mixture was cooled over ice bath before addition of DIAD (1.6 g, 8 mmol)

which is followed by DPPA (2.2 g, 8 mmol). The mixture was stirred for 5 min in ice bath, in addition to another 5 min at rt. This mixture was then allowed to stir at 45°C overnight. The mixture was purified using column chromatography eluting the desired compound with 40:60 Ethyl Acetate: Petroleum Ether. Yellow solid (1 g, 33 %).

Method B: to a stirred solution of 1-(6-chloro-4-oxoquinazolin-3(4*H*)-yl)-3-(4-(cyanomethyl) phenoxy) propan-2-yl 4-methylbenzenesulfonate **2.41** (0.8 g, 1.5 mmol) in DMF, was added NaN₃ (0.3 g, 4.5 mmol). The mixture was stirred for 16 h at 60°C. The mixture was purified using column chromatography eluting the desired compound with 40:60 Ethyl Acetate: Petroleum Ether. Yellow solid (0.4 g, 65 %).

¹H NMR (400 MHz, DMSO-*d*₆) δ 8.40 (s, 1H, C₈H), 8.14 (d, *J* = 2.5 Hz, 1H, C₆H), 7.91 (dd, *J* = 8.8, 2.5 Hz, 1H, C₂H), 7.76 (d, *J* = 8.8, Hz, 1H, C₃H), 7.35 – 7.26 (m, 2H, CH_{Ar}), 7.13 – 6.96 (m, 2H, CH_{Ar}), 4.49 – 4.28 (m, 3H, CH_{Al}), 4.22 – 4.10 (m, 2H, CH_{Al}), 3.97 (s, 2H, C₂₄H). ¹³C NMR (101 MHz, DMSO-*d*₆) δ 160.0, 157.7, 149.0, 147.0, 135.1, 131.9, 130.0, 129.9, 125.6, 124.3, 123.2, 119.9, 115.5, 68.8, 59.1, 46.7, 22.0. LCMS *m/z* calc for C₁₉H₁₆ClN₆O₂⁺ [M+H]⁺: 395.1, found 395.0 with *t*_R 2.90 min.

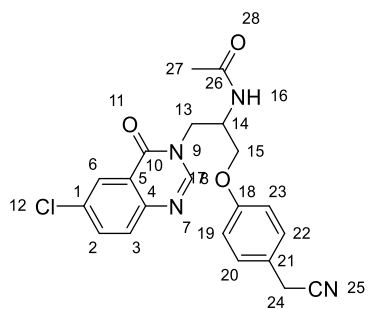
Preparation of 2-(4-(2-amino-3-(6-chloro-4-oxoquinazolin-3(4*H*)-yl) propoxy) phenyl) acetonitrile (**2.40**).



To a mixture of 2-(4-(2-azido-3-(6-chloro-4-oxoquinazolin-3(4*H*)-yl) propoxy) phenyl) acetonitrile **2.39** (1 g, 2.5 mmol) and Ph₃P (1 g, 3.7 mmol), THF (100 mL) was added and stirred for 2 h at 65°C. Then, 10 % water with 0.5 mL of ammonia hydroxide was added and stirred overnight at rt. The mixture was purified using column chromatography eluting the desired compound with 90:10 Ethyl Acetate: MeOH

containing NH₃ (0.7 N). White solid (100 mg, 11 %). ¹H NMR (400 MHz, DMSO-*d*₆) δ 8.38 (s, 1H, C₈H), 8.10 (d, *J* = 2.5 Hz, 1H, C₆H), 7.87 (dd, *J* = 8.8, 2.5 Hz, 1H, C₂H), 7.72 (d, *J* = 8.8 Hz, 1H, C₃H), 7.27 (d, *J* = 8.3 Hz, 2H, CH_{Ar}), 6.94 (d, *J* = 8.3 Hz, 2H, CH_{Ar}), 4.29 (dd, *J* = 13.3, 4.2 Hz, 1H, C₁₅H), 3.94 (d, *J* = 10.9 Hz, 4H, C_{13,24}H), 3.83 (dd, *J* = 13.3, 8.5 Hz, 1H, C₁₅H), 3.38 (t, *J* = 4.2 Hz, 1H, C₁₄H). ¹³C NMR (101 MHz, DMSO-*d*₆) δ 160.0, 158.3, 149.7, 147.2, 134.7, 131.5, 129.8, 125.4, 123.7, 123.4, 120.0, 115.4, 71.8, 60.2, 49.4, 21.9. LCMS *m/z* calc for C₁₉H₁₈ClN₄O₂⁺ [M+H]⁺: 369.1, found 369.1 with *t*_R 2.13 min. HRMS *m/z* calc for C₁₉H₁₈ClN₄O₂⁺ [M + H]⁺: 369.1, found 369.1. Purity of the compound was confirmed to be >95 % by LCMS using a long method run.

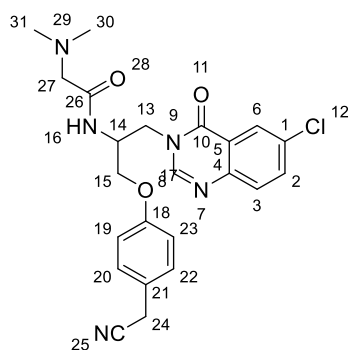
Preparation of *N*-(1-(6-chloro-4-oxoquinazolin-3(4*H*)-yl)-3-(4-(cyanomethyl) phenoxy) propan-2-yl) acetamide (2.47)



To 4 mL of acetic acid anhydride, 2-(4-(2-amino-3-(6-chloro-4-oxoquinazolin-3(4*H*)-yl) propoxy) phenyl) acetonitrile **2.40** (50 mg, 0.1 mmol) was added and stirred at 30 °C for 3h. The reaction was concentrated to the dryness and the residue was dissolved in ethyl acetate and washed with saturated aqueous NaOH and water. The organic phase was concentrated to afford the desired product without further purification. White solid (53 mg, 95 %). ¹H NMR (400 MHz, DMSO-*d*₆) δ 8.28 (s, 1H, C₈H), 8.17 – 8.07 (m, 2H, C₆H, NH), 7.87 (dd, *J* = 8.7, 2.5 Hz, 1H, C₂H), 7.72 (d, *J* = 8.7 Hz, 1H, C₃H), 7.28 (m, CH_{Ar}), 7.02 – 6.94 (m, 2H, CH_{Ar}), 4.55 (tt, *J* = 8.9, 4.8 Hz, 1H, C₁₄H), 4.39 (dd, *J* = 13.6, 4.5 Hz, 1H, C₁₅H), 4.07 (dd, *J* = 5.3, 1.6 Hz, 2H, C₁₃H), 4.01 – 3.90 (m, 3H, C_{15,24}H), 1.76 (s, 3H, C₂₇H). ¹³C NMR (101 MHz, DMSO-*d*₆) δ 170.0, 159.9, 158.0, 149.0, 147.0, 134.9, 131.7, 129.9, 129.8, 125.5,

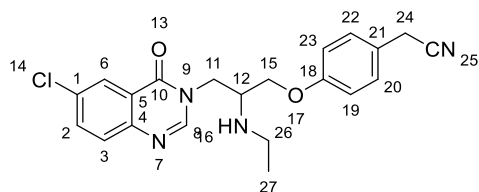
124.0, 123.1, 119.9, 115.5, 68.4, 47.8, 47.3, 22.9, 22.0. LCMS m/z calc for $C_{21}H_{20}ClN_4O_3^+$ $[M+H]^+$: 411.1, found 411.1 with t_R 2.62 min. Purity of the compound was confirmed to be >95 % by LCMS using a long method run.

Preparation of *N*-(1-(6-chloro-4-oxoquinazolin-3(4*H*)-yl)-3-(4-(cyanomethyl) phenoxy) propan-2-yl)-2-(dimethylamino) acetamide (2.48)



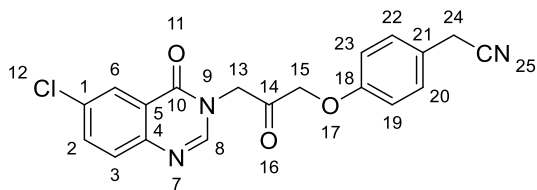
To a stirred solution of (dimethyl amino) acetic acid (12 mg, 0.12 mmol) in DMF (20 mL), was added a mixture of 2-(4-(2-amino-3-(6-chloro-4-oxoquinazolin-3(4*H*)-yl) propoxy) phenyl) acetonitrile **2.40** (60 mg, 0.16 mmol), PyBrop (0.1g, 0.24 mmol) and trimethylamine (46 mg, 0.36 mmol). The mixture was stirred for 4h at rt. The mixture was purified using column chromatography eluting the desired compound with DCM: 10% MeOH containing NH_3 (0.7 N). White solid (28 mg, 54 %). 1H NMR (400 MHz, $DMSO-d_6$) δ 8.32 (s, 1H, C_8H), 8.10 (d, $J = 2.5$ Hz, 1H, C_6H), 8.02 (d, $J = 9.2$ Hz, 1H, NH), 7.87 (dd, $J = 8.7, 2.5$ Hz, 1H, C_2H), 7.71 (d, $J = 8.7$ Hz, 1H, C_3H), 7.29 (d, $J = 8.7$ Hz, 2H, CH_{Ar}), 7.03 – 6.95 (m, 2H, CH_{Ar}), 4.63 (d, $J = 9.2$ Hz, 1H, $C_{14}H$), 4.39 (dd, $J = 13.5, 4.1$ Hz, 1H, $C_{15}H$), 4.16 – 4.04 (m, 3H, $C_{13,15}H$), 3.96 (s, 2H, $C_{24}H$), 2.76 (d, $J = 1.3$ Hz, 2H, $C_{27}H$), 2.12 (s, 6H, $C_{30-31}H$). ^{13}C NMR (101 MHz, $DMSO-d_6$) δ 170.5, 159.9, 158.1, 149.0, 147.0, 134.9, 131.7, 129.9, 129.8, 125.5, 124.0, 123.1, 119.9, 115.5, 68.3, 63.1, 47.5, 46.3, 45.8, 22.0. LCMS m/z calc for $C_{23}H_{25}ClN_5O_3^+$ $[M+H]^+$: 454.1, found 453.9 with t_R 2.17 min. Purity of the compound was confirmed to be >95 % by LCMS using a long method run.

Preparation of 2-(4-(3-(6-chloro-4-oxoquinazolin-3(4H)-yl)-2-(ethylamino) propoxy) phenyl) acetonitrile (2.50)



To a stirred solution of 2-(4-(2-amino-3-(6-chloro-4-oxoquinazolin-3(4H)-yl) propoxy) phenyl) acetonitrile **2.40** (20 mg, 0.054 mmol) in MeCN (20 mL), a mixture of iodoethan (40 uL, 0.54 mmol) and Cs₂CO₃ (13 mg, 0.10 mmol) was added. The mixture was stirred at 60 °C for 16 h. The mixture was purified using column chromatography eluting the desired compound with 95:5 Ethyl Acetate: MeOH containing NH₃ (0.7 N). White solid (13 mg, 65 %). ¹H NMR (400 MHz, DMSO-*d*₆) δ 8.34 (s, 1H, C₈H), 8.10 (d, *J* = 2.5 Hz, 1H, C₆H), 7.87 (dd, *J* = 8.7, 2.5 Hz, 1H, C₂H), 7.72 (d, *J* = 8.7 Hz, 1H, C₃H), 7.26 (d, *J* = 8.4 Hz, 2H, CH_{Ar}), 6.92 (d, *J* = 8.4 Hz, 2H, CH_{Ar}), 4.23 (dd, *J* = 13.5, 5.5 Hz, 1H, C₁₅H), 4.00 (dd, *J* = 10.0, 5.2 Hz, 3H, C_{11,12}H), 3.94 (s, 2H, C₂₄H), 3.23 (s, 1H, C₂₆H), 2.69 (dq, *J* = 13.5, 7.1 Hz, 1H, C₁₅H), 1.90 (s, 1H, C₂₆H), 0.91 (t, *J* = 7.1 Hz, 3H, C₂₇H). ¹³C NMR (101 MHz, DMSO-*d*₆) δ 160.0, 158.2, 149.7, 147.2, 134.8, 131.6, 129.9, 129.7, 125.5, 123.7, 123.2, 120.0, 115.4, 68.7, 55.0, 48.6, 41.2, 21.9, 15.9. LCMS *m/z* calc for C₂₁H₂₂ClN₄O₂⁺ [M+H]⁺: 397.1, found 397.0 with *t*_R 2.65 min. Purity of the compound was confirmed to be >95 % by LCMS using a long method run.

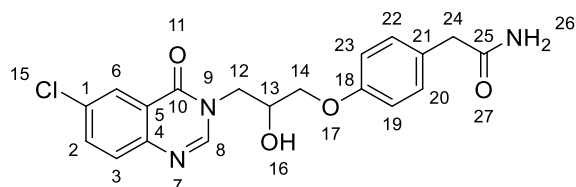
Preparation of 2-(4-(3-(6-chloro-4-oxoquinazolin-3(4H)-yl)-2-oxopropoxy) phenyl) acetonitrile (2.38)



To a mixture of 2-(4-(3-(6-chloro-4-oxoquinazolin-3(4H)-yl)-2-hydroxypropoxy) phenyl) acetonitrile **1.6** (0.5g, 1.3 mmol) in DCM (50 mL),

Dess–Martin periodinane (1g, 2.3 mmol) was added and stirred overnight at rt. The mixture was washed with 1M NaOH, another wash with H₂O, dry it with Na₂SO₄ anhydrous and concentrate the mixture. The residue was purified using column chromatography eluting the desired compound with 70:30 Ethyl Acetate: Petroleum Ether. White solid (0.4g, 76 %). ¹H NMR (400 MHz, DMSO-*d*₆) δ 8.32 (s, 1H, C₈H), 8.09 (d, *J* = 2.5 Hz, 1H, C₆H), 7.88 (dd, *J* = 8.8, 2.5 Hz, 1H, C₂H), 7.75 (d, *J* = 8.8 Hz, 1H, C₈H), 7.30 (d, *J* = 8.5 Hz, 2H, CH_{Ar}), 7.02 (d, *J* = 8.5 Hz, 2H, CH_{Ar}), 5.16 (s, 2H, C₁₅H), 5.09 (s, 2H, C₁₃H), 3.96 (s, 2H, C₂₄H). ¹³C NMR (101 MHz, DMSO-*d*₆) δ 200.3, 159.5, 157.4, 148.9, 147.1, 135.2, 132.0, 130.0, 129.8, 125.5, 124.3, 122.9, 119.9, 115.5, 71.5, 52.6, 22.0. LCMS *m/z* calc for C₁₉H₁₅ClN₃O₃⁺ [M+H]⁺: 368.1, found 367.7 with *t*_R 2.75 min. HRMS *m/z* calc for C₁₉H₁₅ClN₃O₃⁺ [M + H]⁺: 368.1, found 367.7. Purity of the compound was confirmed to be >95 % by LCMS using a long method run.

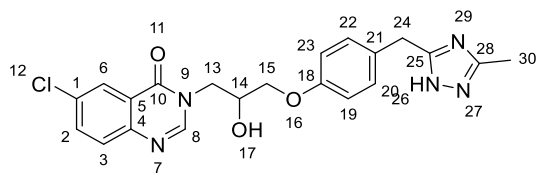
Preparation of 2-(4-(3-(6-chloro-4-oxoquinazolin-3(4*H*)-yl)-2-hydroxypropoxy) phenyl) acetamide (2.51)



A solution of 2-(4-(3-(6-chloro-4-oxoquinazolin-3(4*H*)-yl)-2-hydroxypropoxy) phenyl) acetonitrile **1.6** (0.1g, 0.27 mmol), Cs₂CO₃ (0.3g, 0.54 mmol) in DMSO: 30 % H₂O₂ (100 mL) was stirred for 30 minutes in rt. The mixture was purified using column chromatography eluting the desired compound with 100 % Ethyl Acetate. White solid (0.1g, 96 %). ¹H NMR (400 MHz, DMSO-*d*₆) δ 8.32 (s, 1H, C₈H), 8.12 (d, *J* = 2.5 Hz, 1H, C₆H), 7.88 (dd, *J* = 8.6, 2.5 Hz, 1H, C₂H), 7.73 (d, *J* = 8.6 Hz, 1H, C₃H), 7.40 (s, 1H, NH), 7.18 (d, *J* = 8.2 Hz, 2H, CH_{Ar}), 6.91 – 6.86 (dd, 2H, CH_{Ar}), 6.83 (s, 1H, NH), 5.50 (d, *J* = 5.6 Hz, 1H, OH), 4.35 (dd, *J* = 13.4, 3.6 Hz, 1H, C₁₄H), 4.18 (m, 1H, C₁₃H), 4.02 – 3.84 (m, 3H, C_{12,14}H), 3.30 (s, 2H, C₂₄H). ¹³C NMR (101 MHz, DMSO-*d*₆) δ 173.0, 159.9, 157.4, 149.7, 147.2, 134.8, 131.6, 130.5, 129.9, 129.2, 125.5, 123.3, 114.7, 70.6,

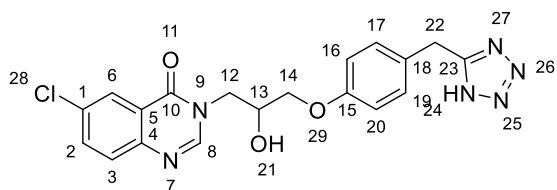
66.5, 50.0, 41.82. LCMS m/z calc for $C_{19}H_{19}ClN_3O_4^+$ $[M+H]^+$: 388.1, found 387.9 with t_R 2.42 min. Purity of the compound was confirmed to be >95 % by LCMS using a long method run.

Preparation of 6-chloro-3-(2-hydroxy-3-(4-((3-methyl-1H-1,2,4-triazol-5-yl) methyl) phenoxy) propyl) quinazolin -4(3H)-one (2.53)



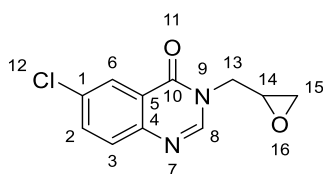
To a stirred solution of 2-(4-(3-(6-chloro-4-oxoquinazolin-3(4H)-yl)-2-hydroxypropoxy) phenyl) acetonitrile **1.6** (0.3g, 0.8 mmol) in methanol (50 mL), acetylhydrazine (0.17g, 2.4 mmol) and 0.1g of sodium methoxide was added. The mixture was refluxed at 80 °C for 16 h. The mixture was diluted with ethyl acetate (50 mL). Then, the ethyl acetate was washed with water (3 x 50 mL), dry it with Na_2SO_4 anhydrous and concentrate the mixture. The residue was purified using column chromatography eluting the desired compound with 95:5 ethyl acetate: MeOH containing NH_3 (0.7 N). White solid (50 mg, 14 %). 1H NMR (400 MHz, $DMSO-d_6$) δ 13.27 (s, 1H, NH), 8.31 (s, 1H, C_8H), 8.10 (d, $J = 2.6$ Hz, 1H, C_6H), 7.87 (dd, $J = 8.7, 2.6$ Hz, 1H, C_2H), 7.72 (d, $J = 8.7$ Hz, 1H, C_3H), 7.16 (d, $J = 8.0$ Hz, 2H, CH_{Ar}), 6.86 (d, $J = 8.0$ Hz, 2H, CH_{Ar}), 5.50 (d, $J = 5.7$ Hz, 1H, OH), 4.34 (dd, $J = 13.4, 3.7$ Hz, 1H, $C_{15}H$), 4.21 – 4.12 (m, 1H, $C_{14}H$), 3.97 (s, 2H, $C_{24}H$), 3.93 – 3.80 (m, 3H, $C_{13,15}H$), 2.25 (s, 3H, $C_{30}H$). ^{13}C NMR (101 MHz, $DMSO-d_6$) δ ^{13}C NMR (126 MHz, $DMSO-d_6$) δ 172.3, 162.7, 159.9, 157.2, 153.1, 149.7, 147.2, 134.8, 131.6, 130.1, 129.9, 125.4, 123.3, 114.8, 70.6, 66.4, 50.0, 33.6, 12.0. LCMS m/z calc for $C_{21}H_{21}ClN_5O_3^+$ $[M+H]^+$: 426.1, found 426.2 with t_R 2.35 min. Purity of the compound was confirmed to be >95 % by LCMS using a long method run.

Preparation of 3-(3-(4-((1*H*-tetrazol-5-yl) methyl) phenoxy)-2-hydroxypropyl)-6-chloroquinazolin-4(3*H*)-one (2.54).



To a stirred solution of 2-(4-(3-(6-chloro-4-oxoquinazolin-3(4*H*)-yl)-2-hydroxypropoxy) phenyl) acetonitrile **1.6** (0.3g, 8 mmol) in DMF (50 mL), NaN₃ (0.15 g, 24 mmol) and Et₃N.HCl (0.3g, 24 mmol) were added. The reaction mixture was heated at 130 °C for 16 h. The reaction was concentrated to the dryness and the desired product was isolated using column chromatography eluting the desired compound with 95:5 Ethyl Acetate: acetic acid. Brown solid (250 mg, 75 %). ¹H NMR (400 MHz, DMSO-*d*₆) δ 8.32 (s, 1H, C₈H), 8.11 (d, *J* = 2.5 Hz, 1H, C₆H), 7.87 (dd, *J* = 8.7, 2.5 Hz, 1H, C₂H), 7.72 (d, *J* = 8.7 Hz, 1H, C₃H), 7.13 (d, *J* = 8.4 Hz, 2H, CH_{Ar}), 6.86 – 6.74 (d, *J* = 8.4 Hz, 2H, CH_{Ar}), 5.64 (s, 1H, OH), 4.34 (dd, *J* = 13.4, 3.6 Hz, 1H, C₁₄H), 4.14 (dt, *J* = 9.0, 4.4 Hz, 1H, C₁₃H), 3.95 (d, *J* = 5.2 Hz, 2H, C₁₂H), 3.91 (s, 2H, C₂₂H), 3.90 – 3.86 (m, 1H, C₁₄H). ¹³C NMR (101 MHz, DMSO-*d*₆) δ 163.9, 160.3, 159.9, 156.8, 149.7, 147.2, 134.8, 133.5, 131.5, 129.9, 125.5, 123.3, 114.5, 70.7, 66.5, 50.0, 31.2. LCMS *m/z* calc for C₁₉H₁₇ClN₆O₃⁺ [M+H]⁺ : 413.1, found 412.7 with *t*_R 2.71 min. Purity of the compound was confirmed to be >95 % by LCMS using a long method run.

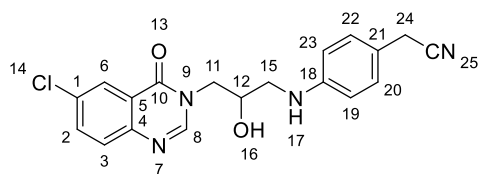
Preparation of 6-chloro-3-(oxiran-2-ylmethyl) quinazolin-4(3*H*)-one (2.55).



A mixture of 6-chloroquinazolin-4(3*H*)-one **2.20** (0.5g, 2 mmol), Cs₂CO₃ (1.3 g, 4 mmol) and TBAI (70 mg, 0.2 mmol) in MeCN (70 mL), (±) epichlorohydrin (250 μL, 3 mmol) was added. The reaction mixture was refluxed overnight. The mixture was

purified using column chromatography eluting the desired compound with 70:30 Ethyl Acetate: Petroleum Ether. White solid (250 mg, 38 %). ^1H NMR (400 MHz, $\text{DMSO-}d_6$) δ 8.32 (s, 1H, C_8H), 8.12 (d, $J = 2.5$ Hz, 1H, C_6H), 7.89 (dd, $J = 8.7, 2.5$ Hz, 1H C_2H), 7.74 (d, $J = 8.7$ Hz, 1H, C_3H), 4.33 (dd, $J = 14.4, 3.7$ Hz, 1H, C_{15}H), 4.10 (dd, $J = 14.4, 5.4$ Hz, 1H C_{15}H), 3.38 – 3.34 (m, 1H, C_{14}H), 2.81 (t, $J = 4.4$ Hz, 1H, C_{13}H), 2.59 (dd, $J = 4.9, 2.6$ Hz, 1H, C_{13}H). ^{13}C NMR (101 MHz, $\text{DMSO-}d_6$) δ 159.8, 148.9, 147.1, 135.1, 131.9, 130.0, 125.5, 123.1, 49.5, 47.4, 45.6. LCMS m/z calc for $\text{C}_{11}\text{H}_{10}\text{ClN}_2\text{O}_2^+$ $[\text{M}+\text{H}]^+$: 237.0, found 236.9 with t_{R} 2.49 min.

Preparation of 2-(4-((3-(6-chloro-4-oxoquinazolin-3(4H)-yl)-2-hydroxypropyl) amino) phenyl) acetonitrile (2.56).

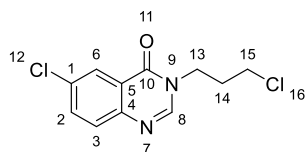


To a 5 mL of ethanol, 6-chloro-3-(oxiran-2-ylmethyl) quinazolin-4(3H)-one **2.55** (50 mg, 0.21 mmol), 2-((4-aminophenyl) acetonitrile) (23 mg, 0.17 mmol), Cs_2CO_3 (130 mg, 0.39 mmol) was dispensed in microwave tube for 30 minutes at 125 $^\circ\text{C}$. The mixture was purified using column chromatography eluting the desired compound with 70:30 Ethyl Acetate: Petroleum Ether. White solid; (37 mg, 47 %). ^1H NMR (400 MHz, $\text{DMSO-}d_6$) δ 8.29 (s, 1H, C_8H), 8.11 (d, $J = 2.4$ Hz, 1H, C_6H), 7.87 (dd, $J = 8.7, 2.5$ Hz, 1H, C_2H), 7.72 (d, $J = 8.7$ Hz, 1H, C_3H), 7.06 (d, $J = 8.3$ Hz, 2H, CH_{Ar}), 6.65 (d, $J = 8.3$ Hz, 2H, CH_{Ar}), 5.73 (t, $J = 6.1$ Hz, 1H, NH), 5.30 (d, $J = 5.4$ Hz, 1H, OH), 4.31 (dd, $J = 13.3, 3.1$ Hz, 1H, CH_{Al}), 4.05 – 3.93 (m, 1H, CH_{Al}), 3.84 – 3.74 (m, 3H, CH_{Al}), 3.22 (s, 2H, C_{24}H). ^{13}C NMR (101 MHz, $\text{DMSO-}d_6$) δ 159.9, 149.7, 148.6, 147.2, 134.8, 131.5, 129.9, 129.2, 125.4, 123.3, 120.3, 118.1, 112.9, 66.7, 50.9, 47.6, 21.9. LCMS m/z calc for $^{19}\text{H}_{18}\text{ClN}_4\text{O}_2^+$ $[\text{M}+\text{H}]^+$: 369.1, found 369.3 with t_{R} 2.70 min. Purity of the compound was confirmed to be >95 % by LCMS using a long method run.

General procedure (2.D) for preparation (2.57, 2.58).

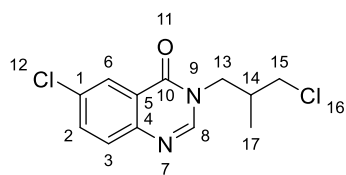
A mixture of 6-chloroquinazolin-4(3*H*)-one **2.20** (0.3 g, 1.6 mmol), 1-bromo-3-chloro-2-propane for **2.57** and 1-bromo-3-chloro-2-methylpropane for **2.58** (0.3 g, 1.9 mmol), Cs₂CO₃ (1 g, 3.2 mmol), TBAI (59 mg, 0.16 mmol) in MeCN (50 mL) was heated at 100 °C, overnight. The mixture was filtered and purified with 50:50 Petroleum Ether: Ethyl Acetate.

6-Chloro-3-(3-chloropropyl) quinazolin-4(3*H*)-one (2.57)



The title compound was prepared in the manner similar to the general procedure (2D) by utilizing 1-bromo-3-chloropropane as the starting material. White solid (0.3g, 73 %). ¹H NMR (400 MHz, DMSO-*d*₆) δ 8.41 (s, 1H, C₈H), 8.09 (d, *J* = 2.5 Hz, 1H, C₆H), 7.86 (dd, *J* = 8.7, 2.5 Hz, 1H, C₂H), 7.71 (d, *J* = 8.7 Hz, 1H, C₃H), 4.11 (t, *J* = 6.6 Hz, 2H, C₁₃H), 3.72 (t, *J* = 6.6 Hz, 2H, C₁₅H), 2.19 (p, *J* = 6.6 Hz, 2H, C₁₄H). ¹³C NMR (101 MHz, DMSO-*d*₆) δ 159.8, 148.9, 147.1, 134.8, 131.7, 129.9, 125.4, 123.3, 44.6, 43.0, 31.5. LCMS *m/z* calc for C₁₁H₁₁Cl₂N₂O⁺ [M+H]⁺: 257.0, found 259.1 with *t*_R 2.74 min.

6-Chloro-3-(3-chloro-2-methylpropyl) quinazolin-4(3*H*)-one (2.58)



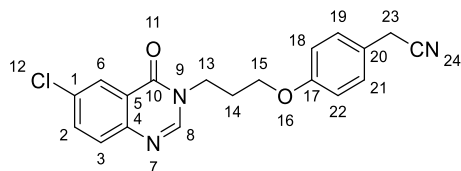
The title compound was prepared in the manner similar to the general procedure (2D) by utilizing 1-bromo-3-chloro-2-methylpropane as the starting material. White solid (0.3g, 71 %). ¹H NMR (400 MHz, DMSO-*d*₆) δ 8.38 (s, 1H, C₈H), 8.10 (d, *J* = 2.5 Hz, 1H, C₆H), 7.86 (dd, *J* = 8.8, 2.5 Hz, 1H, C₂H), 7.72 (d, *J* = 8.8 Hz, 1H, C₃H), 4.08 – 3.88 (m, 2H, C₁₃H), 3.73 – 3.60 (m, 2H, C₁₅H), 2.49 – 2.41 (m, 1H, C₁₄H), 0.99 (d, *J* = 6.8 Hz, 3H, C₁₇H). ¹³C NMR (101 MHz, DMSO-*d*₆) δ 160.02, 149.05, 147.08, 134.98, 131.81,

130.05, 125.63, 123.32, 50.79, 49.03, 34.73, 15.55. LCMS m/z calc for $C_{12}H_{13}Cl_2N_2O^+$ $[M+H]^+$
: 271.0, found 270.8 with t_R 2.83 min.

General procedure (2.E) for preparation (2.59, 2.60).

To a stirred solution of **2.57** or **2.58** (0.3g, 1 mmol), TBAI (37 mg, 0.1 mmol) and CS_2CO_3 (1 g, 1.3 mmol) in MeCN (100 mL), 4-hydroxyphenyl acetonitrile (0.15g, 1.1 mmol) was added. The mixture was heated at 100°C, overnight. The mixture was filtered and purified using column chromatography eluting the desired compound with 40:60 Petroleum Ether: Ethyl Acetate.

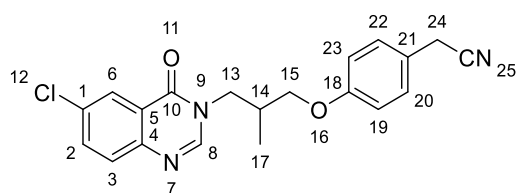
2-(4-(3-(6-Chloro-4-oxoquinazolin-3(4H)-yl) propoxy) phenyl) acetonitrile (2.59)



The title compound was prepared in the manner similar to the general procedure by utilizing 6-chloro-3-(3-chloropropyl) quinazolin-4(3H)-one **2.57** as the starting material. White solid (100 mg, 40 %). 1H NMR (400 MHz, $DMSO-d_6$) δ 8.41 (s, 1H, C_8H), 8.10 (d, $J = 2.6$ Hz, 1H, C_6H), 7.87 (dd, $J = 8.7, 2.6$ Hz, 1H, C_2H), 7.72 (d, $J = 8.7$ Hz, 1H, C_3H), 7.28 – 7.19 (m, 2H, CH_{Ar}), 6.91 – 6.83 (m, 2H, CH_{Ar}), 4.18 (t, $J = 6.4$ Hz, 2H, $C_{15}H$), 4.05 (t, $J = 6.4$ Hz, 2H, $C_{13}H$), 3.93 (s, 2H, $C_{23}H$), 2.18 (p, $J = 6.4$ Hz, 2H, $C_{14}H$). ^{13}C NMR (101 MHz, $DMSO-d_6$) δ 159.8, 158.1, 149.1, 147.2, 134.8, 131.7, 129.9, 129.7, 125.4, 123.6, 123.3, 120.0, 115.3, 65.7, 44.5, 28.2, 21.9. LCMS m/z calc for $C_{19}H_{17}ClN_3O_2^+$ $[M+H]^+$
: 354.1, found 354.0 with 2.72 t_R min. Purity of the compound was confirmed to be >95 % by LCMS using a long method run.

2-(4-(3-(6-Chloro-4-oxoquinazolin-3(4H)-yl)-2-methylpropoxy) phenyl) acetonitrile.

(2.60)



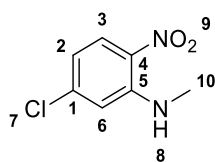
The title compound was prepared in the manner similar to the general procedure by utilizing 6-chloro-3-(3-chloro-2-methylpropyl) quinazolin-4(3H)-one **2.58** as the starting material. White solid (200 mg, 49 %). ¹H NMR (400 MHz, DMSO-*d*₆) δ 8.39 (s, 1H C₈H), 8.09 (d, *J* = 2.5 Hz, 1H C₆H), 7.87 (dd, *J* = 8.7, 2.5 Hz, 1H C₂H), 7.72 (d, *J* = 8.7 Hz, 1H C₃H), 7.24 – 7.20 (m, 2H CH_{Ar}), 6.86 – 6.79 (m, 2H CH_{Ar}), 4.12 (m, 2H, C₁₅H), 4.01 (m, 1H, C₁₄H), 3.92 (d, *J* = 5.5 Hz, 4H, C_{13,24}H), 1.02 (d, *J* = 6.8 Hz, 3H C₁₇H). ¹³C NMR (101 MHz, DMSO-*d*₆) δ 160.0, 158.2, 149.2, 147.1, 134.8, 131.7, 129.9, 129.6, 125.5, 123.6, 123.3, 119.9, 115.2, 70.9, 50.0, 21.9, 14.9. LCMS *m/z* calc for C₂₀H₁₉ClN₃O₂⁺ [M+H]⁺ : 368.1, found 367.7 with *t*_R 2.92 min. Purity of the compound was confirmed to be >95 % by LCMS using a long method run.

6.1.3 Experimental of chapter 3

General procedure (3.A) for preparation of *N*-alkyl-2-nitroaniline (3.8, 3.41-3.55).

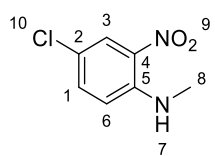
To a solution of 1 g of different substituted (mono or di) chloro-fluoro-1-nitrobenzene (compounds 3.7, 3.39-3.40) in MeOH (20 mL), was added the corresponding amines (5 mL). The mixture was stirred for overnight at 80 °C. The reaction was concentrated to the dryness, and the desired product was used without further purification.

5-Chloro-*N*-methyl-2-nitroaniline (3.8) ²⁰⁵



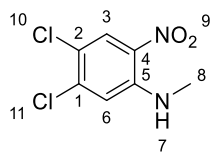
The title compound was prepared in the manner similar to the general procedure (3.A) by utilizing 4-chloro-2-fluoro-1-nitrobenzene 3.7 and methylamine as the starting material. ¹H NMR (400 MHz, DMSO-*d*₆) δ 8.06 (d, *J* = 9.1 Hz, 1H, C₃H), 7.01 (d, *J* = 2.2 Hz, 1H, C₆H), 6.68 (dd, *J* = 9.1, 2.2 Hz, 1H, C₂H), 2.95 (d, *J* = 5.0 Hz, 3H, C₁₀H). ¹³C NMR (101 MHz, DMSO-*d*₆) δ 146.8, 142.0, 130.3, 128.5, 115.4, 113.8, 30.2.

4-Chloro-*N*-methyl-2-nitroaniline (3.41)



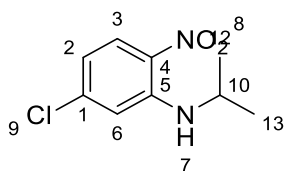
The title compound was prepared in the manner similar to the general procedure (3.A) by utilizing 4-chloro-1-fluoro-2-nitrobenzene 3.39 and methylamine as the starting material. ¹H NMR (400 MHz, DMSO-*d*₆) δ 8.05 (d, *J* = 2.7 Hz, 1H, C₃H), 7.59 (dd, *J* = 9.3, 2.7 Hz, 1H, C₁H), 7.05 (d, *J* = 9.3 Hz, 1H, C₆H), 3.17 (s, 3H, C₈H). ¹³C NMR (101 MHz, DMSO) δ 155.2, 152.6, 136.6, 129.2, 126.3, 120.9, 30.2.

4,5-Dichloro-*N*-methyl-2-nitroaniline (3.42)



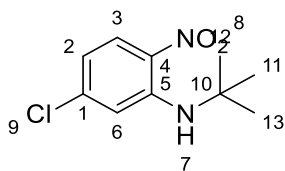
The title compound was prepared in the manner similar to the general procedure (3.A) by utilizing 1,2-dichloro-4-fluoro-5-nitrobenzene **3.40** and methylamine as the starting material. ^1H NMR (400 MHz, $\text{DMSO-}d_6$) δ 8.24 (s, 1H, C_3H), 7.27 (s, 1H, C_6H), 2.96 (d, $J = 5.0$ Hz, 3H, C_8H). ^{13}C NMR (101 MHz, $\text{DMSO-}d_6$) δ 145.3, 139.3, 129.6, 127.5, 119.1, 116.2, 30.4.

5-Chloro-*N*-isopropyl-2-nitroaniline (3.43)



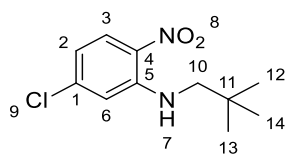
The title compound was prepared in the manner similar to the general procedure (3.A) by utilizing 4-chloro-2-fluoro-1-nitrobenzene **3.7** and *iso*-propylamine as the starting material. ^1H NMR (400 MHz, $\text{DMSO-}d_6$) δ 8.09 (d, $J = 9.2$ Hz, 1H, C_3H), 7.15 (d, $J = 2.1$ Hz, 1H, C_6H), 6.70 (dd, $J = 9.2, 2.1$ Hz, 1H, C_2H), 3.20 – 3.02 (m, 1H, C_{10}H), 1.25 (d, $J = 6.3$ Hz, 6H, $\text{C}_{12,13}\text{H}$).

N-(*tert*-butyl)-5-chloro-2-nitroaniline (3.44)



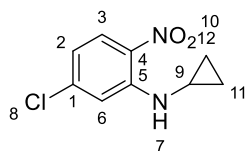
The title compound was prepared in the manner similar to the general procedure (3.A) by utilizing 4-chloro-2-fluoro-1-nitrobenzene **3.7** and *tert*-butylamine as the starting material. ^1H NMR (400 MHz, $\text{DMSO-}d_6$) δ 8.12 (d, $J = 9.2$ Hz, 1H, C_3H), 7.17 (d, $J = 2.2$ Hz, 1H, C_6H), 6.73 (dd, $J = 9.2, 2.2$ Hz, 1H, C_2H), 1.47 (s, 9H, C_{11-13}H). ^{13}C NMR (101 MHz, $\text{DMSO-}d_6$) δ 145.1, 141.5, 129.3, 127.8, 116.2, 115.1, 52.3, 29.4.

5-Chloro-*N*-neopentyl-2-nitroaniline (3.45)



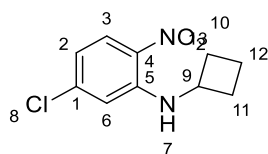
The title compound was prepared in the manner similar to the general procedure (3.A) by utilizing 4-chloro-2-fluoro-1-nitrobenzene **3.7** and neopentylamine as the starting material. ^1H NMR (400 MHz, DMSO- d_6) δ 8.09 (d, $J = 9.1$ Hz, 1H, C_3H), 7.24 (d, $J = 2.2$ Hz, 1H, C_6H), 6.70 (dd, $J = 9.1, 2.2$ Hz, 1H, C_2H), 3.21 (d, $J = 5.9$ Hz, 2H, C_{10}H), 0.99 (s, 9 H, C_{12-14}H). ^{13}C NMR (101 MHz, DMSO- d_6) δ 146.8, 142.3, 130.1, 128.7, 115.8, 114.2, 53.9, 32.3, 27.5.

5-Chloro-*N*-cyclopropyl-2-nitroaniline (3.46) ²⁰⁵



The title compound was prepared in the manner similar to the general procedure (3.A) by utilizing 4-chloro-2-fluoro-1-nitrobenzene **3.7** and cyclopropylamine as the starting material. ^1H NMR (400 MHz, DMSO- d_6) δ 8.09 (d, $J = 9.1$ Hz, 1H, C_3H), 7.38 (d, $J = 2.2$ Hz, 1H, C_6H), 6.80 (dd, $J = 9.1, 2.2$ Hz, 1H, C_2H), 2.69 – 2.63 (m, 1H, C_9H), 0.92 – 0.87 (m, 2H, CH_{Al}), 0.69 – 0.61 (m, 2H, CH_{Al}). ^{13}C NMR (101 MHz, DMSO- d_6) δ 146.9, 141.6, 130.8, 128.5, 116.5, 115.0, 25.1, 7.9.

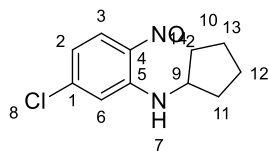
5-Chloro-*N*-cyclobutyl-2-nitroaniline (3.47)



The title compound was prepared in the manner similar to the general procedure (3.A) by utilizing 4-chloro-2-fluoro-1-nitrobenzene **3.7** and cyclobutylamine as the starting material. ^1H NMR (400 MHz, DMSO- d_6) δ 8.08 (d, $J = 9.2$ Hz, 1H, C_3H), 6.94 (d, $J = 2.2$ Hz, 1H, C_6H), 6.74 (dd, $J = 9.1, 2.2$ Hz, 1H, C_2H), 3.45 – 3.31 (m, 1H, C_9H), 2.48 – 2.37

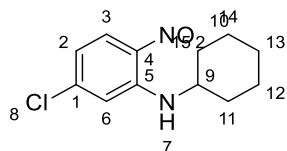
(m, 2H, CH_{Ar}), 2.18 – 1.95 (m, 2H, CH_{Al}), 1.87 – 1.70 (m, 2H, $C_{12}H$). ^{13}C NMR (101 MHz, DMSO- d_6) δ 144.7, 142.0, 130.4, 128.7, 116.1, 114.3, 47.6, 31.3, 15.3.

5-Chloro-*N*-cyclopentyl-2-nitroaniline (3.48)



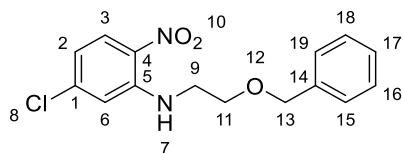
The title compound was prepared in the manner similar to the general procedure (3.A) by utilizing 4-chloro-2-fluoro-1-nitrobenzene **3.7** and cyclopentylamine as the starting material. 1H NMR (400 MHz, DMSO- d_6) δ 8.09 (d, $J = 9.2$ Hz, 1H, C_3H), 7.15 (d, $J = 2.1$ Hz, 1H, C_6H), 6.73 (dd, $J = 9.2, 2.1$ Hz, 1H, C_2H), 4.09 (m, 1H, C_9H), 3.27 (m, 1H, CH_{Al}), 2.08 (m, 1H, CH_{Al}), 1.81 – 1.41 (m, 5H, CH_{Al}), 1.37 – 1.26 (m, 1H, CH_{Al}). ^{13}C NMR (101 MHz, DMSO- d_6) δ 145.6, 142.1, 130.4, 128.7, 115.9, 114.5, 54.0, 33.0, 24.0.

5-Chloro-*N*-cyclohexyl-2-nitroaniline (3.49)



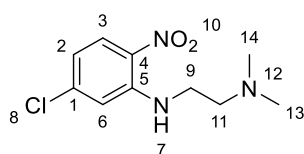
The title compound was prepared in the manner similar to the general procedure (3.A) by utilizing 4-chloro-2-fluoro-1-nitrobenzene **3.7** and cyclohexylamine as the starting material. 1H NMR (400 MHz, DMSO- d_6) δ 8.06 (d, $J = 8.6$ Hz, 1H, C_3H), 7.20 (d, $J = 2.2$ Hz, 1H, C_6H), 6.70 (dd, $J = 8.6, 2.2$ Hz, 1H, C_2H), 1.93 (m, 1H, C_9H), 1.80 – 0.96 (m, 10H, $C_{11-15}H$). ^{13}C NMR (101 MHz, DMSO- d_6) δ 145.2, 142.3, 130.1, 128.9, 115.8, 114.2, 50.5, 34.3, 25.4, 24.4.

N-(2-(benzyloxy) ethyl)-5-chloro-2-nitroaniline (3.50)



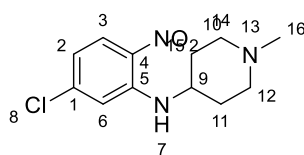
The title compound was prepared in the manner similar to the general procedure (3.A) by utilizing 4-chloro-2-fluoro-1-nitrobenzene **3.7** and 2-(benzyloxy) ethan-amine as the starting material. ^1H NMR (400 MHz, $\text{DMSO-}d_6$) δ 8.09 (d, $J = 9.2$ Hz, 1H, C_3H), 7.40 – 7.24 (m, 5H, CH_{Ar}), 7.20 (d, $J = 2.2$ Hz, 1H, C_6H), 6.72 (dd, $J = 9.2, 2.2$ Hz, 1H, C_2H), 4.55 (s, 2H, C_{13}H), 3.70 (t, $J = 5.2$ Hz, 2H, C_{11}H), 3.59 (t, $J = 5.2$ Hz, 2H, C_9H).

***N*¹-(5-chloro-2-nitrophenyl)-*N*², *N*²-dimethylethane-1,2-diamine (3.51)**



The title compound was prepared in the manner similar to the general procedure (3.A) by utilizing 4-chloro-2-fluoro-1-nitrobenzene **3.7** and 2-(dimethyl amino) ethylamine as the starting material. ^1H NMR (400 MHz, $\text{DMSO-}d_6$) δ 8.08 (d, $J = 9.1$ Hz, 1H, C_3H), 7.09 (d, $J = 2.2$ Hz, 1H, C_6H), 6.71 (dd, $J = 9.1, 2.2$ Hz, 1H, C_2H), 2.22 (s, 6H, $\text{C}_{13,14}\text{H}$), 2.13 (s, 4H, $\text{C}_{9,11}\text{H}$). ^{13}C NMR (101 MHz, $\text{DMSO-}d_6$) δ 146.0, 142.0, 130.2, 128.6, 115.7, 114.4, 57.1, 45.6, 45.3.

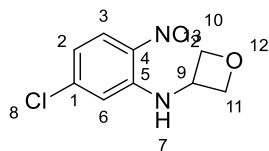
***N*-(5-chloro-2-nitrophenyl)-1-methylpiperidin-4-amine (3.52)**



The title compound was prepared in the manner similar to the general procedure (3.A) by utilizing 4-chloro-2-fluoro-1-nitrobenzene **3.7** and 1-methyl piperidin-4-amine as the starting material. ^1H NMR (400 MHz, $\text{DMSO-}d_6$) δ 8.08 (d, $J = 9.1$ Hz, 1H, C_3H), 7.20 (d, $J = 2.0$ Hz, 1H, C_6H), 6.70 (dd, $J = 9.1, 2.0$ Hz, 1H, C_2H), 3.69 (m, 1H, C_9H), 2.77 – 2.56 (m, 2H, CH_{Al}), 2.19 (s, 3H, C_{16}H), 2.16 (dd, $J = 11.1, 2.6$ Hz, 2H, CH_{Al}), 2.04 – 1.84 (m,

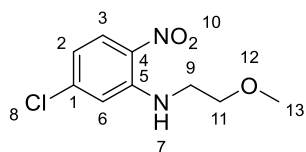
2H, CH_{Al}), 1.57 (m, 2H, CH_{Al}). ^{13}C NMR (101 MHz, DMSO- d_6) δ 145.2, 142.3, 130.3, 128.8, 116.0, 114.3, 53.9, 53.8, 46.4, 31.5.

***N*-(5-chloro-2-nitrophenyl) oxetan-3-amine (3.53)**



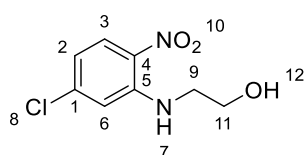
The title compound was prepared in the manner similar to the general procedure (3.A) by utilizing 4-chloro-2-fluoro-1-nitrobenzene **3.7** and oxetan-3-amine as the starting material. 1H NMR (400 MHz, DMSO- d_6) δ 8.17 – 8.03 (m, 1H, C_3H), 6.81 (d, J = 8.3 Hz, 2H, $C_{6,2}H$), 4.97 – 4.78 (m, 3H, C_9H , CH_{Al}), 4.58 (t, J = 5.5 Hz, 2H, CH_{Al}). ^{13}C NMR (101 MHz, DMSO- d_6) δ 144.3, 142.1, 131.2, 128.8, 116.9, 114.0, 77.2, 47.6.

5-Chloro-*N*-(2-methoxyethyl)-2-nitroaniline (3.54)



The title compound was prepared in the manner similar to the general procedure (3.A) by utilizing 4-chloro-2-fluoro-1-nitrobenzene **3.7** and 2-methoxyethylamine as the starting material. 1H NMR (400 MHz, DMSO- d_6) δ 8.09 (d, J = 9.1 Hz, 1H, C_3H), 7.17 (d, J = 2.2 Hz, 1H, C_6H), 6.72 (dd, J = 9.1, 2.2 Hz, 1H, C_2H), 3.61 – 3.50 (m, 5H, CH_{Al}), 3.35 (t, J = 5.6 Hz, 1H, CH_{Al}), 3.26 (s, 1H, CH_{Al}). ^{13}C NMR (101 MHz, DMSO- d_6) δ 146.2, 142.1, 130.4, 128.7, 115.9, 114.3, 70.4, 58.4, 42.5.

2-((5-Chloro-2-nitrophenyl) amino) ethan-1-ol (3.55) ²⁰⁵



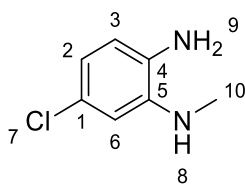
The title compound was prepared in the manner similar to the general procedure (3.A) by utilizing 4-chloro-2-fluoro-1-nitrobenzene **3.7** and 2-aminoethanol as the

starting material. ^1H NMR (400 MHz, DMSO- d_6) δ 8.09 (d, J = 9.1 Hz, 1H, C_3H), 7.17 (d, J = 2.2 Hz, 1H, C_6H), 6.71 (dd, J = 9.1, 2.2 Hz, 1H, C_2H), 6.16 (s, 1H, OH), 3.64 (t, J = 5.5 Hz, 2H, C_{11}H), 3.42 (t, J = 5.5 Hz, 2H, C_9H). ^{13}C NMR (101 MHz, DMSO- d_6) δ 146.4, 142.0, 130.3, 128.7, 115.7, 114.3, 59.4, 45.3.

General procedure (3.B) for preparation of *N*-(alkyl) benzene-1,2-diamine (3.9, 3.56-3.69).

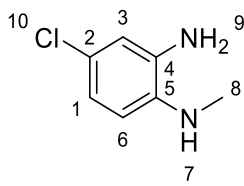
To a solution of the corresponding (chloro- N^l -(alkyl)-2-nitroaniline), prepared previously **3.8**, **3.41-3.55** in MeOH (20 mL) was added zinc (10 equiv), NH_4Cl (5 equiv) and 10 % CH_3COOH . The mixture was stirred overnight at rt. The reaction was concentrated to the dryness, and the desired product was extracted using ethyl acetate and saturated aqueous NaHCO_3 . The organic layer was dried to afford the desired product as a black solid, which was used in the next step without further purification.

5-Chloro- N^l -methylbenzene-1,2-diamine (3.9)



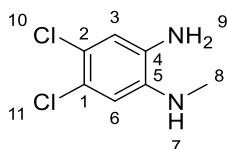
The title compound was prepared in the manner similar to the general procedure (3.B) by utilizing 5-chloro- N -methyl-2-nitroaniline **3.8** as the starting material. ^1H NMR (400 MHz, DMSO- d_6) δ 6.51 (dd, J = 14.9, 7.8 Hz, 1H, CH_{Ar}), 6.44 – 6.36 (m, 1H, CH_{Ar}), 6.30 (d, J = 2.4 Hz, 1H, CH_{Ar}), 2.69 (d, J = 3.3 Hz, 3H, C_{10}H). ^{13}C NMR (101 MHz, DMSO- d_6) δ 138.9, 134.4, 121.6, 115.8, 114.5, 108.7, 21.6.

4-Chloro- N^l -methylbenzene-1, 2-diamine (3.56)



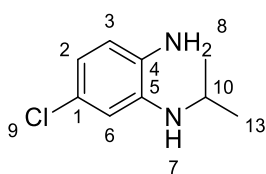
The title compound was prepared in the manner similar to the general procedure (3.B) by utilizing 4-chloro-*N*-methyl-2-nitroaniline **3.41** as the starting material. ^1H NMR (400 MHz, DMSO- d_6) δ 6.59 – 6.45 (m, 2H, CH_{Ar}), 6.31 (d, $J = 8.3$ Hz, 1H, CH_{Ar}), 2.69 (d, $J = 5.0$ Hz, 3H, C_8H). ^{13}C NMR (101 MHz, DMSO- d_6) δ 137.3, 136.3, 120.5, 116.7, 113.0, 110.1, 30.6.

4, 5-Dichloro-*N*¹-methylbenzene-1, 2-diamine (**3.57**)²⁰⁶



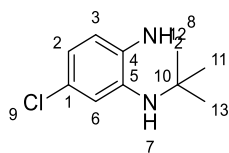
The title compound was prepared in the manner similar to the general procedure (3.B) by utilizing 4,5-dichloro-*N*-methyl-2-nitroaniline **3.42** as the starting material. ^1H NMR (400 MHz, DMSO- d_6) δ 6.65 (s, 1H, CH_{Ar}), 6.40 (s, 1H, CH_{Ar}), 2.70 (d, $J = 5.0$ Hz, 3H, C_8H). ^{13}C NMR (101 MHz, DMSO- d_6) δ 137.8, 136.2, 118.3, 117.3, 113.7, 109.6, 30.4.

5-Chloro-*N*¹-isopropylbenzene-1,2-diamine (**3.12**)



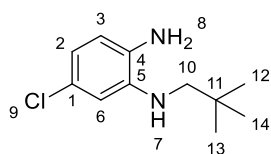
The title compound was prepared in the manner similar to the general procedure (3.B) by utilizing 5-chloro-*N*-isopropyl-2-nitroaniline **3.43** as the starting material. ^1H NMR (400 MHz, DMSO- d_6) δ 6.49 (d, $J = 7.8$ Hz, 1H, CH_{Ar}), 6.43 – 6.31 (m, 2H, CH_{Ar}), 3.52 (dt, $J = 12.9, 6.2$ Hz, 1H, C_{10}H), 1.15 (d, $J = 6.2$ Hz, 6H, $\text{C}_{12,13}\text{H}$). ^{13}C NMR (101 MHz, DMSO- d_6) δ 136.7, 134.5, 121.4, 115.7, 115.0, 109.8, 43.6, 22.8.

*N*¹-(*tert*-butyl)-5-chlorobenzene-1,2-diamine (**3.58**)



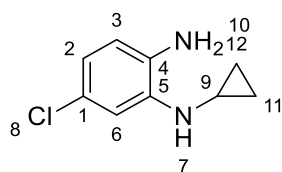
The title compound was prepared in the manner similar to the general procedure (3.B) by utilizing *N*-(*tert*-butyl)-5-chloro-2-nitroaniline **3.44** as the starting material. ^1H NMR (400 MHz, $\text{DMSO-}d_6$) δ 6.66 – 6.54 (m, 2H, CH_{Ar}), 6.50 (dd, $J = 8.3, 2.4$ Hz, 1H, CH_{Ar}), 1.27 (s, 9H, C_{11-13}H). ^{13}C NMR (101 MHz, $\text{DMSO-}d_6$) δ 138.0, 135.3, 120.7, 115.9, 114.5, 111.2, 51.7, 29.9.

5-Chloro-*N*¹-neopentylbenzene-1,2-diamine (3.59)



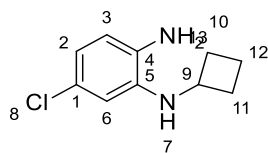
The title compound was prepared in the manner similar to the general procedure (3.B) by utilizing 5-chloro-*N*-neopentyl-2-nitroaniline **3.45** as the starting material. ^1H NMR (400 MHz, $\text{DMSO-}d_6$) δ 6.52 (d, $J = 8.0$ Hz, 1H, CH_{Ar}), 6.42 – 6.37 (m, 2H, CH_{Ar}), 2.84 – 2.79 (m, 2H, C_{10}H), 0.98 (s, 9H, C_{12-14}H). ^{13}C NMR (101 MHz, $\text{DMSO-}d_6$) δ 138.6, 134.4, 121.5, 115.8, 115.1, 109.4, 55.5, 32.4, 28.0.

5-Chloro-*N*¹-cyclopropylbenzene-1,2-diamine (3.60)



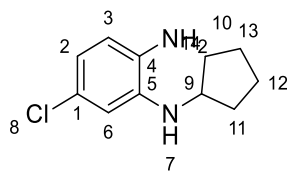
The title compound was prepared in the manner similar to the general procedure (3.B) by utilizing 5-chloro-*N*-cyclopropyl-2-nitroaniline **3.46** as the starting material. ^1H NMR (400 MHz, $\text{DMSO-}d_6$) δ 6.78 (dd, $J = 8.1, 1.5$ Hz, 1H, CH_{Ar}), 6.55 – 6.49 (m, 1H, CH_{Ar}), 6.49 – 6.39 (m, 1H, CH_{Ar}), 2.32 (m, 1H, C_9H), 0.70 (m, 2H, CH_{Al}), 0.39 (m, 2H, CH_{Al}).

5-Chloro-*N*¹-cyclobutylbenzene-1,2-diamine (3.61)



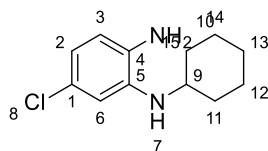
The title compound was prepared in the manner similar to the general procedure (3.B) by utilizing 5-chloro-*N*-cyclobutyl-2-nitroaniline **3.47** as the starting material. ^1H NMR (400 MHz, DMSO- d_6) δ 6.48 (d, $J = 8.2$ Hz, 1H, C₃H), 6.39 (dd, $J = 8.2, 2.3$ Hz, 1H, C₂H), 6.21 (d, $J = 2.3$ Hz, 1H, C₆H), 3.80 (h, $J = 7.1$ Hz, 1H, C₉H), 1.91 – 1.66 (m, 6H, C₁₁₋₁₃H). ^{13}C NMR (101 MHz, DMSO- d_6) δ 136.3, 134.5, 121.2, 116.2, 114.8, 109.8, 48.6, 30.6, 15.4.

5-Chloro-*N*¹-cyclopentylbenzene-1,2-diamine (3.62)



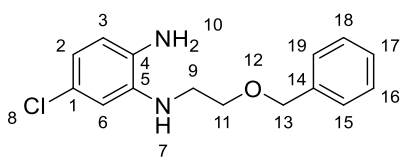
The title compound was prepared in the manner similar to the general procedure (3.B) by utilizing 5-chloro-*N*-cyclopentyl-2-nitroaniline **3.48** as the starting material. ^1H NMR (400 MHz, DMSO- d_6) δ 6.48 (d, $J = 8.0$ Hz, 1H, CH_{Ar}), 6.39 – 6.33 (m, 2H, CH_{Ar}), 3.68 (m, 1H, C₉H), 1.94 (m, 2H, CH_{Al}), 1.76 – 1.41 (m, 6H, CH_{Al}). ^{13}C NMR (101 MHz, DMSO- d_6) δ 137.2, 134.5, 121.3, 115.7, 114.7, 109.9, 54.1, 33.0, 24.3.

5-Chloro-*N*¹-cyclohexylbenzene-1, 2-diamine (3.63)



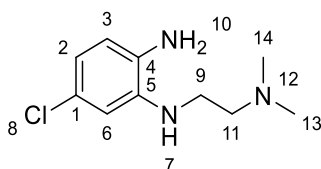
The title compound was prepared in the manner similar to the general procedure (3.B) by utilizing 5-chloro-*N*-cyclohexyl-2-nitroaniline **3.49** as the starting material. ^1H NMR (400 MHz, DMSO- d_6) δ 6.53 – 6.44 (m, 1H, CH_{Ar}), 6.35 (d, $J = 6.4$ Hz, 2H, CH_{Ar}), 1.92 (m, 3H, CH_{Al}), 1.73 (m, 2H, CH_{Al}), 1.62 (m, 1H, CH_{Al}), 1.35 (m, 2H, CH_{Al}), 1.28 – 1.05 (m, 3H, CH_{Al}). ^{13}C NMR (101 MHz, DMSO- d_6) δ 136.7, 133.9, 121.8, 115.7, 111.2, 109.8, 51.2, 33.0, 26.1, 25.1.

***N*¹-(2-(benzyloxy) ethyl)-5-chlorobenzene-1,2-diamine (3.64)**



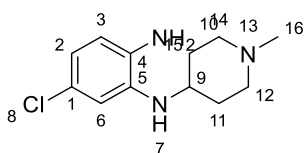
The title compound was prepared in the manner similar to the general procedure (3.B) by utilizing *N*-(2-(benzyloxy) ethyl)-5-chloro-2-nitroaniline **3.50** as the starting material. ¹H NMR (400 MHz, DMSO-*d*₆) δ 7.39 – 7.31 (m, 5H, *CH*_{Ar}), 7.25 (d, *J* = 7.5 Hz, 1H, *CH*_{Ar}), 7.18 (d, *J* = 7.5 Hz, 1H, *CH*_{Ar}), 7.15 – 7.11 (m, 1H, *CH*_{Ar}), 4.53 (s, 2H, *C*₁₃*H*), 3.63 (t, *J* = 5.7 Hz, 2H, *C*₁₁*H*), 3.26 (d, *J* = 5.7 Hz, 2H, *C*₉*H*).

5-Chloro-*N*¹-(2-(dimethylamino) ethyl) benzene-1, 2-diamine (3.65)



The title compound was prepared in the manner similar to the general procedure (3.B) by utilizing *N*¹-(5-chloro-2-nitrophenyl)-*N*², *N*²-dimethylethane-1,2-diamine **3.51** as the starting material. ¹H NMR (400 MHz, DMSO-*d*₆) δ 6.55 – 6.51 (m, 1H, *CH*_{Ar}), 6.47 – 6.42 (m, 2H, *CH*_{Ar}), 3.23 (t, *J* = 6.3 Hz, 2H, *C*₉*H*), 2.88 (t, *J* = 6.3 Hz, 2H, *C*₁₁*H*), 2.49 (s, 6H, *C*_{13,14}*H*). ¹³C NMR (101 MHz, DMSO-*d*₆) δ 137.8, 134.7, 121.7, 116.4, 115.1, 109.6, 57.6, 45.1, 40.9.

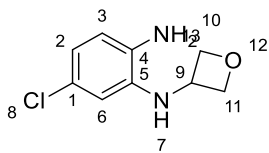
5-Chloro-*N*¹-(1-methylpiperidin-4-yl) benzene-1, 2-diamine (3.66)



The title compound was prepared in the manner similar to the general procedure (3.B) by utilizing *N*-(5-chloro-2-nitrophenyl)-1-methylpiperidin-4-amine **3.52** as the starting material. ¹H NMR (400 MHz, DMSO-*d*₆) δ 6.61 – 6.55 (m, 1H, *CH*_{Ar}), 6.53 – 6.38 (m, 2H, *CH*_{Ar}), 3.45 (d, *J* = 26.7 Hz, 2H, *CH*_{Al}), 3.17 (s, 1H, *CH*_{Al}), 3.07 (m, 2H, *CH*_{Al}), 2.70 (s,

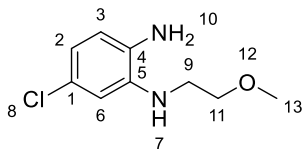
3H, C₁₆H), 2.16 – 2.04 (m, 2H, CH_{Al}), 1.79 (m, 2H, CH_{Al}). ¹³C NMR (101 MHz, DMSO-*d*₆) δ 136.4, 134.3, 117.9, 117.8, 114.9, 111.6, 52.3, 46.50, 42.9, 29.1.

5-Chloro-*N*¹-(oxetan-3-yl) benzene-1,2-diamine (3.67)



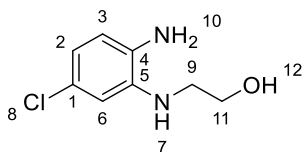
The title compound was prepared in the manner similar to the general procedure (3.B) by utilizing *N*-(5-chloro-2-nitrophenyl) oxetan-3-amine **3.53** as the starting material. ¹H NMR (400 MHz, DMSO) δ 6.53 (d, *J* = 8.2 Hz, 1H, C₃H), 6.46 (dd, *J* = 8.2, 2.3 Hz, 1H, C₂H), 6.06 (d, *J* = 2.3 Hz, 1H, C₆H), 4.87 (t, *J* = 6.2 Hz, 2H, CH_{Al}), 4.50 (dt, *J* = 12.1, 6.2 Hz, 1H, C₉H), 4.43 (t, *J* = 6.2 Hz, 2H, CH_{Al}). ¹³C NMR (101 MHz, DMSO) δ 135.6, 135.1, 121.1, 117.3, 115.0, 109.8, 78.0, 48.1.

5-Chloro-*N*¹-(2-methoxyethyl) benzene-1, 2-diamine (3.68)



The title compound was prepared in the manner similar to the general procedure (3.B) by utilizing 5-chloro-*N*-(2-methoxyethyl)-2-nitroaniline **3.54** as the starting material. ¹H NMR (400 MHz, DMSO-*d*₆) δ 6.52 (d, *J* = 8.0 Hz, 1H, CH_{Ar}), 6.43 – 6.38 (m, 2H, CH_{Ar}), 3.53 (t, *J* = 5.6 Hz, 2H, C₁₁H), 3.30 (s, 3H, C₁₃H), 3.23 – 3.14 (m, 2H, C₉H). ¹³C NMR (101 MHz, DMSO-*d*₆) δ 137.7, 134.4, 121.6, 116.2, 115.1, 109.4, 70.8, 58.4, 43.3.

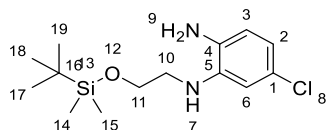
2-((2-Amino-5-chlorophenyl) amino) ethan-1-ol (3.69)



The title compound was prepared in the manner similar to the general procedure (3.B) by utilizing 2-((5-chloro-2-nitrophenyl) amino) ethan-1-ol **3.55** as the starting

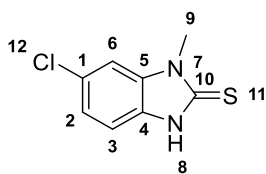
material. ^1H NMR (400 MHz, $\text{DMSO-}d_6$) δ 6.51 (d, $J = 7.9$ Hz, 1H, CH_{Ar}), 6.41 – 6.36 (m, 2H, CH_{Ar}), 3.59 (t, $J = 5.9$ Hz, 2H, C_{11}H), 3.08 (t, $J = 5.9$ Hz, 2H, C_9H). ^{13}C NMR (101 MHz, $\text{DMSO-}d_6$) δ 138.0, 134.5, 121.6, 116.1, 115.0, 109.36, 59.8, 46.2.

N^1 -(2-((*tert*-butyl dimethyl silyl) oxy) ethyl)-5-chlorobenzene-1,2-diamine (3.107)



To a solution of *tert*-butyl(chloro) dimethyl silane (TBDMSCl) (1g, 7 mmol) in DMF (20 mL) was added imidazole (0.8g, 12 mmol). The mixture was stirred for 1 hour at rt. Then the compound 2-((2-amino-5-chlorophenyl) amino) ethan-1-ol **3.69** (1g, 5mmol) was added to the reaction and stirred overnight. The reaction was concentrated to the dryness and the desired product was isolated using column chromatography eluting the desired compound with 50:50 Petroleum Ether: Ethyl Acetate. ^1H NMR (400 MHz, $\text{DMSO-}d_6$) δ 6.52 (d, $J = 7.9$ Hz, 2H, CH_{Ar}), 6.41 (d, $J = 7.9$ Hz, 2H, CH_{Ar}), 4.71 (t, $J = 5.9$ Hz, 1H, N_7H), 4.58 (s, 2H, N_9H), 3.75 (t, $J = 5.9$ Hz, 2H, C_{11}H), 3.16 (t, $J = 5.9$ Hz, 2H, C_{10}H), 0.88 (s, 9H, C_{17-19}H), 0.05 (s, 6H, $\text{C}_{14,15}\text{H}$). ^{13}C NMR (101 MHz, DMSO) δ 137.7, 134.5, 121.6, 116.2, 116.1, 109.6, 61.9, 46.6, 29.7, 26.2, -2.72, -4.84.

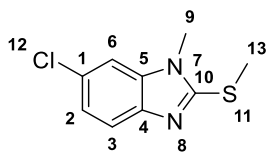
Preparation of 6-chloro-1-methyl-1,3-dihydro-2H-benzo[d]imidazole-2-thione (3.21).



To a solution of 5-chloro- N^1 -methylbenzene-1,2-diamine **3.9** (1g, 6mmol) in EtOH, was added CS_2 (10 mL) and Et_3N (6g, 0.06 mol). The mixture was stirred overnight at rt. The reaction was concentrated to the dryness, and the desired product was isolated using column chromatography eluting the desired compound with 50:50 Petroleum Ether: Ethyl Acetate. Colourless oil (1g, 83 %). ^1H NMR (400 MHz, $\text{DMSO-}d_6$) δ 7.55 (d, $J = 1.8$ Hz, 1H, C_6H), 7.21 (dd, $J = 8.4, 1.8$ Hz, 1H, C_2H), 7.17 (d, $J = 8.4$ Hz, 1H, C_3H), 3.64 (s,

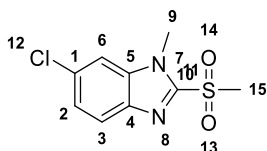
3H, C₉H). ¹³C NMR (101 MHz, DMSO-*d*₆) δ 170.1, 134.6, 130.0, 127.2, 123.1, 111.0, 110.1, 30.7.

Preparation of 6-chloro-1-methyl-2-(methyl thio)-1*H*-benzo[*d*]imidazole (3.22).



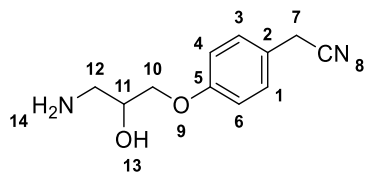
To a solution of 6-chloro-1-methyl-1,3-dihydro-2*H*-benzo[*d*]imidazole-2-thione **3.21** (1g, 5.0 mmol) in 3:1 MeOH: diethyl ether, a methyl iodide CH₃I (0.8g, 6.0 mmol) and 2 eq of 1*N* NaOH was added and stirred at rt for 16 h. The reaction was concentrated to the dryness, and the desired product was isolated using column chromatography eluting the desired compound with 50:50 Petroleum Ether: Ethyl Acetate. Colourless oil (0.6g, 56 %). ¹H NMR (400 MHz, DMSO-*d*₆) δ 7.53 (d, *J* = 1.8 Hz, 1H, C₆H), 7.46 (dd, *J* = 8.4, 1.8 Hz, 1H, C₂H), 7.15 (d, *J* = 8.4 Hz, 1H, C₃H), 3.67 (d, *J* = 3.9 Hz, 3H, C₉H), 2.73 (d, *J* = 3.9 Hz, 3H, C₁₃H). ¹³C NMR (101 MHz, DMSO-*d*₆) δ 153.0, 143.3, 137.4, 126.4, 121.9, 118.9, 117.9, 30.4, 14.7.

Preparation of 6-chloro-1-methyl-2-(methyl sulfonyl)-1*H*-benzo[*d*]imidazole (3.24)



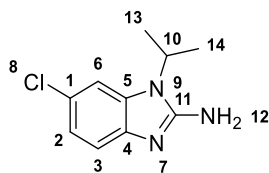
To a solution of 6-chloro-1-methyl-2-(methyl thio)-1*H*-benzo[*d*]imidazole **3.22** (0.6g, 2.9 mmol) in 1:1 MeOH: H₂O, a (5g, 17 mmol) of oxone was added and the mixture was stirred at rt for 16 h. The reaction was concentrated to the dryness, and the desired product was isolated using column chromatography eluting the desired compound with 50:50 Petroleum Ether: Ethyl Acetate. Colourless oil (0.3g, 42 %). ¹H NMR (400 MHz, DMSO-*d*₆) δ 7.57 (d, *J* = 1.8 Hz, 1H, C₆H), 7.49 (dd, *J* = 8.4, 1.8 Hz, 1H, C₂H), 7.19 (d, *J* = 8.4 Hz, 1H, C₃H), 4.14 (d, *J* = 3.9 Hz, 3H, C₉H), 2.95 (d, *J* = 3.9 Hz, 3H, C₁₅H). ¹³C NMR (101 MHz, DMSO-*d*₆) δ 155.0, 143.9, 138.0, 127.2, 122.5, 119.7, 118.9, 42.8, 32.6.

Preparation of 2-(4-(3-amino-2-hydroxypropoxy) phenyl) acetonitrile (3.10)



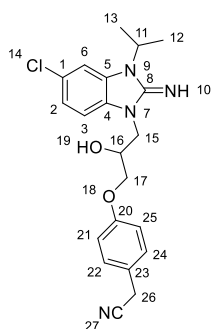
A (1 g) of the previously prepared 2-(4-oxiran-2-ylmethoxy) phenyl) acetonitrile **2.29** was stirred in 10 mL of NH_3/MeOH at rt for 16 h. The reaction was concentrated to the dryness, and the desired product was isolated using column chromatography eluting the desired compound with 90:10 Ethyl Acetate: Methanol. White solid (0.9g, 80 %). ^1H NMR (400 MHz, $\text{DMSO-}d_6$) δ 7.26 (d, $J = 8.3$ Hz, 2H, CH_{Ar}), 6.95 (d, $J = 8.3$ Hz, 2H, CH_{Ar}), 3.94 (s, 2H, C_7H), 3.90 – 3.70 (m, 3H, CH_{Al}), 3.17 – 2.96 (m, 1H, CH_{Al}), 2.79 – 2.54 (m, 1H, CH_{Al}). ^{13}C NMR (101 MHz, $\text{DMSO-}d_6$) δ 158.6, 129.7, 123.4, 120.0, 115.4, 70.7, 70.1, 44.8, 21.9.

Preparation of 6-chloro-1-isopropyl-1H-benzo[d]imidazol-2-amine (3.25)



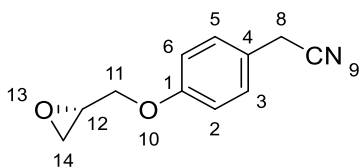
To a solution of previously prepared 5-chloro- N^1 -isopropylbenzene-1,2-diamine **3.12** (3g, 18mm) was dissolved in 1:1 $\text{MeOH}:\text{H}_2\text{O}$, a (6g, 54mm) of cyanogen bromide (CNBr) was added and the mixture was stirred at 30 °C for 3 h. The reaction was concentrated to the dryness, and the desired product was isolated using column chromatography eluting the desired compound with 50:50 Petroleum Ether: Ethyl Acetate. Brown solid (2.8g, 85 %) ^1H NMR (400 MHz, $\text{DMSO-}d_6$) δ 7.96 (br s, 2H, NH_2), 7.65 (d, $J = 1.9$ Hz, 1H, C_6H), 7.31 (d, $J = 8.5$ Hz, 1H, C_3H), 7.17 (dd, $J = 8.5, 9.1$ Hz, 1H, C_2H), 4.75 (hept, $J = 6.9$ Hz, 1H, C_{10}H), 1.51 (d, $J = 6.9$ Hz, 6H, $\text{C}_{13,14}\text{H}$). ^{13}C NMR (101 MHz, $\text{DMSO-}d_6$) δ 152.1, 133.5, 131.3, 125.7, 122.6, 114.3, 111.4, 47.2, 20.0.

Preparation of 2-(4-(3-(5-chloro-2-imino-3-isopropyl-2,3-dihydro-1*H*-benzo[*d*]imidazol-1-yl)-2-hydroxypropoxy) phenyl) acetonitrile (3.26)



To a solution of 6-chloro-1-isopropyl-1*H*-benzo[*d*]imidazol-2-amine **3.25** (50mg, 0.2mmol) was stirred in MeCN. A (160mg, 0.5 mmol) of Cs₂CO₃ and (50mg, 0.3 mmol) of 2-(4-oxiran-2-yl methoxy) phenyl) acetonitrile **2.29** was stirred at 100 °C for 16 h. The reaction was concentrated to the dryness, and the desired product was isolated using column chromatography eluting the desired compound with 100 % Ethyl acetate. White solid (76mg, 80 %) ¹H NMR (400 MHz, DMSO-*d*₆) δ 7.78 (s, 1H, C₆H), 7.54 (d, *J* = 8.8 Hz, 1H, C₂H), 7.30 (dd, *J* = 12.6, 8.8 Hz, 3H, C₃H, CH_{Ar}), 7.04 – 6.94 (m, 2H, CH_{Ar}), 4.85 (p, *J* = 6.9 Hz, 1H, C₁₁H), 4.34 – 4.18 (m, 3H, CH_{Al}), 4.18 – 3.99 (m, 2H, CH_{Al}), 3.96 (s, 2H, C₂₆H), 1.55 (d, *J* = 6.9 Hz, 6H, C_{12,13}H). ¹³C NMR (101 MHz, DMSO-*d*₆) δ 158.3, 150.5, 130.5, 129.7, 129.5, 123.7, 123.1, 120.0, 115.46, 111.9, 108.7, 70.0, 67.1, 48.1, 46.5, 22.0, 19.7. LCMS *m/z* calc for C₂₁H₂₃ClN₄O₂⁺ [M+H]⁺: 399.2, found 399.1 with *t*_R 2.18 min. Purity of the compound was confirmed to be >95 % by LCMS using a long method run.

Preparation of (*S*)-2-(4-(oxiran-2-ylmethoxy) phenoxy) acetonitrile (3.109)



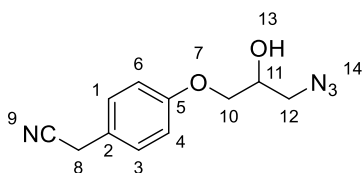
To a stirred solution of 4-hydroxyphenylacetonitrile **2.24** (5g, 0.036mol) in MeCN (50 mL), was added Cs₂CO₃ (24g, 0.074mol) then (*S*)-(+)-glycidyl 3-nitrobenzenesulfonate (11g, 0.043mol). The reaction mixture was heated at 85 °C for 16h. The

mixture was filtered and purified using column chromatography eluting the desired compound with 80:20 Petroleum Ether: Ethyl Acetate. White solid (5g, 70 %). ^1H NMR (400 MHz, $\text{DMSO-}d_6$) δ 7.30 – 7.24 (m, 2H, $\text{C}_{\text{Ar}}\text{H}$), 7.01 – 6.95 (m, 2H, $\text{C}_{\text{Ar}}\text{H}$), 4.33 (dd, $J = 11.4, 2.6$ Hz, 1H, $\text{C}_{\text{Al}}\text{H}$), 3.94 (s, 2H, C_8H), 3.88 – 3.74 (m, 1H, $\text{C}_{\text{Al}}\text{H}$), 3.33 – 3.30 (m, 1H, $\text{C}_{\text{Al}}\text{H}$), 2.85 (dd, $J = 5.1, 4.3$ Hz, 1H, $\text{C}_{\text{Al}}\text{H}$), 2.71 (dd, $J = 5.0, 2.6$ Hz, 1H, $\text{C}_{\text{Al}}\text{H}$). ^{13}C NMR (101 MHz, $\text{DMSO-}d_6$) δ 158.1, 129.8, 123.8, 119.9, 115.4, 69.4, 50.1, 44.2, 21.9.

General procedure (3.C) for preparation of (3.30-3.32, 3.110).

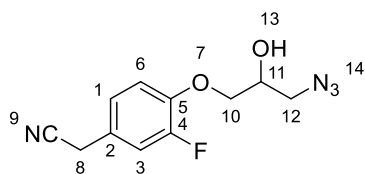
To a solution of **2.29**, **2.31-2.32**, **3.109** (1 eq) in EtOH (100 mL) was added NaN_3 (1.1 eq) and NH_4Cl (2 eq). The mixture was stirred at rt for 16 h. The reaction was concentrated to the dryness and the residue was dissolved in ethyl acetate and washed with water. The organic phase was concentrated to afford the desired product as a colourless oil which was used in the next step without further purification.

2-(4-(3-Azido-2-hydroxypropoxy) phenyl) acetonitrile (3.30)



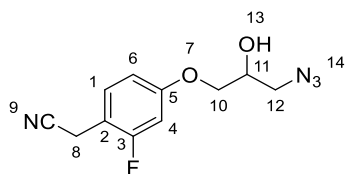
The title compound was prepared in the manner similar to the general procedure (3.C) by utilizing 2-(4-oxiran-2-ylmethoxy) phenyl) acetonitrile **2.29** as a starting material (8g, 0.04 mmol). Colourless oil (9 g, 91 %). ^1H NMR (400 MHz, $\text{DMSO-}d_6$) δ 7.27 (d, $J = 8.2$ Hz, 2H, CH_{Ar}), 6.97 (d, $J = 8.2$ Hz, 2H, CH_{Ar}), 5.57 (d, $J = 5.1$ Hz, 1H, OH), 4.10 – 3.99 (m, 1H, CH_{Al}), 3.93 (s, 4H, C_8H , CH_{Al}), 3.46 – 3.30 (m, 2H, CH_{Al}). ^{13}C NMR (101 MHz, $\text{DMSO-}d_6$) δ 158.2, 129.7, 123.7, 119.9, 115.4, 69.8, 68.7, 53.7, 22.0.

2-(4-(3-Azido-2-hydroxypropoxy)-3-fluorophenyl) acetonitrile (3.31)



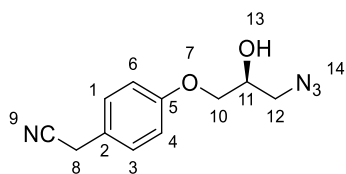
The title compound was prepared in the manner similar to the general procedure (3.C) by utilizing 2-(3-fluoro-4-(oxiran-2-ylmethoxy) phenyl) acetonitrile **2.31** as a starting material (0.6g, 2mmol). Colourless oil (0.6g, 83 %). ^1H NMR (400 MHz, $\text{DMSO-}d_6$) δ 7.27 – 7.18 (m, 2H, CH_{Ar}), 7.13 (dd, $J = 8.8, 2.0$ Hz, 1H, CH_{Ar}), 5.61 (dd, $J = 5.0, 2.4$ Hz, 1H, OH), 4.03 (dt, $J = 4.1, 2.0$ Hz, 3H, $\text{C}_{10,11}\text{H}$), 3.97 (s, 2H, C_8H), 3.44 – 3.34 (m, 2H, C_{12}H). ^{13}C NMR (101 MHz, $\text{DMSO-}d_6$) δ 151.9 (d, $J = 247.2$ Hz), 146.1 (d, $J = 10.2$ Hz), 124.9 (d, $J = 2.7$ Hz), 119.5, 116.4 (d, $J = 19.7$ Hz), 116.0 (d, $J = 1.5$ Hz), 70.9, 68.6, 53.6, 21.9.

2-(4-(3-Azido-2-hydroxypropoxy)-2-fluorophenyl) acetonitrile (3.32)



The title compound was prepared in the manner similar to the general procedure (3.C) by utilizing 2-(2-fluoro-4-(oxiran-2-ylmethoxy) phenyl) acetonitrile **2.32** as a starting material (1.1g, 5mmol). Colourless oil (1g, 75 % yield). ^1H NMR (400 MHz, $\text{DMSO-}d_6$) δ 7.36 (t, $J = 8.8$ Hz, 1H, CH_{Ar}), 6.99 – 6.79 (m, 2H, CH_{Ar}), 5.58 (d, $J = 5.1$ Hz, 1H, OH), 4.09 – 3.98 (m, 1H, CH_{Al}), 3.95 (s, 4H, C_8H , CH_{Al}), 3.46 – 3.35 (m, 2H, CH_{Al}). ^{13}C NMR (101 MHz, $\text{DMSO-}d_6$) δ 161.13 (d, $J = 208.5$ Hz), 159.88 (d, $J = 26.1$ Hz), 131.32 (d, $J = 4.9$ Hz), 118.82, 111.72 (d, $J = 3.1$ Hz), 110.61 (d, $J = 15.5$ Hz), 102.84 (d, $J = 24.3$ Hz), 70.40, 68.61, 53.59, 16.63.

(S)-2-(4-(3-azido-2-hydroxypropoxy) phenyl) acetonitrile (3.110)

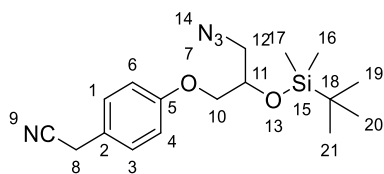


The title compound was prepared in the manner similar to the general procedure (3.C) by utilizing (*S*)-2-(4-(oxiran-2-ylmethoxy) phenoxy) acetonitrile **3.109** as a starting material (5g, 26mmol). Colourless oil (6g, 81 % yield). ¹H NMR (400 MHz, DMSO-*d*₆) δ 7.31 – 7.22 (m, 2H, *CH*_{Ar}), 7.01 – 6.93 (m, 2H, *CH*_{Ar}), 5.56 (d, *J* = 5.2 Hz, 1H, *OH*), 4.01 (m, 1H, *CH*_{Al}), 3.93 (d, *J* = 6.9 Hz, 4H, *C*₈*H*, *CH*_{Al}), 3.44 – 3.37 (m, 1H, *CH*_{Al}), 3.27 (d, *J* = 5.2 Hz, 1H, *CH*_{Al}). ¹³C NMR (101 MHz, DMSO) δ 158.2, 129.7, 123.7, 120.0, 115.4, 69.8, 68.7, 53.7, 22.0.

General procedure (3.D) for preparation of (3.33-3.35, 3.111 step1)

To a solution of TBDMSCl (1.3 eq) in DMF (100 mL) was added imidazole (2.5 eq). The mixture was stirred for 1 hour at rt. Then the compound **3.30-3.32, 3.110** (1 eq) was added to the reaction and stirred for 16h. The reaction was concentrated to the dryness and the desired product was isolated using column chromatography eluting the desired compound with 80:20 Petroleum Ether: Ethyl Acetate.

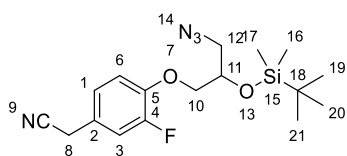
2-(4-(3-Azido-2-((*tert*-butyl dimethyl silyl) oxy) propoxy) phenyl) acetonitrile (3.33 step1)



The title compound was prepared in the manner similar to the general procedure (3.D) by utilizing 2-(4-(3-azido-2-hydroxypropoxy) phenyl) acetonitrile **3.30** (9g, 38 mmol). colourless oil (11g, 82 %). ¹H NMR (400 MHz, DMSO-*d*₆) δ 7.27 (d, *J* = 8.6 Hz 2H, *CH*_{Ar}), 6.93 (d, *J* = 8.6 Hz, 2H, *CH*_{Ar}), 4.08 (m, 1H, *CH*_{Al}), 3.95 (s, 2H, *C*₈*H*), 3.91 (m, 1H, *CH*_{Al}), 3.54 (dd, *J* = 12.9, 3.6 Hz, 1H, *CH*_{Al}), 3.33 (dd, *J* = 12.9, 5.5 Hz, 2H, *CH*_{Al}),

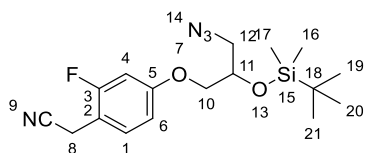
0.89 (s, 9H, C₁₉₋₂₁H), 0.13 (d, *J* = 13.8 Hz, 6H, C_{16,17}H). ¹³C NMR (101 MHz, DMSO-*d*₆) δ 158.1, 129.8, 123.8, 119.9, 115.2, 70.8, 69.8, 54.0, 26.0, 22.0, 18.2, -4.2.

2-(4-(3-Azido-2-((*tert*-butyl dimethyl silyl) oxy) propoxy)-3-fluorophenyl) acetonitrile (3.34 step1)



The title compound was prepared in the manner similar to the general procedure (3.D) by utilizing 2-(4-(3-azido-2-hydroxypropoxy)-3-fluorophenyl) acetonitrile **3.31** (1g, 4 mmol) as the starting material. Colourless oil (0.9 g, 62 % yield). ¹H NMR (400 MHz, DMSO-*d*₆) δ 7.26 – 7.18 (m, 2H, CH_{Ar}), 7.12 (ddd, *J* = 8.3, 2.2, 1.0 Hz, 1H, CH_{Ar}), 4.29 – 4.19 (m, 1H, CH_{Al}), 4.10 – 3.99 (m, 2H, CH_{Al}), 3.97 (s, 2H, C₈H), 3.55 (dd, *J* = 12.8, 3.6 Hz, 1H, CH_{Al}), 3.33 (m, 1H, CH), 0.87 (d, *J* = 4.7 Hz, 9H, C₁₉₋₂₁H), 0.11 (dd, *J* = 18.7, 6.1 Hz, 6H, C_{16,17}H). ¹³C NMR (101 MHz, DMSO-*d*₆) δ 151.8 (d, *J* = 245.3 Hz), 146.0 (d, *J* = 11.2 Hz), 124.9 (d, *J* = 4.9 Hz), 119.5, 116.4 (d, *J* = 18.6 Hz), 115.6 (d, *J* = 1.8 Hz), 71.0, 70.7, 54.0, 26.0, 21.9, 18.1, -4.4.

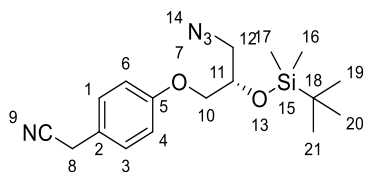
2-(4-(3-Azido-2-((*tert*-butyl dimethyl silyl) oxy) propoxy) -2-fluorophenyl) acetonitrile (3.35 step1)



The title compound was prepared in the manner similar to the general procedure (3.D) by utilizing 2-(4-(3-azido-2-hydroxypropoxy)-2-fluorophenyl) acetonitrile **3.32** (1g, 4 mmol) as the starting material. Colourless oil (0.8 g, 54 %). ¹H NMR (400 MHz, DMSO-*d*₆) δ 7.37 (t, *J* = 8.8 Hz, 1H, CH_{Ar}), 6.95 – 6.79 (m, 2H, CH_{Ar}), 4.20 (ddt, *J* = 7.9, 5.7, 2.7 Hz, 1H, CH_{Al}), 4.03 (dd, *J* = 10.0, 4.4 Hz, 1H, CH_{Al}), 3.96 (d, *J* = 8.0 Hz, 3H, C₈H, CH_{Al}), 3.53 (dd, *J* = 12.9, 3.6 Hz, 1H, CH_{Al}), 3.43 – 3.23 (m, 1H, CH_{Al}), 0.88 (s, 9H, C₁₉₋

$_{21}H$), 0.12 (d, $J = 14.0$ Hz, 6H, $C_{16,17}H$). ^{13}C NMR (101 MHz, $DMSO-d_6$) δ 162.2 (d, $J = 230.6$ Hz), 159.9 (d, $J = 4.6$ Hz), 131.3 (d, $J = 5.3$ Hz), 118.7, 111.6 (d, $J = 3.2$ Hz), 110.8 (d, $J = 17.7$ Hz), 102.6 (d, $J = 24.8$ Hz), 70.6, 70.4, 54.0, 26.0, 18.2, 16.6, -4.2.

(S)-2-(4-(3-azido-2-((*tert*-butyl dimethyl silyl) oxy) propoxy) phenyl) acetonitrile (3.111 step1)

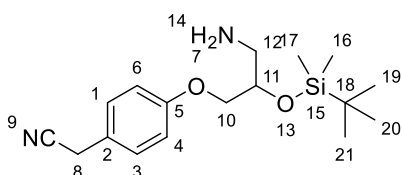


The title compound was prepared in the manner similar to the general procedure (3.D) by utilizing (*S*)-2-(4-(3-azido-2-hydroxypropoxy) phenyl) acetonitrile **3.110** (5g, 25mmol) as the starting material. Colourless oil (5.2g, 70 %). 1H NMR (400 MHz, $DMSO-d_6$) δ 7.30 – 7.25 (m, 2H, CH_{Ar}), 6.99 – 6.92 (m, 2H, CH_{Ar}), 4.26 – 4.14 (m, 1H, CH_{Al}), 4.10 – 3.96 (m, 1H, CH_{Al}), 3.94 (s, 3H, C_8H , CH_{Al}), 3.54 (dd, $J = 12.8, 3.6$ Hz, 1H, CH_{Al}), 0.89 (s, 9H, $C_{19-21}H$), 0.13 (d, $J = 13.6$ Hz, 6H, $C_{16,17}H$). ^{13}C NMR (101 MHz, $DMSO-d_6$) δ 158.1, 129.8, 123.8, 119.8, 115.2, 70.8, 69.8, 54.1, 26.0, 22.0, 18.2, -4.2.

General procedure (3.E) for preparation of (3.33-3.35, 3.111 step2)

To a solution of **3.33-3.35, 3.111 step1** (1 equiv) in THF (20 mL) was added Ph_3P (1.5 equiv) and stirred at rt for 2 hours. Then 20 % water was added and stirred the reaction at rt for 16 h. The reaction was concentrated to the dryness and the desired product was isolated using column chromatography eluting the desired compound with 100 % Ethyl Acetate.

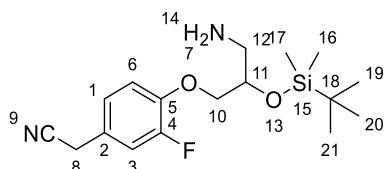
2-(4-(3-Amino-2-((*tert*-butyl dimethyl silyl) oxy) propoxy) phenyl) acetonitrile (3.33 step2)



The title compound was prepared in the manner similar to the general procedure (3.E) by utilizing 2-(4-(3-azido-2-((*tert*-butyl dimethyl silyl) oxy) propoxy)

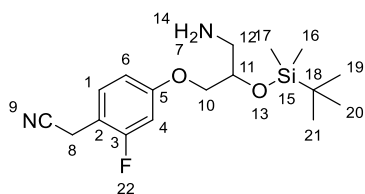
phenyl) acetonitrile **3.33 step1** (11g, 31mmol) as the starting material. Colourless oil (7g, 70 %). ¹H NMR (400 MHz, DMSO) δ 7.26 (d, *J* = 8.5 Hz, 2H, CH_{Ar}), 6.96 – 6.90 (d, *J* = 8.5 Hz, 2H, CH_{Ar}), 4.07 (dd, *J* = 9.8, 3.3 Hz, 1H, CH_{Al}), 3.96 – 3.87 (m, 3H, C₈H, CH_{Al}), 3.82 (dd, *J* = 9.8, 7.1 Hz, 1H, CH_{Al}), 2.71 – 2.58 (m, 2H, CH_{Al}), 0.87 (s, 9H, C₁₉₋₂₁H), 0.08 (d, *J* = 12.9 Hz, 6H, C_{16,17}H). ¹³C NMR (101 MHz, DMSO) δ 158.5, 129.7, 123.4, 120.0, 115.2, 73.3, 70.9, 45.6, 26.2, 21.9, 18.3, -3.9, -4.2.

2-(4-(3-Amino-2-((*tert*-butyl dimethyl silyl) oxy) propoxy)-3-fluorophenyl) acetonitrile (3.34 step2)



The title compound was prepared in the manner similar to the general procedure (3.E) by utilizing 2-(4-(3-azido-2-((*tert*-butyl dimethyl silyl) oxy) propoxy)-3-fluorophenyl) acetonitrile **3.34 step1** (0.9g, 2 mmol) as the starting material. Colourless oil (0.4g, 47 %). ¹H NMR (400 MHz, DMSO-*d*₆) δ 7.26 – 7.09 (m, 3H, CH_{Ar}), 4.14 (td, *J* = 9.2, 3.0 Hz, 1H, CH_{Al}), 4.03 – 3.86 (m, 4H, C₈H, CH_{Al}), 2.67 (dd, *J* = 5.3, 2.6 Hz, 2H, CH_{Al}), 0.92 – 0.77 (m, 9H, C₁₉₋₂₁H), 0.14 – -0.02 (m, 6H, C_{16,17}H). ¹³C NMR (101 MHz, DMSO-*d*₆) δ 151.8 (d, *J* = 243.4 Hz), 146.4 (d, *J* = 10.6 Hz), 124.8 (d, *J* = 3.6 Hz), 124.2 (d, *J* = 6.7 Hz), 119.5, 116.3 (d, *J* = 23.2 Hz), 115.3 (d, *J* = 1.8 Hz), 73.1, 71.9, 45.4, 26.1, 21.8, 18.2, -4.3.

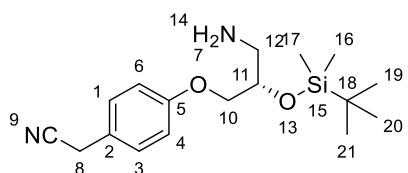
2-(4-(3-Amino-2-((*tert*-butyl dimethyl silyl) oxy) propoxy)-2-fluorophenyl) acetonitrile (3.35 step2)



The title compound was prepared in the manner similar to the general procedure (3.E) by utilizing 2-(4-(3-azido-2-((*tert*-butyl dimethyl silyl) oxy) propoxy)

-2-fluorophenyl) acetonitrile **3.35 step1** (0.8g, 2 mmol) as the starting material. Colourless oil (0.6g, 71 % yield). ^1H NMR (400 MHz, DMSO- d_6) δ 7.36 (td, $J = 8.8, 6.2$ Hz, 1H, CH_{Ar}), 6.94 – 6.77 (m, 2H, CH_{Ar}), 4.09 (td, $J = 10.4, 9.9, 3.4$ Hz, 2H, CH_{Al}), 4.02 – 3.90 (m, 3H, C_8H , CH_{Al}), 3.90 – 3.79 (m, 1H, CH_{Al}), 2.69 – 2.59 (m, 2H, CH_{Al}), 0.90 – 0.83 (m, 9H, C_{19-21}H), 0.08 (d, $J = 13.3$ Hz, 6H, $\text{C}_{16,17}\text{H}$). ^{13}C NMR (101 MHz, DMSO- d_6) δ 162.2 (d, $J = 230.6$ Hz), 159.9 (d, $J = 4.6$ Hz), 131.3 (d, $J = 5.3$ Hz), 118.7, 111.6 (d, $J = 3.2$ Hz), 110.8 (d, $J = 17.7$ Hz), 102.6 (d, $J = 24.8$ Hz), 70.6, 70.4, 54.0, 26.0, 18.2, 16.6, -4.2, -4.5.

(S)-2-(4-(3-Amino-2-((*tert*-butyldimethylsilyl) oxy) propoxy) phenyl) acetonitrile (3.111 step2)

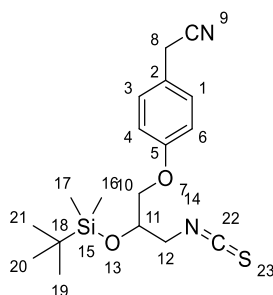


The title compound was prepared in the manner similar to the general procedure (3.E) by utilizing (S)-2-(4-(3-azido-2-((*tert*-butyl dimethyl silyl) oxy) propoxy) phenyl) acetonitrile **3.111 step1** (5.2g, 16mmol) as the starting material. Colourless oil (3g, 65 %). ^1H NMR (400 MHz, DMSO- d_6) δ 7.29 – 7.21 (m, 2H, CH_{Ar}), 6.97 – 6.88 (m, 2H, CH_{Ar}), 4.07 – 4.04 (m, 1H, CH_{Al}), 3.93 (s, 3H, C_8H , CH_{Al}), 3.88 – 3.77 (m, 1H, CH_{Al}), 2.73 – 2.60 (m, 2H, CH_{Al}), 0.91 – 0.80 (m, 9 H, C_{19-21}H), 0.08 (dd, $J = 13.0, 2.8$ Hz, 6H, $\text{C}_{16,17}\text{H}$). ^{13}C NMR (101 MHz, DMSO- d_6) δ 158.5, 129.7, 123.4, 119.9, 115.1, 73.3, 70.9, 49.0, 26.2, 21.9, 18.3, -4.0, -4.2.

General procedure (3.F) for preparation of (3.36-3.38).

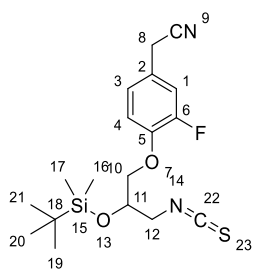
To a solution of **3.33-3.35**, **3.111 step2** (1 eq) in DCM was added 1,1'-thiocarbonyldiimidazole (TCDI) (3 eq) and stirred for 16h at rt. The reaction was concentrated to the dryness and the desired product was isolated using column chromatography eluting the desired compound with 80:20 Petroleum Ether: Ethyl Acetate.

2-(4-(2-((*tert*-Butyl dimethyl silyl) oxy)-3-isothiocyanatopropoxy) phenyl) acetonitrile (3.36)



The title compound was prepared in the manner similar to the general procedure (3.F) by utilizing 2-(4-(3-amino-2-((*tert*-butyl dimethyl silyl) oxy) propoxy) phenyl) acetonitrile **3.33 step2** (1g, 3 mmol) as starting material. Brown oil (0.7g, 63 %). ¹H NMR (400 MHz, DMSO-*d*₆) δ 7.33 – 7.21 (m, 2H, CH_{Ar}), 7.04 – 6.92 (m, 2H, CH_{Ar}), 4.29 (qd, *J* = 5.8, 4.0 Hz, 1H, CH_{Al}), 3.98 (dd, *J* = 10.0, 4.0 Hz, 1H, CH_{Al}), 3.95 – 3.88 (m, 4H, C₈H, CH_{Al}), 3.78 (dd, *J* = 15.1, 5.8 Hz, 1H, CH_{Al}), 0.89 (s, 9H, C₁₉₋₂₁H), 0.13 (d, *J* = 15.1 Hz, 6H, C_{16,17}H). ¹³C NMR (101 MHz, DMSO-*d*₆) δ 158.0, 129.8, 129.5, 123.9, 119.9, 115.3, 69.7, 69.6, 48.8, 26.1, 21.9, 18.1, -4.1, -4.4.

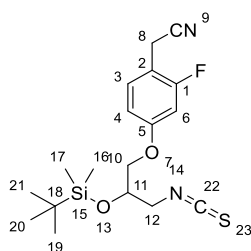
2-(4-(2-((*tert*-Butyl dimethyl silyl) oxy)-3-isothiocyanatopropoxy) -3-fluorophenyl) acetonitrile (3.37)



The title compound was prepared in the manner similar to the general procedure (3.F) by utilizing 2-(4-(3-amino-2-((*tert*-butyl dimethyl silyl) oxy) propoxy)-3-fluorophenyl) acetonitrile **3.34 step2** (0.4g, 1.1mmol) as starting material. Colourless oil (0.2g, 44 %). ¹H NMR (400 MHz, DMSO-*d*₆) δ 7.29 – 7.19 (m, 2H, CH_{Ar}), 7.13 (ddd, *J* = 8.4, 2.1, 0.9 Hz, 1H, CH_{Ar}), 4.32 (tt, *J* = 6.1, 4.1 Hz, 1H, CH_{Al}), 4.15 – 4.01 (m, 2H, CH_{Al}), 3.93 (dd, *J* = 14.8, 3.8 Hz, 1H, CH_{Al}), 3.77 (dd, *J* = 14.7, 5.7 Hz, 1H, CH_{Al}), 0.88 (s, 9H, C₁₉₋₂₁H), 0.17 –

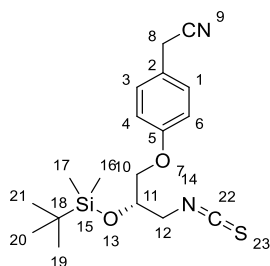
0.07 (m, 6H, C_{16,17}H). ¹³C NMR (101 MHz, DMSO-*d*₆) δ 151.8 (d, *J* = 246.3 Hz), 145.9 (d, *J* = 11.5 Hz), 129.7, 125.0 (d, *J* = 3.7 Hz) 124.9 (d, *J* = 6.8 Hz), 119.5, 116.4 (d, *J* = 18.1 Hz), 115.8 (d, *J* = 1.5 Hz), 70.8, 69.5, 48.7, 26.0, 21.9, 18.1, -4.5.

2-(4-(2-((*tert*-Butyl dimethyl silyl) oxy)-3-isothiocyanatopropoxy)-2-fluorophenyl) acetonitrile (3.38)



The title compound was prepared in similar manner to the general procedure (3.F) by utilizing 2-(4-(3-amino-2-((*tert*-butyl dimethyl silyl) oxy) propoxy)-2-fluorophenyl) acetonitrile **3.35 step** (0.6g, 2 mmol) as the starting material. Colourless oil (0.4g, 45 %). ¹H NMR (400 MHz, DMSO-*d*₆) δ 7.37 (m, 1H, CH_{Ar}), 6.93 (m, 1H, CH_{Ar}), 6.84 (m, 1H, CH_{Ar}), 4.34 – 4.19 (m, 1H, CH_{Al}), 4.12 – 4.00 (m, 1H, CH_{Al}), 4.00 – 3.89 (m, 3H, C₈H, CH_{Al}), 3.83 – 3.66 (m, 2H, CH_{Al}), 0.88 (d, *J* = 4.7 Hz, 9H, C₁₉₋₂₁H), 0.17 – 0.05 (m, 6H, C_{16,17}H). ¹³C NMR (101 MHz, DMSO-*d*₆) δ 161.0 (d, *J* = 228.5 Hz), 159.7 (d, *J* = 6.6 Hz), 131.4 (d, *J* = 5.3 Hz), 129.6, 118.7, 111.6 (d, *J* = 4.6 Hz), 110.7 (d, *J* = 17.2 Hz), 102.9 (d, *J* = 23.9 Hz), 70.4, 69.4, 48.7, 47.0, 26.1, 18.2, -4.1, -4.3.

(*S*)-2-(4-(2-((*tert*-butyl dimethyl silyl) oxy)-3-isothiocyanatopropoxy) phenyl) acetonitrile (3.112)



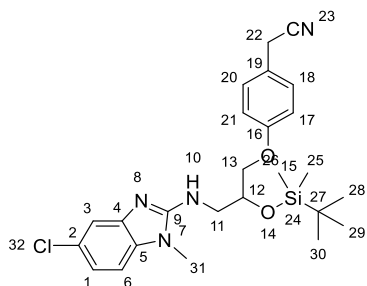
The title compound was prepared in similar manner to the general procedure (3.F) by utilizing (*S*)-2-(4-(3-amino-2-((*tert*-butyldimethylsilyl) oxy) propoxy)

phenyl) acetonitrile **3.111** step2 step2 (0.4g, 1 mmol) as the starting material. Colourless oil (0.3g, 57 %).

General procedure (3.G) for preparation of (3.70-3.86, 3.111).

To a solution of (1 eq) of the corresponding chloro-*N*¹-(alkyl) benzene-1, 2-diamine (**3.12**, **3.56- 3.69**, **3.110**) in EtOH (20 mL) was added (1 eq) of the corresponding isothiocyanate (**3.36- 3.38**, **3.112**) and stirred for 16h at 70 °C. The reaction was concentrated and then dissolved in DMF (20 mL). DIC (1.2 eq) and Et₃N (2 eq) were added to the mixture and stirred for 16h at 80 °C. The reaction was concentrated to the dryness and the desired product was isolated using column chromatography eluting the desired compound with 50:50 Petroleum Ether: Ethyl Acetate for most of the compounds.

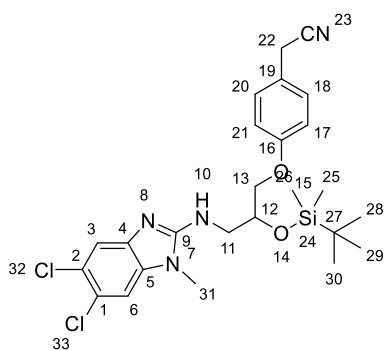
2-(4-(2-((*tert*-Butyl dimethyl silyl) oxy) – 3 - ((5-chloro-1-methyl-1*H*-benzo[*d*]imidazol-2-yl) amino) propoxy) phenyl) acetonitrile (**3.70**)



The title compound was prepared in the manner similar to the general procedure (3.G) by utilizing 4-chloro-*N*¹-methylbenzene-1,2-diamine **3.56** (0.2g, 1mmol) and 2-(4-(2-((*tert*-butyl dimethyl silyl) oxy)-3-isothiocyanatopropoxy) phenyl) acetonitrile **3.36** (0.4g, 1mmol) as starting materials. Brown oil (0.1g, 20 %) ¹H NMR (400 MHz, DMSO-*d*₆) δ 7.30 – 7.23 (m, 2H, CH_{Ar}), 6.96 – 6.80 (m, 4H, CH_{Ar}), 6.55 (ddd, *J* = 15.4, 8.3, 2.4 Hz, 1H, CH_{Ar}), 4.26 (s, 1H, CH_{Al}), 3.94 (s, 3H, C₂₂H, CH_{Al}), 3.85 – 3.69 (m, 2H, CH_{Al}), 3.37 (d, *J* = 8.8 Hz, 4H, C₃₁H, CH_{Al}), 0.89 – 0.69 (m, 9H, C₂₈₋₂₉H), 0.06 (d, *J* = 2.7 Hz, 6H, C_{25,26}H). ¹³C NMR (101 MHz, DMSO-*d*₆) δ 158.5, 155.0, 133.3, 129.7, 128.5, 126.8, 126.0,

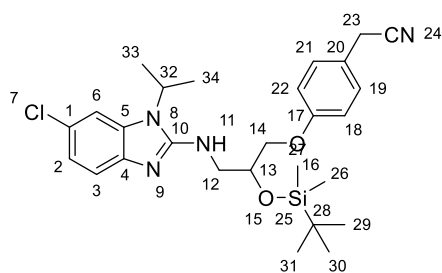
123.5, 120.0, 115.4, 113.7, 109.7, 70.6, 68.1, 46.4, 30.9, 29.2, 26.2, 21.9, -4.1. LCMS m/z calc for $C_{25}H_{33}ClN_4O_2Si^+$ $[M+H]^+$: 485.2, found 485.1 with t_R 2.56 min.

2-(4-(2-((*tert*-Butyl dimethyl silyl) oxy) -3 - ((5, 6-dichloro-1-methyl-1*H*-benzo[*d*]imidazol-2-yl) amino) propoxy) phenyl) acetonitrile (3.71)



The title compound was prepared in the manner similar to the general procedure (3.G) by utilizing 4, 5-dichloro-*N*¹-methylbenzene-1, 2-diamine **3.57** (0.2g, 0.8mmol) and 2-(4-(2-((*tert*-butyl dimethyl silyl) oxy)-3-isothiocyantopropoxy) phenyl) acetonitrile **3.36** (0.3g, 0.8mmol) as a starting material. Brown oil (0.1g, 20 %). ¹H NMR (400 MHz, DMSO-*d*₆) δ 7.46 (s, 1H, CH_{Ar}), 7.35 (s, 1H, CH_{Ar}), 7.29 – 7.24 (m, 2H, CH_{Ar}), 7.14 (t, $J = 5.7$ Hz, 1H, CH_{Ar}), 6.96 – 6.91 (m, 2H, CH_{Ar}), 4.39 (qd, $J = 6.5, 3.0$ Hz, 1H, CH_{Al}), 4.09 (dd, $J = 10.1, 3.0$ Hz, 1H, CH_{Al}), 3.98 – 3.86 (m, 3H, CH_{Al}), 3.58 – 3.41 (m, 5H, CH_{Al}), 0.83 (s, 9H, $C_{28-30}H$), 0.02 (d, $J = 8.4$ Hz, 6H, $C_{25,26}H$). ¹³C NMR (101 MHz, DMSO-*d*₆) δ 158.4, 157.0, 143.1, 135.7, 129.8, 123.5, 122.7, 120.4, 119.9, 116.0, 115.2, 109.2, 71.2, 69.9, 46.0, 29.0, 26.1, 21.9, 18.3, -4.1. LCMS m/z calc for $C_{25}H_{32}Cl_2N_4O_2Si^+$ $[M+H]^+$: 519.1, found 518.7 with t_R 2.91 min.

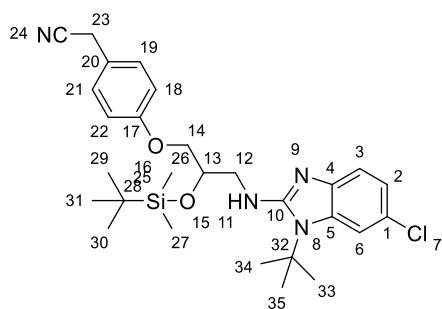
2-(4-(2-((*tert*-Butyl dimethyl silyl) oxy)-3-((6-chloro-1-isopropyl-1*H*-benzo[*d*]imidazol-2-yl) amino) propoxy) phenyl) acetonitrile (3.72)



The title compound was prepared in the manner similar to

the general procedure (3.G) by utilizing 5-chloro-*N*¹-isopropylbenzene-1,2-diamine **3.12** (0.3g, 2mmol) and 2-(4-(2-((*tert*-butyl dimethyl silyl) oxy)-3-isothiocyanatopropoxy) phenyl) acetonitrile **3.36** (0.7g, 2mmol) as starting materials. Brown oil (0.3g, 33 %). ¹H NMR (400 MHz, DMSO-*d*₆) δ 7.37 (d, *J* = 2.0 Hz, 1H, C₆H), 7.26 (dd, *J* = 8.6, 2.0 Hz, 2H, C₂H, CH_{Ar}), 7.17 (d, *J* = 8.6 Hz, 1H, C₃H), 6.97 – 6.91 (m, 3H, CH_{Ar}), 6.82 (t, *J* = 5.6 Hz, 1H, NH), 4.61 (h, *J* = 6.9 Hz, 1H, C₃₂H), 4.41 (qd, *J* = 6.9, 3.0 Hz, 1H, CH_{Al}), 4.09 (dd, *J* = 10.3, 3.0 Hz, 1H, CH_{Al}) 3.93 (s, 2H, C₂₃H), 3.92 – 3.86 (m, 1H, CH_{Al}), 3.57 – 3.39 (m, 2H, CH_{Al}), 1.48 (dd, *J* = 6.9, 1.7 Hz, 6H, C_{33,34}H), 0.85 (s, 9H, C₂₉₋₃₁H), 0.04 (s, 6H, C_{26,27}H). LCMS *m/z* calc for C₂₇H₃₇ClN₄O₂Si⁺ [M+H]⁺: 513.2, found 513.2 with *t*_R 2.64 min.

2-(4-(3-((1-(*tert*-Butyl)-6-chloro-1*H*-benzo[*d*]imidazol-2-yl)amino)-2-((*tert*-butyl dimethyl silyl) oxy) propoxy) phenyl) acetonitrile (3.73)

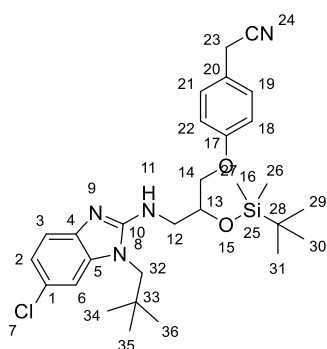


The title compound was prepared in the manner similar to

the general procedure (3.G) by utilizing *N*¹-(*tert*-butyl)-5-chlorobenzene-1,2-diamine **3.58** (0.16g, 0.8mmol) and 2-(4-(2-((*tert*-butyl dimethyl silyl) oxy)-3-isothiocyanatopropoxy) phenyl) acetonitrile **3.36** (0.3g, 0.8mmol) as starting materials. Brown oil (0.12g, 30 %). ¹H NMR (400 MHz, DMSO-*d*₆) δ 7.49 (d, *J* = 2.0 Hz, 1H, C₆H), 7.25 (dd, *J* = 8.6, 2.0 Hz, 2H, C₂H, CH_{Ar}), 7.16 (d, *J* = 8.6 Hz, 1H, C₃H), 7.01 – 6.88 (m, 3H, CH_{Ar}), 6.05 (t, *J* = 5.4 Hz, 1H

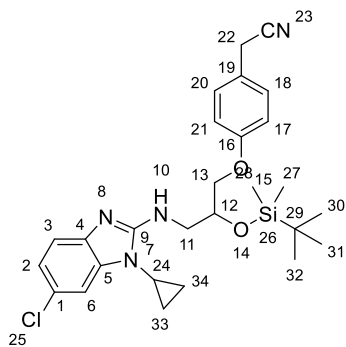
NH), 4.46 (qd, $J = 6.7, 3.0$ Hz, 1H, CH_{Al}), 4.10 (dd, $J = 10.3, 3.0$ Hz, 1H, CH_{Al}), 3.96 – 3.89 (m, 3H, $C_{23}H, CH_{Al}$), 3.61 – 3.45 (m, 2H, CH_{Al}), 1.75 (s, 9H, $C_{33-35}H$), 0.87 (s, 9H, $C_{29-31}H$), 0.08 (d, $J = 5.1$ Hz, 6H, $C_{26,27}H$). ^{13}C NMR (101 MHz, DMSO- d_6) δ 158.4, 156.1, 141.6, 135.3, 129.8, 123.5, 122.7, 120.5, 119.9, 116.6, 115.1, 112.5, 71.6, 69.7, 58.2, 47.2, 41.2, 30.0, 26.2, 21.9, -4.1. LCMS m/z calc for $C_{28}H_{39}ClN_4O_2Si^+ [M+H]^+$: 527.2, found 527.0 with t_R 2.83 min.

2-(4-(2-((*tert*-Butyl dimethyl silyl) oxy)-3-((6-chloro-1-neopentyl-1*H*-benzo[*d*]imidazol-2-yl) amino) propoxy) phenyl) acetonitrile (3.74)



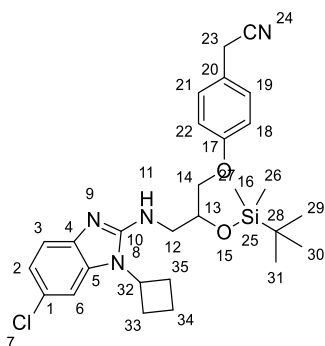
The title compound was prepared in the manner similar to the general procedure (3.G) by utilizing 5-chloro- N^1 -neopentylbenzene-1,2-diamine **3.59** (0.17g, 0.8mmol) and 2-(4-(2-((*tert*-butyl dimethyl silyl) oxy)-3-isothiocyanatopropoxy) phenyl) acetonitrile **3.36** (0.3g, 0.8mmol) as a starting material. Brown oil (0.10g, 21 %). 1H NMR (400 MHz, DMSO- d_6) δ 7.32 – 7.22 (m, 3H, CH_{Ar}), 7.14 (d, $J = 8.3$ Hz, 1H, CH_{Ar}), 6.97 – 6.86 (m, 3H, CH_{Ar}), 6.70 (s, 1H, NH), 4.40 (dq, $J = 7.6, 3.6, 2.5$ Hz, 1H, CH_{Al}), 4.10 (dd, $J = 10.4, 2.8$ Hz, 1H, CH_{Al}), 3.95 – 3.87 (m, 3H, CH_{Al}), 3.82 (s, 2H, $C_{32}H$), 3.55 – 3.46 (m, 2H, CH_{Al}), 0.95 (s, 9H, $C_{34-36}H$), 0.85 (s, 9H, $C_{29-31}H$), 0.08 (d, $J = 4.8$ Hz, 6H, $C_{26,27}H$). ^{13}C NMR (101 MHz, DMSO- d_6) δ 158.4, 156.4, 141.6, 137.1, 129.8, 123.5, 122.8, 120.5, 119.9, 116.0, 115.1, 109.3, 71.3, 70.0, 52.2, 46.2, 28.2, 26.2, 24.5, 21.9, 18.3, -4.1. LCMS m/z calc for $C_{29}H_{41}ClN_4O_2Si^+ [M+H]^+$: 541.2, found 540.7 with t_R 2.86 min.

2-(4-(2-((*tert*-Butyl dimethyl silyl) oxy)-3-((6-chloro-1-cyclopropyl-1*H*-benzo[*d*]imidazol-2-yl) amino) propoxy) phenyl) acetonitrile (3.75)



The title compound was prepared in the manner similar to the general procedure (3.G) by utilizing 5-chloro-*N*¹-cyclopropylbenzene-1,2-diamine **3.60** (0.15g, 0.8mmol) and 2-(4-(2-((*tert*-butyl dimethyl silyl) oxy)-3-isothiocyanatopropoxy) phenyl) acetonitrile **3.36** (0.3g, 0.8mmol) as starting materials. Brown oil (0.08g, 18 %). ¹H NMR (400 MHz, DMSO-*d*₆) δ 7.29 – 7.24 (m, 2H, *CH*_{Ar}), 7.21 – 7.13 (m, 2H, *CH*_{Ar}), 6.94 (m, 3H, *CH*_{Ar}), 6.57 (t, *J* = 5.9 Hz, 1H, *NH*), 4.42 (m, 1H, *CH*_{Al}), 4.11 (dd, *J* = 10.2, 3.0 Hz, 1H, *CH*_{Al}), 3.96 – 3.87 (m, 3H, *C*₂₂*H*, *CH*_{Al}), 3.51 (t, *J* = 6.0 Hz, 2H, *CH*_{Al}), 2.98 (tt, *J* = 7.1, 3.7 Hz, 1H, *C*₂₄*H*), 1.48 – 1.36 (m, 2H, *C*₃₃ or *34H*), 1.36 – 1.23 (m, 2H, *C*₃₃ or *34H*), 0.87 – 0.84 (m, 9H, *C*₃₀₋₃₂*H*), 0.07 (s, 6H, *C*_{26,27}*H*). ¹³C NMR (101 MHz, DMSO-*d*₆) δ 158.4, 156.6, 141.7, 136.5, 129.8, 123.5, 122.9, 120.7, 119.9, 116.4, 115.2, 108.5, 71.3, 69.9, 46.2, 26.2, 22.9, 21.9, 18.3, 8.3, -4.2. LCMS *m/z* calc for C₂₇H₃₅ClN₄O₂Si [M+H]⁺: 511.2, found 511.0 with 2.65 *t*_R min.

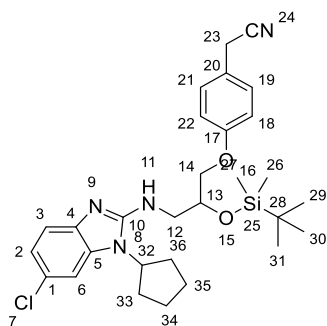
2-(4-(2-((*tert*-Butyl dimethyl silyl) oxy)-3-((6-chloro-1-cyclobutyl-1*H*-benzo[*d*]imidazol-2-yl) amino) propoxy) phenyl) acetonitrile (3.76)



The title compound was prepared in the manner similar to the general procedure (3.G) by utilizing 5-chloro-*N*¹-cyclobutylbenzene-1,2-diamine **3.61** (0.2g, 1mmol) and 2-(4-(2-((*tert*-butyl dimethyl silyl) oxy)-3-isothiocyanatopropoxy) phenyl) acetonitrile **3.36** (0.3g, 0.8mmol) as starting materials. Brown oil (0.08g, 18 %). ¹H NMR (400 MHz, DMSO-*d*₆) δ 7.29 – 7.24 (m, 2H, *CH*_{Ar}), 7.21 – 7.13 (m, 2H, *CH*_{Ar}), 6.94 (m, 3H, *CH*_{Ar}), 6.57 (t, *J* = 5.9 Hz, 1H, *NH*), 4.42 (m, 1H, *CH*_{Al}), 4.11 (dd, *J* = 10.2, 3.0 Hz, 1H, *CH*_{Al}), 3.96 – 3.87 (m, 3H, *C*₂₂*H*, *CH*_{Al}), 3.51 (t, *J* = 6.0 Hz, 2H, *CH*_{Al}), 2.98 (tt, *J* = 7.1, 3.7 Hz, 1H, *C*₂₄*H*), 1.48 – 1.36 (m, 2H, *C*₃₃ or *34H*), 1.36 – 1.23 (m, 2H, *C*₃₃ or *34H*), 0.87 – 0.84 (m, 9H, *C*₃₀₋₃₂*H*), 0.07 (s, 6H, *C*_{26,27}*H*). ¹³C NMR (101 MHz, DMSO-*d*₆) δ 158.4, 156.6, 141.7, 136.5, 129.8, 123.5, 122.9, 120.7, 119.9, 116.4, 115.2, 108.5, 71.3, 69.9, 46.2, 26.2, 22.9, 21.9, 18.3, 8.3, -4.2. LCMS *m/z* calc for C₂₇H₃₅ClN₄O₂Si [M+H]⁺: 511.2, found 511.0 with 2.65 *t*_R min.

acetonitrile **3.36** (0.4g, 1mmol) as starting materials. Brown oil (0.13g, 23 %). ^1H NMR (400 MHz, DMSO- d_6) δ 7.47 (d, $J = 2.0$ Hz, 1H, C_6H), 7.29 – 7.16 (m, 3H, CH_{Ar}), 7.00 – 6.91 (m, 3H, CH_{Ar}), 6.76 (t, $J = 5.7$ Hz, 1H NH), 4.89 (m, 1H, CH_{Al}), 4.40 (m, 2.9 Hz, 1H, CH_{Al}), 4.12 – 3.99 (m, 2H, C_{23}H), 3.99 – 3.86 (m, 3H, CH_{Al}), 2.84 – 2.69 (m, 2H, $\text{C}_{33, 34}$ or 35H), 2.41 – 2.29 (m, 2H, $\text{C}_{33, 34}$ or 35H), 1.99 (d, $J = 2.1$ Hz, 1H, C_{32}H), 1.98 – 1.71 (m, 2H, $\text{C}_{33, 34}$ or 35H), 0.84 (s, 9H, C_{29-31}H). 0.02 (d, $J = 4.4$ Hz, 6H, $\text{C}_{26,27}\text{H}$). ^{13}C NMR (101 MHz, DMSO- d_6) δ 158.4, 155.3, 142.4, 134.8, 129.7, 123.5, 122.8, 120.7, 119.9, 116.6, 115.2, 109.6, 71.3, 69.8, 47.7, 46.3, 28.3, 26.1, 24.5, 21.9, 18.3, -4.2. LCMS m/z calc for $\text{C}_{28}\text{H}_{37}\text{ClN}_4\text{O}_2\text{Si}^+$ $[\text{M}+\text{H}]^+$: 525.2, found 524.6 with t_{R} 2.79 min.

2-(4-(2-((*tert*-Butyl dimethyl silyl) oxy)-3-((6-chloro-1-cyclopentyl-1*H*-benzo[*d*]imidazol-2-yl) amino) propoxy) phenyl) acetonitrile (3.77)

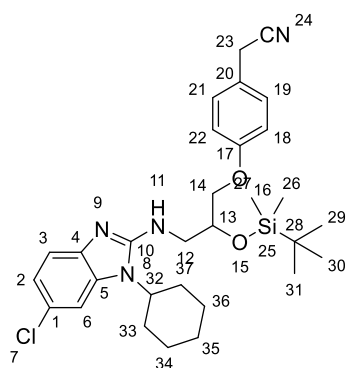


The title compound was prepared in the manner similar to the general

procedure (3.G) by utilizing 5-chloro- N^1 -cyclopentylbenzene-1,2-diamine **3.62** (0.20g, 0.9 mmol) and 2-(4-(2-((*tert*-butyl dimethyl silyl) oxy)-3-isothiocyanatopropoxy) phenyl) acetonitrile **3.36** (0.35g, 0.9mmol) as starting materials. Brown oil (0.12g, 25 %). ^1H NMR (400 MHz, DMSO- d_6) δ 7.29 – 7.24 (m, 2H, CH_{Ar}), 7.20 – 7.16 (m, 2H, CH_{Ar}), 6.99 – 6.92 (m, 3H, CH_{Ar}), 6.88 (t, $J = 5.7$ Hz, 1H, NH), 4.75 (m, 1H, CH_{Al}), 4.41 (m, 1H, CH_{Al}), 4.09 (dd, $J = 10.3, 3.0$ Hz, 1H, CH_{Al}), 3.94 (s, 3H, C_{23}H , CH_{Al}), 3.57 – 3.39 (m, 2H, CH_{Al}), 2.07 – 1.86 (m, $J = 7.9, 6.9$ Hz, 6H, CH_{Al}), 1.74 – 1.60 (m, 2H, CH_{Al}), 0.84 (s, 9H, C_{29-31}H), 0.02 (d, $J = 1.3$ Hz, 6H, $\text{C}_{26,27}\text{H}$). ^{13}C NMR (101 MHz, DMSO- d_6) δ 158.4, 155.6, 142.5, 133.6, 129.8, 123.5,

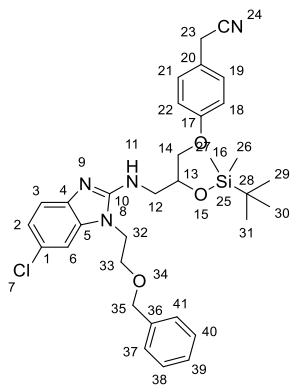
122.6, 120.5, 120.0, 116.6, 115.2, 109.3, 71.3, 69.8, 46.4, 41.2, 28.9, 26.2, 24.7, 21.9, 18.3, -
4.1. LCMS m/z calc for $C_{29}H_{39}ClN_4O_2Si^+$ $[M+H]^+$: 539.2, found 540.1 with t_R 2.75 min.

2-(4-(2-((*tert*-Butyl dimethyl silyl) oxy)-3-((6-chloro-1-cyclo hexyl-1*H*-benzo[*d*] imidazol-2-yl) amino) propoxy) phenyl) acetonitrile (3.78)



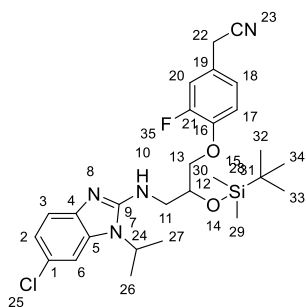
The title compound was prepared in the manner similar to the general procedure (3.G) by utilizing 5-chloro-*N*¹-cyclohexylbenzene-1, 2-diamine **3.63** (0.17g, 0.7mmol) and 2-(4-(2-((*tert*-butyl dimethyl silyl) oxy)-3-isothiocyanatopropoxy) phenyl) acetonitrile **3.36** (0.28g, 0.7mmol) as starting materials. Brown oil (0.09g, 22 %). ¹H NMR (400 MHz, DMSO-*d*₆) δ 7.41 (d, $J = 2.0$ Hz, 1H, C₆H), 7.26 (d, $J = 8.6$ Hz, 2H, C₂H, CH_{Ar}), 7.17 (d, $J = 8.6$ Hz, 1H, C₃H), 6.99 – 6.92 (m, 3H, CH_{Ar}), 6.88 (s, 1H, NH), 4.44 – 4.37 (m, 1H, CH_{Al}), 4.19 (m, 1H, CH_{Al}), 4.09 (dd, $J = 10.3, 3.1$ Hz, 1H, CH_{Al}), 3.93 (s, 2H C₂₃H), 3.54 (m, 1H, CH_{Al}), 3.43 (m, 1H, CH_{Al}), 2.16 – 2.02 (m, 2H, CH_{Al}), 1.77 – 1.61 (m, 3H, CH_{Al}), 1.47 – 1.36 (m, 3H, CH_{Al}), 1.17 – 1.08 (m, 3H, CH_{Al}), 0.85 (s, 9H, C₂₉₋₃₁H), 0.04 (s, 6H, C_{26,27}H). ¹³C NMR (101 MHz, DMSO-*d*₆) δ 158.4, 155.1, 142.2, 134.3, 129.8, 123.5, 122.7, 120.4, 119.9, 116.4, 115.2, 110.1, 71.3, 69.9, 46.5, 42.8, 30.3, 26.2, 24.8, 22.1, 20.8, 18.3, -4.1. LCMS m/z calc for $C_{30}H_{41}ClN_4O_2Si^+$ $[M+H]^+$: 553.2, found 553.2 with t_R 2.84 min.

2-(4-(3-((1-(2-(Benzyloxy) ethyl)-6-chloro-1*H*-benzo[*d*]imidazol-2-yl) amino)-2-((*tert*-butyl dimethyl silyl) oxy) propoxy) phenyl) acetonitrile (3.79)



The title compound was prepared in the manner similar to the general procedure (3.G) by utilizing *N*¹-(2-(benzyloxy) ethyl)-5-chlorobenzene-1,2-diamine **3.64** (0.46g, 1.6mmol) and 2-(4-(2-((*tert*-butyl dimethyl silyl) oxy)-3-isothiocyanatopropoxy) phenyl) acetonitrile **3.36** (0.60g, 1.6mmol) as starting materials. Brown oil (0.31g, 33 %). ¹H NMR (400 MHz, DMSO-*d*₆) δ 7.31 (d, *J* = 2.1 Hz, 1H, CH_{Ar}), 7.28 – 7.21 (m, 5H, CH_{Ar}), 7.18 – 7.12 (m, 3H, CH_{Ar}), 6.95 (dd, *J* = 8.3, 2.1 Hz, 1H, CH_{Ar}), 6.93 – 6.87 (m, 2H, CH_{Ar}), 6.83 (t, *J* = 5.7 Hz, 1H, NH), 4.44 (s, 2H, C₃₅H), 4.22 (q, *J* = 4.6 Hz, 3H, CH_{Al}), 4.11 – 3.99 (m, 3H, CH_{Al}), 3.93 (s, 2H, C₂₃H), 3.88 (dd, *J* = 10.2, 6.9 Hz, 1H, CH_{Al}), 3.68 (t, *J* = 5.2 Hz, 2H, CH_{Al}), 3.47 (t, *J* = 6.2 Hz, 2H, CH_{Al}), 0.85 (s, 9H, C₂₉₋₃₁H), 0.06 (d, *J* = 1.8 Hz, 6H, C_{26,27}H). LCMS *m/z* calc for C₃₃H₄₁ClN₄O₃⁺ [M+H]⁺: 605.3, found 604.5 with *t*_R 2.72 min.

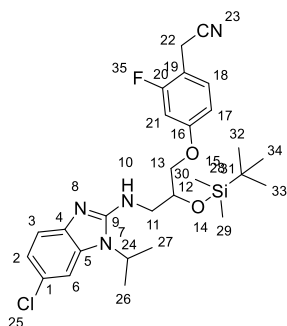
2-(4-(2-((*tert*-Butyl dimethyl silyl) oxy)-3-((6-chloro-1-isopropyl-1*H*-benzo[*d*]imidazol-2-yl) amino) propoxy)-3-fluorophenyl) acetonitrile (3.80)



The title compound was prepared in the manner similar to the general procedure (3.G) by utilizing 5-chloro-*N*¹-isopropylbenzene-1,2-diamine **3.12** (0.1g, 0.5 mmol) and 2-(4-(2-((*tert*-Butyl dimethyl silyl) oxy)-3-isothiocyanatopropoxy) -3-fluorophenyl) acetonitrile **3.37** (0.2g, 0.5 mmol) as starting materials. Brown oil (0.13g, 45 %). ¹H NMR (400

MHz, DMSO-*d*₆) δ 7.38 (d, *J* = 1.9 Hz, 1H, C₆H), 7.23 (dd, *J* = 12.0, 2.1 Hz, 1H, CH_{Ar}), 7.17 (dt, *J* = 8.5, 4.3 Hz, 2H, CH_{Ar}), 7.11 (dd, *J* = 8.6, 2.1 Hz, 1H, CH_{Ar}), 6.95 (dd, *J* = 8.4, 2.0 Hz, 1H, CH_{Ar}), 6.83 (t, *J* = 5.6 Hz, 1H, NH), 4.61 (p, *J* = 6.9 Hz, 1H, C₂₄H), 4.44 (qd, *J* = 6.5, 2.6 Hz, 1H, CH_{Al}), 4.16 (dd, *J* = 10.3, 2.9 Hz, 1H, CH_{Al}), 4.10 – 3.99 (m, 1H, CH_{Al}), 3.96 (s, 2H, C₂₂H), 3.58 – 3.40 (m, 2H, CH_{Al}), 1.48 (dd, *J* = 6.9, 1.6 Hz, 6H, C_{26,27}H), 0.84 (s, 9H, C_{29,30}H), 0.03 (d, *J* = 6.0 Hz, 6H, C₃₂₋₃₄H). ¹³C NMR (101 MHz, DMSO-*d*₆) δ 155.0, 151.9 (d, *J* = 241.1 Hz), 146.4 (d, *J* = 10.5 Hz), 142.4, 134.1, 124.8 (d, *J* = 3.8 Hz), 124.4 (d, *J* = 6.8 Hz), 122.6, 120.4, 119.5, 116.5 (d, *J* = 6.5 Hz), 115.4, 109.7, 72.3, 69.8, 46.3, 45.7, 26.1, 21.8, 20.6, 18.3, -4.4. LCMS *m/z* calc for C₂₇H₃₆ClFN₄O₂Si⁺ [M+H]⁺: 531.2, found 531.0 with *t*_R 2.66 min.

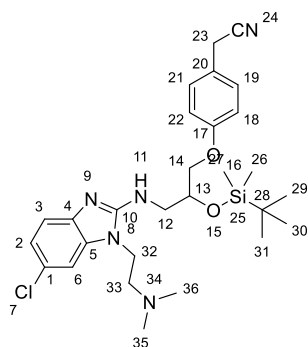
2-(4-(2-((*tert*-Butyl dimethyl silyl) oxy)-3-((6-chloro-1-isopropyl-1*H*-benzo[*d*]imidazol-2-yl) amino) propoxy)-2-fluorophenyl) acetonitrile (3.81)



The title compound was prepared in the manner similar to the general procedure (3.G) by utilizing 5-chloro-*N*¹-isopropylbenzene-1,2-diamine **3.12** (0.15g, 0.8 mmol) and 2-(4-(2-((*tert*-Butyl dimethyl silyl) oxy)-3-isothiocyantopropoxy)-2-fluorophenyl) acetonitrile **3.38** (0.30g, 0.8 mmol) as starting materials. Brown oil (0.16g, 37 %). ¹H NMR (400 MHz, DMSO-*d*₆) δ 7.40 – 7.31 (m, 2H, CH_{Ar}), 6.95 (dd, *J* = 8.5, 1.9 Hz, 1H, CH_{Ar}), 6.93 – 6.77 (m, 3H, CH_{Ar}), 4.65 – 4.56 (m, 2H, CH_{Al}), 4.45 – 4.37 (m, 1H, CH_{Al}), 3.95 (s, 3H, C₂₂H, CH_{Al}), 3.55 – 3.39 (m, 2H, CH_{Al}), 1.53 – 1.45 (m, 6H, C_{26,27}H), 0.86 (d, *J* = 10.2 Hz, 9H, C_{32,34}H), 0.03 (d, *J* = 1.9 Hz, 6H, C_{29,30}H), ¹³C NMR (101 MHz, DMSO-*d*₆) δ 160.9 (d, *J* = 244.8 Hz), 160.4 (d, *J* = 10.9 Hz), 155.4, 142.0, 134.1, 131.3 (d, *J* = 5.3 Hz), 122.8, 120.4, 118.8, 116.3, 111.7 (d, *J* = 3.1 Hz), 110.4 (d, *J* = 16.2 Hz), 109.8, 102.8 (d, *J* = 24.9 Hz), 71.4,

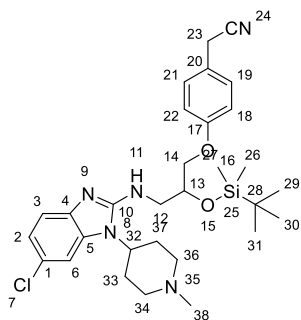
68.1, 46.5, 45.8, 26.1, 20.6, 18.2, 16.6, -4.3. LCMS m/z calc for $C_{27}H_{36}ClFN_4O_2Si^+$ $[M+H]^+$: 531.2, found 531.0 with t_R 2.67 min.

2-(4-(2-((*tert*-Butyl dimethyl silyl) oxy)-3-((6-chloro-1-(2-(dimethyl amino) ethyl)-1*H*-benzo[*d*]imidazol-2-yl) amino) propoxy) phenyl) acetonitrile (3.82)



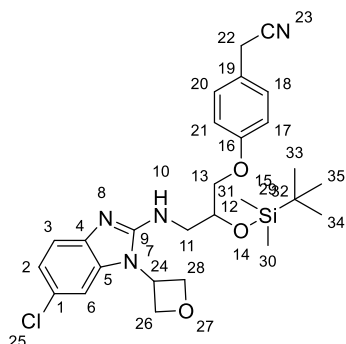
The title compound was prepared in the manner similar to the general procedure (3.G) by utilizing 5-chloro-*N*¹-(2-(dimethylamino) ethyl) benzene-1, 2-diamine **3.67** (0.18g, 0.8 mmol) and 2-(4-(2-((*tert*-butyl dimethyl silyl) oxy)-3-isothiocyanatopropoxy) phenyl) acetonitrile **3.36** (0.30g, 0.8 mmol) as starting materials. Brown oil (0.13g, 32 %). ¹H NMR (400 MHz, DMSO-*d*₆) δ 7.26 (d, $J = 8.6$ Hz, 2H, CH_{Ar}), 7.09 (tt, $J = 7.5, 1.9$ Hz, 1H, CH_{Ar}), 6.97 – 6.80 (m, 4H, CH_{Ar}), 6.61 (dtd, $J = 13.4, 7.5, 1.4$ Hz, 1H, NH), 5.29 (s, 2H, CH_{Al}), 4.24 (dtt, $J = 28.9, 7.3, 3.7$ Hz, 1H, CH_{Al}), 4.00 – 3.90 (m, 3H, CH_{Al}), 3.90 – 3.72 (m, 2H, CH_{Al}), 2.36 (dt, $J = 13.0, 6.0$ Hz, 2H, CH_{Al}), 2.18 (d, $J = 2.7$ Hz, 6H, $C_{35,36}H$), 0.76 (d, $J = 12.3$ Hz, 9H, $C_{29-31}H$), 0.01 (dd, $J = 18.08, 3.2$ Hz, 6H, $C_{26-27}H$). ¹³C NMR (101 MHz, DMSO) δ 158.3, 156.6, 141.1, 135.9, 129.7, 123.9, 122.4, 120.6, 118.7, 116.8, 115.2, 109.3, 70.6, 69.2, 56.8, 51.0, 48.5, 45.8, 26.1, 22.0, 18.1, -4.1. LCMS m/z calc for $C_{28}H_{40}ClN_5O_2Si$ $[M+H]^+$: 542.2, found 541.9 with t_R 2.53 min.

2-(4-(2-((*tert*-Butyl dimethyl silyl) oxy)-3-((6-chloro-1-(1-methyl piperidin-4-yl)-1*H*-benzo[*d*] imidazol-2-yl) amino) propoxy) phenyl) acetonitrile (3.83)



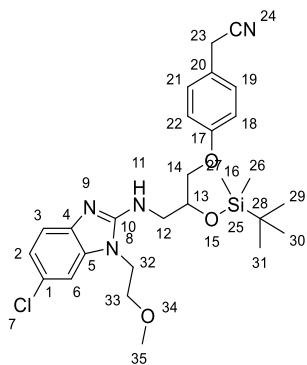
The title compound was prepared in the manner similar to the general procedure (3.G) by utilizing 5-chloro-*N*¹-(1-methylpiperidin-4-yl) benzene-1, 2-diamine **3.65** (0.26g, 1mmol) and 2-(4-(2-((*tert*-butyl dimethyl silyl) oxy)-3-isothiocyanatopropoxy) phenyl) acetonitrile **3.36** (0.40g, 1mmol) as starting materials. Brown oil (0.22g, 36 %). ¹H NMR (400 MHz, DMSO-*d*₆) δ 7.26 (dd, *J* = 8.5, 5.4 Hz, 2H, CH_{Ar}), 7.14 – 6.99 (m, 2H, CH_{Ar}), 6.96 – 6.88 (m, 2H, CH_{Ar}), 6.70 (d, *J* = 8.0 Hz, 1H, CH_{Ar}), 6.58 (t, *J* = 7.6, 1.2 Hz, 1H, NH), 4.58 (d, *J* = 7.6 Hz, 1H, C₁₂H), 4.30 (ddt, *J* = 12.8, 8.8, 5.6 Hz, 1H, CH_{Al}), 4.06 (ddd, *J* = 20.4, 10.3, 2.8 Hz, 1H, CH_{Al}), 3.94 (d, *J* = 5.9 Hz, 2H, CH_{Al}), 3.89 – 3.80 (m, 1H, CH_{Al}), 3.69 (dt, *J* = 12.1, 5.7 Hz, 1H, CH_{Al}), 3.58 (dt, *J* = 12.8, 5.8 Hz, 2H, CH_{Al}), 2.90 (s, 2H, CH_{Al}), 2.32 (s, 3H, C₃₈H), 2.09 (s, 1H, CH_{Al}), 1.91 (dd, *J* = 11.9, 5.8 Hz, 2H, CH_{Al}), 1.63 – 1.47 (m, 2H, CH_{Al}), 0.86 (d, *J* = 16.1 Hz, 9H, C₂₉₋₃₁H), 0.15 – 0.04 (m, 6H, C_{26,27}H). ¹³C NMR (101 MHz, DMSO-*d*₆) δ 158.3, 155.1, 143.1, 134.3, 129.8, 123.7, 122.8, 120.5, 119.6, 116.3, 115.2, 112.2, 71.2, 69.8, 54.2, 53.2, 47.5, 45.5, 29.3, 26.2, 22.0, 18.3, -4.1. LCMS *m/z* calc for C₃₀H₄₂ClN₅O₂Si⁺ [M+H]⁺ : 568.2, found 568.3 with *t*_R 2.62 min.

2-(4-(2-((*tert*-Butyl dimethyl silyl) oxy)-3-((6-chloro-1-(oxetan-3-yl)-1*H*-benzo[*d*]imidazol-2-yl) amino) propoxy) phenyl) acetonitrile (3.87)



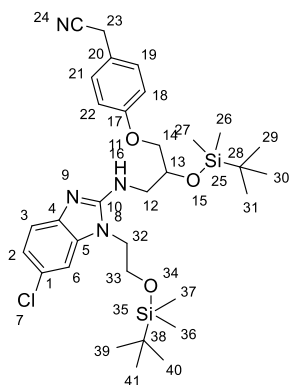
The title compound was prepared in the manner similar to the general procedure (3.G) by utilizing 5-chloro-*N*¹-(oxetan-3-yl) benzene-1,2-diamine **3.69** (0.25g, 1mmol) and 2-(4-(2-((*tert*-butyl dimethyl silyl) oxy)-3-isothiocyanatopropoxy) phenyl) acetonitrile **3.36** (0.50g, 1mmol) as starting materials. Brown oil (0.20g, 28 %). ¹H NMR (400 MHz, DMSO-*d*₆) δ 7.68 (d, *J* = 2.1 Hz, 1H, C₆H), 7.26 (dd, *J* = 8.5, 5.8 Hz, 3H, C₃H, CH_{Ar}), 7.06 (dd, *J* = 8.4, 2.1 Hz, 1H, C₂H), 6.96 – 6.92 (m, 2H, CH_{Ar}), 6.90 (d, *J* = 5.8 Hz, 1H, NH), 5.08 – 4.94 (m, 4H, C_{26,28}H), 4.38 (qd, *J* = 6.5, 3.0 Hz, 1H, C₂₄H), 4.12 – 4.00 (m, 2H, CH_{Al}), 3.97 – 3.87 (m, 3H, C₂₂H, CH_{Al}), 3.46 (ddt, *J* = 26.1, 13.2, 7.1 Hz, 2H, CH_{Al}), 0.82 (s, 9H, C₃₃₋₃₅H), 0.01 (d, *J* = 12.4 Hz, 6H, C_{30,31}H). ¹³C NMR (101 MHz, DMSO-*d*₆) δ 158.4, 155.3, 142.5, 133.7, 129.8, 123.5, 123.4, 121.3, 119.9, 117.0, 115.2, 109.1, 75.1, 71.2, 69.7, 48.3, 46.2, 26.1, 21.9, 18.3, -4.3. LCMS *m/z* calc for C₂₇H₃₅ClN₄O₃Si⁺ [M+H]⁺ : 527.2, found 526.8 with *t*_R 2.64 min.

2-(4-(2-((*tert*-Butyl dimethyl silyl) oxy)-3-((6-chloro-1-(2-methoxyethyl)-1*H*-benzo[*d*]imidazol-2-yl) amino) propoxy) phenyl) acetonitrile (3.88)



The title compound was prepared in the manner similar to the general procedure (3.G) by utilizing 5-chloro-*N*¹-(2-methoxyethyl) benzene-1, 2-diamine **3.70** (0.07g, 0.3 mmol) and 2-(4-(2-((*tert*-butyl dimethyl silyl) oxy)-3-isothiocyanatopropoxy) phenyl) acetonitrile **3.36** (0.13g, 0.3 mmol) as starting materials. Brown oil (0.08g, 40 %). ¹H NMR (400 MHz, DMSO-*d*₆) δ 7.31 – 7.19 (m, 3H, *CH*_{Ar}), 7.16 (d, *J* = 8.3 Hz, 1H, *CH*_{Ar}), 7.00 – 6.87 (m, 3H, *CH*_{Ar}), 6.83 (s, 1H, *NH*), 4.39 (qd, *J* = 6.3, 2.7 Hz, 1H, *CH*_{Al}), 4.20 – 4.14 (m, 1H, *CH*_{Al}), 4.10 (dd, *J* = 10.3, 2.9 Hz, 1H, *CH*_{Al}), 3.97 – 3.89 (m, 3H, *CH*_{Al}), 3.53 (dt, *J* = 32.8, 5.6 Hz, 4H, *CH*_{Al}), 3.20 (s, 4H, *CH*_{Al}), 0.86 (s, 9H, *C*_{29-31H}), 0.07 (d, *J* = 1.1 Hz, 6H, *C*_{26,27H}). ¹³C NMR (101 MHz, DMSO-*d*₆) δ 158.4, 155.7, 141.6, 136.2, 129.8, 123.5, 123.1, 120.7, 119.9, 116.1, 115.1, 108.5, 71.1, 70.7, 70.0, 58.8, 46.2, 42.1, 26.2, 21.9, 18.3, -4.1. LCMS *m/z* calc for C₂₇H₃₇ClN₄O₃Si⁺ [*M*+*H*]⁺ : 529.2, found 529.0 with *t*_R 2.74 min.

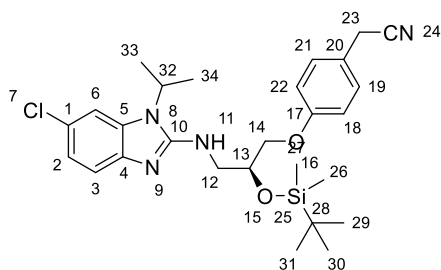
2-(4-(2-((*tert*-Butyl dimethyl silyl) oxy)-3-((1-(2-((*tert*-butyl dimethyl silyl) oxy) ethyl)-6-chloro-1*H*-benzo[*d*]imidazol-2-yl) amino) propoxy) phenyl) acetonitrile (3.111)



The title compound was prepared in the manner similar to the general procedure (3.G) by utilizing *N*¹-(2-((*tert*-butyl dimethyl silyl) oxy) ethyl)-5-chlorobenzene-1,2-

diamine **3.110** (0.15g, 0.5 mmol) and 2-(4-(2-((*tert*-butyl dimethyl silyl) oxy)-3-isothiocyanatopropoxy) phenyl) acetonitrile **3.36** (0.30g, 0.8 mmol) as starting materials. ^1H NMR (400 MHz, $\text{DMSO-}d_6$) δ 7.26 (dd, $J = 8.7, 3.0$ Hz, 3H, CH_{Ar}), 7.15 (d, $J = 8.2$ Hz, 1H, CH_{Ar}), 6.98 – 6.88 (m, 3H, CH_{Ar}), 6.81 (t, $J = 5.7$ Hz, 1H, NH), 4.11 (q, $J = 5.7$ Hz, 1H, CH_{Al}), 4.03 (dt, $J = 14.2, 4.9$ Hz, 3H, CH_{Al}), 3.95 (d, $J = 9.7$ Hz, 3H, C_{23}H , CH_{Al}), 3.66 (q, $J = 5.2$ Hz, 2H, CH_{Al}), 3.60 – 3.41 (m, 2H, CH_{Al}), 0.86 (d, $J = 1.5$ Hz, 9H, C_{29-31}H), 0.70 (s, 6H, $\text{C}_{26,27}\text{H}$), 0.13 – 0.03 (m, 9H, C_{39-41}H), -0.24 (s, 6H, $\text{C}_{36,37}\text{H}$). ^{13}C NMR (101 MHz, $\text{DMSO-}d_6$) δ 158.4, 156.4, 141.5, 136.6, 129.8, 123.5, 123.4, 120.5, 119.9, 116.0, 115.1, 109.0, 71.6, 70.1, 69.7, 61.8, 48.5, 26.26, 26.23, 21.9, 18.3, 18.2, -4.0, -4.1. Brown oil (0.2g, 42 %). LCMS m/z calc for $\text{C}_{32}\text{H}_{49}\text{ClN}_4\text{O}_3\text{Si}_2^+ [\text{M}+\text{H}]^+$: 628.3, found 628.1 with t_{R} 2.82 min.

(*S*)-2-(4-(2-((*tert*-Butyl dimethyl silyl) oxy)-3-((6-chloro-1-isopropyl-1*H*-benzo[*d*]imidazol-2-yl) amino) propoxy) phenyl) acetonitrile (3.113)



The title compound was prepared in the manner similar to

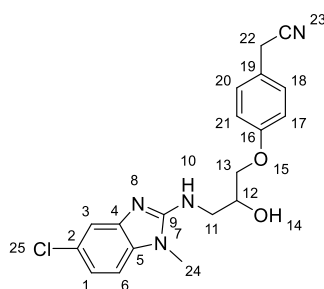
the general procedure (3.G) by utilizing 5-Chloro-*N*¹-isopropylbenzene-1,2-diamine **3.12** (0.13g, 0.7 mmol) and (*S*)-2-(4-(2-((*tert*-Butyl dimethyl silyl) oxy)-3-isothiocyanatopropoxy) phenyl) acetonitrile **3.112** (0.26g, 0.7 mmol) as starting materials. Brown oil (0.1g, 27 %). ^1H NMR (400 MHz, $\text{DMSO-}d_6$) δ 7.38 (d, $J = 2.0$ Hz, 1H, C_6H), 7.26 (d, $J = 8.6$ Hz, 2H, C_2H , CH_{Ar}), 7.17 (d, $J = 8.6$ Hz, 1H, C_3H), 7.01 – 6.89 (m, 3H, CH_{Ar}), 6.83 (t, $J = 5.7$ Hz, 1H, NH), 4.62 (p, $J = 6.9$ Hz, 1H, C_{32}H), 4.41 (qd, $J = 6.5, 2.9$ Hz, 1H, CH_{Al}), 4.09 (dd, $J = 10.3, 2.9$ Hz, 1H, CH_{Al}), 3.96 – 3.88 (m, 3H, CH_{Al}), 3.46 (ddt, $J = 25.9, 12.9, 7.0$ Hz, 2H, CH_{Al}), 1.48 (dd, $J = 7.0, 1.7$ Hz, 6H, $\text{C}_{33,34}\text{H}$), 0.85 (s, 9H, C_{29-31}H) 0.04 (s, 6H, $\text{C}_{26,27}\text{H}$). ^{13}C NMR (101 MHz,

DMSO-*d*₆) δ 158.4, 155.0, 142.4, 134.1, 129.8, 123.5, 122.6, 120.4, 119.9, 116.4, 115.2, 109.7, 71.3, 69.9, 46.4, 45.7, 26.2, 21.9, 20.7, 18.3, -4.1. LCMS *m/z* calc for C₂₇H₃₇ClN₄O₂Si⁺ [M+H]⁺: 512.7, found 512.8 with *t*_R 2.64 min.

General procedure (3.H) for preparation of 3.86-3.100, 3.103, 3.114.

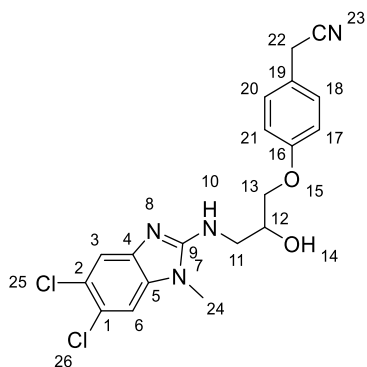
To a solution of (3.72-3.88, 3.111) in MeOH (50 mL) was added 20 % TFA and stirred for 48h at rt. The reaction was neutralized using Et₃N and concentrated to the dryness. The residue was washed by H₂O and the desired compound was extracted using ethyl acetate. The organic layer was concentrated and purified using column chromatography eluting the desired compound with 20:80 Petroleum Ether: Ethyl Acetate for most of the compounds.

2-(4-(3-((5-Chloro-1-methyl-1*H*-benzo[*d*]imidazol-2-yl) amino)-2-hydroxypropoxy) phenyl) acetonitrile (3.86)



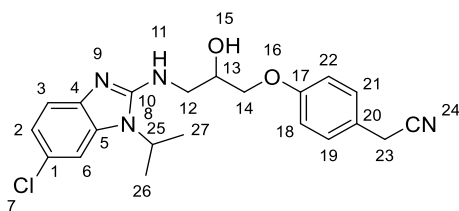
The title compound was prepared in the manner similar to the general procedure (3.H) by utilizing 2-(4-(2-((*tert*-butyl dimethyl silyl) oxy) – 3 - ((5-chloro-1-methyl-1*H*-benzo[*d*]imidazol-2-yl) amino) propoxy) phenyl) acetonitrile **3.72** as a starting material. White solid (0.5, 70 %). ¹H NMR (400 MHz, DMSO-*d*₆) δ 7.71 (d, *J* = 2.0 Hz, 1H, C₃H), 7.33 – 7.23 (m, 4H, CH_{Ar}), 7.07 (dd, *J* = 8.4, 2.0 Hz, 1H, C₁H), 7.01 – 6.93 (m, 2H, CH_{Ar}, NH), 4.13 (m, 1H, CH_{Al}), 4.08 – 3.96 (m, 2H, CH_{Al}), 3.94 (s, 2H, C₂₂H), 3.64 – 3.56 (m, 2H, CH_{Al}), 3.55 (s, 3H, C₂₄H). ¹³C NMR (101 MHz, DMSO-*d*₆) δ 158.5, 155.0, 133.3, 129.7, 128.5, 126.8, 126.0, 123.5, 120.0, 115.4, 113.7, 109.7, 70.6, 68.1, 46.4, 29.2, 21.9. LCMS *m/z* calc for C₁₉H₁₉ClN₄O₂⁺ [M+H]⁺: 371.1, found 371.1 with *t*_R 2.12 min. Purity of the compound was confirmed to be >95 % by LCMS using a long method run.

2-(4-(3-((5, 6-Dichloro-1-methyl-1*H*-benzo[*d*]imidazol-2-yl) amino)-2-hydroxypropoxy) phenyl) acetonitrile (3.87)



The title compound was prepared in the manner similar to the general procedure (3.H) by utilizing 2-(4-(2-((*tert*-butyl dimethyl silyl) oxy) -3 - ((5, 6-dichloro-1-methyl-1*H*-benzo[*d*]imidazol-2-yl) amino) propoxy) phenyl) acetonitrile **3.73** (0.1g, 0.2 mmol) as a starting material. White solid (0.06g, 80 %) ¹H NMR (400 MHz, DMSO-*d*₆) δ 7.47 (s, 1H, CH_{Ar}), 7.36 (s, 1H, CH_{Ar}), 7.26 (d, *J* = 8.7 Hz, 2H, CH_{Ar}), 7.10 (t, *J* = 5.7 Hz, 1H, CH_{Ar}), 6.97 (d, *J* = 8.7 Hz, 2H, CH_{Ar}, NH), 5.44 (d, *J* = 5.5 Hz, 1H, OH), 4.13 (h, *J* = 5.5 Hz, 1H, C₁₂H), 4.02 (dd, *J* = 10.0, 4.3 Hz, 1H, CH_{Al}), 3.95 (d, *J* = 10.2 Hz, 3H, C₂₂H, CH_{Al}), 3.59 – 3.40 (m, 5H, CH_{Al}). ¹³C NMR (101 MHz, DMSO-*d*₆) δ 158.5, 157.4, 142.9, 135.7, 129.7, 123.5, 122.7, 120.4, 120.0, 115.9, 115.4, 109.2, 70.8, 68.1, 46.3, 29.1, 21.9. LCMS *m/z* calc for C₁₉H₁₈Cl₂N₄O₂⁺ [M+H]⁺: 405.0, found 404.7 with *t*_R 2.25min. Purity of the compound was confirmed to be >95 % by LCMS using a long method run.

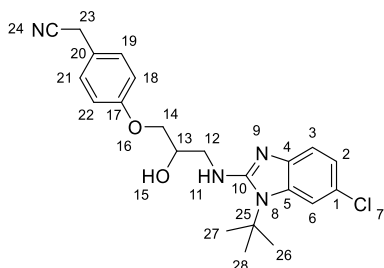
2-(4-(3-((6-Chloro-1-isopropyl-1*H*-benzo[*d*]imidazol-2-yl) amino)-2-hydroxypropoxy) phenyl) acetonitrile (3.20).



The title compound was prepared in the manner similar to the general procedure by utilizing 2-(4-(2-((*tert*-butyl dimethyl silyl) oxy)-3-((6-chloro-1-

isopropyl-1*H*-benzo[*d*]imidazol-2-yl) amino) propoxy) phenyl) acetonitrile **3.74** (0.3g, 0.5 mmol) as a starting material. White solid (0.17g, 77 %). ¹H NMR (400 MHz, DMSO-*d*₆) δ 7.38 (d, *J* = 2.0 Hz, 1H, C₆H), 7.30 – 7.22 (m, 2H, CH_{Ar}), 7.17 (d, *J* = 8.6 Hz, 1H, C₃H), 6.96 (dd, *J* = 8.6, 2.0 Hz, 3H, C₂H, CH_{Ar}), 6.80 (t, *J* = 5.6 Hz, 1H, NH), 5.56 (d, *J* = 4.8 Hz, 1H, OH), 4.63 (hept, *J* = 7.1 Hz, 1H, C₂₅H), 4.13 (q, *J* = 5.6 Hz, 1H, CH_{Al}), 4.01 (dd, *J* = 10.0, 4.4 Hz, 1H, CH_{Al}), 3.94 (d, *J* = 6.8 Hz, 3H, CH_{Al}), 3.60 – 3.40 (m, 2H, CH_{Al}), 1.47 (d, *J* = 7.1 Hz, 6H, C_{26,27}H). ¹³C NMR (101 MHz, DMSO-*d*₆) δ 158.6, 155.5, 142.1, 134.1, 129.7, 123.4, 122.7, 120.4, 120.0, 116.3, 115.4, 109.8, 70.9, 68.3, 46.6, 45.8, 21.9, 20.6. LCMS *m/z* calc for C₂₁H₂₃ClN₄O₂⁺ [M+H]⁺ : 399.2, found 399.1 with *t*_R 2.23 min. Purity of the compound was confirmed to be >95 % by LCMS using a long method run.

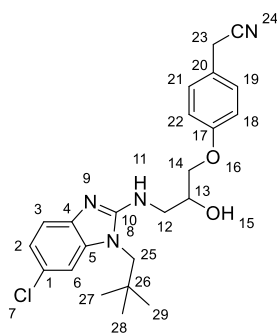
2-(4-(3-((1-(*tert*-Butyl)-6-chloro-1*H*-benzo[*d*]imidazol-2-yl) amino)-2-hydroxypropoxy) phenyl) acetonitrile (3.91**)**



The title compound was prepared in the manner similar to the general procedure by utilizing 2-(4-(3-((1-(*tert*-butyl)-6-chloro-1*H*-benzo[*d*]imidazol-2-yl) amino)-2-((*tert*-butyl dimethyl silyl) oxy) propoxy) phenyl) acetonitrile **3.75** (0.12g, 0.2 mmol) as a starting material. White solid (0.8, 80 %). ¹H NMR (400 MHz, DMSO-*d*₆) δ 7.50 (d, *J* = 1.9 Hz, 1H, CH_{Ar}), 7.28 – 7.23 (m, 2H, CH_{Ar}), 7.18 (d, *J* = 8.4 Hz, 1H, CH_{Ar}), 6.99 – 6.94 (m, 3H, CH_{Ar}), 6.03 (t, *J* = 5.4 Hz, 1H, NH), 5.63 (s, 1H, OH), 4.20 – 4.12 (m, 1H, CH_{Al}), 4.01 (dd, *J* = 10.0, 4.6 Hz, 1H, CH_{Al}), 3.95 (m, 3H, CH_{Al}), 3.66 – 3.43 (m, 2H, CH_{Al}), 1.75 (s, 9H, C₂₆₋₂₈H). ¹³C NMR (101 MHz, DMSO-*d*₆) δ 158.5, 156.2, 141.7, 135.4, 129.8, 123.5, 122.7, 120.5, 120.0, 116.5, 115.4, 112.4, 71.2, 68.1, 58.3, 47.3, 30.0, 21.9. LCMS *m/z* calc for

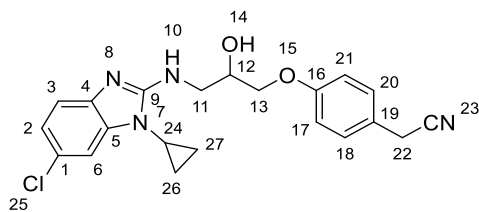
$C_{22}H_{25}ClN_4O_2^+$ $[M+H]^+$: 412.1, found 412.8 with t_R 2.36 min. Purity of the compound was confirmed to be >95 % by LCMS using a long method run.

2-(4-(3-((6-Chloro-1-neopentyl-1*H*-benzo[*d*]imidazol-2-yl) amino)-2-hydroxypropoxy) phenyl) acetonitrile (3.92)



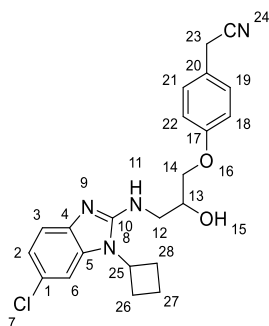
The title compound was prepared in the manner similar to the general procedure by utilizing 2-(4-(2-((*tert*-butyl dimethyl silyl) oxy)-3-((6-chloro-1-neopentyl-1*H*-benzo[*d*]imidazol-2-yl) amino) propoxy) phenyl) acetonitrile **3.76** (0.1g, 0.2 mmol) as a starting material. White solid (0.070g, 90 %). 1H NMR (400 MHz, DMSO- d_6) δ 7.30 (d, J = 2.0 Hz, 1H, C_6H), 7.28 – 7.20 (m, 2H, CH_{Ar}), 7.16 (d, J = 8.3 Hz, 1H, C_3H), 6.94 (dd, J = 8.3, 2.0 Hz, 3H, C_2H , CH_{Ar}), 6.71 (t, J = 5.7 Hz, 1H NH), 5.61 (s, 1H, OH), 4.14 (m, 1H, CH_{Al}), 4.00 (dd, J = 10.0, 4.4 Hz, 1H, CH_{Al}), 3.92 (dd, J = 9.8, 6.1 Hz, 3H, CH_{Al}), 3.84 (s, 2H, $C_{23}H$), 3.51 (m, 2H, CH_{Al}), 0.95 (s, 9H, $C_{27-29}H$). ^{13}C NMR (101 MHz, DMSO- d_6) δ 158.6, 156.8, 141.4, 137.2, 129.7, 123.4, 122.8, 120.5, 120.0, 115.9, 115.3, 109.3, 70.9, 68.4, 52.1, 46.4, 35.3, 28.2, 21.9. LCMS m/z calc for $C_{23}H_{27}ClN_4O_2^+$ $[M+H]^+$: 427.1, found 427.2 with t_R 2.46 min. Purity of the compound was confirmed to be >95 % by LCMS using a long method run.

2-(4-(3-((6-Chloro-1-cyclopropyl-1*H*-benzo[*d*]imidazole-2-yl)amino)-2-hydroxypropoxy) phenyl) acetonitrile (3.90)



The title compound was prepared in the manner similar to the general procedure by utilizing 2-(4-(2-((*tert*-butyl dimethyl silyl) oxy)-3-((6-chloro-1-cyclopropyl-1*H*-benzo[*d*]imidazol-2-yl) amino) propoxy) phenyl) acetonitrile **3.77** (0.08g, 0.2mmol) as a starting material. White solid (0.05g, 80 %). ¹H NMR (400 MHz, DMSO-*d*₆) δ 7.29 – 7.23 (m, 2H, CH_{Ar}), 7.22 – 7.11 (m, 2H, CH_{Ar}), 7.00 – 6.94 (m, 3H, CH_{Ar}), 6.57 (t, *J* = 5.7 Hz, 1H, NH), 5.55 (d, *J* = 4.9 Hz, 1H, OH), 4.15 (q, *J* = 5.2, 4.7 Hz, 1H, CH_{Al}), 4.07 – 4.00 (m, 1H, CH_{Al}), 4.00 – 3.90 (m, 3H, C₂₂H, CH_{Al}), 3.63 – 3.42 (m, 2H, CH_{Al}), 3.00 (tt, *J* = 7.0, 3.7 Hz, 1H, C₂₄H), 1.21 – 1.10 (m, 2H, C₂₆ or ₂₇H), 0.97 – 0.80 (m, 2H, C₂₆ or ₂₇H). ¹³C NMR (101 MHz, DMSO-*d*₆) δ 158.5, 156.9, 141.4, 136.5, 129.7, 123.5, 123.0, 120.8, 120.0, 116.3, 115.4, 108.5, 71.0, 68.2, 46.4, 22.9, 21.9, 7.0. LCMS *m/z* calc for C₂₁H₂₁ClN₄O₂⁺ [M+H]⁺ : 397.1, found 386.8 with 2.21 *t*_R min. Purity of the compound was confirmed to be >95 % by LCMS using a long method run.

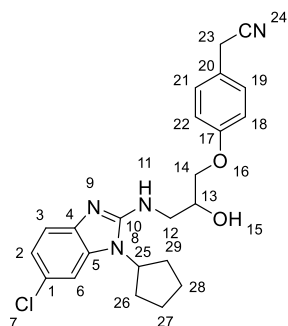
2-(4-(3-((6-Chloro-1-cyclobutyl-1*H*-benzo[*d*]imidazol-2-yl) amino)-2-hydroxypropoxy) phenyl) acetonitrile (3.91)



The title compound was prepared in the manner similar to the general procedure by utilizing 2-(4-(2-((*tert*-butyl dimethyl silyl) oxy)-3-((6-chloro-1-cyclobutyl-1*H*-benzo[*d*]imidazol-2-yl) amino) propoxy) phenyl) acetonitrile **3.78** (0.1g, 0.2 mmol) as a starting material. White solid (0.08, 76 %). ¹H NMR (400 MHz, DMSO-*d*₆) δ 7.46 (d, *J* = 2.1

Hz, 1H, C₆H), 7.30 – 7.13 (m, 3H, CH_{Ar}), 7.03 – 6.91 (m, 3H, CH_{Ar}), 6.70 (t, *J* = 5.6 Hz, 1H NH), 5.52 (d, *J* = 4.9 Hz, 1H OH), 4.88 (m, 1H, C₂₅H), 4.13 (m, 1H, CH_{Al}), 4.01 (dd, *J* = 10.0, 4.4 Hz, 1H, CH_{Al}), 3.97 – 3.90 (m, 3H, CH_{Al}), 3.54 (dt, *J* = 13.4, 5.6 Hz, 1H, CH_{Al}), 3.43 (ddd, *J* = 13.4, 6.8, 5.2 Hz, 1H, CH_{Al}), 2.79 – 2.66 (m, 2H, C₂₆ or 28H), 2.38 (m, 2H, C₂₆ or 28H), 1.94 (m, 1H, C₂₇H), 1.76 (qt, *J* = 10.5, 8.2 Hz, 1H, C₂₇H). ¹³C NMR (101 MHz, DMSO-*d*₆) δ 158.6, 155.7, 142.0, 134.8, 129.7, 123.5, 122.9, 120.7, 120.0, 116.5, 115.4, 109.6, 70.9, 68.2, 47.8, 46.6, 28.3, 21.9, 14.9. LCMS *m/z* calc for C₂₂H₂₃ClN₄O₂⁺ [M+H]⁺: 411.1, found 410.8 with *t*_R 2.39 min. Purity of the compound was confirmed to be >95 % by LCMS using a long method run.

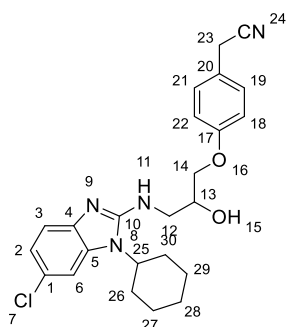
2-(4-(3-((6-Chloro-1-cyclopentyl-1*H*-benzo[*d*]imidazol-2-yl) amino)-2-hydroxypropoxy) phenyl) acetonitrile (3.92)



The title compound was prepared in the manner similar to the general procedure by utilizing 2-(4-(2-((*tert*-butyl dimethyl silyl) oxy)-3-((6-chloro-1-cyclopentyl-1*H*-benzo[*d*]imidazol-2-yl) amino) propoxy) phenyl) acetonitrile **3.79** (0.1 g, 0.2mmol) as a starting material. White solid (0.054g, 54 %). ¹H NMR (400 MHz, DMSO-*d*₆) δ 7.29 – 7.24 (m, 2H, CH_{Ar}), 7.21 – 7.17 (m, 2H, CH_{Ar}), 6.99 – 6.93 (m, 3H, CH_{Ar}), 6.84 (t, *J* = 5.6 Hz, 1H, NH), 5.53 (d, *J* = 5.1 Hz, 1H, OH), 4.76 (p, *J* = 8.6 Hz, 1H, C₂₅H), 4.12 (dd, *J* = 8.2, 3.5 Hz, 1H, CH_{Al}), 4.08 – 3.98 (m, 1H, CH_{Al}), 3.95 (d, *J* = 9.5 Hz, 3H, C₂₃H, CH_{Al}), 3.58 – 3.38 (m, 2H, CH_{Al}), [2.06 – 1.88 (m, 6H), 1.68 (s, 2H), C₂₆₋₂₉H]. ¹³C NMR (101 MHz, DMSO-*d*₆) δ 158.6, 156.1, 142.2, 133.7, 129.7, 123.5, 122.7, 120.6, 120.0, 116.6, 115.3, 109.4, 70.9, 68.3, 54.5, 46.6, 28.9, 24.7, 21.9. LCMS *m/z* calc for C₂₃H₂₅ClN₄O₂⁺ [M+H]⁺: 425.1, found 424.6 with *t*_R

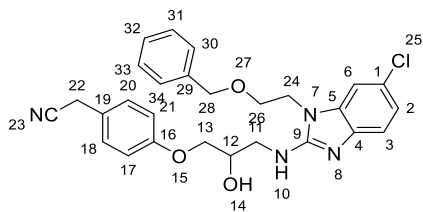
2.33 min. Purity of the compound was confirmed to be >95 % by LCMS using a long method run.

2-(4-(3-((6-Chloro-1-cyclohexyl-1*H*-benzo[*d*]imidazol-2-yl) amino)-2-hydroxypropoxy) phenyl) acetonitrile (3.93)



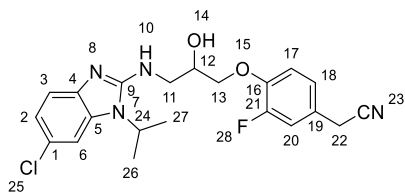
The title compound was prepared in the manner similar to the general procedure by utilizing 2-(4-(2-((*tert*-Butyl dimethyl silyl) oxy)-3-((6-chloro-1-cyclohexyl-1*H*-benzo[*d*] imidazol-2-yl) amino) propoxy) phenyl) acetonitrile **3.80** (0.09g, 0.2 mmol) as a starting material. White solid (0.05g, 75 %). ¹H NMR (400 MHz, DMSO-*d*₆) δ 7.41 (d, *J* = 2.0 Hz, 1H, C₆H), 7.32 (d, *J* = 5.0 Hz, 1H, CH_{Ar}), 7.28 – 7.22 (m, 1H, CH_{Ar}), 7.17 (d, *J* = 8.3 Hz, 1H, C₃H), 6.96 (dd, *J* = 8.6, 2.0 Hz, 3H, C₂H, CH_{Ar}), 6.88 (t, *J* = 5.8 Hz, 1H, NH), 5.60 (s, 1H OH), 4.49 (d, *J* = 5.6 Hz, 1H, C₂₅H), 4.27 – 4.10 (m, 2H, CH_{Al}), 4.01 (dd, *J* = 10.1, 4.4 Hz, 1H, CH_{Al}), 3.94 (d, *J* = 13.7 Hz, 3H, C₂₃H, CH_{Al}), 3.56 (dd, *J* = 9.5, 4.1 Hz, 1H, CH_{Al}), [2.16 – 2.00 (m, 2H, CH_{Al}), 1.84 (d, *J* = 10.9 Hz, 2H, CH_{Al}), 1.69 (dd, *J* = 27.8, 9.9 Hz, 3H, CH_{Al}), 1.51 – 1.34 (m, 3H, CH_{Al})] C₂₆₋₃₀H. ¹³C NMR (101 MHz, DMSO-*d*₆) δ 158.5, 155.5, 141.8, 134.3, 129.7, 123.4, 122.8, 120.5, 120.0, 116.3, 115.4, 110.1, 70.9, 68.3, 63.3, 53.7, 46.6, 30.3, 25.9, 21.9. LCMS *m/z* calc for C₂₄H₂₇ClN₄O₂⁺ [M+H]⁺: 439.1, found 439.7 with *t*_R 2.40 min. Purity of the compound was confirmed to be >95 % by LCMS using a long method run.

2-(4-(3-((1-(2-(Benzyloxy)ethyl)-6-chloro-1*H*-benzo[*d*]imidazol-2-yl)amino)-2-hydroxypropoxy) phenyl) acetonitrile (3.94)



The title compound was prepared in the manner similar to the general procedure by utilizing 2-(4-(3-((1-(2-(benzyloxy) ethyl)-6-chloro-1H-benzo[d]imidazol-2-yl) amino)-2-((*tert*-butyl dimethyl silyl) oxy) propoxy) phenyl) acetonitrile **3.81** (0.3g, 0.5mmol) as a starting material. White solid (0.13g, 65 %). ¹H NMR (400 MHz, DMSO-*d*₆) δ 7.32 (d, *J* = 2.0 Hz, 1H, C₆H), 7.26 (ddt, *J* = 11.2, 6.8, 2.5 Hz, 5H, CH_{Ar}), 7.20 – 7.14 (m, 3H, CH_{Ar}), 6.95 (td, *J* = 8.1, 7.4, 2.1 Hz, 3H, CH_{Ar}), 6.87 (t, *J* = 5.7 Hz, 1H, NH), 5.56 (s, 1H, OH), 4.45 (s, 2H, C₂₈H), 4.24 (t, *J* = 5.2 Hz, 2H, C₂₄ or ₂₆H), 4.11 (p, *J* = 5.8 Hz, 1H, CH_{Al}), 3.99 (dd, *J* = 9.9, 4.4 Hz, 1H, CH_{Al}), 3.95 (s, 2H, C₂₂H), 3.92 – 3.89 (m, 1H, CH_{Al}), 3.68 (t, *J* = 5.1 Hz, 2H, CH_{Al}), 3.61 – 3.39 (m, 2H, CH_{Al}). ¹³C NMR (101 MHz, DMSO-*d*₆) δ 158.5, 156.2, 141.5, 138.5, 136.4, 129.7, 128.6, 127.8, 127.5, 123.4, 123.0, 120.6, 120.0, 116.0, 115.4, 108.7, 72.4, 70.8, 68.5, 68.3, 46.3, 42.2, 21.9. LCMS *m/z* calc for C₂₇H₂₇ClN₄O₃⁺ [M+H]⁺: 491.1, found 490.6 with *t*_R 2.37 min. Purity of the compound was confirmed to be >95 % by LCMS using a long method run.

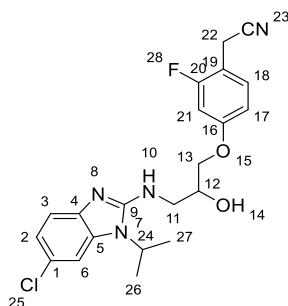
2-(4-(3-((6-Chloro-1-isopropyl-1H-benzo[d]imidazol-2-yl) amino)-2-hydroxypropoxy) -3-fluorophenyl) acetonitrile (3.95)



The title compound was prepared in the manner similar to the general procedure by utilizing 2-(4-(2-((*tert*-Butyl dimethyl silyl) oxy)-3-((6-chloro-1-isopropyl-1H-benzo[d]imidazol-2-yl) amino) propoxy)-3-fluorophenyl) acetonitrile **3.82** (0.13g, 0.2 mmol) as a starting material. White solid (0.08g, 77 %). ¹H NMR (400 MHz, DMSO-*d*₆) δ 7.38 (d, *J* = 2.0 Hz, 1H, C₆H), 7.25 – 7.15 (m, 3H, CH_{Ar}), 7.11 (dd, *J* = 8.4, 2.0

Hz, 1H, C₂H), 6.96 (d, *J* = 8.4 Hz, 1H, C₃H), 6.82 (t, *J* = 5.6 Hz, 1H, NH), 5.62 (d, *J* = 4.4 Hz, 1H, OH), 4.63 (hept, *J* = 6.9 Hz, 1H, C₂₄H), 4.13 – 3.99 (m, 3H, CH_{Al}), 3.99 (s, 2H, C₂₂H), 3.60 – 3.41 (m, 2H, CH_{Al}), 1.47 (d, *J* = 6.8 Hz, 6H, C_{26,27}H).¹³C NMR (101 MHz, DMSO-*d*₆) δ 155.5, 151.9 (d, *J* = 244.5 Hz), 146.5 (d, *J* = 11.2 Hz), 142.0, 134.1, 124.9 (d, *J* = 3.9 Hz), 124.4 (d, *J* = 6.5 Hz), 122.8, 120.4, 119.6, 116.4 (d, *J* = 5.8 Hz), 115.8 (d, *J* = 1.8 Hz), 109.8, 71.9, 68.3, 46.5, 45.8, 21.8, 20.6. LCMS *m/z* calc for C₂₁H₂₃ClFN₄O₂⁺ [M+H]⁺: 417.15, found 416.7 with *t*_R 2.24 min. Purity of the compound was confirmed to be >95 % by LCMS using a long method run.

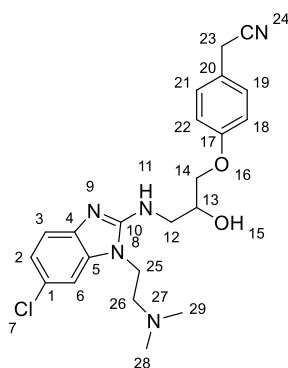
2-(4-(3-((6-Chloro-1-isopropyl-1*H*-benzo[*d*]imidazol-2-yl) amino) -2-hydroxypropoxy) -2-fluorophenyl) acetonitrile (3.96)



The title compound was prepared in the manner similar to the general procedure by utilizing 2-(4-(2-((*tert*-butyl dimethyl silyl) oxy)-3-((6-chloro-1-*isopropyl*-1*H*-benzo[*d*]imidazol-2-yl) amino) propoxy) -2-fluorophenyl) acetonitrile **3.83** (0.16g, 0.2 mmol) as a starting material. White solid (0.10g, 79 %). ¹H NMR (400 MHz, DMSO-*d*₆) δ 7.38 (d, *J* = 2.0 Hz, 1H, C₆H), 7.35 (t, *J* = 8.8 Hz, 1H, C₁₈H), 7.17 (d, *J* = 8.8 Hz, 1H, C₂H), 6.99 – 6.88 (m, 2H, C_{3,21}H), 6.87 – 6.81 (m, 1H, C₁₇H), 6.79 (d, *J* = 5.6 Hz, 1H, NH), 5.57 (s, 1H, OH), 4.63 (m, 1H, C₂₄H), 4.14 (t, *J* = 5.7 Hz, 1H, CH_{Al}), 4.05 (dd, *J* = 10.1, 4.2 Hz, 1H, CH_{Al}), 4.02 (m, 1H, CH_{Al}) 3.90 (s, 2H, C₂₂H), 3.59 – 3.39 (m, 2H, CH_{Al}), 1.47 (d, *J* = 6.9 Hz, 6H, C_{26,27}H).¹³C NMR (101 MHz, DMSO-*d*₆) δ 160.9 (d, *J* = 244.8 Hz), 160.4 (d, *J* = 10.9 Hz), 155.4, 142.0, 134.1, 131.3 (d, *J* = 5.3 Hz), 122.8, 120.4, 118.8, 116.3, 111.7 (d, *J* = 3.1 Hz), 110.4 (d, *J* = 16.2 Hz), 109.8, 102.8 (d, *J* = 24.9 Hz), 71.4, 68.1, 46.5, 45.8, 20.6, 16.6. LCMS

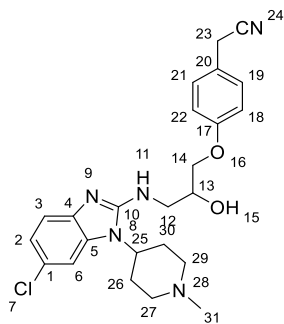
m/z calc for $C_{21}H_{22}ClFN_4O_2^+$ $[M+H]^+$: 417.15, found 416.6 with t_R 2.26 min. Purity of the compound was confirmed to be >95 % by LCMS using a long method run.

2-(4-(3-((6-Chloro-1-(2-(dimethylamino) ethyl)-1*H*-benzo[*d*]imidazol-2-yl) amino)-2-hydroxypropoxy) phenyl) acetonitrile (3.97)



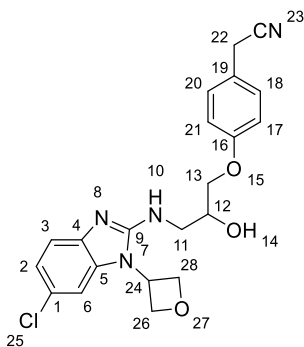
The title compound was prepared in the manner similar to the general procedure by utilizing 2-(4-(2-((*tert*-Butyl dimethyl silyl) oxy)-3-((6-chloro-1-(2-(dimethyl amino) ethyl)-1*H*-benzo[*d*]imidazol-2-yl) amino) propoxy) phenyl) acetonitrile **3.85** (0.13g, 0.2mmol) as a starting material. White solid (0.08 g, 80 %). 1H NMR (400 MHz, DMSO- d_6) δ 7.26 (d, $J = 8.5$ Hz, 2H, CH_{Ar}), 7.14 (ddd, $J = 8.5, 7.3, 1.5$ Hz, 1H, CH_{Ar}), 6.98 (ddd, $J = 13.9, 7.8, 1.5$ Hz, 1H, CH_{Ar}), 6.91 – 6.84 (m, 3H, CH_{Ar}), 6.64 (dtd, $J = 9.1, 7.6, 1.5$ Hz, 1H, CH_{Al}), 5.18 (t, $J = 4.4$ Hz, 1H, CH_{Al}), 4.63 – 4.49 (m, 1H, CH_{Al}), 3.94 (s, 2H $C_{23}H$), 3.89 – 3.72 (m, 2H, CH_{Al}), 3.67 (dq, $J = 13.1, 5.3$ Hz, 1H, CH_{Al}), 3.60 – 3.44 (m, 1H, CH_{Al}), 3.27 – 3.03 (m, 2H, CH_{Al}), 2.76 (s, 6H, $C_{28,29}H$). ^{13}C NMR (101 MHz, DMSO- d_6) δ 158.4, 156.8, 141.1, 136.2, 129.7, 123.5, 122.0, 119.9, 118.6, 117.2, 115.4, 108.3, 70.9, 67.2, 60.2, 50.7, 48.9, 43.6, 21.9. LCMS m/z calc for $C_{22}H_{26}ClN_5O_2^+$ $[M+H]^+$: 428.1, found 427.9 with t_R 2.05 min. Purity of the compound was confirmed to be >95 % by LCMS using a long method run.

2-(4-(3-((6-Chloro-1-(1-methylpiperidin-4-yl) -1*H*-benzo[*d*]imidazol-2-yl) amino)-2-hydroxypropoxy) phenyl) acetonitrile (3.98)



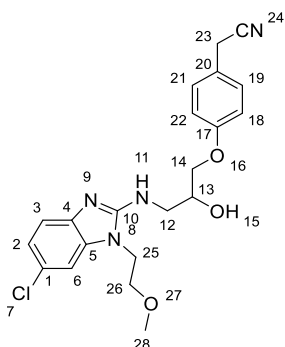
The title compound was prepared in the manner similar to the general procedure by utilizing 2-(4-(2-((*tert*-Butyl dimethyl silyl) oxy)-3-((6-chloro-1-(1-methyl piperidin-4-yl)-1*H*-benzo[*d*]imidazol-2-yl) amino) propoxy) phenyl) acetonitrile **3.86** (0.2g, 0.3mmol) as a starting material. White solid (0.08 g, 80 %). ¹H NMR (400 MHz, DMSO-*d*₆) δ 7.26 (d, *J* = 8.6 Hz, 2H, CH_{Ar}), 7.12 – 7.06 (m, 1H, CH_{Ar}), 7.02 (d, *J* = 7.7 Hz, 1H, CH_{Ar}), 6.94 – 6.90 (m, 2H, CH_{Ar}), 6.72 (d, *J* = 8.1 Hz, 1H, CH_{Ar}), 6.59 (td, *J* = 7.5, 1.3 Hz, 1H, NH), 5.27 (s, 1H, OH), 4.35 (d, *J* = 7.9 Hz, 1H, CH_{Al}), 4.07 – 3.98 (m, 2H, CH_{Al}), 3.93 (d, *J* = 9.5 Hz, 3H, C₂₃H, CH_{Al}), 3.90 – 3.81 (m, 1H, CH_{Al}), 3.71 (s, 1H, CH_{Al}), 3.53 (dt, *J* = 12.7, 5.7 Hz, 1H, CH_{Al}), 2.67 (d, *J* = 11.5 Hz, 2H, CH_{Al}), 2.16 (s, 3H, C₃₁H), 1.85 (d, *J* = 12.5 Hz, 2H, CH_{Al}), 1.37 (q, *J* = 10.1 Hz, 2H, CH). ¹³C NMR (101 MHz, DMSO-*d*₆) δ 158.4, 155.2, 143.7, 134.7, 129.8, 123.3, 122.8, 120.0, 119.6, 116.4, 115.4, 112.5, 71.0, 67.8, 54.3, 48.9, 47.9, 46.3, 31.1, 21.9. LCMS *m/z* calc for C₂₄H₂₈ClN₅O₂⁺ [M+H]⁺: 454.2, found 454.2 with *t*_R 2.08 min. Purity of the compound was confirmed to be >95 % by LCMS using a long method run.

2-(4-(3-((6-Chloro-1-(oxetan-3-yl)-1*H*-benzo[*d*]imidazol-2-yl)amino)-2-hydroxypropoxy) phenyl) acetonitrile (3.99)



The title compound was prepared in the manner similar to the general procedure by utilizing 2-(4-(2-((*tert*-butyl dimethyl silyl) oxy)-3-((6-chloro-1-(oxetan-3-yl)-1*H*-benzo[*d*]imidazol-2-yl) amino) propoxy) phenyl) acetonitrile **3.87** (0.2g, 0.4 mmol) as a starting material. White solid (0.08 g, 80 %). ¹H NMR (400 MHz, DMSO-*d*₆) δ 7.67 (d, *J* = 2.0 Hz, 1H, C₆H), 7.26 (dd, *J* = 8.6, 2.0 Hz, 3H, C₂H, CH_{Ar}), 7.06 (d, *J* = 8.6 Hz, 1H, C₃H), 6.97 (m, 2H, CH_{Ar}), 6.86 (t, *J* = 5.4 Hz, 1H, NH), 5.61 (tt, *J* = 7.6, 5.4 Hz, 1H, OH), 5.46 (s, 1H, CH_{Al}), 5.11 – 4.90 (m, 4H, CH_{Al}), 4.12 (t, *J* = 5.7 Hz, 1H, CH_{Al}), 4.01 (dd, *J* = 10.0, 4.6 Hz, 1H, CH_{Al}), 3.98 – 3.90 (m, 3H, C₂₂H, CH_{Al}), 3.59 – 3.35 (m, 2H, CH_{Al}). ¹³C NMR (101 MHz, DMSO-*d*₆) δ 158.5, 155.7, 142.2, 133.8, 129.7, 123.5, 123.4, 121.3, 120.0, 116.9, 115.4, 109.2, 75.1, 70.8, 68.0, 48.5, 46.6, 21.9. LCMS *m/z* calc for C₂₁H₂₁ClN₄O₃⁺ [M+H]⁺: 413.1, found 412.5 with *t*_R 2.17 min. Purity of the compound was confirmed to be >95 % by LCMS using a long method run.

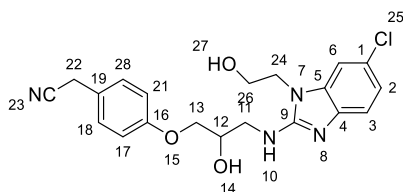
2-(4-(3-((6-Chloro-1-(2-methoxyethyl)-1*H*-benzo[*d*]imidazol-2-yl)amino)-2-hydroxypropoxy) phenyl) acetonitrile (3.100)



The title compound was prepared in the manner similar to the general procedure by utilizing 2-(4-(2-((*tert*-butyl dimethyl silyl) oxy)-3-((6-chloro-1-(2-

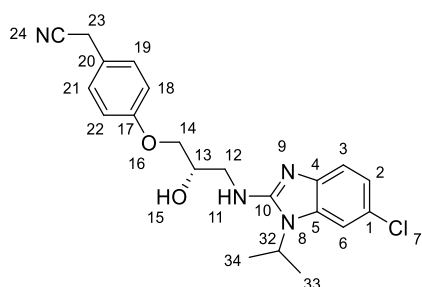
methoxyethyl)-1*H*-benzo[*d*]imidazol-2-yl) amino) propoxy) phenyl) acetonitrile **3.88** (0.08g, 0.1 mmol) as a starting material. (0.05, 85 %). ¹H NMR (400 MHz, DMSO-*d*₆) δ 7.29 (d, *J* = 2.1 Hz, 1H, *CH*_{Ar}), 7.27 (d, *J* = 1.9 Hz, 1H, *CH*_{Ar}), 7.25 (s, 1H, *CH*_{Ar}), 7.16 (d, *J* = 8.3 Hz, 1H, *CH*_{Ar}), 7.00 – 6.93 (m, 3H, *CH*_{Ar}), 6.81 (t, *J* = 5.7 Hz, 1H, *NH*), 5.50 (d, *J* = 22.6 Hz, 1H, *OH*), 4.20 – 4.07 (m, 3H, *CH*_{Al}), 3.95 (d, *J* = 8.9 Hz, 3H, *CH*_{Al}), 3.68 – 3.39 (m, 5H, *CH*_{Al}), 3.20 (s, 3H, *C*₂₈*H*). ¹³C NMR (101 MHz, DMSO-*d*₆) δ 158.6, 156.2, 141.5, 136.4, 129.7, 123.5, 123.0, 120.6, 120.0, 116.1, 115.4, 108.4, 70.8, 68.2, 58.8, 46.3, 42.1, 23.7, 21.9. LCMS *m/z* calc for C₂₁H₂₃ClN₄O₃⁺ [*M*+*H*]⁺ : 415.1, found 414.8 with *t*_R 2.21 min. Purity of the compound was confirmed to be >95 % by LCMS using a long method run.

2-(4-(3-((6-Chloro-1-(2-hydroxyethyl)-1*H*-benzo[*d*]imidazol-2-yl)amino)-2-hydroxypropoxy) phenyl) acetonitrile (3.103)



The title compound was prepared in the manner similar to the general procedure by utilizing 2-(4-(2-((*tert*-butyl dimethyl silyl) oxy)-3-((1-(2-((*tert*-butyl dimethyl silyl) oxy) ethyl)-6-chloro-1*H*-benzo[*d*]imidazol-2-yl) amino) propoxy) phenyl) acetonitrile **3.111** (0.2g, 0.3mmol) as a starting material. (0.09g, 72 %). ¹H NMR (400 MHz, DMSO-*d*₆) δ 7.31 – 7.22 (m, 3H, *CH*_{Ar}), 7.17 (d, *J* = 8.3 Hz, 1H, *CH*_{Ar}), 7.00 – 6.93 (m, 3H, *CH*_{Ar}), 6.81 (t, *J* = 5.6 Hz, 1H, *NH*), 5.55 (s, 1H, *O*₁₄*H*), 5.01 (t, *J* = 5.1 Hz, 1H, *O*₂₇*H*), 4.11 (q, *J* = 5.6 Hz, 1H, *CH*_{Al}), 4.03 (dt, *J* = 14.2, 4.9 Hz, 3H, *CH*_{Al}), 3.95 (d, *J* = 9.7 Hz, 3H, *C*₂₂*H*, *CH*_{Al}), 3.66 (q, *J* = 5.1 Hz, 2H, *C*₂₆*H*), 3.59 – 3.41 (m, 2H, *C*₂₄*H*). ¹³C NMR (101 MHz, DMSO-*d*₆) δ 158.5, 156.4, 141.5, 136.6, 129.7, 123.4, 123.0, 120.4, 120.0, 116.0, 115.4, 108.52, 70.8, 68.3, 60.1, 46.3, 44.8, 21.9. LCMS *m/z* calc for C₂₀H₂₁ClN₄O₃⁺ [*M*+*H*]⁺ : 401.1, found 401.8 with *t*_R 2.08 min. Purity of the compound was confirmed to be >95 % by LCMS using a long method run.

(S)-2-(4-(3-(((6-Chloro-1-isopropyl-1H-benzo[d]imidazol-2-yl)amino)-2-hydroxypropoxy) phenyl) acetonitrile (3.114)



The title compound was prepared in the manner similar to the general procedure by utilizing (S)-2-(4-(2-((*tert*-butyl dimethyl silyl) oxy)-3-(((6-chloro-1-isopropyl-1H-benzo[d]imidazol-2-yl) amino) propoxy) phenyl) acetonitrile **3.113** (0.1g, 0.2mmol) as a starting material. (0.05g, 71 %). ¹H NMR (400 MHz, DMSO-*d*₆) δ 7.38 (d, *J* = 2.4 Hz, 1H, C₆H), 7.30 – 7.22 (m, 2H, CH_{Ar}), 7.17 (d, *J* = 8.6 Hz, 1H, C₃H), 6.96 (dd, *J* = 8.6, 2.4 Hz, 3H, C₂H), 6.80 (t, *J* = 5.6 Hz, 1H, NH), 5.56 (d, *J* = 4.8 Hz, 1H, OH), 4.63 (hept, *J* = 6.8 Hz, 1H, C₃₂H), 4.13 (q, *J* = 5.6 Hz, 1H, C₁₄H), 4.01 (dd, *J* = 10.0, 4.4 Hz, 1H, CH_{Al}), 3.94 (d, *J* = 6.9 Hz, 3H, C₂₃H, CH_{Al}), 3.60 – 3.40 (m, 2H, CH_{Al}), 1.47 (d, *J* = 7.1 Hz, 6H, C_{33,34}H). ¹³C NMR (101 MHz, DMSO-*d*₆) δ 158.6, 155.5, 142.1, 134.1, 129.7, 123.4, 122.7, 120.4, 120.0, 116.3, 115.4, 109.8, 70.9, 68.3, 46.6, 45.8, 21.9, 20.6. LCMS *m/z* calc for C₂₁H₂₃ClN₄O₂⁺ [M+H]⁺ : 399.4, found 399.1 with *t*_R 2.23 min. Purity of the compound was confirmed to be >95 % by LCMS using a long method run.

Preparation of (R)-2-(4-(3-(((6-chloro-1-isopropyl-1H-benzo[d]imidazol-2-yl) amino)-2-hydroxypropoxy) phenyl) acetonitrile (3.115) and testing the purity of both enantiomers.

The analytical chiral high performance liquid chromatography (HPLC) technique was performed on Dionex ICS-3000 with an 581Ultimate-3000 detector equipped with Lux 5 μm Cellulose-4, LC column 250 × 4.6 mm column. This technique was used to separate the racemic compound 2-(4-(3-(((6-chloro-1-isopropyl-1H-benzo[d]imidazol-2-yl) amino)-2-hydroxypropoxy) phenyl) acetonitrile **3.20** into enantiomerically pure isomers: **3.114** (S

isomer) and **3.115** (*R* isomer). **3.20** was separated using ethanol in hexane solvent system and the result showed that the mixture contains 54.5% of *S* isomer and 44.3% of the *R* isomer (Figure 6-1).

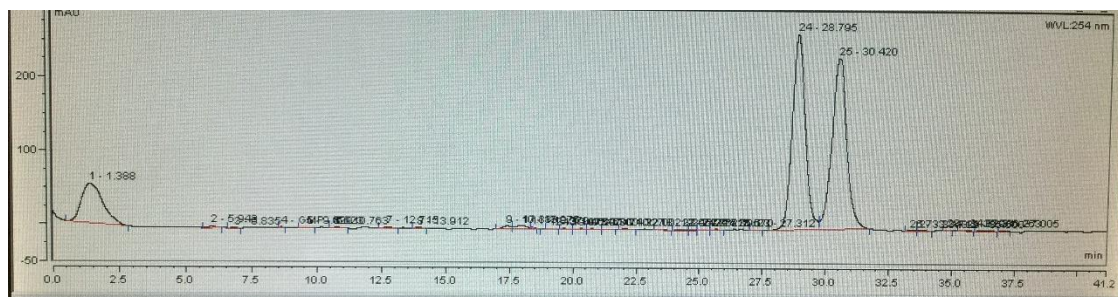


Figure 6-1: Chiral HPLC trace of **3.20**. The method used was (10/90 %, ethanol/hexane) over 40 min at 2 mL/min. Eluent detection was monitored by UV absorbance at 254 nm.

Further analysis was employed by mixing 1:1 of **3.20** and the synthesised (*S*) enantiomer **3.114** which showed in (Figure 6-2). This analysis showed that the (*S*) enantiomer **3.114** has a lower affinity for the stationary phase, and therefore was eluted from the column first, followed by the (*R*) enantiomer **3.115**.

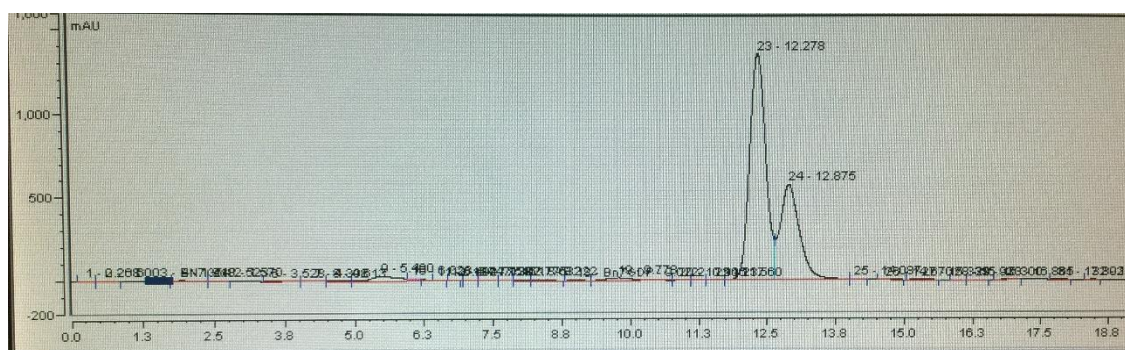


Figure 6-2: Chiral HPLC trace of 1:1 mixture of **3.20** and **3.114**. The method used was (15/85 %, ethanol/hexane) over 20 min at 2 mL/min. Eluent detection was monitored by UV absorbance at 254 nm.

In addition, the purity of synthesised *S* isomer was analysed using the same solvent system. According to this analysis, the purity of **3.114** was 95.6 ee% as shown in Figure 6-3.

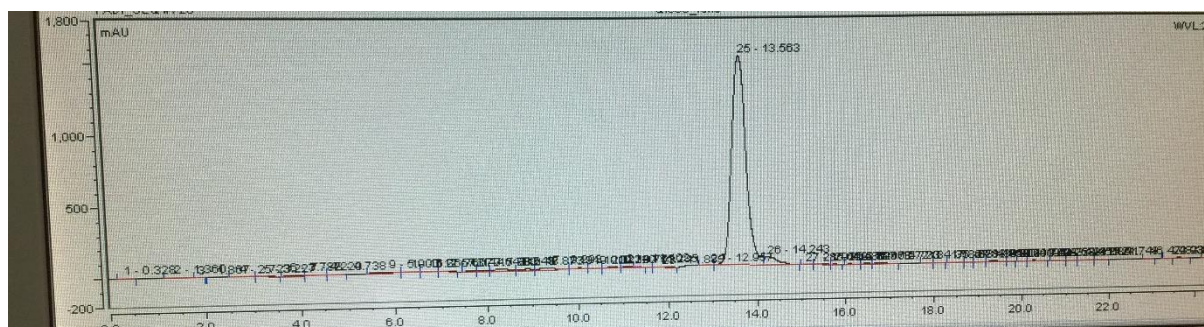


Figure 6-3: Chiral HPLC trace of synthesised **3.114**. The method used was (15/85 %, ethanol/hexane) over 25 min at 2 mL/min. Eluent detection was monitored by UV absorbance at 254 nm.

Further investigation after the separation to analyse the purity of each enantiomer as demonstrated below showed that the purity of **3.114** was 96.9 ee% while the purity of **3.115** was 96.1 ee%.

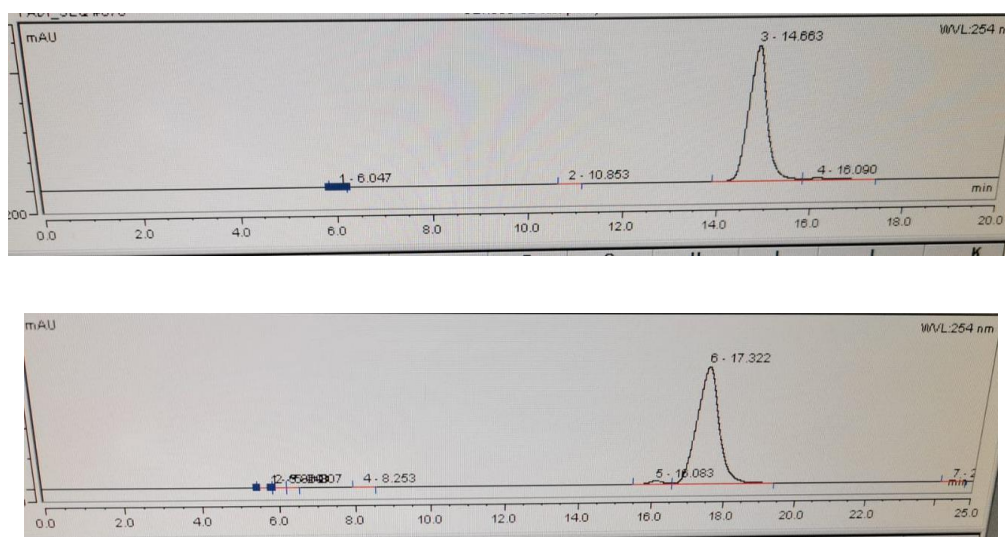
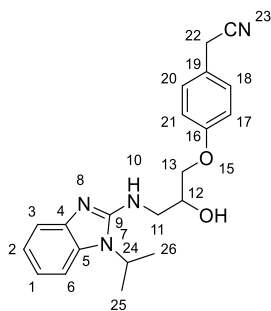


Figure 6-4: Chiral HPLC trace of separated isomers (**3.114** above and **3.115** below). The method used was (15/85 %, ethanol/hexane) over 20 or 25 min, respectively at 2 mL/min. Eluent detection was monitored by UV absorbance at 254 nm.

Preparation of 2-(4-(2-Hydroxy-3-((1-isopropyl-1*H*-benzo [*d*]imidazol -2- yl) amino) propoxy) phenyl) acetonitrile (3.101)



A solution of 2-(4-(3-((6-chloro-1-isopropyl-1*H*-benzo[*d*]imidazol-2-yl) amino)-2-hydroxypropoxy) phenyl) acetonitrile **3.20** (0.1g, 0.3 mmol) in MeOH, and 10% Pd on activated carbon (20% w/w) was stirred under balloon of H₂ at rt for 16 h. The mixture was filtered and purified eluting the desired compound with 20:80 Petroleum Ether: Ethyl Acetate. White solid (0.09 g, 95 %). ¹H NMR (400 MHz, DMSO-*d*₆) δ 7.34 (d, *J* = 7.7 Hz, 1H, CH_{Ar}), 7.29 – 7.23 (m, 2H, CH_{Ar}), 7.20 (d, *J* = 7.7 Hz, 1H, CH_{Ar}), 7.00 – 6.92 (m, 3H, CH_{Ar}), 6.88 (t, *J* = 7.7, 1.3 Hz, 1H, CH_{Ar}), 6.70 (t, *J* = 5.6 Hz, 1H, NH), 5.78 (d, *J* = 5.6 Hz, 1H, OH), 4.63 (p, *J* = 6.8 Hz, 1H, C₂₄H), 4.12 (d, *J* = 6.3 Hz, 1H, CH_{Al}), 4.01 (dd, *J* = 9.9, 4.5 Hz, 1H, CH_{Al}), 3.95 – 3.90 (m, 3H, C₂₂H, CH_{Al}), 3.59 – 3.39 (m, 2H, CH_{Al}), 1.49 (d, *J* = 6.8 Hz, 6H, C₂₅ or C₂₆H). ¹³C NMR (101 MHz, DMSO-*d*₆) δ 158.6, 154.7, 142.9, 133.2, 129.7, 123.4, 120.5, 120.0, 118.8, 115.6, 115.4, 110.1, 70.9, 68.7, 46.7, 45.6, 21.9, 20.8. LCMS *m/z* calc for C₂₁H₂₅N₄O₂⁺ [M+H]⁺ : 365.2, found 364.6 with 2.05 *t*_R min. Purity of the compound was confirmed to be >95 % by LCMS using a long method run.

6.2 Biological evaluation

Bacterial Strains. The *P. aeruginosa* strains and plasmids used in this study are listed in Table 6-1. Bacteria were grown in (LB) at 37 °C unless stated otherwise. Where required, tetracycline (Tc) was added to the media at 125 µg/ mL to select recombinants, and synthetic alkyl quinolones added at the concentrations indicated.

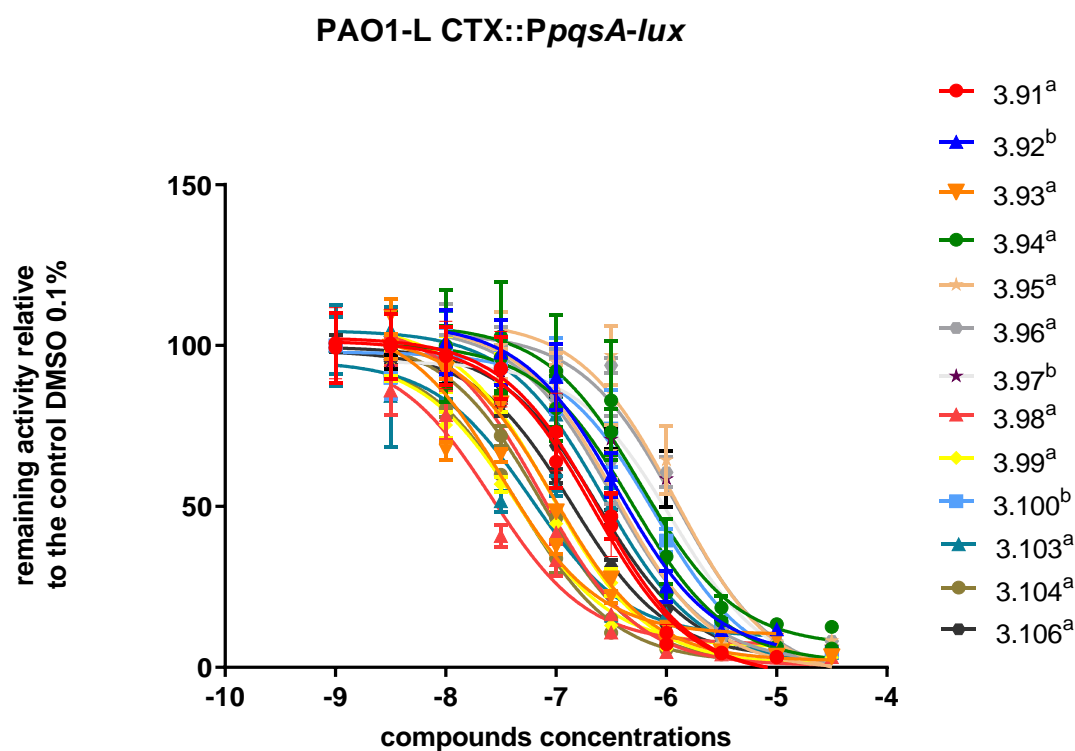
Table 6-1: **Bacterial strains and plasmids used in this study.**

Strain ^a or Plasmid ^b	Relevant Characteristics
PAO1-L ^a	Wild type PAO1, Lausanne subline. ²⁰⁷
PAO1-L CTX::P _{pqsA-lux} ^a	PAO1-L with chromosomal mini-CTX::P _{pqsA-lux} insertion; TcR. ¹²⁸
PA14 ^a	Wild type UCBPP-PA14. ²⁰⁸
PA14 CTX::P _{pqsA-lux} ^a	PA14 with chromosomal mini-CTX::P _{pqsA-lux} insertion; TcR. ¹²⁸
mini-CTX::P _{pqsA-lux} ^b	R6K-based mini-CTX suicide plasmid for the chromosomal insertion of a P _{pqsA-lux} transcriptional reporter fusion; TcR. ¹²⁹

6.2.1 Bioluminescence reporter gene fusion assay

The whole cell based assay was established here according to a published protocol with some modifications ¹³¹ by employing a constructed bacterial strains which are (PAO1-L CTX::P_{pqsA-lux} and PA14 CTX::P_{pqsA-lux}). These strains produce luminescence upon PqsR activation with endogenous ligands and the inhibition can therefore be quantified based on light reduction compared to a solvent vehicle control (DMSO). The desired strain was grown in Lysogen broth (LB) at 37 °C overnight and the final optical density (OD₆₀₀) was measured using a

spectrophotometer. The bacterial culture was prepared by dilute the bacterial stock in LB to a final concentration of 0.01 OD₆₀₀. The 10 mM concentration of the compounds DMSO stocks were diluted to a final concentration (10 μM) using the LB solution. In 96 well-plate, 100 μl of each compound and 100 μl of 0.01 bacterial culture were dispensed in triplicate and incubated overnight at 37 °C. The automated luminometer- spectrometer was used to determine the luminescence and turbidity automatically at 30 minutes interval for a duration of 8 hours. The luminescence data were normalised to the absorbance values for each well and they were then related to the solvent control to determine the remaining activity. The primary screening was performed at 10 μM and a selection threshold of 50 % or less in relative to the untreated sample was set for actives. Following this, IC₅₀ values were determined following the same protocol by employing a concentration-response curve with fixed decreasing concentrations to accommodate the logarithmic scale (10, 3.1, 1, 0.31, 0.1, 0.031, 0.01 and 0.0031 μM) and related the normalized values to the solvent control.



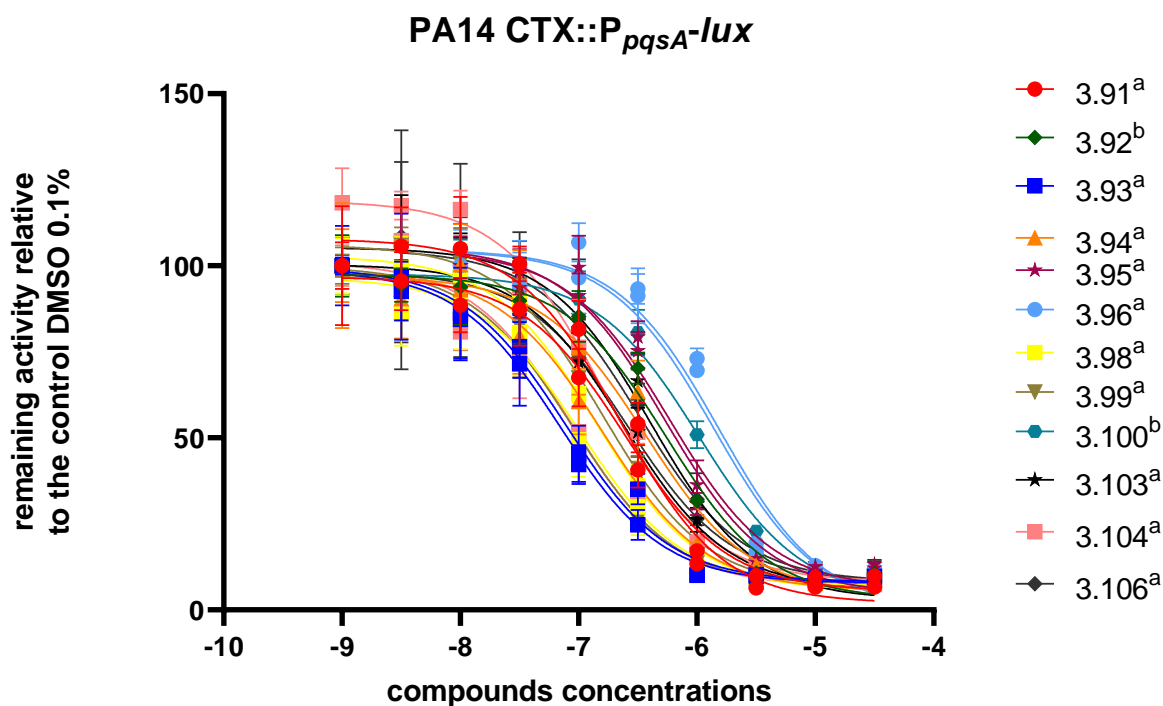


Figure 6-5: **Concentration-response curve of compounds presented in chapter three.** The inhibition of PqsR activity measured in a) PAO1-L *PpqsA::lux*. and b) PA14 *PpqsA::lux* strains. Data shown based on n = 6^a or 3^b.

6.2.2 Pyocyanin and alkyl quinoline quantification

Supernatant preparation. For pyocyanin and alkyl quinolone quantification, the same protocol was applied to prepare the supernatant as the following: the desired wild type strain was cultured in fresh LB at 37 °C overnight. The targeted concentration of the bacterial culture in each flask is OD₆₀₀ 0.05. The compounds from the other hand were assayed in triplicate at 3× IC₅₀ concentration with negative control of DMSO at the same concentration of the tested compound. The flasks incubated in shaker at 37 °C overnight with 200 rpm. The culture was centrifuged at 10,000 RCF for 10 min and the supernatant was filtered with HSW 10 mL Soft-Ject Syringe and a 0.22 μM Sartorius syringe-driven filter (Fisher Brand, Loughborough, UK).

Pyocyanin Quantification. The extraction of pyocyanin pigment was obtained by mixing 7.5 ml of the previous prepared supernatant with 4.5 ml of chloroform which then extracted again with 1.5 ml of 0.2 M HCL. The layer of HCL will be turned to pink or red depending on the

concentration of the pyocyanin which is determined by a spectrophotometer with OD₅₂₀. The triplicate readings for each compound are related to the corresponding negative control to calculate the percentage of pyocyanin production in the presence of the tested compound.

LCMS-MS Alkyl Quinoline Quantification. 10µl of each previous prepared supernatant was diluted with 90µl of an internal standard solution (500nM d4-HHQ in MeOH solution). The samples were vortex mixed for several minutes and then centrifuged (5min at 13k rpm). Samples were transferred to LC vials prior to analysis. The injection volume for each sample was 5.0µl. Analysis was conducted with the MS operating in MRM (multiple reaction monitoring) mode under positive electrospray (+ES) conditions, screening the LC eluent for the four AQs (HHQ, HQNO, PQS and d4-HHQ). Change in performance of the MS was assessed by repeat injection (x3 pre-batch and x3 post-batch) of a system suitability standard sample (containing 500nM of each analyte in MeOH). Confirmation that detection of AQs in analytical samples fell within the linear response range of the MS was performed by analysis of a range of calibration samples (of HHQ, HQNO and PQS) up to 1µM.

6.2.3 *Ex vivo* pig lung model

Bacterial strain. The Wild type PAO1 strain of *P. aeruginosa* was used as an examples of standard laboratory strains. This strain grew in LB agar plate overnight at 37°C.

Artificial sputum medium and culture conditions. Artificial sputum medium was prepared following the method of Palmer *et al.* (2007)²⁰⁹ mentioned in Harrison and Diggle (2016)²¹⁰, the latter showed slight modification by excluding the glucose from the recipe. They found that the glucose facilitated growth of any resident bacteria left on the lung tissue without affecting the growth of *P. aeruginosa*. In addition, they added 50 µg/mL of ampicillin in all used media to further minimize the growth of any resident bacteria present in the lung tissue.

Lung dissection and infection. The lungs were collected from a local butcher (JT Beedham & Sons) as soon as possible after they arrived in the shop from the abattoir and they were used immediately when arriving at the laboratory. The chilled cool box was used for transportation to The University of Nottingham and the dissection was in a room not used for microbiological work. The standard sterile technique was applied throughout the process by working under Bunsen burner, dissection tools were autoclaved and dipped in ethanol and flaming as necessary during the experiment. The lung surface was briefly seared using a hot pallet knife to kill the surface contaminants. Using razor blades to cut along the tissue to expose the cartilage of the bronchus and separate the bronchus from the trachea and the surrounding alveolar tissue. The bronchus was washed with a 1:1 mix of RPMI and DMEM (Sigma-Aldrich). It was cut into strips and after washing again with the same solution the strips were cut to cubes. These cubes were washed once with the previous solution and once with the ASM. Under sterilizing condition, they were transferred to the wells of a 24-well tissue culture plate which was prepared previously with soft pad of 400 μ l ASM supplemented with 0.8 % w/v agarose. Then, 500 μ l of ASM was added to each well. By 1 mL insulin syringe, the colony of PAO1 strain of *P. aeruginosa* was touched lightly and then touch the tissue which was incubated at 37°C on a rocking platform for 24 hours (acute infection) or 72 hours (chronic infection). After building a mock infection, 0.2 μ M of **3.20** was added and incubated for further 8 hours. After incubation, the cubes were transferred to metal bead tubes with 1 mL phosphate-buffered saline and homogenized using a Precellys24 homogenizer. The supernatant was used to measure the growth and count the colony of bacteria by serial dilution in 96 well plate and then transfer it to LB plate.

Furthermore, after a process of extraction by ethyl acetate, the LC/MS was used to quantify the concentration of HHQ and PQS with and without treatment as described in Section 6.2.2.

6.2.4 Cytotoxicity study

Cell viability was assessed according to O'Brien *et al.*¹⁹⁹ on A549 adenocarcinomic human alveolar basal epithelial cell line. The viability of A549 cell line after overnight incubation with three concentrations (1, 50 and 100 μM) of the corresponding compound were determined using alamar blue (resazurin) dye. Cells were maintained in the Dulbecco's Modified Essential Medium (DMEM) supplemented with 10 % fetal bovine serum (FBS) and 1 % Penicillin-Streptomycin-Neomycin. After that, 100 μL of suspended cells with a final concentration (1×10^4 cells/wall) was seeded in 96-well plates with 100 μL of (1, 50, 100 μM) concentration of the tested compound was dispensed in sextuplicate. In addition, the highest concentration of the solvent vehicle (1 % DMSO) employed as a negative control. On the other hand, 100 μM of $\text{K}_2\text{Cr}_2\text{O}_7$ was added as a positive control (kill cells). The plate incubated at 37°C, 5 % carbon dioxide for 24 hours. After 24 hours of incubation, 20 μL of alamar blue dye was added to the corresponding walls. The plates were further incubated for 4-6 hours and the intensity of the fluorescence was measured by exciting the light at 510 nm and measuring the fluorescence at 590 nm. The percentage of cell viability in each column was normalised to the DMSO reading.

7 Appendix

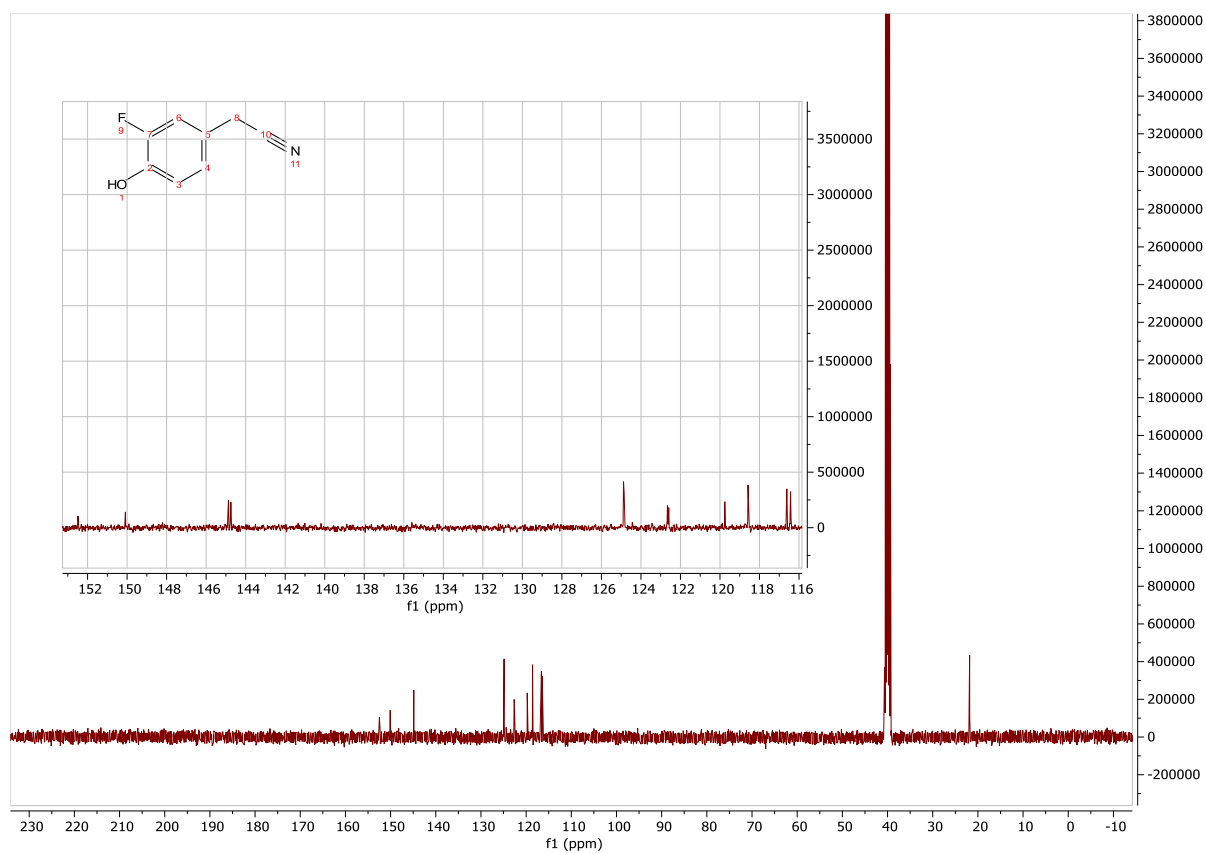


Figure 7-1: The ^{13}C NMR spectra of 2-(3-Fluoro-4-hydroxyphenyl) acetonitrile **2.26** with enlarged section of the aromatic region, in $\text{DMSO-}d_6$ solvent at 100.66 MHz.

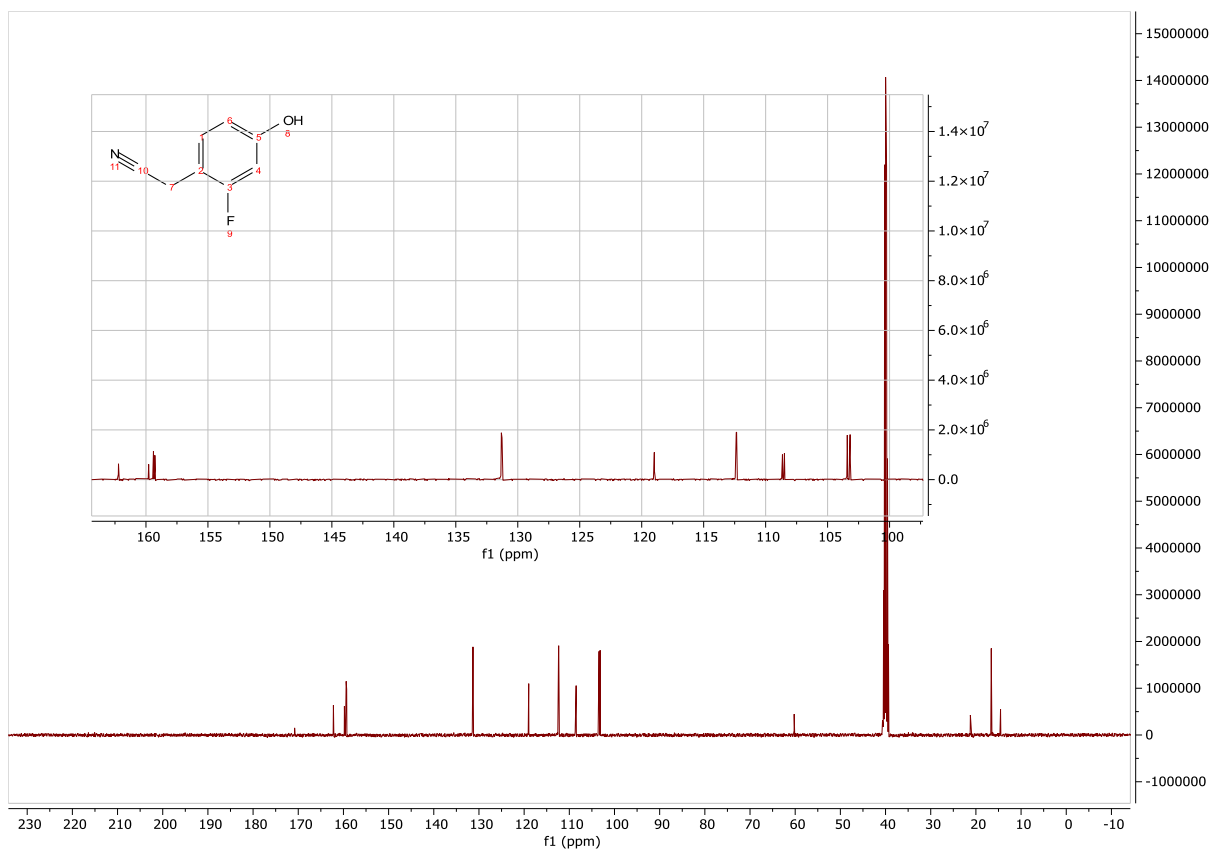


Figure 7-2: The ^{13}C NMR spectra of 2-(2-Fluoro-4-hydroxyphenyl) acetonitrile **2.27** with enlarged section of the aromatic region, in $\text{DMSO-}d_6$ solvent at 100.66 MHz.

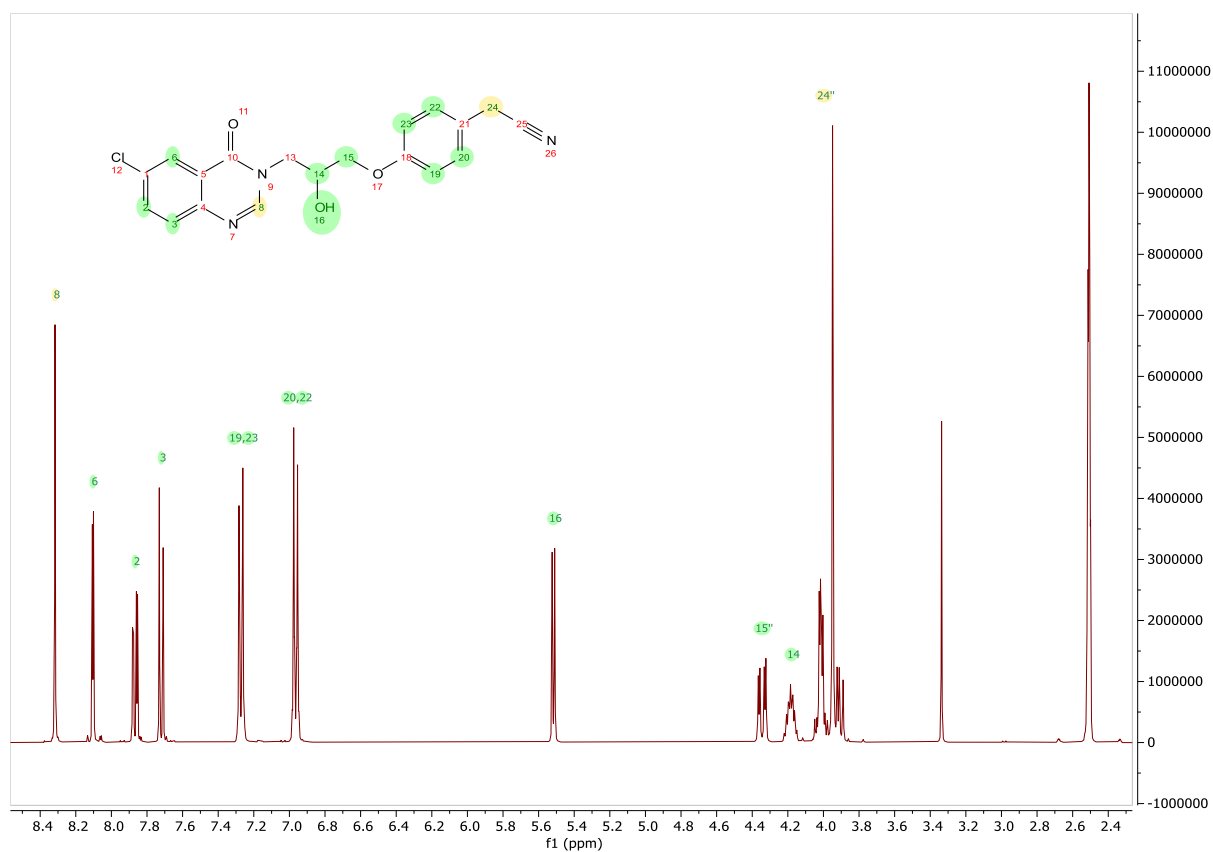


Figure 7-3: The $^1\text{H-NMR}$ spectra of 2-(4-(3-(6-chloro-4-oxoquinazolin-3(4*H*)-yl)-2-hydroxypropoxy) phenyl) acetonitrile **1.6**, in $\text{DMSO-}d_6$ solvent at 400.25 MHz.

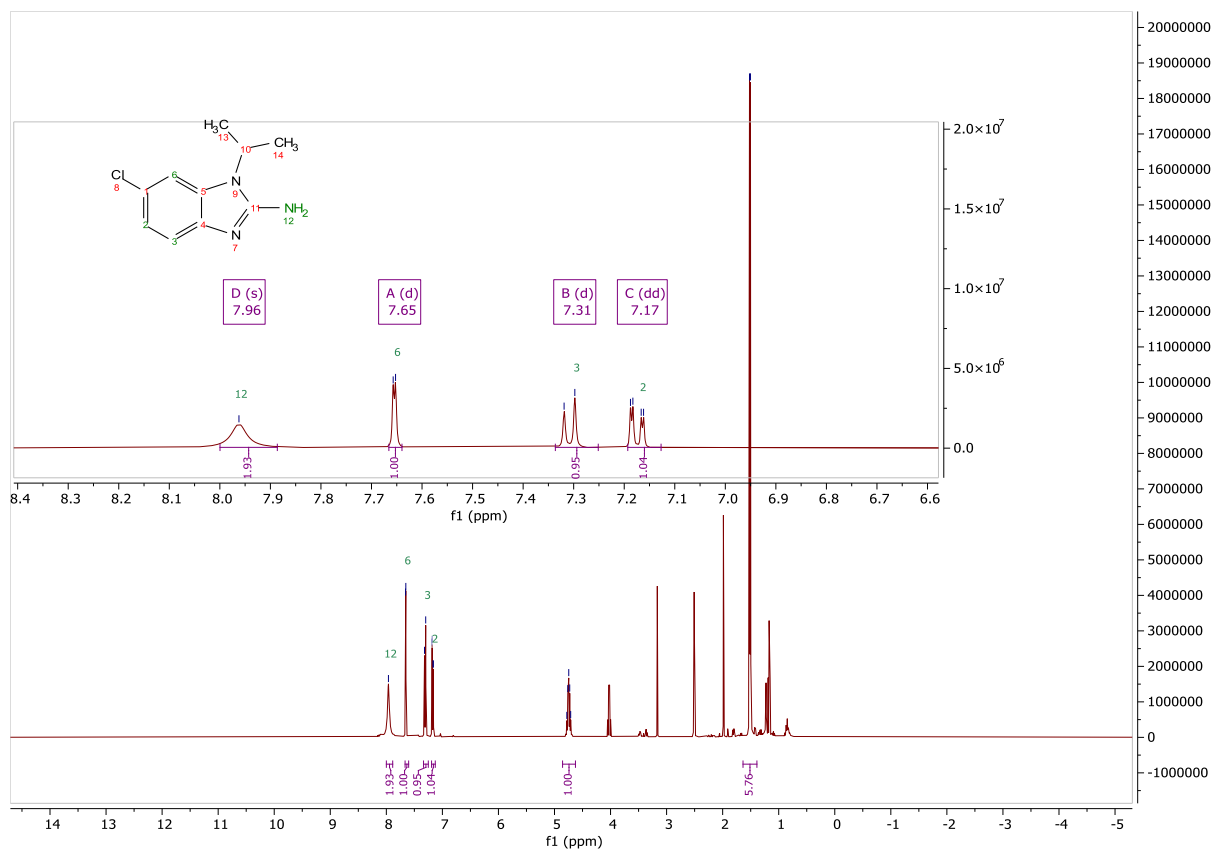


Figure 7-4: The $^1\text{H-NMR}$ spectra of 6-chloro-1-isopropyl-1H-benzo[d]imidazol-2-amine **3.25**, with enlarged section of the aromatic region in $\text{DMSO-}d_6$ solvent at 400.25 MHz.

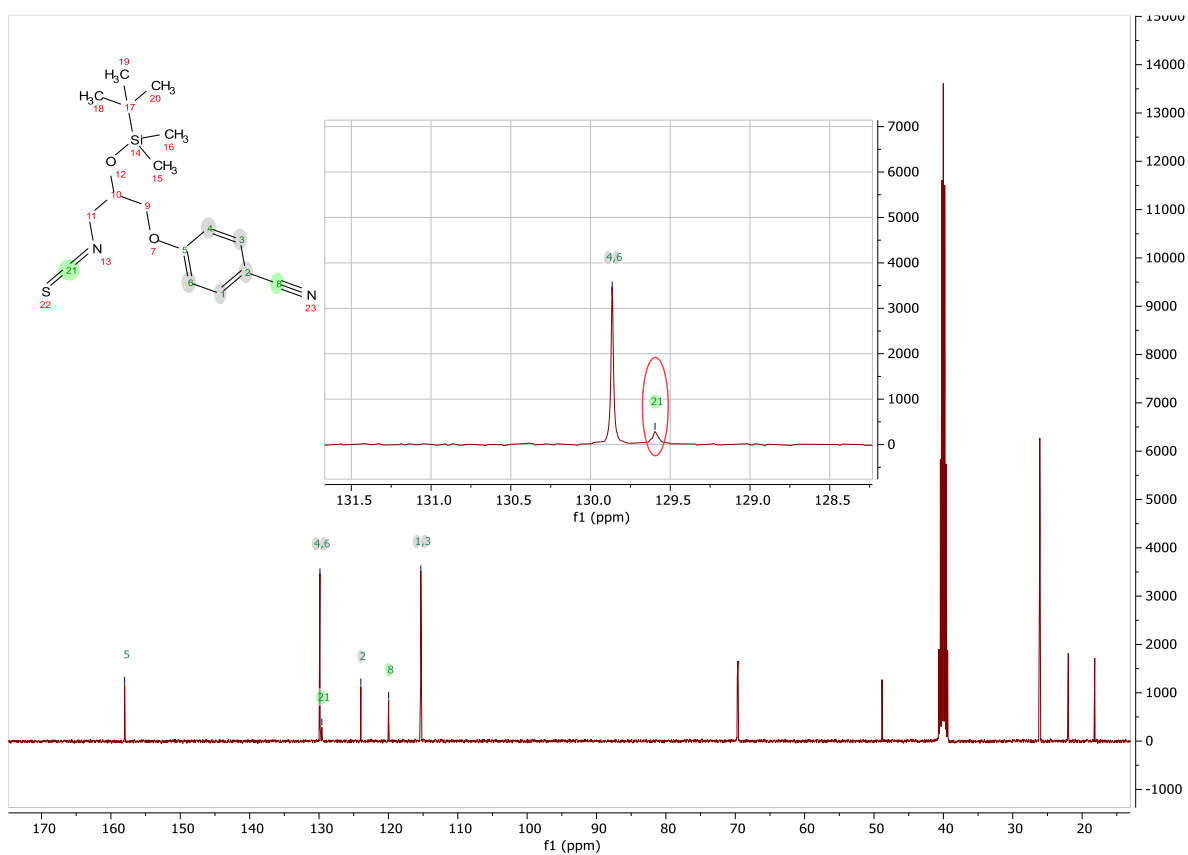
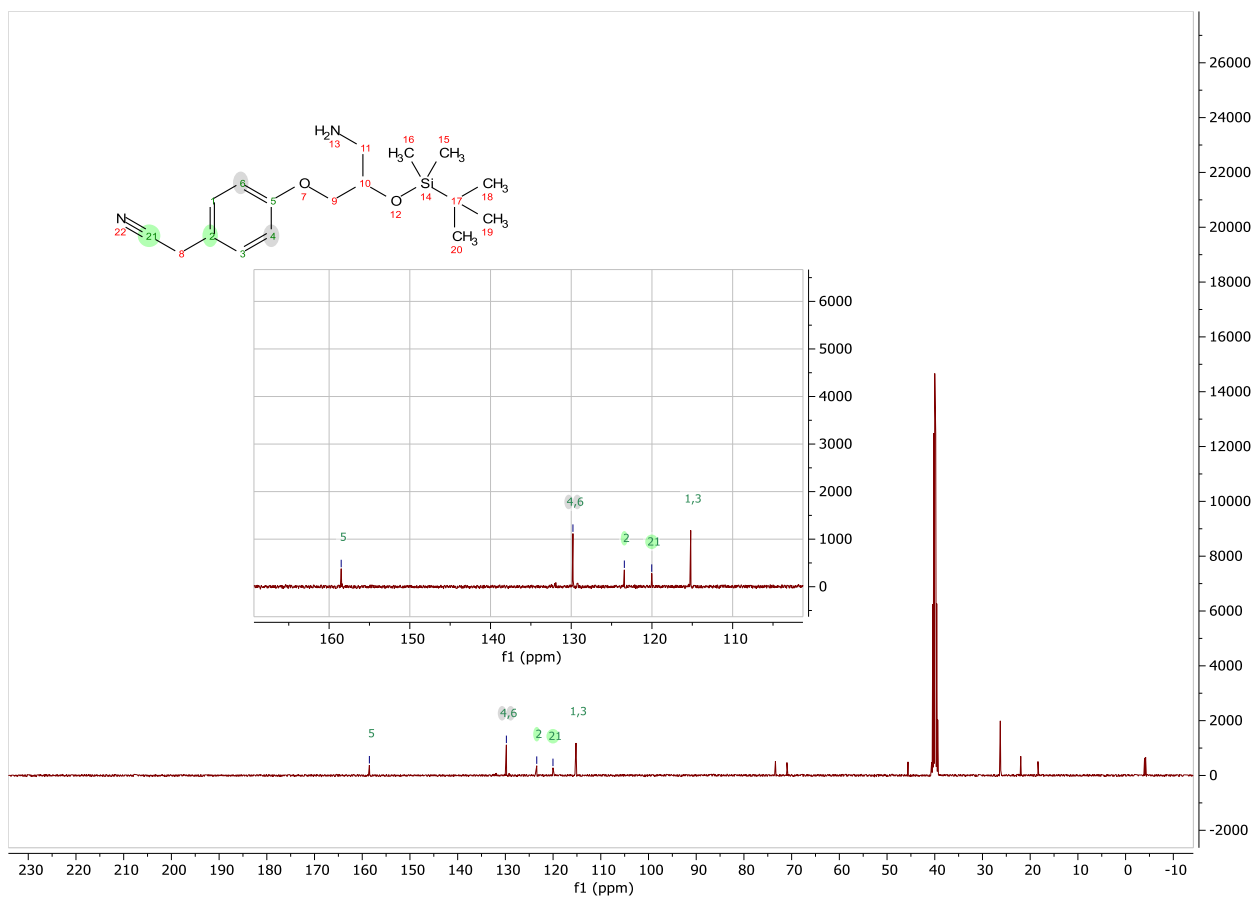


Figure 7-5: The ^{13}C NMR spectra of 2-(4-(3-Amino-2-((*tert*-butyl dimethyl silyl) oxy) propoxy) phenyl) acetonitrile **3.33 step2** (above) and 2-(4-(2-((*tert*-Butyl dimethyl silyl) oxy)-3-isothiocyanatopropoxy) phenyl) acetonitrile **3.36** (below) with enlarged section of the aromatic region, in $\text{DMSO-}d_6$ solvent at 100.66 MHz

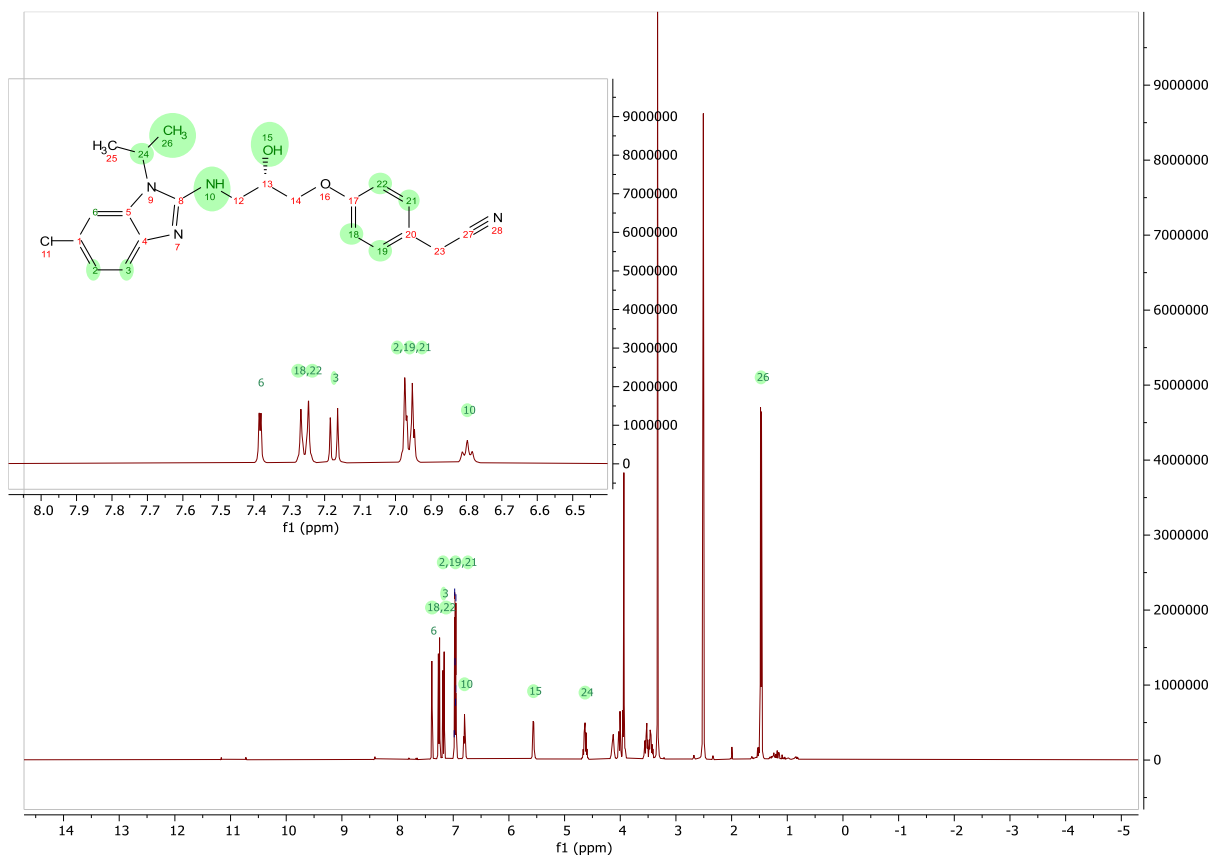


Figure 7-6: The ^1H -NMR spectra of (*S*)-2-(4-(3-((6-Chloro-1-isopropyl-1*H*-benzo[*d*]imidazol-2-yl)amino)-2-hydroxypropoxy) phenyl) acetonitrile **3.114**, with enlarged section of the aromatic region in $\text{DMSO-}d_6$ solvent at 400.25 MHz.

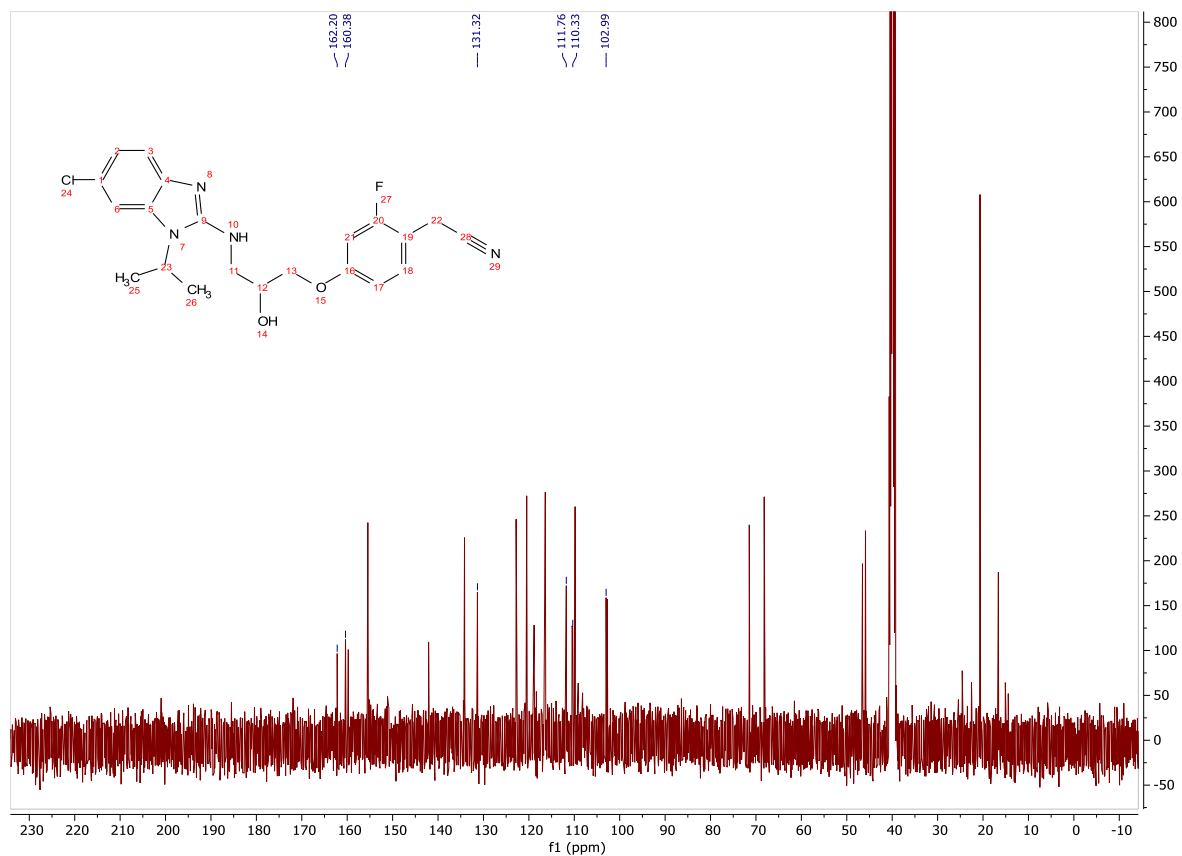


Figure 7-7: The ^{13}C NMR spectra of 2-(4-(3-((6-chloro-1-isopropyl-1*H*-benzo[*d*]imidazol-2-yl) amino) -2-hydroxypropoxy) -2-fluorophenyl) acetonitrile **3.96** in $\text{DMSO-}d_6$ solvent at 100.66 MHz, the highlighted peaks in the spectrum are coupling with the fluorine.

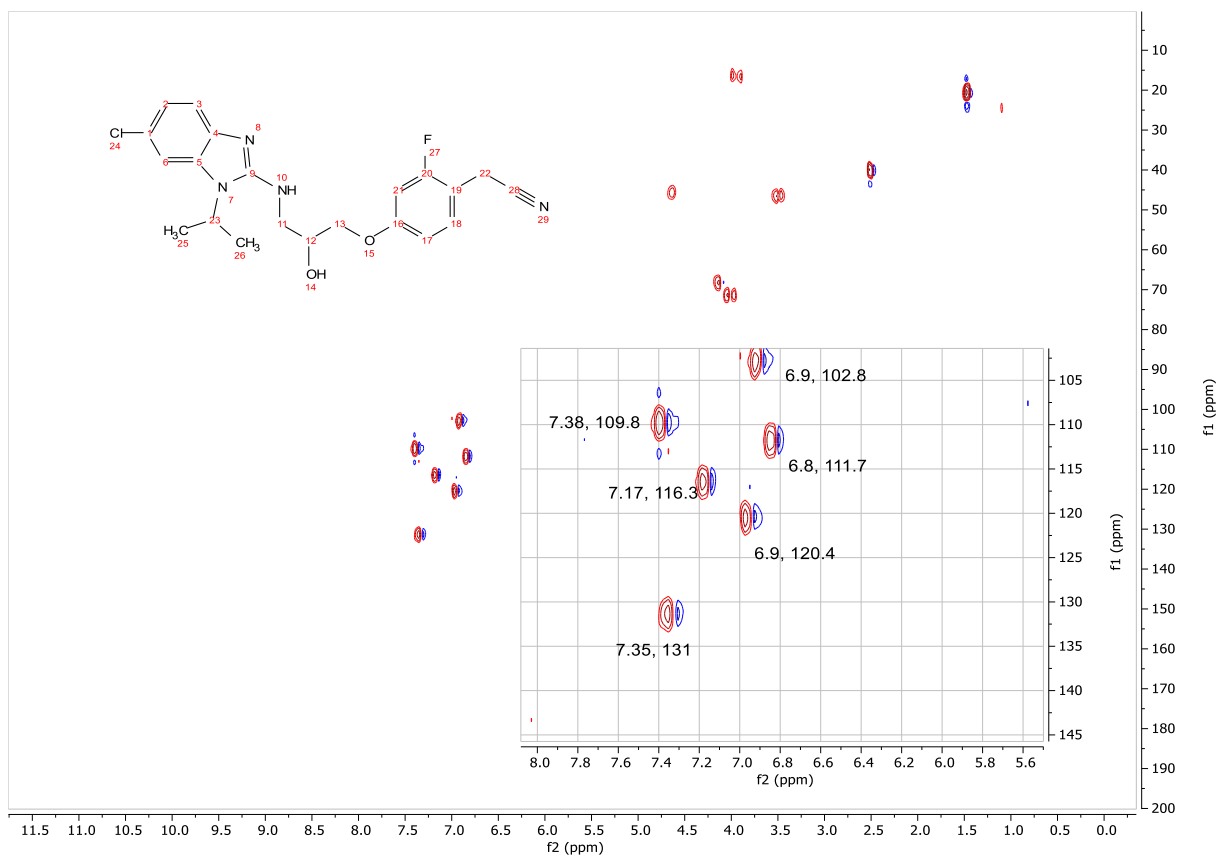


Figure 7-8: The heteronuclear single quantum correlation (HSQC) analysis of 2-(4-(3-((6-chloro-1-isopropyl-1*H*-benzo[*d*]imidazol-2-yl) amino) -2-hydroxypropoxy) -2-fluorophenyl) acetonitrile **3.96**, with enlarged section of the aromatic region, in DMSO-*d*₆ solvent at 100.66 MHz.

8 References

1. Tamma, P., Cosgrove, S. & Maragakis, L. Combination therapy for treatment of infections with gram-negative bacteria. *Clin. Microbiol. Rev.* **25**, 450–470 (2012).
2. Abraham, E. & Chain, E. An Enzyme from Bacteria able to destroy penicillin. *Nature* **146**, 837 (1940).
3. Smith, J. & Marples, M. A Natural Reservoir of Penicillin-resistant Strains of *Staphylococcus aureus*. *Nature* **201**, 844 (1964).
4. Davies, J. Origins and evolution of antibiotic resistance. *Microbiologia* **12**, 9–16 (1996).
5. World Health Organization. Global priority list of antibiotic-resistant bacteria to guide research, discovery, and development of new antibiotics. (2017).
6. Wu, W., Jin, Y., Bai, F. & Jin, S. *Pseudomonas aeruginosa*. *Molecular Medical Microbiology* (Academic Press, 2014).
7. Bonten, M., Bergmans, D., Speijer, H. & Stobberingh, E. Characteristics of polyclonal endemicity of *pseudomonas aeruginosa* colonization in intensive care units implications for infection control. *AJRCCM* **160**, 1212–1219 (1999).
8. Gellatly, S. & Hancock, R. *Pseudomonas aeruginosa*: New insights into pathogenesis and host defenses. *Pathog. Dis.* **67**, 159–173 (2013).
9. Bodey, G., Bolivar, R., Fainstein, V. & Jadeja, L. Infections Caused by *Pseudomonas aeruginosa*. *Rev Infect Dis* **5**, 279–313 (1983).
10. Bassetti, M., Vena, A., Croxatto, A., Righi, E. & Guery, B. How to manage *Pseudomonas aeruginosa* infections. *Drugs Context* **7**, 1–18 (2018).
11. Martin, A., Smalley, C., George, R., Healing, D. & Anderson, C. Gentamicin and tobramycin compared in the treatment of mucoid *pseudomonas* lung infections in cystic fibrosis. *Arch Dis Child* **55**, 604–607 (1980).
12. Riordan, J. *et al.* Identification of the cystic fibrosis gene: Cloning and characterization of complementary DNA. *Science* **245**, 1066–1073 (1989).
13. National Center for Biomedical Communications. CFTR gene. *U.S. National Library of*

- Medicine*, www.ghr.nlm.nih.gov/gene/CFTR (2017).
14. Kragh, K. *et al.* Polymorphonuclear leukocytes restrict growth of *Pseudomonas aeruginosa* in the lungs of cystic fibrosis patients. *Infect Immun* **82**, 4477–4486 (2014).
 15. Sadikot, R. T., Blackwell, T. S., Christman, J. W. & Prince, A. S. Pathogen-host interactions in *Pseudomonas aeruginosa* pneumonia. *Am J Respir Crit Care Med* **171**, 1209–1223 (2005).
 16. Høiby, N. *et al.* The clinical impact of bacterial biofilms. *Int J Oral Sci* **3**, 55–65 (2011).
 17. Micek, S. *et al.* *Pseudomonas aeruginosa* bloodstream infection: importance of appropriate initial antimicrobial treatment. *Am Soc Microbiol* **49**, 1306–1311 (2005).
 18. Kathryn, S. & Moffett, M. *Pseudomonas aeruginosa* in patients with Cystic Fibrosis. *infection disease & antimicrobial agents*, <http://www.antimicrobe.org/new/b260.asp> (2010).
 19. Iglewski, B. H. *Medical Microbiology. 4th edition. University of Texas Medical Branch at Galveston* (University of Texas Medical Branch at Galveston, 1996).
 20. Klockgether, J., Cramer, N., Wiehlmann, L., Davenport, C. F. & Tümmler, B. *Pseudomonas aeruginosa* genomic structure and diversity. *Front Microbiol* **2**, 1–18 (2011).
 21. Kung, V., Ozer, E. & Hauser, A. The Accessory Genome of *Pseudomonas aeruginosa*. *Microbiol Mol Biol Rev* **74**, 621–641 (2010).
 22. Stover, C. *et al.* Complete genome sequence of *Pseudomonas aeruginosa* PAO1, an opportunistic pathogen. *Nature* **406**, 959–964 (2000).
 23. He, J. *et al.* The broad host range pathogen *Pseudomonas aeruginosa* strain PA14 carries two pathogenicity islands harboring plant and animal virulence genes. *Proc Natl Acad Sci U S A* **101**, 2530–2535 (2004).
 24. Winstanley, C. *et al.* Newly introduced genomic prophage islands are critical determinants of in vivo competitiveness in the liverpool epidemic strain of *Pseudomonas aeruginosa*. *Genome Res* **19**, 12–23 (2009).
 25. Tümmler, B. Emerging therapies against infections with *Pseudomonas aeruginosa*. *F1000Research* **8**, 1371 (2019).

26. Pandey, N. & Cascella, M. *Beta Lactam Antibiotics*. *StatPearls* (StatPearls Publishing, 2020).
27. Ramirez, M. & Tolmasky, M. Aminoglycoside Modifying Enzymes. *Drug Resist Updat*. **13**, 151–171 (2010).
28. Jeannot, K., Bolard, A. & Plésiat, P. Resistance to polymyxins in Gram-negative organisms. *Int J Antimicrob Agents* **49**, 526–535 (2017).
29. Bassetti, M., Peghin, M., Vena, A. & Giacobbe, D. R. Treatment of infections due to MDR gram-negative bacteria. *Front Med* **6**, 1–10 (2019).
30. Wu, J., Srinivas, P. & Pogue, J. Cefiderocol: a novel agent for the management of multidrug-resistant gram-negative organisms. *Infect Dis Ther* **9**, 17–40 (2020).
31. Sader, H. S., Dale, G. E., Rhomberg, P. R. & Flamm, R. K. Antimicrobial activity of murepavadin tested against clinical isolates of pseudomonas aeruginosa from the United States, Europe, and China. *Antimicrob Agents Chemother* **62**, 1–6 (2018).
32. Saiman, L. *et al.* Azithromycin in patients with Cystic Fibrosis chronically infected with Pseudomonas aeruginosa. *JAMA* **290**, 1749–1756 (2003).
33. Lamers, R., Cavallari, J. & Burrows, L. The efflux inhibitor phenylalanine-arginine beta-naphthylamide (PABN) permeabilizes the outer membrane of gram-negative bacteria. *PLoS One* **8**, 1–7 (2013).
34. Stokes, J. *et al.* Pentamidine sensitizes Gram-negative pathogens to antibiotics and overcomes acquired colistin resistance. *Nat Microbiol* **2**, 1–21 (2017).
35. Bernardini, F., Dale, G., Wach, A. & Obrecht, D. Pharmacokinetics and pharmacodynamics of murepavadin (POL7080) in neutropenic lung infection models when evaluated by aerosol administration. *J Cyst Fibros* **18**, S2 (2019).
36. Vaara, M. & Vaara, T. Polycations as outer membrane-disorganizing agents. *Antimicrob Agents Chemother* **24**, 114–122 (1983).
37. Köhler, T., Perron, G., Buckling, A. & Van Delden, C. Quorum sensing inhibition selects for virulence and cooperation in pseudomonas aeruginosa. *PLoS Pathog* **6**, 1–6 (2010).
38. Chevalier, S. *et al.* Structure, function and regulation of Pseudomonas aeruginosa porins.

- FEMS Microbiol Rev* **41**, 698–722 (2017).
39. Hancock, R. & Brinkman, F. Function of *Pseudomonas* porins in uptake and efflux. *Annu Rev Microbiol* **56**, 17–38 (2002).
 40. Ballesteros, S. *et al.* Carbapenem resistance in *Pseudomonas aeruginosa* from cystic fibrosis patients. *J Antimicrob Chemother* **38**, 39–45 (1996).
 41. Putman, M., Veen, H. & Konings, W. Molecular properties of bacterial multidrug transporters. *Am Soc Microbiol* **64**, 672–693 (2000).
 42. Pang, Z., Raudonis, R., Glick, B., Lin, T. & Cheng, Z. Antibiotic resistance in *Pseudomonas aeruginosa*: mechanisms and alternative therapeutic strategies. *Biotechnol Adv* **37**, 177–192 (2019).
 43. Drawz, S. & Bonomo, R. Three decades of β -Lactamase inhibitors. *Clin Microbiol Rev* **23**, 160–201 (2010).
 44. Breidenstein, E., de la Fuente-Núñez, C. & Hancock, R. *Pseudomonas aeruginosa*: all roads lead to resistance. *Trends Microbiol* **19**, 419–426 (2011).
 45. Munita, J. & Arias, C. Mechanisms of Antibiotic Resistance. *Microbiol Spectr* **4**, 1–37 (2016).
 46. Taylor, P., Yeung, A. & Hancock, R. Antibiotic resistance in *Pseudomonas aeruginosa* biofilms: towards the development of novel anti-biofilm therapies. *J Biotechnol* **191**, 121–130 (2014).
 47. Valentini, M. & Filloux, A. Biofilms and Cyclic di-GMP (c-di-GMP) Signaling: Lessons from *Pseudomonas aeruginosa* and Other Bacteria. *J Biol Chem* **291**, 12547–12555 (2016).
 48. Petrova, O. & Sauer, K. SagS contributes to the motile-sessile switch and acts in concert with BfiSR to enable *Pseudomonas aeruginosa* biofilm formation. *J Bacteriol* **193**, 6614–6628 (2011).
 49. Banin, E., Vasil, M. & Greenberg, P. Iron and *Pseudomonas aeruginosa* biofilm formation. *PNAS* **102**, 11076–11081 (2005).
 50. Rasamiravaka, T., Labtani, Q., Duez, P. & El Jaziri, M. The formation of biofilms by *Pseudomonas aeruginosa*: a review of the natural and synthetic compounds interfering

- with control mechanisms. *Biomed Res Int* **2015**, (2015).
51. Ciofu, O. & Tolker-Nielsen, T. Tolerance and resistance of *Pseudomonas aeruginosa* biofilms to antimicrobial agents-How *P. aeruginosa* Can escape antibiotics. *Front Microbiol* **10**, (2019).
 52. Fernández-Barat, L. *et al.* Phenotypic shift in *Pseudomonas aeruginosa* populations from cystic fibrosis lungs after 2-week antipseudomonal treatment. *J Cyst Fibros* **16**, 222–229 (2017).
 53. Wang, H., Wu, H., Ciofu, O., Song, Z. & Høiby, N. In Vivo pharmacokinetics/pharmacodynamics of colistin and imipenem in *Pseudomonas aeruginosa* biofilm infection. *Antimicrob Agents Chemother* **56**, 2683–2690 (2012).
 54. Wood, T., Knabel, S. & Kwan, B. Bacterial persister cell formation and dormancy. *Appl Env. Microbiol* **79**, 7116–7121 (2013).
 55. Lyczak, J., Cannon, C. & Pier, G. Establishment of *Pseudomonas aeruginosa* infection: Lessons from a versatile opportunist. *Microbes Infect* **2**, 1051–1060 (2000).
 56. Sato, H., Okinaag, K. & Saito, H. Role of pili in the pathogenesis of *Pseudomonas aeruginosa* burn infection. *Microbiol Immunol* **32**, 131–139 (1988).
 57. Chemani, C. *et al.* Role of LecA and LecB lectins in *Pseudomonas aeruginosa*-induced lung injury and effect of carbohydrate ligands. *Infect Immun* **77**, 2065–2075 (2009).
 58. Zulianello, L. *et al.* Rhamnolipids are virulence factors that promote early infiltration of primary human airway epithelia by *Pseudomonas aeruginosa*. *INFECT IMMUN* **74**, 3134–3147 (2006).
 59. Glick, R. *et al.* Increase in rhamnolipid synthesis under iron-limiting conditions influences surface motility and biofilm formation in *Pseudomonas aeruginosa*. *J BACTERIOL* **192**, 2973–2980 (2010).
 60. Filloux, A. Protein secretion systems in *Pseudomonas aeruginosa*: an essay on diversity, evolution, and function. *Front Microbiol* **2**, 1–21 (2011).
 61. Lau, G., Hassett, D., Ran, H. & Kong, F. The role of pyocyanin in *Pseudomonas aeruginosa* infection. *Trends Mol Med* **10**, 599–606 (2004).
 62. Anderson, R., Roddam, L., Bettiol, S., Sanderson, K. & Reid, D. Biosignificance of

- bacterial cyanogenesis in the CF lung. *J Cyst Fibros* **9**, 158–164 (2010).
63. Muller, M. Pyocyanin induces oxidative stress in human endothelial cells and modulates the glutathione redox cycle. *Free Radic Biol Med* **33**, 1527–1533 (2002).
 64. Bejarano, P., Langeveld, J., Hudson, B. & Noelken, M. Degradation of basement membranes by *Pseudomonas aeruginosa* elastase. *Infect Immun* **57**, 3783–3787 (1989).
 65. Ostroff, R., Vasil, A. & Vasil, M. Molecular Comparison of a Nonhemolytic and a Hemolytic Phospholipase C from *Pseudomonas aeruginosa*. *J Bacteriol* **172**, 5915–5923 (1990).
 66. Foley, B., Moehring, J. & Moehring, T. Mutations in the elongation factor 2 gene which confer resistance to diphtheria toxin and *Pseudomonas* exotoxin A. *J Biol Chem* **270**, 23218–23336 (1995).
 67. Wolz, C. *et al.* Iron release from transferrin by pyoverdinin and elastase from *Pseudomonas aeruginosa*. *Infect Immun* **62**, 4021–4027 (1994).
 68. Waters, C. & Bassler, B. Quorum Sensing: cell-to-cell communication in bacteria. *Annu Rev Cell Dev Biol* **21**, 319–346 (2005).
 69. Pesci, E. *et al.* Quinolone signaling in the cell-to-cell communication system of *Pseudomonas aeruginosa*. *Biochemistry* **96**, 11229–11234 (1999).
 70. Atkinson, S. & Williams, P. Quorum sensing and social networking in the microbial world. *J R Soc Interface* **6**, 959–978 (2009).
 71. Eberhard, A. *et al.* Structural identification of autoinducer of photobacterium fischeri luciferase. *Biochemistry* **20**, 2444–2449 (1981).
 72. Soukariéh, F., Williams, P., Stocks, M. & Cámara, M. *Pseudomonas aeruginosa* quorum sensing systems as drug discovery targets: current position and future perspectives. *J Med Chem* **61**, 10385–10402 (2018).
 73. Lee, J. & Zhang, L. The hierarchy quorum sensing network in *Pseudomonas aeruginosa*. *Protein Cell* **6**, 26–41 (2014).
 74. Pearson, J. *et al.* Structure of the autoinducer required for expression of *Pseudomonas aeruginosa* virulence genes. *PNAS* **91**, 197–201 (1994).
 75. Pearson, J., Passadori, L., Iglewski, B. & Greenberg, E. A second N-acylhomoserine

- lactone signal produced by *Pseudomonas aeruginosa*. *PNAS* **92**, 1490–1494 (1995).
76. Choi, Y. *et al.* Growth phase-differential quorum sensing regulation of anthranilate metabolism in *Pseudomonas aeruginosa*. *Mol Cells* **32**, 57–65 (2011).
 77. Ochsner, U., Koch, A., Fiechter, A. & Reiser, J. Isolation and characterization of a regulatory gene affecting rhamnolipid biosurfactant synthesis in *Pseudomonas aeruginosa*. *J Bacteriol* **176**, 2044–2054 (1994).
 78. Ochsner, U. & Reiser, J. Autoinducer-mediated regulation of rhamnolipid biosurfactant synthesis in *Pseudomonas aeruginosa*. *PNAS* **92**, 6424–6428 (1995).
 79. Rampioni, G. *et al.* Unravelling the genome-wide contributions of specific 2-alkyl-4-quinolones and PqsE to quorum sensing in *Pseudomonas aeruginosa*. *PLoS Pathog.* **12**, 1–25 (2016).
 80. De'ziel, E. *et al.* Analysis of *Pseudomonas aeruginosa* 4-hydroxy-2-alkylquinolines (HAQs) reveals a role for 4-hydroxy-2-heptylquinoline in cell-to-cell communication. *PNAS* **101**, 1339–1344 (2004).
 81. Gallagher, L., Mcknight, S., Kuznetsova, M., Pesci, E. & Manoil, C. Functions required for extracellular quinolone signaling by *Pseudomonas aeruginosa*. *J Bacteriol* **184**, 6472–6480 (2002).
 82. Heeb, S. *et al.* Quinolones: From antibiotics to autoinducers. *FEMS Microbiol Rev* **35**, 247–274 (2011).
 83. Rampioni, G. *et al.* Transcriptomic analysis reveals a global alkyl-quinolone-independent regulatory role for PqsE in facilitating the environmental adaptation of *Pseudomonas aeruginosa* to plant and animal hosts. *Env. Microbiol* **12**, 1659–1673 (2010).
 84. Farrow, J. *et al.* PqsE functions independently of PqsR-*Pseudomonas* quinolone signal and enhances the rhl quorum-sensing system. *J Bacteriol* **190**, 7043–7051 (2008).
 85. Hazan, R., He, J., Xiao, G., Dekimpe, V. & Apidianakis, Y. Homeostatic interplay between bacterial cell-cell signaling and iron in virulence. *PLoS Pathog* **6**, e1000810 (2010).
 86. Folch, B., Déziel, E. & Doucet, N. Systematic mutational analysis of the putative

- hydrolase PqsE: toward a deeper molecular understanding of virulence acquisition in *Pseudomonas aeruginosa*. *PLoS One* **8**, e73727 (2013).
87. Ilangovan, A. *et al.* Structural basis for native agonist and synthetic inhibitor recognition by the *Pseudomonas aeruginosa* quorum sensing regulator PqsR (MvfR). *PLoS Pathog.* **9**, (2013).
 88. Rampioni, G., Leoni, L. & Williams, P. The art of antibacterial warfare: deception through interference with quorum sensing-mediated communication. *Bioorg Chem* **55**, 60–68 (2014).
 89. Mashburn, L. & Whiteley, M. Membrane vesicles traffic signals and facilitate group activities in a prokaryote. *Nature* **437**, 422–425 (2005).
 90. Jinshui, L., Juanli, C., Yao, W. & Xihui, S. The *Pseudomonas* quinolone signal (PQS): not just for quorum sensing anymore. *Front Cell Infect Microbiol* **8**, 1–9 (2018).
 91. Orazi, G. & O’Toole, G. *Pseudomonas aeruginosa* alters *Staphylococcus aureus* sensitivity to vancomycin in a biofilm model of cystic fibrosis infection. *MBio* **8**, e00873-17 (2017).
 92. Nguyen, A. *et al.* Cystic fibrosis isolates of *Pseudomonas aeruginosa* retain iron-regulated antimicrobial activity against *Staphylococcus aureus* through the action of multiple alkylquinolones. *Front Microbiol* **7**, 1171 (2016).
 93. Proctor, R. *et al.* Small colony variants: a pathogenic form of bacteria that facilitates persistent and recurrent infections. *Nat Rev Microbiol* **4**, 295–305 (2006).
 94. Lightbown, J. & Jackson, F. Inhibition of cytochrome systems of heart muscle and certain bacteria by the antagonists of dihydrostreptomycin: 2-alkyl-4-hydroxyquinoline N-oxides. *Biochemistry* **63**, 130–137 (1956).
 95. Machan, Z., Taylor, G., Pitt, T., Cole, P. & Wilson, R. 2-Heptyl-4-hydroxyquinoline N-oxide, an antistaphylococcal agent produced by *Pseudomonas aeruginosa*. *J Antimicrob Chemother* **30**, 615–623 (1992).
 96. Alanis, A. Resistance to antibiotics: are we in the post-antibiotic era? *Arch Med Res* **36**, 697–705 (2005).
 97. Clatworthy, A., Pierson, E. & Hung, D. Targeting virulence: a new paradigm for

- antimicrobial therapy. *Nat Chem Biol* **3**, 541–548 (2007).
98. Allen, R., Popat, R., Diggle, S. & Brown, S. Targeting virulence: can we make evolution-proof drugs? *Nat Rev Microbiol* **12**, 300–308 (2014).
 99. Soukarieh, F. *et al.* Hit identification of new potent PqsR antagonists as inhibitors of quorum sensing in planktonic and biofilm grown *Pseudomonas aeruginosa*. *Front Chem* **8**, 1–14 (2020).
 100. Amara, N. *et al.* Fine-tuning covalent inhibition of bacterial quorum sensing. *ChemBioChem* **17**, 825–835 (2016).
 101. O’Loughlin, C. *et al.* A quorum-sensing inhibitor blocks *Pseudomonas aeruginosa* virulence and biofilm formation. *PNAS* **110**, 17981–17986 (2013).
 102. Nora, E., Joseph, M., Margrith, M. & Helen, B. Potent and selective modulation of the RhIR quorum sensing receptor using non-native ligands – an emerging target for virulence control in *Pseudomonas aeruginosa*. *ChemBioChem* **16**, 2348–2356 (2015).
 103. Starkey, M. *et al.* Identification of anti-virulence compounds that disrupt quorum-sensing regulated acute and persistent pathogenicity. *PLoS Pathog.* **10**, e1004321 (2014).
 104. Feltner, J. *et al.* LasR variant cystic fibrosis isolates reveal an adaptable quorum-sensing hierarchy in *Pseudomonas aeruginosa*. *MBio* **7**, e01513-16 (2016).
 105. Welsh, M., Eibergen, N., Moore, J. & Blackwell, H. Small molecule disruption of quorum sensing cross-regulation in *Pseudomonas aeruginosa* causes major and unexpected alterations to virulence phenotypes. *J Am Chem Soc* **137**, 1510–1519 (2015).
 106. Barr, H. *et al.* *Pseudomonas aeruginosa* quorum sensing molecules correlate with clinical status in cystic fibrosis. *Eur Respir J* **46**, 1046–1054 (2015).
 107. Dickey, S., Cheung, G. & Otto, M. Different drugs for bad bugs: antivirulence strategies in the age of antibiotic resistance. *Nat Rev Drug Discov* **16**, 457–471 (2017).
 108. Déziel, E. *et al.* The contribution of MvfR to *Pseudomonas aeruginosa* pathogenesis and quorum sensing circuitry regulation: multiple quorum sensing-regulated genes are modulated without affecting IasRI, rhIRI or the production of N-acyl-L-homoserine lactones. *Mol Microbiol* **55**, 998–1014 (2005).

109. Xiao, G. *et al.* MvfR, a key *Pseudomonas aeruginosa* pathogenicity LTTR-class regulatory protein, has dual ligands. *Mol Microbiol* **62**, 1689–1699 (2006).
110. Cao, H. *et al.* A quorum sensing-associated virulence gene of *Pseudomonas aeruginosa* encodes a LysR-like transcription regulator with a unique self-regulatory mechanism. *PNAS* **98**, 14613–14618 (2001).
111. Lu, C. *et al.* Discovery of antagonists of PqsR, a key player in 2-alkyl-4-quinolone-dependent quorum sensing in *Pseudomonas aeruginosa*. *Chem Biol* **19**, 381–390 (2012).
112. Kitao, T. *et al.* Molecular insights into function and competitive inhibition of *Pseudomonas aeruginosa* multiple virulence factor regulator. *MBio* **9**, 2158–2175 (2018).
113. Schell, M. Molecular biology of the LysR family of transcriptional regulators. *Annu Rev Microbiol* **47**, 597–626 (1993).
114. Maddocks, S. & Oyston, P. Structure and function of the LysR-type transcriptional regulator (LTTR) family proteins. *Microbiology* **154**, 3609–3623 (2008).
115. Wade, D. *et al.* Regulation of pseudomonas quinolone signal synthesis in *Pseudomonas aeruginosa*. *J Bacteriol* **187**, 4372–4380 (2005).
116. Zender, M. *et al.* Flexible fragment growing boosts potency of quorum-sensing inhibitors against *Pseudomonas aeruginosa* virulence. *ChemMedChem* **15**, 188–194 (2020).
117. Grossman, S. *et al.* Novel quinazolinone inhibitors of the *Pseudomonas aeruginosa* quorum sensing transcriptional regulator PqsR. *Eur J Med Chem* **208**, (2020).
118. O’Shea, R. & Moser, H. Physicochemical properties of antibacterial compounds: Implications for drug discovery. *J Med Chem* **51**, 2871–2878 (2008).
119. Waring, M. *et al.* An analysis of the attrition of drug candidates from four major pharmaceutical companies. *Nat Rev Drug Discov* **14**, 475–486 (2015).
120. Lipinski, C., Lombardo, F., Dominy, B. & Feeney, P. Experimental and computational approaches to estimate solubility and permeability in drug discovery and development settings. *Adv Drug Deliv Rev* **23**, 3–25 (1997).
121. Leeson, P. & Springthorpe, B. The influence of drug-like concepts on decision-making

- in medicinal chemistry. *Nat Rev Drug Discov* **6**, 881–890 (2007).
122. Krause, K., Serio, A., Kane, T. & Connolly, L. Aminoglycosides: an overview. *Cold Spring Harb Perspect Med* **6**, a027029 (2016).
 123. Tillotson, G. Quinolones: Structure-activity relationships and future predictions. *J Med Microbiol* **44**, 320–324 (1996).
 124. Preethi, P. J. *et al.* Benzimidazole: An important Scaffold in Drug Discovery. *Asian J. Pharm. Technol.* **5**, 138 (2015).
 125. Henderson, R., Bechtold, W., Medinsky, M., P.-Fischer, J. & Lee, T. The effect of molecular weight/lipophilicity on clearance of organic compounds from lungs. *Toxicol Appl Pharmacol* **95**, 515–521 (1988).
 126. Boer, F. Drug handling by the lungs. *Br J Anaesth* **91**, 50–60 (2003).
 127. Labiris, N. & Dolovich, M. Pulmonary drug delivery. part I: physiological factors affecting therapeutic effectiveness of aerosolized medications. *Br J Clin Pharmacol* **56**, 588–599 (2003).
 128. Soukarieh, F. *et al.* In silico and in vitro-guided identification of inhibitors of alkylquinolone-dependent quorum sensing in *Pseudomonas aeruginosa*. *Molecules* **23**, (2018).
 129. Fletcher, M. *et al.* A dual biosensor for 2-alkyl-4-quinolone quorum-sensing signal molecules. *Env. Microbiol* **9**, 2683–2693 (2007).
 130. Moore, J., Gerdt, J., Eibergen, N. & Blackwell, H. Active efflux influences the potency of quorum sensing inhibitors in *Pseudomonas aeruginosa*. *ChemBioChem* **15**, 435–442 (2014).
 131. Fletcher, M., Diggle, S., Cámara, M. & Williams, P. Biosensor-based assays for PQS, HHQ and related 2-alkyl-4-quinolone quorum sensing signal molecules. *Nat Protoc* **2**, 1254–1262 (2007).
 132. Roberts, A., Kragh, K., Bjarnsholt, T. & Diggle, S. The limitations of in vitro experimentation in understanding biofilms and chronic infection. *J Mol Biol* **427**, 3646–3661 (2015).
 133. Azeredo, J. *et al.* Critical review on biofilm methods. *Crit Rev Microbiol* **43**, 313–351

- (2017).
134. Soukarieh, F. *et al.* Supplementary Material, Hit Identification of new potent PqsR antagonists as inhibitors of quorum sensing in planktonic and biofilm grown *Pseudomonas aeruginosa*. *Front Chem* **8**, 1–14 (2020).
 135. Bjarnsholt, T., Ciofu, O., Molin, S., Givskov, M. & Høiby, N. Applying insights from biofilm biology to drug development-can a new approach be developed? *Nat Rev Drug Discov* **12**, 791–808 (2013).
 136. Maura, D. & Rahme, L. G. Pharmacological Inhibition of the Formation and Potentiates Antibiotic Mediated Biofilm Disruption. *Antimicrob Agents Chemother* **61**, e01362-17 (2017).
 137. Welsh, M. & Blackwell, H. Chemical probes of quorum sensing: from compound development to biological discovery. *FEMS Microbiol Rev* **40**, 774–794 (2016).
 138. Lu, C., Maurer, C., Kirsch, B., Steinbach, A. & Hartmann, R. Overcoming the unexpected functional inversion of a PqsR antagonist in *Pseudomonas aeruginosa*: An in vivo potent antivirulence agent targeting pqs quorum sensing. *Angew Chem Int Ed Engl* **53**, 1109–1112 (2014).
 139. Sou, T. *et al.* Model-based drug development in pulmonary delivery: pharmacokinetic analysis of novel drug candidates for treatment of *pseudomonas aeruginosa* lung infection. *J Pharm Sci* **108**, 630–640 (2019).
 140. Tiwary, B. K., Pradhan, K., Nanda, A. K. & Chakraborty, R. Implication of quinazoline-4(3H)-ones in medicinal chemistry: a brief review. *J Chem Biol Ther* **1**, 104 (2016).
 141. Niementowski, S. Synthesen der chinolinderivate. *chemistry* **27**, 1394–1403 (1894).
 142. Lemahieu, R. *et al.* (E)-3-(4-oxo-4H-quinazolin-3-yl)-2-propenoic acids, a new series of antiallergy agents. *J Med Chem* **26**, 420–425 (1983).
 143. Roelens, F. *et al.* Regioselective synthesis and estrogenicity of (±)-8-alkyl-5,7-dihydroxy-4-(4-hydroxyphenyl)-3,4-dihydrocoumarins. *Eur J Med Chem* **40**, 1042–1051 (2005).
 144. Parker, R. & Isaacs, N. Mechanisms of epoxide reactions. *Chem Rev* **59**, 737–799 (1959).

145. Špulák, M. *et al.* The unambiguous synthesis and NMR assignment of 4-alkoxy and 3-alkylquinazolines. *Tetrahedron* **69**, 1705–1711 (2013).
146. Lizarzaburu, M. & Shuttleworth, S. Convenient preparation of aryl ether derivatives using a sequence of functionalized polymers. *Tetrahedron Lett* **44**, 4873–4876 (2003).
147. Kokatla, H. & Lakshman, M. One-pot etherification of purine nucleosides and pyrimidines. *Org Lett* **12**, 4478–4481 (2010).
148. Hu, B. *et al.* Hexachlorocyclotriphosphazene (HCCP)-mediated direct formation of thioethers and ethers from quinazolin-4(3H)-ones. *Molecules* **18**, 5580–5593 (2013).
149. Burbuliene, M., Mazeikaite, R. & Vainilavicius, P. Regioselective synthesis of N(3)- and O-acylmethyl derivatives of 2-methylthio-4(3H)-quinazolinone. *J Heterocycl Chem* **45**, 607–610 (2008).
150. Dess, D. & Martin, J. Readily accessible 12-I-51 oxidant for the conversion of primary and secondary alcohols to aldehydes and ketones. *J Org Chem* **48**, 4155–4156 (1983).
151. Dong, L., Roosenberg, J. & Miller, M. Total synthesis of desferrisalmycin B. *J Am Chem Soc* **124**, 15001–15005 (2002).
152. Ramanathan, A. & Jimenez, L. Reductive dehalogenation of aryl bromides and chlorides and their use as aryl blocking groups. *Synthesis* **41**, 217–220 (2010).
153. Amundsen, L. & Nelson, L. Reduction of nitriles to primary amines with Lithium Aluminum Hydride. *J Am Chem Soc* **73**, 242–244 (1950).
154. Albericio, F. & El-Faham, A. Choosing the right coupling reagent for peptides: a twenty-five-year journey. *Org Process Res Dev* **22**, 760–772 (2018).
155. Montalbetti, C. & Falque, V. Amide bond formation and peptide coupling. *Tetrahedron* **61**, 10827–10852 (2005).
156. Abdel-Magid, A. & Mehrman, S. A review on the use of sodium triacetoxyborohydride in the reductive amination of ketones and aldehydes. *Org Process Res Dev* **10**, 971–1031 (2006).
157. Wiberg, K. The mechanisms of hydrogen peroxide reactions. I. The conversion of benzonitrile to benzamide. *J Am Chem Soc* **75**, 3961–3964 (1953).
158. Mantalo, N., Navarro, A., Saeed, A. & Gernert, D. Preparation of triazole, oxadiazole

- and thiadiazole derivatives as PPAR modulators for the treatment of diabetes. (2005).
159. Roh, J., Artamonova, T., Vávrová, K., Koldobskii, G. & Hrabálek, A. Practical synthesis of 5-substituted tetrazoles under microwave irradiation. *Synthesis* 2175–2178 (2009).
 160. Velázquez-Campoy, A., Ohtaka, H., Nezami, A., Muzammil, S. & Freire, E. Isothermal Titration Calorimetry. *Curr Protoc Cell Biol* **23**, 17821–17824 (2004).
 161. Meanwell, N. Improving drug candidates by design: a focus on physicochemical properties as a means of improving compound disposition and safety. *Chem Res Toxicol* **24**, 1420–1456 (2011).
 162. Bissantz, C., Kuhn, B. & Stahl, M. A medicinal chemist's guide to molecular interactions. *J Med Chem* **53**, 5061–5084 (2010).
 163. Hansch, C., Leo, A. & Taft, R. A Survey of Hammett Substituent Constants and Resonance and Field Parameters. *Chem Rev* **91**, 165–195 (1991).
 164. Nepali, K., Lee, H. & Liou, J. Nitro group containing drugs. *J Med Chem* **62**, 2851–2893 (2019).
 165. Ahmed, A. & Farooqui, M. Comparative toxicities of aliphatic nitriles. *Toxicol Lett* **12**, 157–163 (1982).
 166. Wang, Y., Du, Y. & Huang, N. A survey of the role of nitrile groups in protein-ligand interactions. *Futur. Med Chem* **10**, 2713–2727 (2018).
 167. McConathy, J. & Owens, M. Stereochemistry in Drug Action. *Prim Care Companion J Clin Psychiatry* **5**, 70–73 (2003).
 168. Development of new stereoisomeric drugs. *U.S. Food & Drug administration*. <https://www.fda.gov/regulatory-information/search-fda-guidance-documents/development-new-stereoisomeric-drugs> (1992).
 169. Thakuria, R., Nath, N. & Saha, B. The nature and applications of π - π interactions: a perspective. *Cryst Growth Des* **19**, 523–528 (2019).
 170. Vergalli, J. *et al.* Spectrofluorimetric quantification of antibiotic drug concentration in bacterial cells for the characterization of translocation across bacterial membranes. *Nat Protoc* **13**, 1348–1361 (2018).
 171. Singh, P. & Silakari, O. Chapter 2- Benzimidazole: journey from single targeting to

- multitargeting molecule. in *Key Heterocycle Cores for Designing Multitargeting Molecules* 31–52 (Elsevier Ltd, 2018).
172. Kuzniewski, C., Gertsch, J., Wartmann, M. & Altmann, K.-H. Total synthesis of hypermodified epothilone analogs with potent in vitro antitumor activity. *Org Lett* **10**, 1183–1186 (2008).
 173. Whiting, M., Harwood, K., Hossner, F., Turner, P. & Wilkinson, M. Selection and development of the manufacturing route for EP1 antagonist GSK269984B. *Org Process Res Dev* **14**, 820–831 (2010).
 174. Kennedy, R. & Stock, A. The Oxidation of Organic Substances by Potassium Peroxymonosulfate. *J Org Chem* **25**, 1901–1906 (1960).
 175. Betterton, E. & Hoffmann, M. Kinetics and mechanism of the oxidation of aqueous hydrogen sulfide by peroxymonosulfate. *Env. Sci Technol* **24**, 1819–1824 (1990).
 176. O'Donovan, D. & Rozas, I. A concise synthesis of asymmetrical N,N'-disubstituted guanidines. *Tetrahedron Lett* **52**, 4117–4119 (2011).
 177. Beesu, M. *et al.* Human toll-like receptor 8-selective agonistic activities in 1-alkyl-1h-benzimidazol-2-amines. *J Med Chem* **57**, 7325–7341 (2014).
 178. Kinsman, A. & Kerr, M. Total synthesis of (±)-Hapalindole Q. *Org Lett* **3**, 3189–3191 (2001).
 179. Corey, E. & Venkateswarlu, A. Protection of hydroxyl groups as tert-Butyldimethylsilyl derivatives. *J Am Chem Soc* **94**, 6190–6191 (1972).
 180. Patschinski, P., Zhang, C. & Zipse, H. The lewis base-catalyzed silylation of alcohols—a mechanistic analysis. *J Org Chem* **79**, 8348–8357 (2014).
 181. Romero, M., Morales, C., González-Zamora & Gutiérrez-Carillo. 2,4-Dinitrophenyl and pentaerythrityl trinitrate as explosophoric units in the synthesis of new energetic materials. *Synthesis* **48**, 3794–3802 (2016).
 182. Ramurthy, S. *et al.* Design and synthesis of orally bioavailable benzimidazoles as Raf kinase inhibitors. *J Med Chem* **51**, 7049–7052 (2008).
 183. Poitout, L. *et al.* Identification of a novel series of benzimidazoles as potent and selective antagonists of the human melanocortin-4 receptor. *Bioorganic Med Chem Lett* **17**, 4464–

- 4470 (2007).
184. Wan, Z.-K., Ousman, E.-F., Papaioannou, N. & Saiah, E. Phosphonium-mediated cyclization of N-(2-aminophenyl)thioureas: Efficient synthesis of 2-aminobenzimidazoles. *Tetrahedron Lett* **52**, 4149–4152 (2011).
 185. Zhong, M. *et al.* An efficient stereoselective synthesis of methyl (S)-3-amino-3-(3-pyridyl)propanoate. *Tetrahedron Lett* **40**, 7721–7725 (1999).
 186. Masi, M., Réfregiers, M., Pos, K. & Pagès, J.-M. Mechanisms of envelope permeability and antibiotic influx and efflux in Gram-negative bacteria. *Nat Microbiol* **2**, 17001 (2017).
 187. Hall, S. *et al.* Cellular effects of pyocyanin, a secreted virulence factor of *Pseudomonas aeruginosa*. *Toxins* **8**, 236 (2016).
 188. Oton, E. *Pseudomonas aeruginosa* PQS mediated virulence regulation and interference. (2018).
 189. Marvig, R., Johansen, H., Molin, S. & Jelsbak, L. Genome analysis of a transmissible lineage of *pseudomonas aeruginosa* reveals pathoadaptive mutations and distinct evolutionary paths of hypermutators. *PLoS Genet* **9**, e1003741 (2013).
 190. Wee, B. *et al.* Whole genome sequencing reveals the emergence of a *Pseudomonas aeruginosa* shared strain sub-lineage among patients treated within a single cystic fibrosis centre. *BMC Genomics* **19**, 644 (2018).
 191. Roy, P. *et al.* Complete genome sequence of the multiresistant taxonomic outlier *Pseudomonas aeruginosa* PA7. *PLoS One* **5**, e8842 (2010).
 192. Diggle, S. *et al.* The *Pseudomonas aeruginosa* quinolone signal molecule overcomes the cell density-dependency of the quorum sensing hierarchy, regulates rhl-dependent genes at the onset of stationary phase and can be produced in the absence of LasR. *Mol Microbiol* **50**, 29–43 (2003).
 193. Mashburn-Warren, L. *et al.* Interaction of quorum signals with outer membrane lipids: Insights into prokaryotic membrane vesicle formation. *Mol Microbiol* **69**, 491–502 (2008).
 194. Cain, A., Nolan, L., Sullivan, G., Whitchurch, C. & Filloux, A. Complete Genome

- Sequence of *Pseudomonas aeruginosa* Reference Strain PAK. *Am Soc Microbiol* **8**, e00865-19 (2019).
195. Jiang, Q., Chen, J., Yang, C., Yin, Y. & Yao, K. Quorum Sensing: a prospective therapeutic target for bacterial diseases. *Biomed Res Int* **2019**, 2015978 (2019).
 196. Baishya, J. & Wakeman, C. Selective pressures during chronic infection drive microbial competition and cooperation. *npj Biofilms Microbiomes* **5**, (2019).
 197. Harrison, F., Muruli, A., Higgins, S. & Diggle, S. Development of an ex vivo porcine lung model for studying growth, virulence, and signaling of *Pseudomonas aeruginosa*. *Infect Immun* **82**, 3312–3323 (2014).
 198. Hefti, F. Requirements for a lead compound to become a clinical candidate. *BMC Neurosci* **9**, (2008).
 199. O'Brien, J., Wilson, I., Orton, T. & Pognan, F. Investigation of the Alamar blue (resazurin) fluorescent dye for the assessment of mammalian cell cytotoxicity. *Eur J Biochem* **267**, 5421–5426 (2000).
 200. Rémy, B. *et al.* Interference in bacterial quorum sensing: a biopharmaceutical perspective. *Front Pharmacol* **9**, 1–17 (2018).
 201. Smith, W. *et al.* Current and future therapies for *Pseudomonas aeruginosa* infection in patients with cystic fibrosis. *FEMS Microbiol Lett* **364**, 1–9 (2017).
 202. Ertl, P., Rohde, B. & Selzer, P. Fast calculation of molecular polar surface area as a sum of fragment-based contributions and its application to the prediction of drug transport properties. *J Med Chem* **43**, 3714–3717 (2000).
 203. Negash, K., Norris, J. & Hodgkinson, J. Siderophore-antibiotic conjugate design: new drugs for bad bugs? *Molecules* **24**, 3314 (2019).
 204. Zhang, J. *et al.* Design, synthesis and evaluation of a series of 3- or 4-alkoxy substituted phenoxy derivatives as PPARs agonists. *Oncotarget* **8**, 20766–20783 (2017).
 205. Zotova, N., Kushakova, P., Kuznetsov, V., Rodin, A. & Garabadzhiu, A. Specific features of nucleophilic substitution in 1-chloro-3,4-dinitrobenzene. *Russ J Org Chem* **40**, 1473–1476 (2004).
 206. Bieszczad, B. *et al.* Unsymmetrically-substituted 5,12-dihydrodibenzo[b,f]

- [1,4]diazocine-6,11-dione scaffold—a useful tool for unsymmetrically-substituted 5,12-dihydrodibenzo[b,f] [1,4]diazocine-6,11-dione scaffold—a useful tool for bioactive molecules design. *Molecules* **25**, 2855 (2020).
207. Holloway, B. Genetic recombination in *Pseudomonas aeruginosa*. *J gen microbiol* **13**, 572–581 (1955).
208. Rahme, L. *et al.* Common virulence factors for bacterial pathogenicity in plants and animals. *Science* **268**, 1899–1902 (1995).
209. Palmer, K., Aye, L. & Whiteley, M. Nutritional cues control *pseudomonas aeruginosa* multicellular behavior in cystic fibrosis sputum. *J Bacteriol* **189**, 8079–8087 (2007).
210. Harrison, F. & Diggle, S. An ex vivo lung model to study bronchioles infected with *Pseudomonas aeruginosa* biofilms. *Microbiol* **162**, 1755–1760 (2016).